University of Sheffield
Department of Physics and Astronomy

Quantum effects in nonlinear optics and polaritonics

Giuseppe Buonaiuto

Submitted in part fulfilment of the requirements for the degree of
Doctor of Philosophy in Physics of the University of Sheffield
September 2018

Abstract

The main scope of this thesis is the investigation of quantum properties of nonlinear, dissipative, optical and condensed matter systems. Compared with previous studies on this subjects, we reached several milestone of general interests for the theoretical and experimental community. The main experimental platform we refer to in this thesis is microcavity polaritons: polaritons arise from the coupling of light with excitons in a quantum well, i.e., a 2D semiconductor material embedded in the microcavity. They have attracted the interest of the scientific community for their rich physics. Polaritons can form out-of-equilibrium Bose-Einstein condensates, they can experience superfluid phase transition and, due to their interaction via the excitonic component, they show a variety of phenomena which are typical of nonlinear physics, such as bistability and parametric scattering. In particular, motivated by recent proposals about the generation of single photons from weakly nonlinear system, like the unconventional photon blockade, and by the production of squeezed states in polariton systems, we studied the possibility of obtaining antibunched light and other quantum states (like squeezed states and entangled states), when the nonlinear system shows some peculiar features: in particular we consider polariton soliton and cascade systems. Finally, when considering nonlinear incoherent processes, we investigate the effect of the $\mathcal{PT}$-symmetry and the $\mathcal{PT}$-symmetry breaking on the quantum state of the emitted light.

Hence, this research work has two main objectives: first, from the fundamental physics point of view, to understand the interplay between nonlinear phenomena and quantum optics, second to provide useful tools for future technological applications. Specifically, for the latter case, we demonstrate a theorem that links the measurement of intensity correlations with the occurrence of certain phase transitions, and we propose a setup to maximize the non-classicality of the light emitted by weakly non-linear systems via a cascade configuration.

Acknowledgements

I would like to express my gratitude and professional appreciation to my supervisor David M. Whittaker, who made possible the realization of this thesis and of the underlying research.

A special acknowledgement goes to Emiliano Cancellieri, who taught me a lot about how research works. The discussions we had, about physics and beyond, were a constant stimulus for me to improve and to reflect about what I was doing: his help was fundamental and for this he has my gratitude.

It was interesting to share the office with people who have proven to be often better than me. It was a test of tolerance and humility, which made me realize that, often, narcissism prevented me from seeing and exceeding my limits: for this I thank you all, Jasminder, David, Mark, Luke, Scott, Mark P., Zixin.

A special mention goes to all the colleagues in the department with whom I have established a human and professional relationship. In particular I want to refer to those who gave me friendship and listened to me when I needed them, even without realizing it: Rahul, for the quality time we spent together, Kyriakos, for his relaxing presence and amazing empathy, Harriet, for incredible courage and strength, Armando, for his profound soul and friendly personality, Charles, for the quality of the discussion we manage to have and Ruggero, for the patience showed in listening to my complains.

Making a Ph.D. can be complicated, not only because of the difficulties encountered in research, but because of the stress, frustration and psychological anxiety that comes with it. This is why it was fundamental for me to have good relationships outside the workplace. Everyone helped me to maintain my mental health and to remind myself that beauty and dignity do not necessarily live among the four walls of a university. So I thank Fabio, for the piece of road we did together, Baptiste, for the beautiful evenings full of music, Josie and Neri, for their joyful madness, Jamal, for the passionate political and artistic discussions, Paolo, for the passion for sport and nature that it is able to communicate.

A special thought goes to John: we spent days and nights talking about Physics, Philosophy, Zen and so on. An intense human and spiritual exchange, which often made the difference in my days.

Another special thought goes to Sofia, with whom I have had difficult moments, but I preserve the affection intact. She showed me my human limits, made me understand that it's never over, and the work I have to do on myself is always a lot.

As an immigrant, the thought of home, of what I have left, is salvation and damnation. I missed my friends and relatives, every day, but I also felt their constant closeness, in my memories and in my soul, whatever that is. So all I did in these years in England, I did it thanks to you, Ciro, Giuseppe, Antonietta, Rocco, Davide, Federica, Pierpaolo, Pasquale, Walter (which was always here with me, but that's

fine).
And of course my family. They have supported me since I was born and continue to do so, perhaps not in the most traditional ways, but always with great unconditional love. So a special thank you goes to my Father, my Mother, to my brothers Giovanni and Alfonso and my four-legged friend, Cloe.
Finally, the deepest gratitude goes to the family I have built here, the one with whom I have shared daily life, pain, joy and every other human feeling. Claudio, with an immense heart, Caterina, with an immense heart, Ebaa, with an immense heart. Immense people, struggling, each in their own way, every day the battle for personal freedom and that of others. People who believe in Good, beyond appearances. People who are a living example of the fact that humanity has hope. To them, my deep thanks.

Dedicated to all the people that try to improve this world, a bit, every day.

Contents

List of Figures

Chapter 1

Introduction

1.1 Structure of the Thesis

The Thesis is organised as follows. In the first Chapter, we summarise the main theoretical background used for the rest of the work. This basically consists in the physics of open quantum systems and the definition of the phase-space methods implemented. In the second Chapter, the basics of polariton physics are presented: in particular we demonstrate the possibility of manipulating the spin-orbit state of microcavity polaritons, generated by the TE-TM energy splitting, by the means of Stark pulses. In Chapter three, we analyse the main computational techniques used to address the quantum dynamics of nonlinear photonic system: using a gauged version of the Positive P-representation we are able to perform large scale simulations, with arbitrary number of particles, avoiding moving singularities and the growth of systematic errors. Hence, we make use of the gauge P-representation, to quantify the statistics, and in particular the second order correlation function, of polariton solitons: these non dispersive waves have been observed experimentally both in monolithic cavities and in nonlinear waveguides. In Chapter four, we demonstrate a theorem which states that the $m-th$ order correlation function, in a multimode system, is stationary if the system itself is $U(1)$-symmetric, i.e., the Hamiltonian commutes with the number operator. The breaking of the $U(1)$ symmetry corresponds to a non stationary correlation function, hence giving a potential experimental tool to investigate whether such phase transition is occurring. The

result has a potential impact in the investigation of phase transition both in condensed matter systems and in photonic systems. We provide an analytical proof of the theorem, together with numerical simulations, which confirm the validity of the results. In Chapter five we propose a scheme, based on a cascade configuration, to generate highly non-classical states. A nonlinear optical cavity is driven with a classical light field until it produces photons with non-coherent statistics: then these states are used to feed another nonlinear system, with a unidirectional coupling. We show that the light emitted by the second system experiences an increase in the sub-Poissonianity. Moreover we demonstrate that the two subsystems are in an entangled state, which is produced by the dissipative coupling between them. The last Chapter is dedicated to quantum effects in non-Hermitian optical systems. In the last few years, a big effort has been dedicated to the investigation of the physics behind non-Hermitian systems, i.e., systems decribed by non-Hermitian Hamiltonians, and in particular to $\mathcal{PT}$-symmetric systems. Here we investigate the effect of the interplay between the non-Hermitianity and the nonlinearity on the quantum properties of a class of nonlinear optical systems. In particular we consider a photonic molecule, with one mode experiencing a saturable gain and the other a saturable loss. We demonstrate that the breaking of the $\mathcal{PT}$-symmetry has a direct effect on the quantum statistics of the emitted light: moreover, the numerical simulation of the Wigner function reveals that the PT-symmetry breaking pushes one mode towards a coherent vacuum state, and the other towards a Fock state, with high fidelity. Hence we propose the $\mathcal{PT}$-symmetric optical system as a possible candidate for the production of Fock states, useful in principle for quantum computing and quantum communication protocols.

1.2 Statement of Originality

The material presented in this thesis is original, to the best of the knowledge of the author, except where otherwise specified. Parts of the work containing general information and the theoretical framework are inspired by the standard literature

related to the subject, which hence have been properly referenced.

1.3 Publications

- Feng Li, E. Cancellieri, **G. Buonaiuto**, M. S. Skolnick, D. N. Krizhanovskii, and D. M. Whittaker, *Full Stark control of polariton states on a spin-orbit hypersphere*, Physical Review B, 94, 20,1301, 2016.

- C.E. Whittaker, B. Dzurnak, O.A. Egorov, **G. Buonaiuto**, P.M. Walker, E. Cancellieri, D.M. Whittaker, E. Clarke, S.S. Gavrilov, M.S. Skolnick, and D.N. Krizhanovskii, *Polariton Pattern Formation and Photon Statistics of the Associated Emission*, Physical Review X, 7,3,031033, 2017.

- **Giuseppe Buonaiuto**, David M. Whittaker, Emiliano Cancellieri, *Conservation of Quantum Correlations in Multimode Systems with U(1) Symmetry*, Phys. Rev. Lett. 121, 020404, 2018.

1.3.1 Submitted Journal Publications

- **Giuseppe Buonaiuto**, David M. Whittaker, Emiliano Cancellieri, *Quantum optics of nonlinear systems in cascade*, Submitted to Physical Review Letter, arXiv:1805.09272 [quant-ph].

1.3.2 Papers in Preparation

- **Giuseppe Buonaiuto**, David M. Whittaker, Emiliano Cancellieri, *Quantum effects of PT-symmetric nonlinear gain-loss systems.*

1.3.3 Presentations

Oral

- PLMCN17, Quantum effects in polariton solitons, Nara, Japan Mar 2016

- ISPP17, Qunantum nonlinear systems in cascade, Cefalu, Sicily, IT Aug 2017

- PLMCN19, Conservation of Correlation functions in U(1)-symmetric systems, Chengdu,China May 2018

Poster

- Topolight 2015,Topological effects in Condensed Matter, Trento, IT Feb 2015
- QFLM, Quantum fluid of light-matter, Cargese, Corsica. Apr 2017

Chapter 2

Background Theory

In this Chapter, we revise the basic theoretical tools which will be used throughout the rest of this thesis. These tools come from the theory of quantum optics and open quantum systems: hence, in the following, we will refer mostly to standard textbooks, such as *Quantum Optics*, by Walls and Milburn [8], *Statistical methods in Quantum Optics I* by H. Carmichael [9] and the *Theory of open quantum systems* by Breuer and Petruccione [10]. In the following sections, we first review the quantum harmonic oscillator and the relevant quantum states commonly found in quantum optics. We then focus on the basic model for dissipative dynamics, defining and deriving the master equation for a damped harmonic oscillator. Finally, the main instruments implemented for the theoretical and numerical investigations in this thesis are revised, such as the intensity correlation function and the phase-space methods.

2.1 Quantum Harmonic Oscillator

In this section we briefly revise the theoretical description of the quantum harmonic oscillator, following the approach of Carmichael in [9]. This simple model underlines many physical systems, especially for quantum optics, as we can describe the electromagnetic field as a collection of quantized harmonic oscillators. The harmonic

oscillator is described by the following Hamiltonian:

$$\mathcal{H} = \frac{1}{2m}p^2 + \frac{1}{2}m\omega^2 q^2, \tag{2.1}$$

with frequency ω and mass m, where the position q and momentum p operators obey to the commutation relation:

$$[p, q] = i\hbar. \tag{2.2}$$

The Heisenberg uncertainty principle follows from the commutation relation: the principle constitutes a limit to the precision for the measurements of the position and momentum of the particle, as we explicitly show in the following section. The standard approach for finding the eigenvalues of (2.1) is based on the definition of the ladder operators:

$$\begin{aligned} a &= \sqrt{\frac{\omega}{2\hbar}}q + \frac{i}{\sqrt{2\hbar\omega}}p \\ a^\dagger &= \sqrt{\frac{\omega}{2\hbar}}q - \frac{i}{\sqrt{2\hbar\omega}}p, \end{aligned} \tag{2.3}$$

these are called, when referring to quantum fields, annihilation and creation operators, respectively. In term of such quantities, the commutation relation can be written as:

$$[a, a^\dagger] = 1, \tag{2.4}$$

through which the Hamiltonian of the harmonic oscillator can be rewritten,

$$\mathcal{H} = \hbar\omega(a^\dagger a + \frac{1}{2}). \tag{2.5}$$

Without going too much into details, it can be demonstrated that the eigenstates of $a^\dagger a$ are the states $|n\rangle$ with $n \in \mathbb{N}$, which are called, when referring to field excitations, *Fock states*. The lowest state satisfies:

$$a\,|0\rangle = 0, \tag{2.6}$$

and starting from this is possible to reconstruct the action of the annihilation/creation operators on the Fock states:

$$a\,|n\rangle = \sqrt{n}\,|n-1\rangle \tag{2.7}$$

$$a^\dagger\,|n\rangle = \sqrt{n+1}\,|n+1\rangle\,. \tag{2.8}$$

The states $|n\rangle$ are also called *number states*, because they are states with a definite number of excitations. In particular, they constitutes a complete, orthonormal, basis for any vector Hilbert space of an harmonic oscillator. If we return to the Hamiltonian (2.1), from the arguments above it follows that the energy spectrum consists of equally spaced energy levels:

$$E_n = \hbar\omega(n + \frac{1}{2}). \tag{2.9}$$

In the laboratory, photon number states can be obtained using various techniques, mostly relying on nonlinear optical processes [11], like the parametric down conversion, with micromasers [12] and with superconducting circuits [13]. In parametric down conversion, a continuous wave laser is used to drive a nonlinear crystal: as a consequence of the nonlinearity, photons in the pump are spontaneously down converted into pairs of lower energy photons, following the conservation of energy and momentum. The detection of a single photon in one of the two spatial mode, heralds the presence of a single photon in the other mode. Among the Fock states, the single photon state is particularly intereroberstingly, as it can be used as a *qubit*, i.e. the fundamental unit in which quantum information can be encoded, for potential applications in quantum computing and quantum communication. Obtaining such states, especially with high efficiency, remains a difficult task. Among the possible strategies implemented, we mention here quantum dots and NV-centers in diamonds [14], which have attracted a lot of attention for their ability to generate higly indistinguishable single photons, together with less standard approaches, like the *unconventional photon blockade*, which is a mechanism based on the interference effect arising from the coherent coupling between specific nanostructures [15].

2.1.1 Quantization of the electromagnetic field

The harmonic oscillator is the basic model used to describe a quantised electromagnetic field. In fact, each mode of the electromagnetic field can be described as a set of harmonic oscillator, labelled with the subscript k, wich has the following effect on the n-th energy eigenstate:

$$a_k |n_k\rangle = \sqrt{n_k} |n_k - 1\rangle , \tag{2.10}$$

where the creation and annihilation operators for the k-mode obey the following commutation relations:

$$\begin{aligned} [a_k, a_{k'}] &= [a_k^\dagger, a_{k'}^\dagger] = 0 \\ [a_k, a_{k'}^\dagger] &= \delta_{kk'}, \end{aligned} \tag{2.11}$$

so that they destroy (or create) one unit of energy $\hbar\omega_k$, one *photon*. The total energy of the system is described by the Hamiltonian:

$$\mathcal{H}_{em} = \sum_k \hbar\omega_k \left(\frac{1}{2} + a_k^\dagger a_k \right), \tag{2.12}$$

where each mode of the electromagnetic field contributes only with quantised packet of energy. The electric field, including the degree of polarization e_k, can be written as:

$$E(\mathbf{r}, t) = \frac{1}{\sqrt{V}} \sum_k e_k \frac{\hbar\omega_k}{2\epsilon_0} (X_k \cos(\Theta_k(\mathbf{r}, t)) + P_k \sin(\Theta_k(\mathbf{r}, t)), \tag{2.13}$$

with V the volume element of the quantization region arising from the considered boundary conditions, ϵ_0 the dielectric constant of vacuum and $\Theta_k = \omega t - \mathbf{k} \cdot \mathbf{r}$ the phase of the wavefront. The quantities X_k and P_k are the quadratures of the field:

$$\begin{aligned} X_k &= (a_k + a_k^\dagger) \\ P_k &= i(-a_k + a_k^\dagger), \end{aligned} \tag{2.14}$$

which are often called the in-phase and out-of-phase components of the field, respectively, defined respect to a reference field, implemented in a homodyne detection. By convention, the X component is called the amplitude quadrature, as it retains most of the information about the amplitude of the wave. Conversely, P describes the phase shift of the EM field, hence is conventionally called the phase quadrature. To have a complete tomography of the electromagnetic field in the phase-space spanned by X and P, hence to fully reconstruct the quantum state of the system, it is often necessary to consider all the possible two dimensional basis obtain through a rotation by an angle ϕ of (2.14):

$$\begin{aligned} X_k^{\phi} &= X_k \cos(\phi) + P_k \sin(\phi) \\ X_k^{\phi+\pi/2} &= -X_k \sin(\phi) + P_k \cos(\phi) \end{aligned} \tag{2.15}$$

2.1.2 Quadrature Uncertainty

Let us consider the quadrature operators for a single mode, $X = (a + a^{\dagger})$ and $P = i(-a + a^{\dagger})$. From (2.4) it follows that these operators do not commute, and in particular they obey to the following relation:

$$[X, P] = 2i, \tag{2.16}$$

which leads to the uncertainty principle between the quadratures. The uncertainty principle, in the most general mathematical formulation, consists in a lower bound for the variance in the distribution of two observables O_1 and O_2:

$$\Delta(O_1^2)\Delta(O_2^2) \geq (\frac{i}{2}\langle[O_1, O_2]\rangle)^2, \tag{2.17}$$

which is known as *Robertson relation*, where $\Delta(O^2) = \langle(O - \langle O\rangle)^2\rangle$, and (2.17) can be obtained from the commutator $[O_1, O_2]$ making use the Schwarz inequality. Substituting (2.16) in (2.17), we obtain:

$$\Delta(X^2)\Delta(P^2) \geq 1. \tag{2.18}$$

The fact that the minimum of the product of the two variances is non-zero, sets a limit to the precision of the simultaneous measurement of the quadratures: this precision needs not be equally distributed, as long as the product of the variances satisfies the inequality. Hence the variance of the X quadrature for a given state may be smaller than the one possessed by a coherent state, but this need to be compensated by a larger variance for the relative orthogonal quadrature, so that (2.18) is always satisfied.

2.1.3 Coherent State

The coherent state $|\alpha\rangle$ is formally defined as the right eigenstate of the annihilation operator with eigenvalue $\alpha \in \mathbb{C}$:

$$a|\alpha\rangle = \alpha|\alpha\rangle . \tag{2.19}$$

In particular coherent states minimize the Heisenberg uncertainty relation, which means that, considering the ground state of a harmonic oscillator, the inequality (2.18) is saturated, $\Delta(X^2)\Delta(P^2) = 1$ and $\Delta(P^2) = \Delta(X^2)$: in this sense, coherent states are often referred as the *most classical quantum states*. The mean photon number and the variance of a coherent state can be calculated by considering the action of the number operator on these states:

$$\begin{aligned} \bar{n} &= \langle\alpha|n|\alpha\rangle = |\alpha|^2 \\ \Delta(n^2) &= |\alpha|^2, \end{aligned} \tag{2.20}$$

hence, the variance of the number of detected excitations is equal in magnitude to the mean number of particles. As the quadrature uncertainty is fixed, in the limit of large α, the quantum noise becomes less significant and the field can be approximated by a classical wave. It is possible to expand any normalized coherent state into a Fock state basis $|n\rangle$. In fact if we express $|\alpha\rangle$ as:

$$|\alpha\rangle = \sum_{n=0}^{\infty} c_n |n\rangle , \tag{2.21}$$

hence, since the action of the annihilation operator on a Fock state is $a|n\rangle = \sqrt{n}|n-1\rangle$, the above expression becomes

$$\sum_{n=1}^{\infty} c_n \sqrt{n}\,|n-1\rangle = \alpha \sum_{n=0}^{\infty} c_n |n\rangle\,. \tag{2.22}$$

We now make use of the orthogonality of the Fock states, multiplying the equation above on the left by $\langle m|$, obtaining:

$$\sum_{n=1}^{\infty} c_n \sqrt{n}\delta_{m,n-1} = \alpha \sum_{n=0}^{\infty} c_n \delta_{m,n}, \tag{2.23}$$

or, equivalently:

$$c_{m+1}\sqrt{m+1} = \alpha c_m, \tag{2.24}$$

which means that:

$$c_n = \frac{\alpha^n}{\sqrt{n!}} c_0. \tag{2.25}$$

The first term of the series c_0 can be derived from the normalization condition $\langle\alpha|\alpha\rangle = 1$, leading to:

$$|\alpha\rangle = e^{-\frac{|\alpha|^2}{2}} \sum_{n=0}^{\infty} \frac{\alpha^n}{\sqrt{n!}} |n\rangle\,, \tag{2.26}$$

with the corresponding Poisson-photon number distribution:

$$p(n) = |\langle n|\alpha\rangle|^2 = e^{-|\alpha|^2} \frac{|\alpha|^2}{n!}. \tag{2.27}$$

It is also possible to define the coherent state by considering the vacuum state, which is the ground state of the harmonic oscillator, and applying to it a displacement operator:

$$|\alpha\rangle = D(\alpha)|0\rangle = \exp(\alpha a^\dagger - \alpha^* a)|0\rangle\,, \tag{2.28}$$

where $\alpha = |\alpha|e^{-i\phi}$ is a complex number, which can be put in correspondence with the phasor representation of the classical electromagnetic field. The displacement operator acquires its name because of its action on the annihilation operator, $D(\alpha)^{-1} a D(\alpha) = a + \alpha$. From expansion (2.26) it follows that coherent states do not form an orthog-

onal set. The overlap between the state $|\alpha\rangle$ and $|\beta\rangle$ is given by:

$$|\langle\alpha|\beta\rangle|^2 = e^{-|\alpha-\beta|^2}. \tag{2.29}$$

The orthogonality is exactly recovered in the limit of large $|\alpha-\beta|^2$. Another property of coherent states, which will be used later in this thesis, is the *over-completeness*: coherent states obey to the closure relation,

$$\frac{1}{\pi}\int d^2\alpha\,|\alpha\rangle\langle\alpha| = 1, \tag{2.30}$$

where the integration is taken over the entire complex plane. Hence, any quantum states can be decomposed in term of a diagonal set of coherent states.
It is worth to mention here the physical importance of a coherent state: a laser field that is operating well above threshold, is well approximated by a coherent state.

2.1.4 Squeezed states

Generally, a *squeezed state* is a quantum state which has a smaller variance than a coherent state in one of the quadrature: as we mentioned before, to satisfy the Heisenberg uncertainty principle, this noise reduction in one quadrature always comes with an increase in the noise in the other quadrature. Mathematically, squeezed states can be obtained by considering the action of the following operator:

$$S(\xi) = e^{((\frac{\xi}{2})^* a^2 - \frac{\xi}{2}a^{\dagger 2})}, \tag{2.31}$$

with $\xi = re^{2i\phi}$. In particular the action of the squeezing operator is understood considering the following transformation properties:

$$S^\dagger(\xi)aS(\xi) = a\cosh(r) - a^\dagger e^{-2i\phi}\sinh(r)$$
$$S^\dagger(\xi)a^\dagger S(\xi) = a^\dagger\cosh(r) - ae^{-2i\phi}\sinh(r)$$
$$S^\dagger(\xi)(X_\phi + iP_\phi)S(\xi) = X_\phi e^{-r} + iP_\phi e^{r},$$

where $X_\phi + iP_\phi = (X + iP)e^{-i\phi}$ is the rotated complex amplitude, and from the transformation relations, it is clear that the squeezing operator reduces one component of the complex amplitude and amplifies the other, by a factor $r = |\xi|$. Considering a squeezed vacuum state:

$$|\zeta\rangle = S(\zeta)\,|0\rangle\,, \tag{2.32}$$

it is possible to show that variances of the quadratures are:

$$\Delta(X_\phi^2) = e^{-r} \quad \Delta(P_\phi^2) = e^{r}, \tag{2.33}$$

showing that squeezed states have unequal uncertainties for the two orthogonal quadratures. Multiplying the two variances in (2.33), we obtain:

$$\Delta(X_\phi^2)\Delta(P_\phi^2) = 1, \tag{2.34}$$

hence, like for coherent states, squeezed vacuum states have minimum uncertainty, as the Heiseberg inequality is saturated.

2.2 The density operator

In quantum mechanics, pure states are defined as the states which can be fully described by a vector in a complex Hilbert space. In particular they can be expressed as a superposition of number states in the Fock basis. Some physical systems cannot be represented via single vectors in the Hilbert space, as they might be constituted by a statistical ensemble of different pure states, with different weights. The density operator is a mathematical tool that completely characterizes a quantum state as a statistical collection of individual pure states, in a diagonal representation, hence a collection of states together with the respective probabilities of finding them. In particular, for a pure state, the density operator corresponds to the *projection* operator on the subspace spanned by the state vector itself:

$$\rho = |\psi\rangle\,\langle\psi|\,. \tag{2.35}$$

Consider a discrete set of pure states, $|\psi_i\rangle$, the density matrix for a general mixed state is defined as:

$$\rho = \sum_i p_i |\psi_i\rangle \langle\psi_i| , \tag{2.36}$$

with p_i the probability of the system to be in the pure state $|\psi_i\rangle \langle\psi_i|$. The mean value of any operator O, in the framework of density operators, becomes:

$$\langle O\rangle = \sum_i \langle\psi_i| O |\psi_i\rangle = \mathrm{Tr}(O\rho), \tag{2.37}$$

where $\mathrm{Tr}(\cdot)$ denotes the trace operation.
The off-diagonal elements of a density matrix are related to quantum coherences and their presence into the dynamical equation of motion discriminates quantum dynamics from the classical one.

The density matrix is a Hermitian operator, with unit trace, in agreement with its statistical interpretation. The trace of the square of the density operator is also one in the case of pure states, which can be easily demonstrated by considering the fact that if $\rho = |\psi\rangle \langle\psi|$, so $\rho^2 = |\psi\rangle \langle\psi| |\psi\rangle \langle\psi| = |\psi\rangle \langle\psi| = \rho$. Following this argument, it is possible to define the *purity* of a density operator via the relation:

$$\mathrm{Tr}(\rho^2) \leq 1, \tag{2.38}$$

with the inequality saturated by pure states.

2.2.1 Dissipative processes

In this section we briefly introduce the master equation formulation for describing dissipative processes. More details will be given through the whole thesis. Consider a system A interacting with a reservoir B, living in a Hilbert space $A \otimes B$, all described by the total Hamiltonian:

$$H = H_A + H_B + H_{AB}, \tag{2.39}$$

with H_{AB} the interaction term. As we will not consider the dynamics of the reservoir, its properties are not defined specifically, but only in very general terms. If the total system is described by the density matrix ρ_T, its dynamics will be given by:

$$\dot{\rho}_T = -\frac{i}{\hbar}[H, \rho_T] + \frac{\partial}{\partial t}\rho, \tag{2.40}$$

which is the Von-Neumann equation, with H given by (2.39) and the last term $\frac{\partial}{\partial t}\rho$ is zero if the initial probability distribution is not time-dependent, as we shall assume in the following. In the interaction picture, the total density matrix reads:

$$\tilde{\rho}_T = e^{(i/\hbar)(H_A+H_B)t}\rho_T e^{-(i/\hbar)(H_A+H_B)t}, \tag{2.41}$$

hence obtaining, after some manipulation:

$$\dot{\tilde{\rho}}_T = -\frac{i}{\hbar}[\tilde{H}_{AB}(t), \tilde{\rho}_T], \tag{2.42}$$

where $\tilde{H}_{AB}(t)$ has an explicit time-dependence. Integrating we formally obtain:

$$\dot{\tilde{\rho}}_T = -\frac{i}{\hbar}[\tilde{H}_{AB}(t), \tilde{\rho}_T(0)] - \frac{1}{\hbar^2}\int_0^t dt'[\tilde{H}_{AB}(t'), [\tilde{H}_{AB}(t'), \tilde{\rho}_T(t')]]. \tag{2.43}$$

At this point, we assume that there is no correlation between the systems A and B at the initial time, hence the total density matrix initially is in the product state $\rho_T(0) = \rho(0)B_0$, with B_0 the initial density matrix of the reservoir. It is possible to eliminate the degrees of freedom of the reservoir, by performing a *partial trace*:

$$\mathrm{Tr}_B(\tilde{\rho}_T(t)) = \tilde{\rho}(t), \tag{2.44}$$

which applied on (2.43), gives the formal master equation for the system A:

$$\dot{\tilde{\rho}} = -\frac{1}{\hbar^2}\int_0^t dt' \,\mathrm{Tr}_B([\tilde{H}_{AB}(t'), [\tilde{H}_{AB}(t'), \tilde{\rho}_T(t')]]). \tag{2.45}$$

We now perform two major approximations, which will be assumed to be valid for the rest of the thesis. The first one is the *Born approximation*, which basically consists in assuming that the influence of the system on the bath is small, because

the interaction between them is weak. Hence, at time t, we can write the total density matrix as a tensor product between the density matrix of the system and of the bath:

$$\tilde{\rho}_T(t) = \tilde{\rho}(t) \bigotimes \tilde{B}(t). \tag{2.46}$$

Another important approximation we shall assume is the *Markovian approximation*, which consists in making the master equation local in time, i.e. the state of the system at a future time only depends on its present state. We realize this by replacing $\tilde{\rho}_T(t')$ with $\tilde{\rho}_T(t)$ in (2.45). Hence we end up with the *Born-Markov master equation* for the system A:

$$\dot{\tilde{\rho}} = -\frac{1}{\hbar^2} \int_0^t dt' \, \mathrm{Tr}_B([\tilde{H}_{AB}(t'), [\tilde{H}_{AB}(t'), \tilde{\rho}(t) B_0]]). \tag{2.47}$$

2.2.2 The dissipative Harmonic Oscillator

Following the arguments of the previous section, we now derive the master equation for a dissipative harmonic oscillator, which is the basis for the models used in the main part of this thesis. The starting point consists in the definition of the Hamiltonian for the system, living in a Hilbert space S, and for the reservoir, defined on a different space B, together with an interaction term between them, living in the composite Hilbert space $S \bigotimes B$. In the case of a damped harmonic oscillator we have:

$$\begin{aligned} H_S &= \hbar\omega_0 a^\dagger a \\ H_B &= \sum_j \hbar\omega_j b_j^\dagger b_j \\ H_{SB} &= \sum_j \hbar\left(k_j^* b_j^\dagger a + k_j b_j a^\dagger\right) = \hbar(aM^\dagger + a^\dagger M), \end{aligned}$$

where the ω_j are the frequencies of the oscillator used to model the reservoir and $M = \sum_j k_j^* b_j^\dagger$. The oscillator a is coupled to the j^{th} bath oscillator through a coupling constant k_j, in the rotating wave approximation, i.e. terms in a Hamiltonian which oscillate faster than the resonance frequency (as for $b_j^\dagger a^\dagger$) are neglected. After writing these quantities in the interaction picture, substituting in (2.47), and with some

algebraic manipulation, we obtain:

$$\dot{\tilde{\rho}} = -\int_0^t dt'([aa\tilde{\rho}(t') - a\tilde{\rho}(t')a]e^{-i\omega_0(t-t')}\langle\tilde{M}^\dagger(t)\tilde{M}^\dagger(t')\rangle_B + ([a^\dagger a^\dagger\tilde{\rho}(t') - a^\dagger\tilde{\rho}(t')a^\dagger]e^{i\omega_0(t-t')}\langle\tilde{M}(t)\tilde{M}(t')\rangle_B + ([aa^\dagger\tilde{\rho}(t') - a^\dagger\tilde{\rho}(t')a]e^{i\omega_0(t+t')}\langle\tilde{M}^\dagger(t)\tilde{M}(t')\rangle_B + ([a^\dagger a\tilde{\rho}(t') - a\tilde{\rho}(t')a^\dagger]e^{i\omega_0(t+t')}\langle\tilde{M}(t)\tilde{M}^\dagger(t')\rangle_B, \tag{2.48}$$

where the reservoir correlation functions $\langle\tilde{M}(t')\tilde{M}(t')\rangle_B$ are defined as:

$$\langle\tilde{M}(t')\tilde{M}(t)\rangle_B = \mathrm{Tr}_B[M_0\tilde{M}(t')\tilde{M}(t)]. \tag{2.49}$$

It is easy to check that the only non-zero correlation functions are the ones containing both $\tilde{M}(t')$ and $\tilde{M}^\dagger(t')$, which have the form:

$$\begin{aligned}\langle\tilde{M}^\dagger(t)\tilde{M}(t')\rangle_B &= \sum_j |k_j|^2 e^{-i\omega_j(t-t')}\bar{n}(\omega_j,T)\\ \langle\tilde{M}(t)\tilde{M}^\dagger(t')\rangle_B &= \sum_j |k_j|^2 e^{i\omega_j(t-t')}(\bar{n}(\omega_j,T)+1),\end{aligned} \tag{2.50}$$

where we assume a reservoir in thermal equilibrium, at temperature T, with mean number of excitations for the j-th mode given by the Bose-distribution $\bar{n}(\omega_j,T) = \frac{e^{-\hbar\omega_j/k_BT}}{1-e^{-\hbar\omega_j/k_BT}}$. It is possible and convenient to transform equations (2.50) in the continuum limit: this can be achieved by defining a function $g(\omega)$, called the *density of states*, such that $g(\omega)d\omega$ quantifies the number of oscillators having frequencies within the range ω and $\omega + d\omega$. Performing a transformation of variables in terms of the time shift $\tau = t - t'$, we obtain:

$$\begin{aligned}\dot{\tilde{\rho}} = -\int_0^t d\tau([aa^\dagger\tilde{\rho}(t-\tau) - a^\dagger\tilde{\rho}(t-\tau)a]e^{-i\omega_0\tau}\langle\tilde{M}^\dagger(t)\tilde{M}(t-\tau)\rangle_B +\\ + ([a^\dagger a\tilde{\rho}(t-\tau) - a\tilde{\rho}(t-\tau)a^\dagger]e^{i\omega_0\tau}\langle\tilde{M}(t)\tilde{M}^\dagger(t-\tau)\rangle_B,\end{aligned} \tag{2.51}$$

where now the correlations are defined as:

$$\langle\tilde{M}^\dagger(t)\tilde{M}(t-\tau)\rangle_B = \int_0^\infty d\omega g(\omega)|k(\omega)|^2\bar{n}(\omega,T)e^{i\omega\tau}, \tag{2.52}$$

$$\langle\tilde{M}(t)\tilde{M}^\dagger(t-\tau)\rangle_B = \int_0^\infty d\omega g(\omega)|k(\omega)|^2(\bar{n}(\omega,T)+1)e^{-i\omega\tau}. \tag{2.53}$$

It can be demonstrated, but here we avoid this detail, that the Markov approximation requires the reservoir correlation time $t_R = \hbar/k_B T$ to be much smaller than the system characteristic decay time t_S. If we find ourselves in this regime, it is possible to consider $\tilde{\rho}(t)$ rather than $\tilde{\rho}(t-\tau)$ in (2.51), as the integration in τ is dominated by times shorter than the evolution time scale of $\tilde{\rho}$. This condition, together with the evaluation of the frequency integrals (2.52), allows us to write down the Markovian master equation for the dissipative Harmonic Oscillator:

$$\dot{\tilde{\rho}} = -i\Delta[a^\dagger a, \tilde{\rho}] + \gamma(a\tilde{\rho}a^\dagger - \frac{1}{2}(a^\dagger a\tilde{\rho} - \tilde{\rho}a^\dagger a)) + \gamma\bar{n}(a\tilde{\rho}a^\dagger + a^\dagger\tilde{\rho}a - a^\dagger a\tilde{\rho} - \tilde{\rho}aa^\dagger), \quad (2.54)$$

with $\gamma = 2\pi g(\omega)|k(\omega)|^2$, $\bar{n} = \bar{n}(\omega, T)$ and Δ the dressed frequency coming out from the interaction with the reservoir, all derived from the frequency integrals. It may be convenient to rewrite equation (2.54), which is in the interaction picture, back into the Schrödinger picture, obtaining:

$$\dot{\rho} = -i\omega'[a^\dagger a, \rho] + \gamma(a\rho a^\dagger - \frac{1}{2}(a^\dagger a\rho - \rho a^\dagger a)) + \gamma\bar{n}(a\rho a^\dagger + a^\dagger\rho a - a^\dagger a\rho - \rho aa^\dagger), \quad (2.55)$$

with $\omega' = \omega_0 + \Delta$. Such a master equation is said to be in the Lindblad form, from the work of the eponymous scientist, who related the dissipative dynamics of quantum systems with semigroups. The master equations we shall consider in the following are all Markovian and in the Lindblad form: however there is an ongoing research interest in non-Markovian master equations that cannot be always expressed in a Lindblad form. To give a physical interpretation of (2.55), we write down the rate equations, obtained by evaluating the diagonal matrix elements of ρ, $p_n = \langle n|\,\rho\,|n\rangle$, which defines the probability for the oscillator to be found in the nth energy state:

$$\dot{p}_n = \gamma(\bar{n}+1)(n+1)p_{n+1} - \gamma\bar{n}np_n + \gamma\bar{n}np_{n-1} - \gamma\bar{n}(n+1)p_n. \quad (2.56)$$

This clearly describes the transition rates from and into the n-th energy levels. Equation (2.55) can be written formally as:

$$\dot{\rho} = \mathcal{L}\rho, \quad (2.57)$$

$\mathcal{L}$ is a superoperator, which means that it operates on operators rather than on states, and is called Liouvillian. The action of the Liouvillian superoperator on a generic operator O is defined by:

$$\mathcal{L}O = -i[H, O] + \sum_i \gamma_i (f_i O f_i^\dagger - f_i^\dagger f_i O - O f_i^\dagger f_i), \tag{2.58}$$

with f_i the *collapse operators*, which are derived from the interaction between the system and the bath. From (2.58) and (2.37) follows that the derivative of the expectation value of an operator, in a dissipative regime, is given by:

$$\langle \dot{O} \rangle = \mathrm{Tr}(\dot{O}\rho) + \mathrm{Tr}(O\dot{\rho}) = \mathrm{Tr}(O\mathcal{L}\rho) = \langle O\mathcal{L} \rangle \,, \tag{2.59}$$

which is the *action of the Liouvillian* from the left, and we have used the fact that the operator O is in the Schroedinger picture, which means that it does not depend explicitly on time.

2.3 Measure of coherence and correlations

Coherence is defined as of waves that enables stationary interference [16]. Coherent waves are waves which possess a well-defined phase relation between them. A standard way to quantify coherence in classical mechanics is by means of correlation functions: as an example, if we calculate the time correlation function for the position quadrature X of an electromagnetic wave, $\langle X(t)X(0) \rangle$, with $\langle ... \rangle$ denoting a statistical average, the result would give a constant multiplied by a $\cos(\omega t)$ factor, with ω being the frequency of the oscillation. In this sense the field has a constant self-coherence over time. Coherence functions, as introduced by Glauber and others [17], are a rigorous mathematical tool which intuitively captures the concept behind coherence, defining it in terms of correlations between the component of an electric field. These correlations can be defined and measured to any order in the fields variables, thus giving rise to the definition of different orders of coherence. One of the earliest experiment regarding coherence and the interference effects between waves is the double slit experiment [18], proposed and performed by Young, where

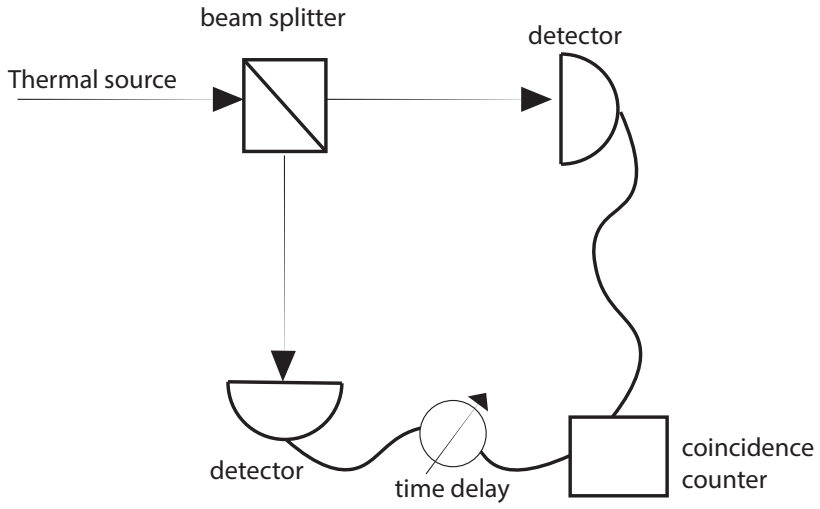

Figure 2.1: Schematic arrangement of the Hambury-Brown-Twiss experiment, used to measure intensity correlations.

the relevant quantity which is effectively measured is the first order coherence of the light beam. This quantity is defined as:

$$g^{(1)}(\boldsymbol{r}_1, t_1; \boldsymbol{r}_2, t_2) = \frac{\langle E^*(\boldsymbol{r}_1, t_1) E(\boldsymbol{r}_2, t_2)\rangle}{\sqrt{\langle E^*(\boldsymbol{r}_1, t_1) E(\boldsymbol{r}_1, t_1)\rangle}\sqrt{\langle E^*(\boldsymbol{r}_2, t_2) E(\boldsymbol{r}_2, t_2)\rangle}}, \tag{2.60}$$

with r_1, r_2 the coordinates of the slits. If we consider a single mode, and recast the time variable as $t_1 = t$, $t_2 = t + \tau$, it is possible to define the temporal first order coherence for a quantum field through:

$$G^{(1)}(t, \tau) = \langle a^\dagger(t) a(t + \tau)\rangle\,, \tag{2.61}$$

and the normalized version:

$$g^{(1)}(t, \tau) = \frac{\langle a^\dagger(t) a(t + \tau)\rangle}{\langle a^\dagger(t) a(t)\rangle}. \tag{2.62}$$

The second-order coherence, also called the intensity correlation function, has proven to be a useful tool in a variety of fields, including astronomy and nuclear physics, as from its measurements it is possible to extract the angular diameter of distant bodies [19]. The first optical experiment involving a measurement of intensity correlation was conducted by Hanbury Brown and Twiss in the 1956, to perform astronomical measurements on the star Sirius. Morgan and Mandel, inspired by the Hambury

Brown experiment, designed a detection apparatus to measure intensity correlation: a thermal light source is divided by a beam splitter in two components which are then detected by two different detectors, as showed in the scheme in Fig (2.1). With this apparatus it is possible to measure coincidences in the photon counting, i.e. counting the number of events where a photon is detected by one detector and another is detected by the other detector after τ seconds. This scheme allows to measure the joint probability of counting a photon at time t and another at time $t+\tau$: Glauber [20] was the first one to demonstrate that there is a direct correspondence between this probability and the intensity correlation function:

$$G^{(2)}(t,\tau) = \langle a^\dagger(t)a^\dagger(t+\tau)a(t+\tau)a(t)\rangle\,, \tag{2.63}$$

which normalized gives:

$$g^{(2)}(t,\tau) = \frac{\langle a^\dagger(t)a^\dagger(t+\tau)a(t+\tau)a(t)\rangle}{\langle a^\dagger(t)a(t)\rangle^2}. \tag{2.64}$$

Putting things in a different perspective, as suggested by [21], (2.64) describes the probability of photons in the light beam to group together or to be separated: if $g^{(2)}(t,\tau) = 1$, joint detection, i.e. the numerator of (2.64), and independent detection, the denominator of (2.64), coincide. This should always be the case at $\tau \to \infty$, since the memory of the first detection vanishes over time. In the case where $g^{(2)}(t,\tau) < g^{(2)}(t,0)$, as the time delay increases, the probability of detecting the second photon decreases, and this indicates that photons tend to arrive together (bunching). Finally, if $g^{(2)}(t,\tau) > g^{(2)}(t,0)$, as the time delay τ increases, the probability of counting a second photon at the detector increases, which is characteristic of photon *antibunching*. It is easy to show that for a coherent state $|\alpha\rangle$, the second order correlation function is $g^{(2)}(t,0) = 1$, while for a Fock state $|n\rangle$, it reads:

$$g^{(2)}(t,0) = 1 - \frac{1}{n}. \tag{2.65}$$

Consider now (2.64) with $\tau = 0$: we can omit the time dependence if we consider a stationary process. The expression for the second order correlation can be rewritten

as:

$$g^{(2)}(t,\tau) = \frac{\langle a^\dagger a^\dagger a a\rangle}{\langle a^\dagger a\rangle}^2 = 1 + \frac{\langle \Delta n^2\rangle - \langle n\rangle}{\langle n\rangle}^2 . \tag{2.66}$$

where we have used the fact that, from the commutation relations, $a^\dagger a^\dagger a a = n^2 - n$, and that $\langle \Delta n^2\rangle = \langle n^2\rangle - \langle n\rangle^2$. The statistics are defined to be *sub-Poissonian* if the variance of the number of photon detected is smaller than the average number of photons, hence the statistics deviates from the Poisson distribution typical of coherent states. This is a purely quantum phenomenon which has no counterpart in the classical regime. From (2.66) follows that, having a sub-Poissonian statistics is equivalent to:

$$g^{(2)}(0) < 1. \tag{2.67}$$

Sub-Poissonianity and antibunching are closely related, even though they are not exactly the same thing: a quantum field can have a sub-Poissonian statistics and yet showing bunching in the intensity correlation function.

2.4 Quasiprobability distribution

An alternative way to represent the density matrix of a given field is offered by *quasiprobability* distributions. These mathematical objects resemble classical probability distributions: they are real-valued functions wich obey a normalization condition and allow the calculation of statistical moments through an integration of c-number functions, weighted by the distribution function. However, contrary to classical probability distributions, the quasiprobability distribution may not be always positive, hence the interpretation in terms of a probability distribution is not always meaningful. Negative values of the probability distribution are allowed in quantum mechanics as they can be used to describe efficiently phenomana such as destructive interference, in term of distributions. Depending on the ordering of the operators in the average values we wish to calculate, it is possible to obtain different representation of the field. For example, normal ordering gives the Glauber quasiprobability distribution, while anti-normal ordering gives the Husimi Q-function [22]. In the following we consider the *normal ordering* (annihilation

operators to the right, creation operators to the left).

2.4.1 P-representation

The *Glauber-Sudarshan P-representation*, is based upon the non-orthogonality and overcompleteness of coherent states, hence on the fact that any density operator ρ can be written in terms of diagonal sums over a set of coherent states:

$$\rho = \int d^2\alpha \, |\alpha\rangle \langle\alpha| \, P(\alpha). \tag{2.68}$$

The function $P(\alpha)$ is a c-number which possesses some analogy with a classical probability distribution, provided that it does not show any pathological behaviour: in particular $P(\alpha)$ has a normalization condition and allows the calculation of statistical moments through the usual integral formulation, hence proving to be a very powerful computational tool. Indeed we first notice that:

$$\begin{aligned} \int d^2\alpha P(\alpha) &= \int d^2\alpha \, \langle\alpha|\alpha\rangle \, P(\alpha) \\ &= \mathrm{Tr}\Big(\int d^2\alpha \, |\alpha\rangle \langle\alpha| \, P(\alpha)\Big) = \mathrm{Tr}(\rho) = 1. \end{aligned} \tag{2.69}$$

The statistical moments can be evaluated from:

$$\begin{aligned} \langle a^{\dagger p} a^q \rangle = \quad & \mathrm{Tr}(\rho a^{\dagger p} a^q) = \mathrm{Tr}\Big(\int d^2\alpha \, |\alpha\rangle \langle\alpha| \, P(\alpha) a^{\dagger p} a^q \Big) = \\ & \int d^2\alpha \, \langle\alpha| \, P(\alpha) a^{\dagger p} a^q \, |\alpha\rangle = \int d^2\alpha P(\alpha) \alpha^{*p} \alpha^q. \end{aligned} \tag{2.70}$$

However, it suffers from a pathological behaviour for a certain class of states: if the state considered has a classical analogue, like coherent states and thermal states, the P-distribution is always non-negative. But if we consider highly quantum states or states, such as Fock states, the P-function can be negative or more singular than a Delta-function. Hence it fails to be a properly defined probability distribution. For a coherent state $\rho_c = |\alpha_0\rangle \langle\alpha_0|$, equation (2.70) gives:

$$\langle a^{\dagger p} a^q \rangle = \alpha_0^{*p} \alpha_0^q, \tag{2.71}$$

hence $P(\alpha) = \delta(\alpha - \alpha_0)$ is a delta function. It is worth noticing here that, from the overcompleteness of coherent states, the P-representation is not unique, i.e. a given state can be represented by different P distributions. For squeezed states, $P(\alpha)$ takes negative values [8], as it can be seen explicitly by calculating the variance for the quadrature X:

$$\begin{aligned}\langle \Delta X^2 \rangle &= \langle (a + a^\dagger)^2 - \langle a + a^\dagger \rangle^2 \rangle \\ &= 1 + \int d^2\alpha P(\alpha)(\alpha + \alpha^* - (\alpha + \alpha^*)^2)^2, \end{aligned} \tag{2.72}$$

which gives $\langle \Delta X^2 \rangle < 1$ only if $P(\alpha)$ is negative.

2.4.2 Q-representation

If the operators, whose expectation values we wish to calculate, are written in *anti-normal* order, a useful phase-space representation is the Q-function, or Husimi function. The definition of the Q distribution can be derived from the overcompleteness of the coherent state, and is:

$$Q(\alpha) = \frac{1}{\pi} \langle \alpha | \rho | \alpha \rangle , \tag{2.73}$$

hence $\pi Q(\alpha)$ effectively corresponds to the trace of the density matrix, evaluated on the coherent state basis spanned by $|\alpha\rangle$. In this representation, a coherent state is Gaussian in the phase-space, i.e. its Husimi function is $Q(\alpha) = \frac{1}{\pi} \exp(-|\alpha - \alpha_0|^2)$. It is clear from the definition (2.73) that the Q-function is always positive, since ρ is a positive-definite operator: hence, contrarily to the P-function, the Husimi function allows the description of squeezed states in term of a well defined, positive, distribution function. In terms of the Q-function the mean values of the quantum operators have the form:

$$\langle a^q a^{\dagger p} \rangle = \int d^2\alpha Q(\alpha) \alpha^q \alpha^{p*}. \tag{2.74}$$

We mention here that it is possible to obtain the Q-function from a suitable *Weiestrass transform* of the P-function:

$$Q(\alpha) = \frac{1}{\pi}\int P(\beta)e^{-|\alpha-\beta|^2}d^2\beta, \tag{2.75}$$

which follows from the expansion of the density matrix on the basis spanned by $|\beta\rangle$ as showed in equation (2.68).

2.4.3 Wigner function

The Wigner function, for a single mode field, is the function of the complex variable, α, defined as:

$$W(\alpha) = \frac{1}{\pi^2}\int d^2\zeta\, \mathrm{Tr}(\rho e^{\zeta a^\dagger - \zeta^* a})e^{\zeta^*\alpha - \zeta\alpha^*}, \tag{2.76}$$

where ζ is a complex number and the term:

$$C_S(\zeta) = \mathrm{Tr}(\rho e^{\zeta a^\dagger - \zeta^* a}) \tag{2.77}$$

is called the symmetric *characteristic function*, which is a function completely characterizing the density matrix and which can be used to evaluate the expectation value of the annihilation and creation operator, using the relation

$$\langle a^{\dagger p}a^q\rangle_S = \frac{\partial^{p+q}}{\partial\zeta^p\partial\zeta^{*q}}C_S(\zeta)|_{\zeta=0}. \tag{2.78}$$

Notice that it is possible to make to define a generalized characteristic function, which parametrizes the possible ordering of the operators products, to obtain all the quasi-probability distribution discussed above (**??**). The Wigner function can be used, as mentioned before, to evaluate *symmetrically ordered* products of creation and annihilation operators, which is defined as follows: the symmetrically ordered product is the average of all the different ways of ordering m creation and n annihilation operators (there are $(n+m)!/n!m!$ possible orderings), for example $(a^\dagger a)_S = \frac{1}{2}(a^\dagger a + aa^\dagger)$. From (2.78), and inverting (2.76), the average values of the

operators in terms of the Wigner function is:

$$\langle a^{\dagger p} a^q \rangle_S = \int d^2 W(\alpha) \alpha^{*p} \alpha^q. \tag{2.79}$$

The Wigner function is non singular, but it can be negative: the negativity of this quasiprobability distribution is a signature of non-classicality. Furthermore, for pure states, the Wigner distribution can be used as a tool measure the *Gaussianity* of pure states, i.e., measure if the state is Gaussian or not: if the Wigner function shows a 2D Gaussian distribution, the state can be considered as Gaussian, while any other shape gives non-Gaussian states. In particular, when the Wigner function is negative, i.e., when the state is certainly non-classical, is not possible, for any convolution over a set made entirely of Gaussian states, to reproduce the negative distribution. However, the Wigner function of a non-Gaussian state is not necessarily negative hence the non-classicality in not guaranteed by the non-Gaussianity. Indeed, as showed by [23], pure states can have non-negative Wigner function only if they are Gaussian states.

2.5 The positive P-representation

In this section we will discuss the *positive P-representation*, which is going to be one of the main theoretical tool used for the rest of the thesis. The importance of the positive P-representation is given by the computational advantages it provides. The Glauber P-representation is not always positive semidefinite, as we showed for squeezed states, hence the interpretation in terms of stochastic differential equation is not always possible, the same applies to the Wigner function, as the evolution equation for the distribution $W(\alpha)$ may contain derivatives in α of the third order or higher, hence preventing one to write it down as a Fokker-Planck equation [24]. The positive P, on the contrary, can be always positive semidefinite, thus we can represent the system's dynamics as a set of stochastic differential equations, as described in the next sections. Typically, this representation is used to address the dynamics of complex multimode systems, hence we start immediately by considering

the general multimode case, giving a definition for the generalized P-representation. A multimode quantum state of light can be defined as a M-mode coherent state $|\boldsymbol{\alpha}\rangle$, living on a Hilbert space of M bosonic modes:

$$|\boldsymbol{\alpha}\rangle = \exp\left(\sum_{n=1}^{M} \alpha_n a_n^\dagger - \frac{|\boldsymbol{\alpha}|^2}{2}\right)|0\rangle\,, \tag{2.80}$$

where $|0\rangle$ is the vacuum state. The generalized P-representations are defined as:

$$\rho = \int\int d\mu(\boldsymbol{\alpha},\boldsymbol{\beta}) P(\boldsymbol{\alpha},\boldsymbol{\beta}) \Lambda(\boldsymbol{\alpha},\boldsymbol{\beta}), \tag{2.81}$$

where $d\mu(\boldsymbol{\alpha},\boldsymbol{\beta})$ is an integration measure, the choice of which allows one to define different possible P representations. The operator $\Lambda(\boldsymbol{\alpha},\boldsymbol{\beta})$ is a projection operator on an off-diagonal pair of coherent states:

$$\Lambda(\boldsymbol{\alpha},\boldsymbol{\beta}) = \frac{|\boldsymbol{\alpha}\rangle\langle\boldsymbol{\beta}^*|}{\langle\boldsymbol{\beta}^*|\boldsymbol{\alpha}\rangle}, \tag{2.82}$$

with $\mathrm{Tr}(\Lambda(\boldsymbol{\alpha},\boldsymbol{\beta})) = 1$, from the cyclic properties of the trace. We can derive from (2.81) the Glauber P-representation. This can be done by choosing the integration measure as:

$$d\mu(\boldsymbol{\alpha},\boldsymbol{\beta}) = \delta^{2M}(\boldsymbol{\alpha}-\boldsymbol{\beta}) d^{2M}\alpha\, d^{2M}\beta, \tag{2.83}$$

which gives immediately, inserting it into (2.81):

$$\rho = \int d^{2M}\alpha P(\boldsymbol{\alpha})\,|\boldsymbol{\alpha}\rangle\langle\boldsymbol{\alpha}|\,. \tag{2.84}$$

Different integration measures lead to other types of generalized P-representation. The *positive-P-representation* is defined by choosing the integration measure as a volume measure in the phase space, with the standard doubling of the basis:

$$d\mu(\boldsymbol{\alpha},\boldsymbol{\beta}) = d^{2M}\boldsymbol{\alpha}\, d^{2M}\boldsymbol{\beta}. \tag{2.85}$$

This gives the following expression for the density operator:

$$\rho = \int\int d^{2M}\boldsymbol{\alpha}\, d^{2M}\boldsymbol{\beta} P(\boldsymbol{\alpha},\boldsymbol{\beta}) \Lambda(\boldsymbol{\alpha},\boldsymbol{\beta}). \tag{2.86}$$

The modes described by $\boldsymbol{\alpha}$ and $\boldsymbol{\beta}$ correspond to every possible mode of excitation of the system, whether they are photon field or the damping reservoirs. It has been demonstrated that is always possible to obtain an explicitly non-singular, positive-definite distribution of this type, given by:

$$P(\boldsymbol{\alpha},\boldsymbol{\beta}) = \frac{1}{(4\pi^2)^M} e^{-\frac{1}{4}|\boldsymbol{\alpha}-\boldsymbol{\beta}^*|^2} \langle \frac{\boldsymbol{\alpha}+\boldsymbol{\beta}^*}{2} | \rho | \frac{\boldsymbol{\alpha}+\boldsymbol{\beta}^*}{2} \rangle , \tag{2.87}$$

which is clearly positive, although not unique. The Positive-P, like other representation examined above, allows us to build a correspondence between the normally ordered operator products and the moments of the distribution, hence allowing us to calculate the expectation value of quantum operators. Suppose now that $O_N(\boldsymbol{a},\boldsymbol{a}^\dagger)$ is an operator function of the multimode annihilation and creation operators, expressed in normally ordered form, so that:

$$O_N(\boldsymbol{a},\boldsymbol{a}^\dagger) = \sum_{\boldsymbol{n},\boldsymbol{m}} c_{\boldsymbol{n},\boldsymbol{m}} \prod_{j=1}^{M} (a_j^\dagger)^{m_j} \prod_{j=1}^{M} a_j^{m_j} . \tag{2.88}$$

The expectation value of O_N is given by:

$$\begin{aligned} \langle O_N(\boldsymbol{a},\boldsymbol{a}^\dagger)\rangle &= \mathrm{Tr}(O_N(\boldsymbol{a},\boldsymbol{a}^\dagger)\rho) \\ &= \int\int d^{2M}\boldsymbol{\alpha}\, d^{2M}\boldsymbol{\beta}\, P(\boldsymbol{\alpha},\boldsymbol{\beta})\, \mathrm{Tr}\Big(\sum_{\boldsymbol{n},\boldsymbol{m}} c_{\boldsymbol{n},\boldsymbol{m}} \prod_{j=1}^{M} (\alpha_j)^{m_j}\Big) \frac{|\boldsymbol{\alpha}\rangle\langle\boldsymbol{\beta}^*|}{\langle\boldsymbol{\beta}^*|\boldsymbol{\alpha}\rangle} \prod_{j=1}^{M} \beta_j^{m_j}\Big) \\ &= \int\int d^{2M}\boldsymbol{\alpha}\, d^{2M}\boldsymbol{\beta}\, P(\boldsymbol{\alpha},\boldsymbol{\beta})\Big(\sum_{\boldsymbol{n},\boldsymbol{m}} c_{\boldsymbol{n},\boldsymbol{m}} \prod_{j=1}^{M} (\alpha_j)^{m_j}\Big) \prod_{j=1}^{M} \beta_j^{m_j}\Big), \end{aligned} \tag{2.89}$$

and here we used the eigenvalue property of the coherent states together with the fact that the trace of a coherent state projection operator is one. We can express a quantum expectation value in terms of c-number quantities: a probability distribution which is related to the density matrix and complex functions for the considered operator.

As we will clarify in the following, it is possible to estimate the expectation variable of a given operator by sampling the distribution $P(\boldsymbol{\alpha},\boldsymbol{\beta})$, using stochastic trajectory

from a sample space s:

$$\bar{O}_N = \langle \mathrm{Re}(\mathrm{Tr}(O_N\Lambda)\rangle_{\mathrm{stoch}} + \langle \mathrm{Re}(\mathrm{Tr}(O_N\Lambda^\dagger)\rangle_{\mathrm{stoch}}\,, \tag{2.90}$$

where we indicate the average over a sample of stochastic trajectories as $\langle . \rangle_{stoch}$ and the correspondence between the above quantities and the exact expectation value holds in the limit:

$$\lim_{s\to\infty} \bar{O}_N = \langle O \rangle_N\,. \tag{2.91}$$

2.5.1 Quantum dynamics and operator identities

The temporal dynamics of a quantum system can be calculated using the Positive P-representation, by applying differential operators correspondence rules to the density matrix of the system. This procedure gives an evolution equation for the Positive-P distribution: in this case, as the equation contains at most derivatives of the second order in the field variables, the evolution equation is equivalent to a Fokker-Planck equation, originally derived for the description of Brownian motion [25]. The Fokker-Planck is not easy to solve analytically or numerically, in most practical cases: however it possible to transform it, as we shall see in more details in the next sections, into the stochastic formulation of a diffusion process, which resolves the Fokker-Planck as an ensemble average over a set of stochastic trajectories.

We can rewrite (2.82) more explicitly, using the definition of a coherent state as a displaced vacuum state:

$$\Lambda(\boldsymbol{\alpha},\boldsymbol{\beta}) = e^{(\boldsymbol{a}^\dagger - \boldsymbol{\beta})\cdot\boldsymbol{\alpha}}\,|\mathbf{0}\rangle\,\langle\mathbf{0}|\,e^{\boldsymbol{a}\cdot\boldsymbol{\beta}}, \tag{2.92}$$

where we used the fact that $\langle \boldsymbol{\beta}^*\boldsymbol{\alpha}\rangle = \exp(-\frac{1}{2}(|\boldsymbol{\alpha}| + |\boldsymbol{\beta}|) + \boldsymbol{\beta}\cdot\boldsymbol{\alpha})$. Differentiating (2.92) with respect to α_n, we get the following result:

$$\partial_{\alpha_n}\Lambda(\boldsymbol{\alpha},\boldsymbol{\beta}) = [a_n^\dagger - \beta_n]\Lambda(\boldsymbol{\alpha},\boldsymbol{\beta}). \tag{2.93}$$

Combining eq. (2.93) and the relative conjugate equation with the eigenvalues for

coherent states, we obtain the identities:

$$\begin{aligned} a_n^\dagger \Lambda &= [\partial_{\alpha_n} + \beta_n]\Lambda \\ a_n \Lambda &= \alpha_n \Lambda \\ \Lambda a_n &= [\partial_{\beta_n} + \alpha_n]\Lambda \\ \Lambda a_n^\dagger &= \beta_n \Lambda. \end{aligned} \tag{2.94}$$

Let us consider a typical master equation, describing the quantum dynamics of a system. We have now, in the framework of the Positive-P:

$$\partial_t \rho = -i[H, \rho] = \int \int d^{2M}(\boldsymbol{\alpha}) d^{2M}(\boldsymbol{\beta}) P(\boldsymbol{\alpha}, \boldsymbol{\beta}) [H, \Lambda(\boldsymbol{\alpha}, \boldsymbol{\beta})]. \tag{2.95}$$

As an example, consider an Hamiltonian $H = a^\dagger a$. Then from the identities (2.94) it can be derived:

$$\begin{aligned} \partial_t \rho &= -i[a^\dagger a, \rho] = -i \int \int d^2(\boldsymbol{\alpha} d^2(\boldsymbol{\beta}) P(\boldsymbol{\alpha}, \boldsymbol{\beta}) [a^\dagger a, \Lambda(\boldsymbol{\alpha}, \boldsymbol{\beta})] \\ &= -i \int \int d^2(\boldsymbol{\alpha} d^2(\boldsymbol{\beta}) P(\boldsymbol{\alpha}, \boldsymbol{\beta}) (\partial_\alpha \alpha - \partial_\beta \beta) \Lambda(\boldsymbol{\alpha}, \boldsymbol{\beta}). \end{aligned}$$

From the definition (2.86), follows that the maser equation, in general, can be rewritten as:

$$\partial_t \rho = \partial_t \int \int d^{2M}(\boldsymbol{\alpha}) d^{2M}(\boldsymbol{\beta}) P(\boldsymbol{\alpha}, \boldsymbol{\beta}) \Lambda(\boldsymbol{\alpha}, \boldsymbol{\beta}) = \int \int d^{2M}(\boldsymbol{\alpha}) d^{2M}(\boldsymbol{\beta}) \partial_t P(\boldsymbol{\alpha}, \boldsymbol{\beta}) \Lambda(\boldsymbol{\alpha}, \boldsymbol{\beta}), \tag{2.96}$$

which, combining the two relations, leads to the equation of motion for the probability distribution, as shown in [26]:

$$\partial_t P(\boldsymbol{\alpha}, \boldsymbol{\beta}) = i(\partial_\alpha \alpha - \partial_\beta \beta) P(\boldsymbol{\alpha}, \boldsymbol{\beta}). \tag{2.97}$$

This is a general result for the harmonic oscillator: the motion in phase space for this type of quadratic Hamiltonian is exactly the same as the corresponding classical trajectory, regardless of the operator ordering of the representation.

2.5.2 The Fokker-Planck equation

We now want to give a more detailed definition and description of the Fokker-Planck equation. As showed in the previous section, equation (2.97) describes the time evolution of the P-distribution, and it basically represents a Fokker-Planck equation with no diffusion term.
In general, the Fokker-Planck equation indeed describes the evolution of the quasi-probability distribution function. It is usually presented in the form:

$$\partial_t P(\boldsymbol{\alpha}, t) = [\partial_{\alpha_\mu} A_\mu(\boldsymbol{\alpha}) + \frac{1}{2}\partial^2_{\alpha_\mu \alpha_\nu} D_{\mu\nu}(\boldsymbol{\alpha})]P(\boldsymbol{\alpha}, t), \tag{2.98}$$

where $A_\mu(\boldsymbol{\alpha})$ are drift terms, $D_{\mu\nu}(\boldsymbol{\alpha})$ are elements of the diffusion matrix and summation over repeated indices is assumed. The D matrix contains all the terms proportional to the second derivatives in the phase space variables $(\boldsymbol{\alpha}, \boldsymbol{\beta})$, arising after the application of the operator identities. As we mentioned, the Wigner function contains third order derivatives, hence undermining any formulations in terms of FPE: however, the third order derivatives are significant when the effects of quantum noise are large, which typically is the case when the mean number of particles is small. Hence it is sometimes possible to truncate the evolution equation for the Wigner function by neglecting the high order derivatives, thus recovering the Fokker Planck formulation [27].

Our aim is to make use of the stochastic formulation of the diffusion process, which allows us to transform a Fokker-Planck equation into an ensemble average over a set of trajectories. To interpret the Fokker-Planck equation as a set of stochastic differential equations, the D matrix needs to be semipositive definite, i.e., all real eigenvalues are non-negative, as shown in [28]. For example, the Q-distribution can show both non-positive diffusion terms and higher-than-third derivatives in the Fokker-Planck equation, hence the Q function also cannot always be interpreted in terms of stochastic evolution. To better understand the meaning of the Fokker-Planck equation and of the A and D matrices, we follow the apporoach of [9] and

consider the random variable y of a one-dimensional process. Its mean value and variance are defined as:

$$\langle y(t)\rangle = \int dyyP(y,t) \tag{2.99}$$

$$\langle \Delta y^2(t)\rangle = \int dy(y-\langle y\rangle)^2 P(y,t), \tag{2.100}$$

and consider the equation of motion for them, derived from equation (2.98),

$$\langle \dot{y}(t)\rangle = \int dyy\partial_t P(y,t) = -\int dyy\partial_y A(y)P(y,t) + \frac{1}{2}\int dyy\partial_y^2 D(y)P(y,t). \tag{2.101}$$

Integrating the above relation by part and assuming that the distribution goes fast to zero at infinity (as required for every phase-space method), we obtain:

$$\langle \dot{y}(t)\rangle = \langle A(y)\rangle . \tag{2.102}$$

Similarly, it can be shown that for the variance:

$$\langle \dot{\Delta y^2}(t)\rangle = 2\langle yA(y)\rangle - 2\langle y\rangle\langle A(y)\rangle + \langle D(y)\rangle . \tag{2.103}$$

The dynamics of the average value (2.102), is defined by A, which is called the drift term because it generates a drift of the distribution in phase-space, i.e. the mean of the distribution function shifts according to the evolution of the mean. Similarly, D acts as a source of fluctuation, as it is responsible for the dynamical change of the variance, in the most simple case (a linear Fokker-Planck equation) broadening or sharpening the distribution itself.

2.5.3 Stochastic processes

It is possible to demonstrate rigorously that the solution of a Fokker-Planck equation is equivalent to the statistical average on a set of stochastic trajectories, when the sampling space goes to infinity [29]. The same result holds in the other direction: given a Markov random process, described by a set of stochastic differential equations, it is possible to derive the associated Fokker-Planck equation for the probability distribution [30]. This equivalence is well-posed only if the diffusion matrix

D, written with real entries corresponding to the real and imaginary part of α_i, β_i, being these the components of a $4M$-dimensional vector $\boldsymbol{\alpha} \to (\alpha_1, ..., \alpha_M, \beta_1, ..., \beta_M)$, is *positive semidefinite*, i.e. all its eigenvalues have non-negative real parts. In this the case, the diffusion matrix $D(\boldsymbol{\alpha})$ can always be factorized in the non-unique form:

$$D(\boldsymbol{\alpha}) = B(\boldsymbol{\alpha})B^T(\boldsymbol{\alpha}) \tag{2.104}$$

and the stochastic differential equations (SDE) for the α_i, β_i, equivalent to the Fokker-Planck equation, are:

$$d\alpha_i = A_i(\boldsymbol{\alpha}, t)dt + \sum_{ij} B_{ij}(\boldsymbol{\alpha}, t)dW_j(t), \tag{2.105}$$

with A_i and B_{ij} being elements of the drift matrix and of the square root of the diffusion matrix, respectively. A detailed proof of the equivalence between equation (2.105) and a Fokker-Planck equation can be found in [31]. The noise terms $dW_j(t)$ are Weiner increments, defined in terms of the Weiner process $W(t)$ [28], satisfying at each t:

$$\langle dW_i(t)dW_j(t')\rangle = \delta_{ij}\delta(t-t')dt.$$
$$\langle dW_i(t)\rangle = 0.$$

Equation (2.105) can be equivalently put in a compact notation as follows:

$$\frac{d\boldsymbol{\alpha}(t)}{dt} = A(\boldsymbol{\alpha}, t) + B(\boldsymbol{\alpha}, t)\xi(t), \tag{2.106}$$

where $\xi(t)$ is a vector made of real, independent Gaussian white noise terms with zero mean and the following non-zero correlations:

$$\langle \xi_i(t)\xi_j(t')\rangle = \delta_{ij}\delta(t-t'), \tag{2.107}$$

such that $\xi_i(t) = \frac{d}{dt}W_i(t)$. The above stochastic differential equation can be written down in the so called Ito or Stratonovich form. Without going in the details of those two stochastic rules, it is worth to mention that only in the Stratonovich form the integration rules are the same of ordinary calculus. The Ito form has advantages

arising from the fact that, in this form, the stochastic increments are independent of the integration variables. However the rule of the differential calculus are different from the ordinary ones. For example the usual chain rule of the standard calculus, in the Ito calculus is modified as follows:

$$dh(\boldsymbol{y}) = \sum_j \partial_{y_i} h(\boldsymbol{y}) dy_j + \frac{dt}{2} \sum_{j,i} \frac{\partial^2}{\partial y_j \partial y_i} h(\boldsymbol{y}) D_{j,i}(\boldsymbol{y}), \tag{2.108}$$

which shows a dependence on the diffusion matrix.

In the following, unless otherwise specified, we are going to use SDE in the Ito formulation: in this way, considering (2.105), the random variables $d\alpha_i$ are made independent of the same-time Weiner increments $dW_i(t)$, which is not the case in the Stratonovich formulation. For the small time intervals Δt, the stochastic increments $dW_i(t)$ are usually implemented by real Gaussian noise, independent for each i and each time step, having mean zero, and variance Δt. To give a simple example, if we follow the example of the harmonic oscillator in (2.97), we notice that there is no diffusion term, which means that, in the stochastic formulation, there is no noise there appearing, so every $B_{ij}(\boldsymbol{\alpha}, t) = 0$. The equation of motion for the harmonic oscillator in the positive P-representation is then:

$$\frac{d\boldsymbol{\alpha}}{dt} = -i\omega\boldsymbol{\alpha}, \tag{2.109}$$

that is the expected solution for an oscillatory motion, which in phase space gives a circular path around the origin, so that the initial coherent state, stays coherent with a rotated amplitude $\boldsymbol{\alpha}(t) = \boldsymbol{\alpha}(0)e^{-i\omega t}$. Among all the representation, it is only the positive-P that can generally be used in a stochastic form for nonlinear quantum systems: the diffusion matrix, in fact, can always be obtained in a positive semidefinite form in this representation, due to the additional degrees of freedom arising from the doubling of the phase space, to guarantee the positivity. However, the corresponding stochastic equations in the doubled-dimensions, in some cases, show numerical instabilities. This is particularly true when we consider systems with low damping rate and large non-linearity: in this case the dynamics can lead

to distribution tails that vanish only as fast as a power law, which means that some boundary terms cannot be neglected, when dealing with the solution of the Fokker-Planck equation. Hence sampling error become large and systematic errors occur due to the neglected boundary terms.

2.5.4 The gauge P-representation

In the previous section we showed that the positive P-representation always gives a Fokker-Planck equation for the probability distribution $P(\alpha, \beta)$, with positive semidefinite diffusion: this property allows us to solve the dynamical problem considered in term of a well-defined stochastic process. However, the doubling of the phase-space variables can give rise to numerical instabilities in the solution of the stochastic differential equations. In order to avoid these problems, we now introduce a new type of representation, named gauge P-representation, described for the first time by Drummond [32].

Compared to the standard positive P-representation, the gauge P-representation presents a modified time evolution, obtained via the introduction of an additional complex field, Ω, in the expansion of the density matrix of the system. The additional degree of freedom come from the non-orthogonal nature of the coherent state basis: in fact any non-orthogonal basis set possesses an implicit global phase freedom for the expansion of a given state. The gauge field leaves the statistical moments unaffected, while it is able to stabilise the stochastic simulations and to minimise the systematic errors in the sampling. These computational advantages can be achieved by effectively modifying both the drift terms (*drift gauges*) and the diffusion terms (*diffusion gauges*) in the Fokker-Planck equation: the original probability distribution, and its associated statistical moments, are then recovered by evaluating the time evolution of the field Ω, which absorbs the quantum phase factor, as we shall see in the following.

The gauge representation is based on the possibility of expanding any density

matrix ρ on the un-normalized basis $\Lambda(\vec{\alpha})$, with $\vec{\alpha} = (\boldsymbol{\alpha}, \boldsymbol{\beta}, \Omega)$, and

$$\Lambda(\vec{\alpha}) = \Omega \frac{|\boldsymbol{\alpha}\rangle \langle \boldsymbol{\beta}|}{\langle \boldsymbol{\beta}|\boldsymbol{\alpha}\rangle}, \tag{2.110}$$

where the Ω is the additional gauge field mentioned above. We define the gauge representation $G(\boldsymbol{\alpha}, \boldsymbol{\beta}, \Omega)$ as a real and positive function, satisfying:

$$\rho = \int \int d^{2M}(\boldsymbol{\alpha})\, d^{2M}(\boldsymbol{\beta})\, d\Omega\, G(\boldsymbol{\alpha}, \boldsymbol{\beta}, \Omega) \Lambda(\boldsymbol{\alpha}, \boldsymbol{\beta}, \Omega), \tag{2.111}$$

together with the normalization condition:

$$\mathrm{Tr}(\Lambda(\boldsymbol{\alpha}, \boldsymbol{\beta}, \Omega)) = \Omega. \tag{2.112}$$

For the gauge representation, the identities (2.94) are still valid, together with the additional one coming from the Ω variable:

$$\partial_\Omega \Lambda = \frac{1}{\Omega} \Lambda. \tag{2.113}$$

The observables are calculated in the same way as with the positive P-representation: it is sufficient to know how to evaluate the expectation of creation and annihilation operators in terms of the representation as in (2.89), as the operators whose averages corresponds to the statistical moments, can always be expressed as a combination of powers of a and $a^\dagger$. In terms of sampling trajectories, the main difference here is that we need to include the variable Ω and normalize the result accordingly (this follows from the fact that for a gauge representation the trace of Λ is not unity). In the limit of infinite trajectories:

$$\langle a^{\dagger p} a^q \rangle = \frac{\langle \boldsymbol{\beta}^p \boldsymbol{\alpha}^q \Omega \rangle_{\mathrm{stoch}} + \langle \boldsymbol{\beta}^q \boldsymbol{\alpha}^p \Omega^* \rangle_{\mathrm{stoch}}}{\langle \Omega + \Omega^* \rangle_{\mathrm{stoch}}}. \tag{2.114}$$

In analogy to what we showed in the previous sections, it is possible to derive a for the gauge representation:

$$\partial_t G(\boldsymbol{\alpha}, \boldsymbol{\beta}, \Omega, t) = [\partial_{\alpha_\mu} A_\mu(\boldsymbol{\alpha}, \boldsymbol{\beta}, \Omega) + \frac{1}{2} \partial^2_{\alpha_\mu \alpha_\nu} D_{\mu\nu}(\boldsymbol{\alpha}, \boldsymbol{\beta}, \Omega)] G(\boldsymbol{\alpha}, \boldsymbol{\beta}, \boldsymbol{\Omega}, t), \tag{2.115}$$

from which is clear that is possible to have different kind of gauge, applying to the drift and diffusion terms individually or simultaneously. The diffusion gauge freedom is a direct consequence of the non-unique decomposition of the diffusion matrix . In fact, given a suitable decomposition of D of the form:

$$D = BB^T, \tag{2.116}$$

it is easy to show that any matrix defined as $B' = BO$, where O is an orthogonal matrix ($O^T O = \mathbb{1}$), will give:

$$B'B'^T = BOO^T B^T = BB^T = D, \tag{2.117}$$

hence leaving unchanged the diffusion matrix. The diffusion gauges allow to control error in the sampling but they fail to eliminate singularities in the drift equations: for this specific purpose is necessary to implement another kind stochastic gauge which act on the drift part of the equations and, potentially, is able to stabilize the results removing pathological behaviours. Without too many details, which will be given for the specific system of interest in the next Chapters, it is possible to demonstrate that the SDE with such a drift and diffusion gauge terms has the general Ito form:

$$\begin{aligned} &\frac{d\boldsymbol{\alpha}(t)}{dt} = A(\boldsymbol{\alpha}, t) + B'(\boldsymbol{\alpha}, t)(\xi(t) - g(\boldsymbol{\alpha})) \\ &\partial_t \Omega = \Omega g(\boldsymbol{\alpha}) \cdot \xi(t) \end{aligned} \tag{2.118}$$

where $B' = BO$ with $O = e^G$ being an arbitrary orthogonal matrix, which represents the diffusion gauge, while $g(\boldsymbol{\alpha})$ is the drift gauge function, which acts on the elements of the drift matrix $A(\boldsymbol{\alpha}, t)$, as it does not depends on the white noise term $\xi(t)$. The above system of equations gives the dynamics of the field c-number variables and of the gauge term, which needs to be tracked to evaluate properly the average values of the operators (2.114). If the coherent states become highly non-classical during the dynamics in the phase space, the presence of the guage terms are able to stabilize their stochastic evolution. In this sense this strategy turns the overcompleteness of coherent states into a computational resource, helpful in reducing sampling errors

and eliminating singular trajectories.

2.5.5 Numerical methods for SDE

Equation (2.118) is a typical system of stochastic differential equations, which can be written in a general form:

$$dX_t = \mu(X_t, t)dt + \sigma(X_t, t)dW \tag{2.119}$$

where X_t is a random variable and dW is a Wiener process. Equation (2.119) can be equivalently expressed in the integral form:

$$X_{t+s} - X_t = \int_t^{t+s} \mu(X_u, u)du + \int_t^{t+s} \sigma(X_u, u)dW_u \tag{2.120}$$

To properly find the numerical solution of equation (2.119) we need to consider some approximation scheme: there are huge amount of algorithms availabe. Here we are going to consider briefly some of the easiest to implement. Details can be found in [33].

Consider a time interval $[t_0, t_{\text{fin}}]$ and assign to it a grid of points:

$$t_0 < t_1 < ... < t_{\text{fin}},$$

to which we will assign approximate values of the random variable X:

$$w_0 < w_1 < ... < w_{\text{fin}}.$$

The *Euler-Maruyama* approximation of X_t, with $w_0 = X(t = t_0)$, is

$$w_{i+1} = w_i + \mu(w_i)\Delta t_{i+1} + \sigma(w_i)\Delta W_{i+1} \tag{2.121}$$

with $\Delta t_{i+1} = t_{i+1} - t_i$, the equidistant time steps, and $\Delta W_{i+1} = W_{t_{i+1}} - W_{t_i}$ are the Wiener increments, i.e. Gaussian random variables with mean zero and variance Δt:

$$\Delta W_i \approx N(0, \Delta t). \tag{2.122}$$

It is clear that the set of $(w_0 ... w_{\text{fin}})$, produced by this method would be an approximate solution of the stochastic process $X(t)$.

The approximation is said to converge strongly to X_T, at time T, if the following condition holds:

$$\lim_{\Delta t \to 0} \mathbb{E}(|X_T - w_{\Delta t}(T)|) = 0 \tag{2.123}$$

where $\mathbb{E}(\cdot)$ is the ensemble average over a set of realizations of the stochastic process, and $w_{\Delta t}$ is the approximate solution calculated making use of a fixed time step Δt. The approximation is said to *converges strongly* with order γ if:

$$\forall\, \Delta t,\ \exists\, C \in \mathbb{R} :\ \mathbb{E}(|X_T - w_{\Delta t}(T)|) \leq C|\Delta t|^{\gamma}. \tag{2.124}$$

In particular, it can be demonstrated that the Euler-Maruyama scheme converges strongly with order $\gamma = \frac{1}{2}$ to the real solution. An improvement on the order of convergence can be achieved through the implementation of another numerical approximation, the *Millestein method*, which is implemented in the following chapters for the numerical simulations, unless otherwise specified. The Millestein method can be derived from a stochastic Taylor series expansion and the order of convergence of scheme is $\gamma = \frac{3}{2}$. The Millestein approximation of the evolution equation for X_t is:

$$w_{i+1} = w_i + \mu(w_i)\Delta t_i + \sigma(w_i)\Delta W_i + \frac{1}{2}\sigma(w_i)\sigma'(w_i)(\Delta W_i^2 - \Delta t_i) \tag{2.125}$$

where $\sigma'(w_i)$ is the derivative of σ evaluated at w_i. The application of the Euler-Maruyama methods or of the Millestein method, with decreasing steps, gives an increasingly good approximation.

2.6 Quantum jumps approach

When the population of the system under investigation is not excessively large, or the system itself is not composed by many subsystems, it is convenient to address its dynamics by the so-called *Quantum jumps approach*, first introduced by Carmichael in [34].

The incoherent dynamics of a quantum state, described by the master equation in the Born-Markov approximation:

$$\partial_t \rho = -i[H, \rho] + \sum_j \gamma_j (f_j \rho f_j^\dagger - f_j^\dagger f_j \rho - \rho f_j^\dagger f_j), \tag{2.126}$$

can be equivalently described via a stochastic evolution of a given initial pure state $|\Psi(0)\rangle$, generated by the effect of the *collapse operators*, f_j, and by the non-Hermitian Hamiltonian:

$$H_{eff} = H - \frac{i}{2} \sum_j \gamma_j f_j^\dagger f_j. \tag{2.127}$$

If the time step is kept sufficiently small, then the state at time t, $|\Psi(t)\rangle$, evolves according to:

$$|\Psi(t + dt)\rangle = (1 - H_{eff} dt) |\Psi(t)\rangle, \tag{2.128}$$

which is un-normalized, as the Hamiltonian is not Hermitian, hence:

$$\langle \Psi(t + dt) | \Psi(t + dt) \rangle = (1 - \delta p), \tag{2.129}$$

with $\delta p = \sum_j \delta p_j$ and $\delta p_j = \gamma_j dt \, \langle \Psi(t + dt) | f_j^\dagger f_j | \Psi(t + dt) \rangle$. The effects of the collapse operator on $|\Psi(t)\rangle$ is a jump, which happens with probability δp_j: the jump can be associated with the detection of a particular event, for the spontaneous emission of photons or the change in the spin of a quantum dot. If the jump is registered, the wavefunction jumps into an normalised state which is defined by a projection via the collapse operator:

$$|\Psi(t + dt)\rangle = \frac{f_j |\Psi(t)\rangle}{(\langle \Psi(t)| f_j^\dagger f_j |\Psi(t)\rangle)^{1/2}}. \tag{2.130}$$

On the contrary, if no events is detected with probability $1 - \sum_j \delta p_j$, the states evolve under the action of H_{eff} only, as showed above, resulting in the normalized state:

$$|\Psi(t + dt)\rangle = \frac{(1 - H_{eff} dt) |\Psi(t)\rangle}{(1 - \sum_j \delta p_j)^2}. \tag{2.131}$$

The facts that the jump occurs with a certain probability, makes the evolution of the state intrinsically stochastic.

The density operator $\rho(t)$ which describes the system, is then recovered by grouping together the states obtained via different realization of the stochastic evolution.

In particular we make use of *QuTip* [35], a Python package for the simulation of open quantum systems, which has an embedded library for the evaluation of the quantum trajectories of a given system, defined via the Hamiltonian and the collapse operators.

Chapter 3

Polariton physics

In this chapter we introduce the main system investigated during the research work: microcavity polaritons. Polaritons are often described as "half-light half-matter" systems, as they arise from the strong coupling between an exciton in a semicondutor structure and a photon. They have attracted a lot of interest in recent years as they constitute a platform to study a rich variety of physical phenomena: non-linear optics, Bose-Einstein condensation [36], topological photonics [37] and the quantum properties of driven-dissipative systems. Here we focus mainly on the latter field, even though, as it will be clear in the following, part of the research was devoted to the investigation of semi-classical properties of polaritons. The structure where it is possible to obtain polariton and hence investigate their physical properties are semiconductor *microcavities*: microcavities are semiconductor-based structures that allow to efficiently confine the light and the electronic excitations of a given material in a small volume, ultimately leading to strong interaction between them. We first focus on the specific case of excitons and photons in a microcavity, and then we derive the polariton Hamiltonian, considering the mean field equation which describes their dynamics. Finally, including the polarization degree of freedom and the spin-orbit coupling arising from TE-TM splitting (due to the confinement), allows us to describe the control of the polariton state through a Stark-pulse. This result was published in *Physical Review B* [2].

3.1 Polariton Hamiltonian model

Microcavities are semiconductor devices that trap the light and control the coupling with the material inside. Their basic building blocks are a structures where the excitons occur and a cavity for trapping light: the structure we consider here consists of a number of semiconductor quantum wells embedded in a cavity made by distributed Bragg reflectors (DBRs), with alternating layers of low and high refractive index, each of them having thickness of $\lambda/4$, where λ is the centre wavelength of reflection. Interference effects created by successive reflections creates the *stop band*, which is a region of the spectrum with high reflectivity ($\approx 99\%$) : in this way light is trapped in standing waves. The two dimensional quantum wells, where the excitons are formed, are placed at the antinodes of the cavity such that the resonance frequency of the cavity match with the frequency of the exciton.

3.1.1 Excitons

Excitons are defined as bound states arising from the Coulomb interaction between electrons in the conduction band and holes in the valence band. They are the lowest energy excited state in a semiconductor. The Hamiltonian describing the electron-hole interaction, with certain assumptions about the form of the band structure, has a similar structure to the hydrogen atom:

$$H_{e-h} = \frac{\boldsymbol{P}^2}{2M} + \frac{\boldsymbol{p}^2}{2\mu} - \frac{e^2}{4\pi\epsilon_0\epsilon_r|\boldsymbol{r'}|}, \tag{3.1}$$

where the first term on the right and side is the total kinetic term, while the second term is the kinetic term in the reduced mass frame. In equation (3.1) M is the total mass, μ the reduced mass $(\frac{m_e m_h}{m_e+m_h})$, $\boldsymbol{r'} = r_e - r_h$ and the presence of all the surrounding charges is taken into account via the dielectric constant ϵ_r. This model described the so-called *Wannier excitons*. The existence of bound states, i.e. excitons, is due to the Coulomb potential in the Hamiltonian (3.1): the energy dispersion of a semiconductor exciton is given by the binding energy E_b, together with the standard

kinetic term,

$$E_{ex}(\boldsymbol{k}) = E_b + \frac{\hbar^2 \boldsymbol{k}^2}{2M}, \tag{3.2}$$

where $\boldsymbol{k} = k_e + k_h$ is the centre-of-mass momentum and the binding energy is given by:

$$E_b = -\frac{\hbar^2}{2\mu a_0^2 n^2}, \tag{3.3}$$

where a_0 is the Bohr radius. Since excitons are bound states between two fermions, they can be approximately described as bosons. In fact, it is possible to define the creation operator $b_k^\dagger$, in terms of the electron-hole creation operators, $c_{k_e}^\dagger, d_{k_h}^\dagger$:

$$b_k^\dagger = \sum_{k_e k_h} \langle k_e, k_h | b_k \rangle \, c_{k_e}^\dagger d_{k_h}^\dagger, \tag{3.4}$$

where $\langle k_e, k_h | b_k \rangle$ is the unbounded electron-hole state vector:

$$\langle k_e, k_h | b_k \rangle = \delta_{k_e + k_h, \boldsymbol{k}} \langle \alpha_h k_e - \alpha_e k_h | \phi_n \rangle, \tag{3.5}$$

and $|\phi_n\rangle$ is such that $\langle \boldsymbol{r} | \phi_n \rangle = \int \delta_{\boldsymbol{r},\boldsymbol{r}'} \phi_n(\boldsymbol{r}') d\boldsymbol{r}'$, i.e., the state vector associated with the internal structure of the exciton. It can be demonstrated, as showed in [38], that the operators defined in (3.4), at low exciton densities, obey the standard bosonic commutation relations:

$$[b_k, b_{k'}^\dagger] = \delta_{k,k'}, \tag{3.6}$$

which confirms that we can treat exciton as composite bosons. Electrons in a semiconductor interact via the Coulomb interaction in (3.1): it is then expected that excitons will experience the same interaction. In term of the exciton creation and annihilation operator, defined previously, such a Coulomb term will have the form:

$$H_{ex-ex} = \sum_{\boldsymbol{k},\boldsymbol{k}',\boldsymbol{q}} V_q b_{\boldsymbol{k}+\boldsymbol{q}}^\dagger b_{\boldsymbol{k}'-\boldsymbol{q}}^\dagger b_{\boldsymbol{k}} b_{\boldsymbol{k}'}. \tag{3.7}$$

where $V_{\boldsymbol{q}} \approx V_0 = 6e^2 a_0/\epsilon_0$, provided that the Bohr radius of the exciton $a_0 << \frac{1}{|\boldsymbol{q}|}$ [39].

3.1.2 Photon dispersion

As mentioned above, the optical cavities considered here are made of a thin layer of semiconductor material, confined between two dielectric mirrors. If high quality mirrors are fabricated, the confining system acts like a Fabry-Perot resonator, hence it is able to trap the light efficiently, making possible strong interactions between light and matter, embedded in the cavity in the form of electronic resonances. The Bragg mirrors confine the light, say in the z direction, but not in the $x-y$, so the light entering the microcavity with an angle θ will have a dispersion of the form:

$$E_{ph}(k_\parallel) = \frac{\hbar c}{n}\sqrt{k_\parallel^2 + k_\perp^2}, \tag{3.8}$$

where the cavity has a refractive index n and $k_\parallel$ is the wavevector component parallel to the surface, while $k_\perp$ is the wavevector component perpendicular to the surface. In particular:

$$k_\perp = n\frac{2\pi}{\lambda}, \tag{3.9}$$

where λ is the resonance wavelength at normal incidence. Making a Taylor expansion of (3.8), defining the photon "mass" term as $m = \frac{n}{c}k_\perp$, which is orders of magnitude smaller than the exciton mass, we obtain the quadratic dispersion relation:

$$E_{ph}(k_\parallel) \approx E_0 + \frac{\hbar^2 k_\parallel^2}{2m}, \tag{3.10}$$

with $E_0 = \frac{\hbar c}{n}k_\perp$.

3.1.3 Polariton Hamiltonian

The basic starting point to provide a theoretical description of polariton is to consider two multimode bosonic fields, b_k and a_k, which describe, respectively, the excitons of the semiconductor structure and the photons, coming from a light source and interacting with the structure:

$$H_{ex-ph} = \sum_k E_{ex}^{(k)} b_k^\dagger b_k + E_{ph}^{(k)} a_k^\dagger a_k + \frac{\Omega}{2}(a_k^\dagger b_k + b_k^\dagger a_k), \tag{3.11}$$

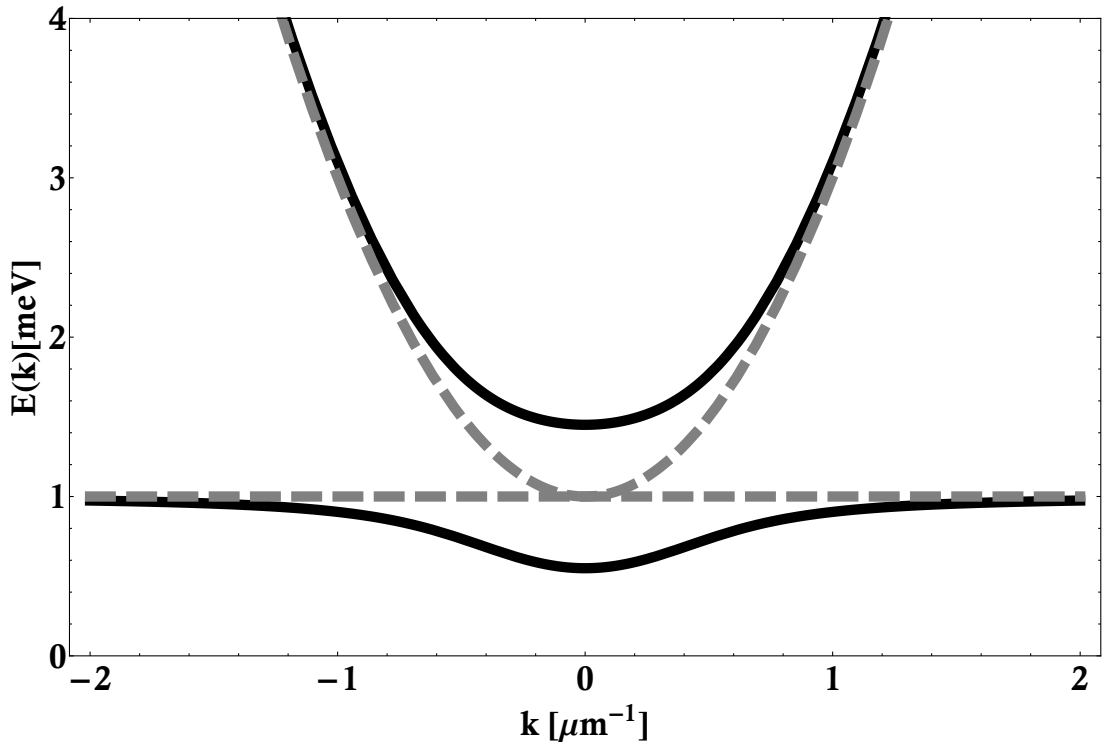

Figure 3.1: Polariton dispersion relation: The upper and lower polariton branches (dark lines) are separated by a Rabi splitting Ω. We have included the photon parabolic dispersion relation and the exciton energy in gray.

where Ω is the Rabi coupling between photons and exciton, which, for quantum wells at the antinode of the electromagnetic field, is calculated approximately from the following expression:

$$\Omega = \sqrt{\frac{N_{qw}e^2}{2\epsilon m_0 L_{\text{eff}}} f_{osc}}, \tag{3.12}$$

with N_{qw} quantum wells embedded in the cavity, having effective length L_{eff} (including penetration in the mirrors) and where f_{osc} is the oscillator strength of the transition. Because of the translational invariance in the cavity plane, photons only interact with excitons with the same $\boldsymbol{k}$, that is $k_\parallel$. Fixing the value of $k_\parallel$, it is possible to write the single particle Hamiltonian associated with (3.11), in the basis $|X\rangle$,$|P\rangle$, representing the single exciton state and the single photon state, respectively. In such a basis, the Hamiltonian reduces to a two-dimensional square matrix:

$$\begin{pmatrix} E_{ex} & \frac{\Omega}{2} \\ \frac{\Omega}{2} & E_{ph} \end{pmatrix}, \tag{3.13}$$

which is that of a *coupled oscillator model*. The eigenenergies of the the above matrix are:

$$E_{lp} = \frac{1}{2}[E_{ex} + E_{ph} - \sqrt{\Omega^2 + \Delta^2}] \tag{3.14}$$

$$E_{up} = \frac{1}{2}[E_{ex} + E_{ph} + \sqrt{\Omega^2 + \Delta^2}], \tag{3.15}$$

where $\Delta = E_{ex} - E_{ph}$ is the exciton-photon *detuning* and the dispersion relation is showed in Fig.(3.1). In the eigenbasis, we can diagonalize (3.11), obtaining:

$$H_{pol} = \sum_k E_{lp}^{(k)} l_k^\dagger l_k + E_{up}^{(k)} u_k^\dagger u_k, \tag{3.16}$$

where $l_k^\dagger, u_k^\dagger$ are called *upper and lower polaritons*, and can be obtained from the unitary transformation:

$$\begin{pmatrix} l_k^\dagger \\ u_k^\dagger \end{pmatrix} = \begin{pmatrix} X_k & C_k \\ -C_k & X_k \end{pmatrix} \begin{pmatrix} b_k^\dagger \\ a_k^\dagger \end{pmatrix}, \tag{3.17}$$

where X_k and C_k are called *Hopfield coefficients* [40],

$$\begin{aligned} X_k &= \sqrt{\frac{\Delta + \sqrt{\Delta^2 + \Omega^2}}{2\sqrt{\Delta^2 + \Omega^2}}} \\ C_k &= \sqrt{\frac{\Omega^2}{(\Delta + \sqrt{\Delta^2 + \Omega^2})2\sqrt{\Delta^2 + \Omega^2}}}, \end{aligned} \tag{3.18}$$

which satisfy the normalization condition, $|X_k|^2 + |C_k|^2 = 1$. As we have mentioned in the previous section, the Coulomb interaction between the carriers gives rise to an effective exciton-exciton interaction term (we discard the anharmonic saturation in the photon-exciton coupling). Considering (3.7), as long as the interaction strength is small, it is possible to neglect scattering between the lower and the upper branch modes, as they give rise to non-secular terms. In this sense the two branches are virtually decoupled and it is convenient to work directly in one of the polariton basis: thus, we express the Hamiltonian (3.11), together with the exciton-exciton interaction term (3.7), in the lower polariton basis ($l^\dagger$), to obtain:

$$H = \sum_{\boldsymbol{k}} E_{lp} l_{\boldsymbol{k}}^\dagger l_{\boldsymbol{k}} + \sum_{\boldsymbol{k},\boldsymbol{k}',\boldsymbol{q}} V_{\boldsymbol{k},\boldsymbol{k}',\boldsymbol{q}} l_{\boldsymbol{k}+\boldsymbol{q}}^\dagger l_{\boldsymbol{k}'-\boldsymbol{q}}^\dagger l_{\boldsymbol{k}} l_{\boldsymbol{k}'}, \tag{3.19}$$

where $V_{\boldsymbol{k},\boldsymbol{k}',\boldsymbol{q}} = V_0 X_{|\boldsymbol{k}'-\boldsymbol{q}|} X_k X_{|\boldsymbol{k}+\boldsymbol{q}|} X_{k'}$. The scattering between polaritons of different modes, whose physics is incorporated in (3.19), give rise to the collision broadening calculated by C. Ciuti in [41]: here a threshold behaviour of the broadening was predicted, with an exciton density at threshold, approximately, $n_{ex} = 7.109\,\mathrm{cm}^2$ at $\Delta = 3\,\mathrm{meV}$ for a sample with a Rabi splitting $\Omega = 3\,\mathrm{meV}$. Below this threshold the collision broadening can be neglected [42] and we can keep the lowest order term, obtaining, at $k = 0$:

$$H = E_{lp} l_0^\dagger l_0 + V_0 l_0^\dagger l_0^\dagger l_0 l_0, \tag{3.20}$$

which is a Kerr-like Hamiltonian, with a nonlinearity which is quadratic in the field annihilation-operators. Even though the approximation (3.20) is cutting out of the physical model different kind of scattering processes, it is a minimum model for interacting polaritons and its relative simplicity allows us to investigate the quantum properties and dynamics of polaritons.

3.1.4 Polariton decay

In order to have a realistic model which describes the physics of polaritons, other phenomena need to be included in (3.11). So far we have considered the polariton-polariton interaction, which is generated by the excitonic component of the quasiparticles. However, both exciton and photon, in real experiment, have a finite lifetime, i.e. every mode present in the system, once populated, will tend to dissipate. For the photons, this is ultimately due to the finite reflectivity of the mirrors. In fact, to realize *strong coupling* between the excitons and photons, high-quality cavities are required: experimentally, the strong coupling regime is demonstrated by the presence of two dips in the reflectivity spectrum. For microcavity polaritons, the strong coupling regime takes place when the exciton and cavity linewidths are smaller than the Rabi splitting, Ω, which means that the decay is smaller than the coupling. It is possible to add phenomenologically a damping term as an imaginary term, $i\gamma$, in the photon energy in (3.43), as showed in [39], As depicted schematically in Fig. 3.2, as γ approaches the same value as $\Omega = 1$, the two branches of the dispersion merge

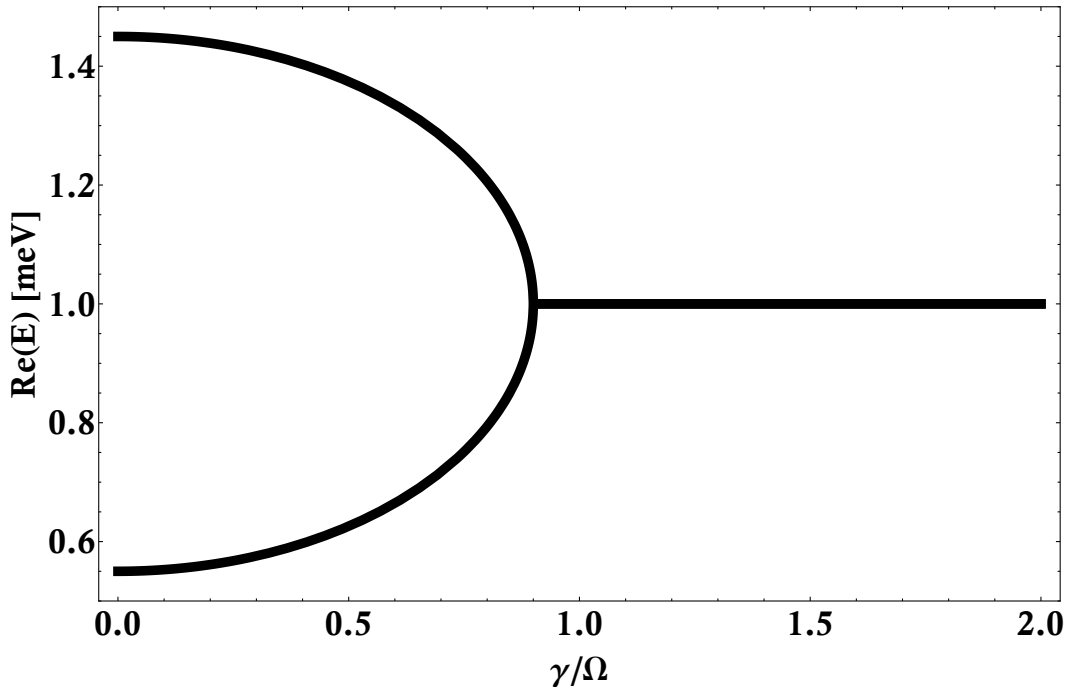

Figure 3.2: Transition from the strong coupling regime to the weak coupling, for cavity modes at $k = 0$. In the strong coupling, the interaction is splitting the spectrum in two branches. Notice that $\gamma/\Omega \geq 1$ the transition from strong to weak coupling regime takes place.

into one, and the system is then in the weak coupling regime. The excitons in a quantum well have a finite linewidth too: we can the introduce both decay processes phenomenologically, in the dispersion relations:

$$\begin{aligned} E'_{ex} &= E_{ex} - i\gamma_{ex} \\ E'_{ph} &= E_{ph} - i\gamma_{ph}. \end{aligned} \tag{3.21}$$

Incorporating this in the polariton Hamiltonian (i.e. in the strong coupling regime), the upper and lower polariton energy dispersions become:

$$E_{lp} = \frac{1}{2}[E_{ex} + E_{ph} - i(\gamma_{ex} + \gamma_{ph}) - \sqrt{\Omega^2 + (\Delta - i(\gamma_{ex} - \gamma_{ph}))^2}] \tag{3.22}$$

$$E_{up} = \frac{1}{2}[E_{ex} + E_{ph} - i(\gamma_{ex} + \gamma_{ph}) + \sqrt{\Omega^2 + (\Delta - i(\gamma_{ex} - \gamma_{ph}))^2}], \tag{3.23}$$

which at resonance, i.e. $\Delta = 0$, gives as a condition for being in the strong coupling regime, $\Omega^2 > (\gamma_{ex} - \gamma_{ph})^2$. A proper treatment of the strong to weak coupling transition can be obtained both semiclassicaly and with a quantum approach [43], the

former through the transfer matrices method [44].

3.2 Driven-dissipative cavity polariton

Microcavity polaritons are intrinsically driven-dissipative systems, as the injection of photons inside the cavity requires a photon source and the imperfection of the mirrors cause the leaking of the photons from the cavities, discussed in the last section. There are two standard ways to drive a polaritonic system: resonant excitation and non-resonant excitation. For *resonant excitation* the pump signal is resonant to the polariton state, in fact the light is matched in energy and in-plane momentum, hence the polaritons generated will inherit the same properties. This means that it is possible to engineer the polariton state with the coherence imprinted by the source. The usual way to describe a resonant excitation is through a coupling term, in the Hamiltonian, between the cavity mode and a classical field with amplitude $f(t)$:

$$H_{pump} = f(t)e^{-i\omega_p t}a^\dagger + f^*(t)e^{i\omega_p t}a, \tag{3.24}$$

with frequency ω_p. On the other hand another pumping scheme can be implemented called *non-resonant excitation*: this pumping scheme is the one implemented to generate a Bose-Einstein condensate of polaritons, which forms spontaneously from the thermal distribution. The pump excites high-energy exciton states which, via scattering with the lattice, lose energy and cool down: the reservoir created by these excitations, at high momentum, while losing energy, moves towards $k_\parallel = 0$, hence entering the region described by the polariton dispersion and populating the polariton energy levels with particles having a quasi-thermal distribution. The relaxation process keeps taking place, until the minimum of the energy is reached, at $k_\parallel = 0$: here polaritons can condense forming a peculiar out-of-equilibrium Bose-Einstein condensate, if the BEC-phase transition density threshold is reached. The pumping scheme described above is incoherent, as no coherence coming from the laser is present in the reservoir, and non-resonant with the polariton level: a general way to

model such processes is via a Lindblad term in the master equation, as in (2.54):

$$\mathcal{L}_{pump} = \sum_{\boldsymbol{k}} \Gamma_{\boldsymbol{k}} \bar{n}(\boldsymbol{k})(a^{\dagger}_{\boldsymbol{k}} \rho a_{\boldsymbol{k}} - \frac{1}{2}(a_{\boldsymbol{k}} a^{\dagger}_{\boldsymbol{k}} \rho - \rho a_{\boldsymbol{k}} a^{\dagger}_{\boldsymbol{k}})), \tag{3.25}$$

where $\Gamma_{\boldsymbol{k}}$ is the pump rate at a given $\boldsymbol{k}$ and $\bar{n}(\boldsymbol{k})$ is the reservoir distribution function. As mentioned above, making use of this pumping scheme, most properties of the pump, such as polarization and coherence, are lost, hence we can study the features of the condensate without worrying too much about memory effects coming from the pump. Note here that the incoherent pumping scheme by itself is necessary but not sufficient to generate a stable polariton condensate: in fact, a complete model of polariton condensation needs to take into account a variety of scattering mechanisms, which allow the quasi-thermal distribution to cool down and to macroscopically occupie the bottom state of the polariton dispersion. In particular these mechanisms include *polariton-phonons* interaction and *polariton-polariton* interaction, at different k-vectors, as showed in [45].

3.2.1 Mean field equations

Consider now the Hamiltonian (3.11) for a single mode exciton and a single mode photon, inclusive of the exciton interaction term:

$$H_{ex-ph} = E_{ex} b^{\dagger} b + E_{ph} a^{\dagger} a + \frac{\Omega}{2}(a^{\dagger} b + b^{\dagger} a) + V_0 b^{\dagger} b^{\dagger} b b. \tag{3.26}$$

From the above Hamiltonian it is possible to derive the equation of motion for the exciton and the photon operators, as well as for the exciton number operator. To do this, we use the Heisenberg equation of motion:

$$\hbar \frac{d}{dt} a^{\dagger} = -i[a^{\dagger}, H], \tag{3.27}$$

which leads us to:

$$\begin{aligned} i\hbar\frac{d}{dt}N_{ex} &= -\Omega(a^\dagger b - ab^\dagger) \\ i\hbar\frac{d}{dt}a &= E_{ph}a + \Omega b \\ i\hbar\frac{d}{dt}b &= E_{ex}b + V_0 b^\dagger b^\dagger bb + \Omega a, \end{aligned} \tag{3.28}$$

where $N_{ex} = b^\dagger b$. The equations above couple different species of operators in a non-trivial way. Hence, in order to to solve them, we need to consider a nested structure of commutators, or, equivalently, terms made of an increasing number of products between operators: this problem is well-knowns as *quantum hierarchy problem* [46]. We can solve the system of equations (3.28) considering the mean values of the operators: $\langle N_{ex}\rangle$, $\langle a\rangle$, $\langle b\rangle$, together with the approximations:

$$\begin{aligned} \langle bb\rangle &= 0 \\ \langle b^\dagger b^\dagger b\rangle &= \langle b^\dagger b\rangle \langle b^\dagger\rangle \\ \langle b^\dagger bb\rangle &= \langle b^\dagger b\rangle \langle b\rangle , \end{aligned} \tag{3.29}$$

which truncate the hierarchy. The assumption in (3.29) consists in removing the purely correlatad terms in the expansion of the mean values of the high order products of operators, hence obtating factors with at most second order products: this stategy ensures that we are dealing with particle-number conserving quantities. In particular, the assumption is justified, phenomenologically, in the polaritonic case, by the experimental results [47]. It follows that the equation of motion for the mean values, from (3.28), are:

$$\begin{aligned} i\hbar\frac{d}{dt}\langle N_{ex}\rangle &= 2i\Omega\mathrm{Im}(\langle b\rangle \langle a^\dagger\rangle) \\ i\hbar\frac{d}{dt}\langle a\rangle &= E_{ph}\langle a\rangle + \Omega\langle b\rangle \\ i\hbar\frac{d}{dt}\langle b\rangle &= (E_{ex} + V_0\langle N\rangle)\langle b\rangle + \Omega\langle a\rangle , \end{aligned} \tag{3.30}$$

where we have used the fact that $\langle a^\dagger\rangle\langle b\rangle - \langle b^\dagger\rangle\langle a\rangle = 2i\mathrm{Im}(\langle b\rangle\langle a^\dagger\rangle)$. The set of equations (3.30) is called the *Excitonic-Bloch equations*, due to its analogy with the

optical Bloch equations [39]. This analogy is not precise: in the excitonic-Bloch equation we are dealing with excitons and not with two-level systems; in the latter case there is an intrinsic saturation which comes from the fact that a two level system cannot be further excited once it is inverted. By contrast, bosonic systems like excitons, in an ideal case, can be excited with arbitrary large number in the Fock basis.

If we move to the lower polariton base (which we rewrite as ψ_{lp}), i.e. we transform the equations (3.30) through the Hopfield coefficients, we obtain:

$$i\hbar\frac{d}{dt}\psi_{lp} = (E_{lp} - i\gamma_{lp} + g|\psi_{lp}|^2)\psi_{lp} + f_{\text{ext}}e^{-i\omega_p t}, \tag{3.31}$$

where $g = |X|^4 V_0$ and we have included the finite linewidth of the lower polariton mode γ_{lp}, and a coherent driving term, $f_{\text{ext}}e^{-i\omega_p t}$ with frequency ω_p. Equation (3.31) is called the single mode *Gross-Pitaevski equation*, in analogy to the equation that describes the order parameter in atom condensates. The Gross-Pitaevskii equation can be generalized to deal with spatially extended condensate of atoms, and of other bosonic fields, providing a remarkable mean-field model for many-body systems. For an order parameter with a spatial dependence $\Psi_{lp}(\boldsymbol{r})$, which describes the lower polariton modes, the driven-dissipative Gross-Pitaevskii equation is [48]:

$$i\hbar\partial_t\Psi_{lp}(\boldsymbol{r},t) = (-\frac{\hbar^2}{2m}\nabla^2 + \omega^0 - i\gamma_{lp} + g|\Psi_{lp}|^2 + V_{\text{ext}}(\boldsymbol{r}))\Psi_{lp} + F_{\text{ext}}(\boldsymbol{r},t), \tag{3.32}$$

with $m = m_{ph}/|X|^2$, where m_{ph} is the effective mass of the photon in the cavity, V_{ext} is an external potential felt by the lower polariton and $F_{\text{ext}}(\boldsymbol{r},t)$ is the driving field that, in general, possesses a spatial profile. The same equation holds for cavity with a generic nonlinear medium embedded, but in this case equation (3.32) describes pure photonic states, with the interaction strength related to the nonlinear susceptibility of the medium considered.

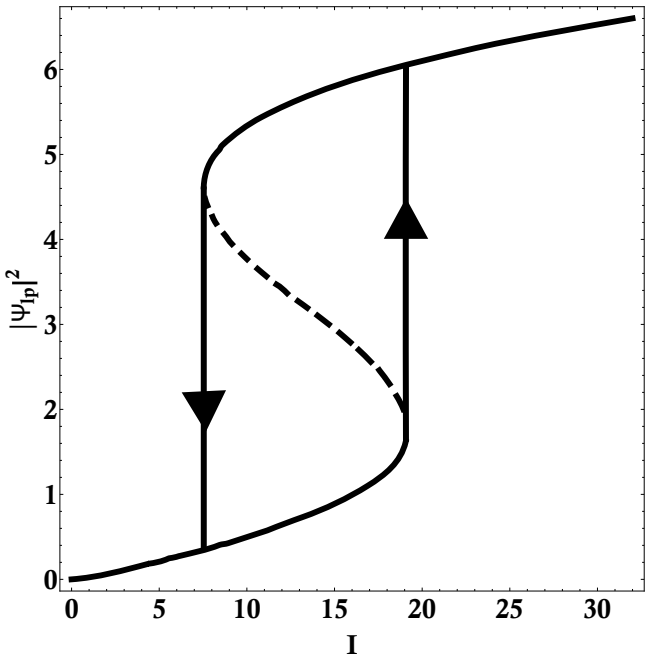

Figure 3.3: Bistable curve (S-curve) for a single mode Kerr oscillator with $g = \gamma = 0.1$ and $\delta = 0.2 > \sqrt{3}\gamma$, showing the density of polaritons as a function of the intensity of the pump I. The dotted lines indicate the unstable points, where the population is weak against small fluctuation, which eventually drive the system either on the upper or on the lower stable branches (solid lines).

3.2.2 Optical bistability

The optical bistability is a phenomenon observed in some optical systems, where two possible stable states are present in transmission, depending on the input field. Optical bistability is well known in literature and was first studied in the framework of nonlinear optics, where the presence of a Kerr interaction induces a bistable behaviour in some region of the system's parameter space. The bistability of microcavity polaritons has been extensively studied both theoretically [42] and experimentally [49], and is based on the use of a coherent resonant excitation of the cavity, blue detuned with respect to the lower polariton. If the driving power is cycled within a range of intensities, it is possible to observe the typical hysteresis curve in the transmitted laser intensity. Let us start by considering the steady-state of the Gross-Pitaevskii equation in the polariton basis (3.31), with an external driving

amplitude $f_{\text{ext}} = \sqrt{I}$:

$$(E_{lp} - i\gamma_{lp} + g|\psi_{lp}|^2)\psi_{lp} = -\sqrt{I}e^{-i\omega_p t}. \tag{3.33}$$

Multiplying the equation by its complex conjugate, we obtain a third order polynomial equation for the number of polaritons $|\psi_{lp}|^2$:

$$I = [(g|\psi_{lp}|^2 - \delta)^2 + \gamma_{lp}^2]|\psi_{lp}|^2, \tag{3.34}$$

where $\delta = \omega_p - E_{lp}$ is the laser-polariton detuning.

Now, we demonstrate that if $\delta \geq \sqrt{3}\gamma_{lp}$ this equation solutions show an S-curve, meaning that for a range of intensities, it has three solutions, with two stable and one unstable, as illustrated in Fig. (3.3). In fact, consider the condition for turning points of I:

$$\frac{d}{d|\psi_{lp}|^2} I = 3g^2|\psi_{lp}|^4 - 4g|\psi_{lp}|^2\delta^2 + \gamma_{lp}^2 + \delta = 0, \tag{3.35}$$

and we can see that real solution exist when:

$$g^2(\delta^2 - 3\gamma^2) \geq 0, \tag{3.36}$$

which yields the condition $\delta \geq \sqrt{3}\gamma_{lp}$.

As the power increases, when the polariton density $|\psi_{lp}|^2$ reaches the local maximum, it jumps to the upper branch, then when the power decreases, the intensity goes down until it drops reaching the local minimum. When the detuning $\delta < \sqrt{3}\gamma_{lp}$ the pump is too close to resonance and the polaritons rapidly blueshift above the laser energy. The transmitted intensity increases and saturates: such a configuration is called *optical limiter*. Finally, if $\delta = \sqrt{3}\gamma_{lp}$ the solutions have a degeneracy and a single jump occurs, due to the discontinuity of the derivative and the system is called *optical discriminator* [50].

3.3 Control of polariton spin-orbit state

In this section we present original research carried out in collaboration with Feng Li et al. in Sheffield, which lead to the publication of a paper in *Physical Review B* [2]. The research concerns the manipulation and control of polaritonic states on the hypersphere, i.e. a sphere in higher dimensions, that can be built considering the spin-orbit coupling, via a Stark pulse. In the previous section we have introduced the basic physics and model describing exciton-polaritons: however we have so far ignored the polarization degrees of freedom, which plays a crucial role in investigating peculiar optical phenomena, like the *Optical Spin Hall effect*, in this systems, due to the interplay between the polarization of the state, the effective magnetic field induced by the TE-TM splitting in the cavity and the driven-dissipative nature of polaritons. In the following, we first introduce a general model of polarization for polaritons, then we briefly describe the physics of the TE-TM splitting in microcavities and, finally, we present the research results about the state control on the hypersphere.

3.3.1 Polarization degrees of freedom

The polariton spin is a direct consequence of the band structure of the semiconductor material embedded in the microcavity. For standard GaAs cavities, electrons in the conduction s-band have a spin of $m_e = \pm\frac{1}{2}$ and orbital angular momentum (OAM) $J_e = 0$. In the valence band with p-symmetry, holes have a spin angular momentum of $m_h = \pm 1/2, \pm 3/2$. Hence, for an exciton, the total angular momentum is $m_{ex} = \pm 1, \pm 2$. Due to the conservation of the angular momentum, only excitons with spin projection 1 can be created through the absorption of a photon, as photons have a spin of either 0 or ± 1. Excitons with a spin of ± 2 are often referred to as *dark excitons*, as they are not optically active, i.e., they do not couple with light. The *bright excitons*, i.e., the one that couples with light having a spin of ± 1, can emit photons with the two polarisations, respectively σ^+ and σ^-: it follows that the

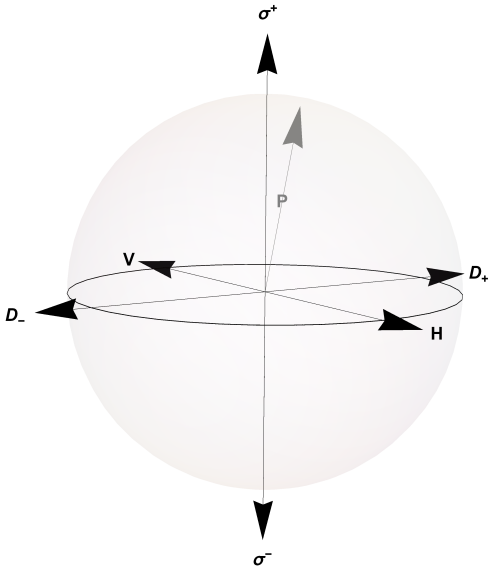

Figure 3.4: Schematic representation of the Poincare sphere, with the pseudospin vectors on each axis S_k. The information about the polarisation of light are contained in the vector P on the sphere, having the Stokes parameters (S_c, S_l, S_p) as coordinates.

polariton polarisation, can be written as a linear superposition:

$$|\psi\rangle = \psi_+ |\sigma^+\rangle + \psi_- |\sigma^-\rangle . \tag{3.37}$$

It is possible to build a one-to-one correspondence between polariton spin angular momentum, and a $\frac{1}{2}$ pseudo-spin representation, where the pseudo-spin component normal to the plane carries the information about the exciton spin and the in-plane components characterize the orientation of the dipole moment of the exciton [51]. Hence the density matrix of a polariton with momentum $\boldsymbol{k}$ is:

$$\rho_{\boldsymbol{k}} = \frac{N_{\boldsymbol{k}}}{2}(\mathbb{1}_2 + S_{\boldsymbol{k}} \cdot \sigma_{\boldsymbol{k}}), \tag{3.38}$$

where $S_{\boldsymbol{k}}$ is the pseudospin vector, $N_{\boldsymbol{k}}$ is the number of polaritons at a given $\boldsymbol{k}$ and $\sigma_{\boldsymbol{k}}$ are the Pauli matrices. Following this argument, it is clear that it is possible to represent polaritons with spin angular momentum $|+1\rangle$, $|-1\rangle$, as pseudospin

vectors $|\uparrow\rangle$,$|\downarrow\rangle$, respectively. The information about the polariton spin orientation is then contained in the emitted light and it can be retrieved with a polarization resolved analysis. The polarisation of light can be fully characterised by the Stokes parameters, that compose the polarisation vector $\boldsymbol{S}$:

$$\begin{pmatrix} S_c \\ S_l \\ S_d \end{pmatrix}, \tag{3.39}$$

expressed in the circular (σ^+, σ^-), linear (H, V) and diagonal (D_+, D_-) basis:

$$\begin{aligned} S_c &= \frac{I_{\sigma^+} - I_{\sigma^-}}{I_{\sigma^+} + I_{\sigma^-}} \\ S_l &= \frac{I_H - I_V}{I_H + I_V} \\ S_d &= \frac{I_{D_+} - I_{D_-}}{I_{D_+} + I_{D_-}}, \end{aligned} \tag{3.40}$$

with $|\boldsymbol{S}| = \sqrt{S_c^2 + S_l^2 + S_d^2} \leq 1$. When $|\boldsymbol{S}|$ is zero, the light is *unpolarized*. If we ignore polariton-polariton interactions, the dynamics of the system density operator is fully characterized, in the basis spanned by the pseudo spin eigenvectors, by the following Heisenberg equation:

$$\frac{d}{dt}\rho_{\boldsymbol{k}} = -i[H_{\boldsymbol{k}}, \rho_k], \tag{3.41}$$

where it is possible to write the Hamiltonian in this basis as an effective spin-orbit interaction:

$$H_{\boldsymbol{k}} = E_{\boldsymbol{k}} - B_{\text{eff},\boldsymbol{k}} \cdot \boldsymbol{S}_k, \tag{3.42}$$

where $E_{\boldsymbol{k}}$ is the energy of the branch considered and $B_{\text{eff},\boldsymbol{k}}$ is an effective magnetic field, which couples with the polarisation degrees of freedom. The effective field has the same mathematical structure of a magnetic field, but it is not a real field: it takes action only on the bright states, whereas a magnetic field would mix the dark and the bright exciton. Note that the last term in (3.42) gives the minimum of the energy for the system when the effective field and the polarisation are parallel.

3.3.2 TE-TM splitting

In empty confining structures, such as microcavities, the transverse electric (TE) and transverse magnetic (TM) normal modes of the cavity are non-degenerate in energy, for finite value of in-plane momentum.

Additionally, the long range interaction between electrons and holes, in confined systems, generates a TE-TM splitting for excitons [52]: it basically consists in a splitting in the energy between the excitons that have a dipole moment parallel (TM) and perpendicular (TE) to the wave-vector [53]. The TE-TM splitting is phenomenologically equivalent to an effective magnetic field, acting in the plane of the quantum well, which affects the polariton polarisation. The strength of this effective magnetic field depends on the energy splitting between the exciton TE and TM mode. These effect result in polariton TE-TM splitting, which, following the arguments above, depends is on k. It can be demonstrated that the dispersion relations for the polariton branches have the general following form:

$$E_{lp}^{TE} = \frac{1}{2}[E_{ex}^{TE} + E_{ph}^{TE} - \sqrt{\Omega^2 + \Delta_{TE}^2}] \tag{3.43}$$

$$E_{lp}^{TM} = \frac{1}{2}[E_{ex}^{TM} + E_{ph}^{TM} - \sqrt{\Omega^2 + \Delta_{TM}^2}] \tag{3.44}$$

$$E_{up}^{TE} = \frac{1}{2}[E_{ex}^{TE} + E_{ph}^{TE} + \sqrt{\Omega^2 + \Delta_{TE}^2}] \tag{3.45}$$

$$E_{up}^{TM} = \frac{1}{2}[E_{ex}^{TM} + E_{ph}^{TM} + \sqrt{\Omega^2 + \Delta_{TM}^2}], \tag{3.46}$$

where Δ_{TE} and Δ_{TM} are, respectively, the TE and TM exciton-photon detunings, and, in the lower polariton base, the magnitude of the splitting is given by $\Delta_{EM} = E_{lp}^{TE} - E_{lp}^{TM}$. In principle, the TE-TM splitting acts both on the photonic modes and on the exciton modes: however the effect of the splitting on the exciton energy is significantly smaller than the photonic one, hence it can be ignored to a good approximation. An important property of the effective field induced by the splitting is its k-dependece: in a space where the x axis is defined by the direction of the horizontal polarised light and the y axis by the direction of the vertical polarised

light, the Hamiltonian that describes the effective field, as shown in [54], reads:

$$B_{\text{eff},\boldsymbol{k}} = \Delta_{EM,\boldsymbol{k}} \begin{pmatrix} \cos(2\phi) \\ \sin(2\phi) \end{pmatrix} \tag{3.47}$$

where ϕ define the orientation of $k_{\parallel}$.

An explicit expression for the x and y component of (3.47) can be found by considering that the dispersion of the photonic field is parabolic and, since we ignore the effect of the exciton, the splitting grows quadratically in $|\boldsymbol{k}|$. It can be shown that [55]:

$$B_{\text{eff},x} = \beta(k_x^2 + k_y^2)$$

$$B_{\text{eff},y} = \beta(2k_x k_y)$$

where $\beta = \hbar^2(\frac{1}{m_{TE}} - \frac{1}{m_{TM}})$ depends on the effective mass of the TE and TM modes. Consequently, the Hamiltonian (3.42) in the basis (3.37) reads:

$$H = \begin{pmatrix} \hbar E_{lp}^{\sigma^+} - \frac{\hbar^2\nabla^2}{2m_{lp}} & B_{\text{eff},x} - iB_{\text{eff},y} \\ B_{\text{eff},x} + iB_{\text{eff},y} & \hbar E_{lp}^{\sigma^-} - \frac{\hbar^2\nabla^2}{2m_{lp}} \end{pmatrix}, \tag{3.48}$$

and $B_{\text{eff},x} \mp iB_{\text{eff},y} = \beta(k_x \pm ik_y)^2 = \beta(\partial_x \mp i\partial_y)^2$, where we have used the correspondence of the momentum to the differential operator.

3.3.3 Spin-Orbit Hypersphere

We have previously shown that the pseudospin of photons can be graphically represented by the Poincaré sphere, where every state is expressed through a linear combination of the polarisations eigenstates, for example consider a combination of σ^+ circularly polarized light and σ^-:

$$|\psi\rangle = \psi_+|\sigma^+\rangle + \psi_-|\sigma^-\rangle, \tag{3.49}$$

with ψ_+ and ψ_- the complex amplitudes, which satisfies the normalisation condition, $|\psi_+|^2 + |\psi_-|^2 = 1$. The states $|\sigma^+\rangle$ and $|\sigma^-\rangle$ correspond, respectively, to the north and

the south poles of the Poincaré sphere, with unit radius. All the other states on the sphere are determined by amplitudes and the relative phase between ψ_+ and ψ_-: in this sense they are spanned by a two-parameter space. We consider now an expanded Hilbert space, spanned by all the possible coherent superposition of circularly polarized photons which carry an orbital angular momentum $l = \pm 1$. We can build a basis for this Hilbert space by considering the four vectors:

$$\boldsymbol{\sigma} = (|\circlearrowleft, \sigma^+\rangle, |\circlearrowright, \sigma^+\rangle, |\circlearrowleft, \sigma^-\rangle, |\circlearrowright, \sigma^-\rangle), \tag{3.50}$$

where the symbols $\circlearrowright$ is used to represent the eigenstate having OAM $l = 1$and $\circlearrowleft$ for $l = -1$. Each of these basis vectors can be expressed via the Jones vector form [56]:

$$\begin{aligned} |1\rangle = |\circlearrowleft, \sigma^+\rangle = G(r)\begin{pmatrix} e^{-i\theta} \\ 0 \end{pmatrix}, |2\rangle = |\circlearrowright, \sigma^+\rangle = G(r)\begin{pmatrix} e^{i\theta} \\ 0 \end{pmatrix}, \\ |3\rangle = |\circlearrowleft, \sigma^-\rangle = G(r)\begin{pmatrix} 0 \\ e^{-i\theta} \end{pmatrix}, |4\rangle = |\circlearrowright, \sigma^-\rangle = G(r)\begin{pmatrix} 0 \\ e^{i\theta} \end{pmatrix}. \end{aligned} \tag{3.51}$$

The elements of the above vectors correspond to the σ^+ or σ^- polarisation, while θ is the azimuthal angle in real space, and $G(r)$ is a function describing the density profile of the state, in the radial coordinate. In this new space, the four states in (3.51), corresponds to the poles of a hypersphere where any arbitrary state can be expressed as: $|\psi\rangle = \boldsymbol{\psi} \cdot \boldsymbol{\sigma}$, with $\boldsymbol{\psi} = (\psi_1, \psi_2, \psi_3, \psi_4)$. Such states now are spanned by a six parameter space: four complex numbers ψ_{1-4} and the two relative phases, while the other degrees of freedom are removed making use of the arbitrary choice for one of the phase factors and the additional constraint imposed by the normalisation condition. Hence, states on the SO hypersphere can be used to describe eigenstates of orbital angular momentum and pseudospin: we call this new set of eigenstates *spin-orbit vectors* (SOV). Every set made of two orthogonal spin orbit vectors, can be used to build the corresponding two parameters spin-orbit Poincaré sphere (SOPS), constructed as a pseudospin Poincaré sphere, hence sharing with it the same mathematical properties. As an example, the "purely orbital" Poincaré

sphere, studied in [57], is obtained from the basis (3.51) by selecting $\psi = (1,0,0,0)$ and $(0,1,0,0)$ as the two poles of the sphere.

3.3.4 Polariton Hypersphere

In the previous section we showed that it is possible to interpret the TE-TM splitting on polaritons as an "effective magnetic field" ([58]), having a specific k-dependence. The structure we consider in the following is an open microcavity: it consists of a planar bottom layer of DBRs and a concave top DBR, which can be controlled by nanopositioner. This structure allows to free tune the spectral resonance by changing the separation between the mirrors. Moreover, the concave mirror induces an effective harmonic confinement, as it focus the beam on a small region of the quantum well. Taking into account the effect of the TE-TM splitting and of the concave mirror and neglecting polariton-polariton interaction, in the basis of σ^+ and σ^- lower polariton modes, the system is described by the following Hamiltonian:

$$H = \begin{pmatrix} \hbar\omega_{LP}^{\sigma^+} - \frac{\hbar^2\nabla^2}{2m_{LP}} + V & \beta\left(\frac{\partial}{\partial x} - i\frac{\partial}{\partial y}\right)^2 \\ \beta\left(\frac{\partial}{\partial x} + i\frac{\partial}{\partial y}\right)^2 & \hbar\omega_{LP}^{\sigma^-} - \frac{\hbar^2\nabla^2}{2m_{LP}} + V \end{pmatrix}, \tag{3.52}$$

where $\omega_{LP}^{\sigma^+}$ ($\omega_{LP}^{\sigma^-}$) is the frequency corresponding to the σ^+ (σ^-) polarisation, m_{LP} is the effective mass, $V = \frac{1}{2}m_{LP}\omega_h^2(x^2+y^2)$ is a harmonic potential, generated by the in-plane confinement and the terms proportional to $\beta = \hbar^2(1/m_t - 1/m_l)/4$ describe the effective magnetic field, induced by the TE-TM splitting, as shown in the previous section. We can add the photon leakage rate by inserting the non-Hermitian term, $-i\gamma_{LP}/2$, in the diagonal elements of Hamiltonian (3.52). When the TE-TM is switched off, i.e., when $\beta = 0$, eq. (3.52) simply describes a two mode system with a 2D harmonic potential: in this case, it is well known [59], that the Laguerre-Gauss modes form a basis that spans the Hilbert space for the system, and, in particular, the Laguerre-Gauss corresponding to $l = \pm 1$, $LG_{0,\pm1}^{\sigma^\pm}$, are a basis for the first excited manifold of the harmonic potential. The first excited manifold has a radial distribution structurally equivalent to the one in eqs. (3.51), with $G(r) = r\,e^{-r^2/2a^2}/\sqrt{\pi a^2}$ and $a = \sqrt{\hbar/m_{LP}\omega_h}$.

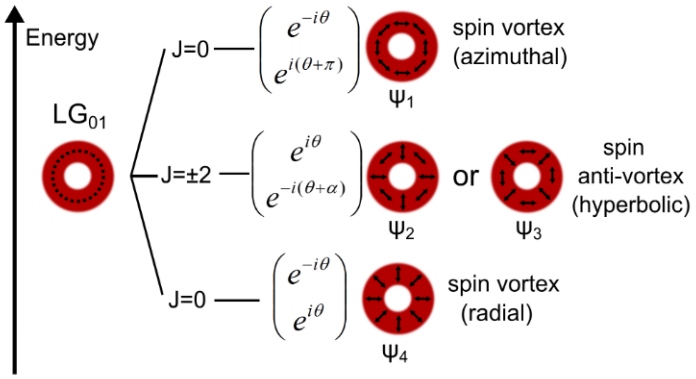

Figure 3.5: From [1]. Sketch of the eigenstates formed by the Laguerre-Gauss mode, LG_{01}, when a TE-TM splitting in the cavity is present. The presence of the in-plane effective field removes the degeneracy of the modes, giving three energy levels.

If we add now a small TE-TM splitting, the new eigenmodes of the system can be calculated perturbatively, as demonstrate in [1]: in particular, for $\omega_{LP}^{\sigma^+} = \omega_{LP}^{\sigma^-} = 0$, they consist of two spin vortices, split in energy, one radial ($\boldsymbol{\psi_{RA}} = (1,0,0,1)/\sqrt{2}$) and one azimuthal ($\boldsymbol{\psi_{AZ}} = (1,0,0,-1)/\sqrt{2}$), together with the degenerate subspace, spanned by $\boldsymbol{\psi_{HY1}} = (0,1,1,0)/\sqrt{2}$ and $\boldsymbol{\psi_{HY2}} = (0,1,-1,0)/\sqrt{2}$, of the hyperbolic spin anti-vortex, as depicted in Fig.(3.5). These four states can be written in the base of $\sigma^+ = (1\,0)^T$ and $\sigma^- = (0\,1)^T$ states as:

$$|\boldsymbol{\psi_{RA}}\rangle = \frac{1}{\sqrt{2}}\begin{pmatrix} e^{-i\theta} \\ e^{i\theta} \end{pmatrix} \quad |\boldsymbol{\psi_{AZ}}\rangle = \frac{1}{\sqrt{2}}\begin{pmatrix} e^{-i\theta} \\ -e^{i\theta} \end{pmatrix} \quad |\boldsymbol{\psi_{HY1}}\rangle = \frac{1}{\sqrt{2}}\begin{pmatrix} e^{i\theta} \\ e^{-i\theta} \end{pmatrix} \quad |\boldsymbol{\psi_{HY2}}\rangle = \frac{1}{\sqrt{2}}\begin{pmatrix} e^{i\theta} \\ -e^{-i\theta} \end{pmatrix}.$$

The energy of the spin-vortex modes is equal, respectively, to $E = E_1 \pm 2\beta/a^2$, while the energy of the two hyperbolic spin anti-vortex is $E = E_1$, where E_1 is the energy of the unperturbed modes. The structure of the new eigenstates of the system can be easily understood if we notice that the total angular momentum $J = l + s$ is the actual constant of motion of the system. In the first excited manifold, both the orbital angular momentum and the pseudospin are equal to $l = \pm 1$, hence J can have only three possible values, namely $0, \pm 2$. The spin-orbit coupling induce by the TE-TM splitting, removes the degeneracy of the states with $J = 0$, while the states with $J = 2$ are not affected.

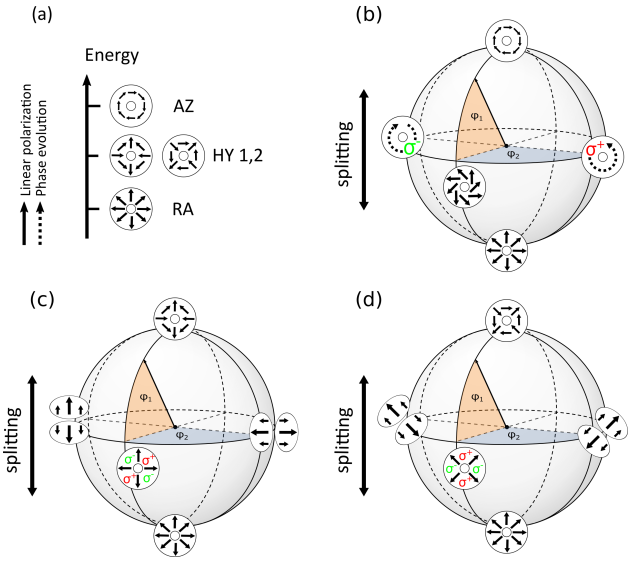

Figure 3.6: From [2]. (a) Energy levels and eigenstates structures of a 2D harmonic potential in presence of TE-TM splitting. (b),(c) and (d): A representation of the SOPSs which can be obtained considering the following states as poles: $\boldsymbol{\psi_{RA}}$ and $\boldsymbol{\psi_{AZ}}$ (b), $\boldsymbol{\psi_{RA}}$ and $\boldsymbol{\psi_{HY1}}$ (c), and $\boldsymbol{\psi_{RA}}$ and $\boldsymbol{\psi_{HY2}}$ (d). The vector on the sphere represents the field intensity and the and φ_1 and φ_2 correspond to the angular coordinates.

3.3.5 Stark Control

Considering the new energy structure of the eigenstates on the spin-orbit hypersphere in (3.6), it is possible to obtain a class of SOPSs, again described by a two-parameters space, defining as poles every pair of modes which are split in energy. For example, any spin-orbit state on the sphere in Fig.(3.6)(b) can be written in a parametric form as:

$$|\boldsymbol{\psi_b}\rangle = \left[\cos\left(\frac{\phi_1}{2}\right) e^{-i\frac{\phi_2}{2}} |\boldsymbol{\psi_{AZ}}\rangle + \sin\left(\frac{\phi_1}{2}\right) e^{i\frac{\phi_2}{2}} |\boldsymbol{\psi_{RA}}\rangle\right], \tag{3.53}$$

hence spanned by the two parameters ϕ_1 and ϕ_2. The splitting induces a precession of the spin-orbit vector around the vertical axis of the sphere considered, hence acting as an *effective* magnetic field [55]. We can make use of the AC Stark effect to manipulate the states on this spin-orbit Poincaré sphere: the Stark pulse consists of a laser pulse, generally red detuned with respect to the bare energy of the exciton. It is used, especially in the context of semiconductor microcavities, to induce a transient blue-shift of the exciton resonance possessing the same polarisation of the

laser. The blue-shift of the exciton line results in a shift in the polariton line, as was demonstrated in [60]. Hence, making use of Stark pulse having a σ^+ polarisation, we induce a pulsed *effective* magnetic field, arising from the splitting between the σ^+ and σ^- polaritons. Specifically, considering the spin orbit sphere depicted in Fig. 3.6(b), the σ^+ Stark pulse induces a precession of the spin-orbit vector around the axis having the two $\sigma^\pm$ vortex as extremes. Effectively, the precession lasts until the Stark pulse is over. Let us consider then a $\sigma^\pm$ polarised Stark pulse: the dynamics of the states can be obtained by making use of time-dependent perturbation theory, as the strength of the harmonic confinement is usually much higher than the TE-TM splitting. On the basis (3.50), the pertubation matrix $M_{\sigma^\pm}$, whose elements are $\langle i|\, H\, |j\rangle$, is:

$$M_{\sigma^\pm} = \begin{pmatrix} \hbar\delta\omega_{lp}^{\sigma^+}(t) & 0 & 0 & -2\beta/a^2 \\ 0 & \hbar\delta\omega_{lp}^{\sigma^+}(t) & 0 & 0 \\ 0 & 0 & \hbar\delta\omega_{lp}^{\sigma^-}(t) & 0 \\ -2\beta/a^2 & 0 & 0 & \hbar\delta\omega_{lp}^{\sigma^-}(t) \end{pmatrix}, \tag{3.54}$$

where $\hbar\delta\omega_{lp}^{\sigma^\pm}(t) = \hbar\delta\omega_{lp}^{\sigma^\pm}\exp[-(t-t_{st})^2/2\sigma_{st}^2]$ the term that describe the time dependent Stark pulse, acting as a shift in the energy of the $\sigma^\pm$ polaritons, centred at t_{st}, having a width of σ_{st}. From eq.(3.54) it is possible to obtain the system of linear differential equations and hence describe the system's temporal evolution. The system is analytically intractable, but can be solved numerically, using *Mathematica*, obtaining the solution at each time for the system in the presence of a Stark pulse. Clearly, the result is not limited to the case of a $\sigma^\pm$ polarised pulse, and the analysis can be easily extended to other bases. For example, the M matrix for a Stark pulse, polarised in the H-V basis and in the $D^\pm$ basis, are:

$$M_{H-V} = \begin{pmatrix} \frac{\hbar\delta\omega_{lp}^{H}(t)+\hbar\delta\omega_{lp}^{V}(t)}{2} & \frac{\hbar\delta\omega_{lp}^{H}(t)-\hbar\delta\omega_{lp}^{V}(t)}{2} & 0 & -2\beta/a^2 \\ \frac{\hbar\delta\omega_{lp}^{H}(t)-\hbar\delta\omega_{lp}^{V}(t)}{2} & \frac{\hbar\delta\omega_{lp}^{H}(t)+\hbar\delta\omega_{lp}^{V}(t)}{2} & 0 & 0 \\ 0 & 0 & \frac{\hbar\delta\omega_{lp}^{H}(t)+\hbar\delta\omega_{lp}^{V}(t)}{2} & \frac{\hbar\delta\omega_{lp}^{H}(t)-\hbar\delta\omega_{lp}^{V}(t)}{2} \\ -2\beta/a^2 & 0 & \frac{\hbar\delta\omega_{lp}^{H}(t)-\hbar\delta\omega_{lp}^{V}(t)}{2} & \frac{\hbar\delta\omega_{lp}^{H}(t)+\hbar\delta\omega_{lp}^{V}(t)}{2} \end{pmatrix}, \tag{3.55}$$

and for the diagonal one,

$$M_{D^{\pm}} = \begin{pmatrix} \frac{\hbar\delta\omega_{lp}^{D^+}(t)+\hbar\delta\omega_{lp}^{D^-}(t)}{2} & i\frac{\hbar\delta\omega_{lp}^{D^+}(t)-\hbar\delta\omega_{lp}^{D^-}(t)}{2} & 0 & -2\beta/a^2 \\ -i\frac{\hbar\delta\omega_{lp}^{D^+}(t)-\hbar\delta\omega_{lp}^{D^-}(t)}{2} & \frac{\hbar\delta\omega_{lp}^{D^+}(t)+\hbar\delta\omega_{lp}^{D^-}(t)}{2} & 0 & 0 \\ 0 & 0 & \frac{\hbar\delta\omega_{lp}^{D^+}(t)+\hbar\delta\omega_{lp}^{D^-}(t)}{2} & i\frac{\hbar\delta\omega_{lp}^{D^+}(t)-\hbar\delta\omega_{lp}^{D^-}(t)}{2} \\ -2\beta/a^2 & 0 & -i\frac{\hbar\delta\omega_{lp}^{D^+}(t)-\hbar\delta\omega_{lp}^{D^-}(t)}{2} & -i\frac{\hbar\delta\omega_{lp}^{D^+}(t)+\hbar\delta\omega_{lp}^{D^-}(t)}{2} \end{pmatrix}. \tag{3.56}$$

We now focus the analysis on the $\sigma^{\pm}$ pulse, i.e. the matrix (3.54), without loss of generality, as all the other cases will show the same basic features. Analyzing the new eigenenergies of the systems,

$$\begin{aligned} E_1' &= E_1 + \hbar\delta\omega_{LP}^{\sigma^+} \\ E_2' &= E_1 + \hbar\delta\omega_{LP}^{\sigma^-} \\ E_3' &= \frac{\hbar}{2}\left(\delta\omega_{lp}^{\sigma^+} + \delta\omega_{lp}^{\sigma^+} \pm \sqrt{(\delta\omega_{lp}^{\sigma^+} - \delta\omega_{lp}^{\sigma^-})^2 + 16\beta^2/a^2\hbar^2}\right), \end{aligned} \tag{3.57}$$

it can be noticed that the $\sigma^{\pm}$ energy splitting is mapped into a transient blueshift of the eigenmodes of the systems. In particular, considering $\delta\omega^{\sigma\pm} = 0$, the experimental results studied in [1] are recovered. The complete control over a SOV state, by means of a Stark pulse, can be demonstrated by showing that is always possible to manipulate the state on the corresponding spin-orbit Poincaré sphere of Fig. 3.6, i.e. by demonstrating the possibility of moving from a certain eigenstate on one basis to every other state on the spheres. In Fig. 3.7, this is achieved by considering the spatial polariton distribution and the corresponding polarisation, during the Stark pulse, hence while the manipulation on the SOPS in Fig. 3.6(b) is occurring. In particular we demonstrate the manipulation from the $\boldsymbol{\psi_{AZ}}$ state to the $\boldsymbol{\psi_{RA}}$ state. We initialize the system, at $t = 0$ ps , in the $\boldsymbol{\psi_{AZ}}$ state, which is characterized by σ^+ and σ^- components having identical intensities, as is apparent from the polariton distribution and polarisation in the lower panel in Fig. 3.7. The manipulation can be performed by making use of two Stark pulses, both σ^+-polarised and red-detuned. The first Stark pulse, which arrives at $t = t_{st}^1 = 6.58$ ps, is used to flip the spin-orbit vector from the state in the north pole of the sphere, to the equatorial line. Here the

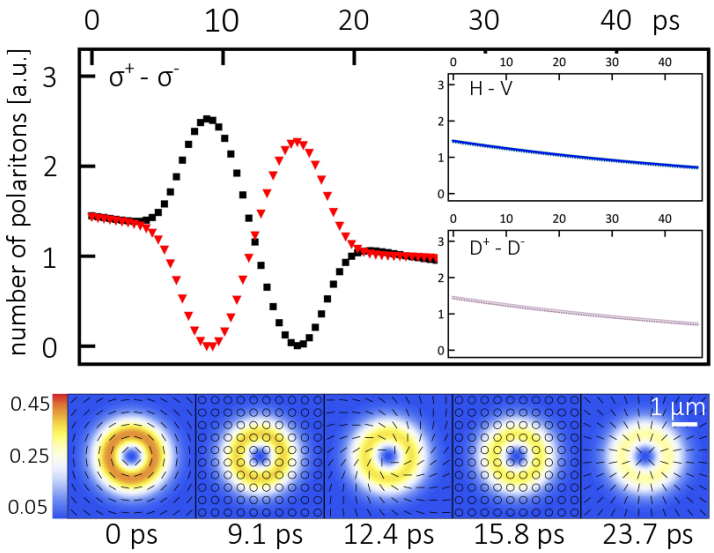

Figure 3.7: From [2]. Control of the SOV using a Stark pulse on the states of the SOPS. Upper panel (main): the population of polariton, for σ^+ and σ^- polarisation. Upper panel (side): population difference of polaritons for H, V and $D^{\pm}$ polarisation, which stays always identical during this control protocol. The presence of the decay term in the equations, induces a dissipation of the population, as expected. Lower panel: intensity distribution (colors) and polarisation (lines) evaluated at different times. The manipulation is performed via two σ^+ polarised Stark pulses, whose effect can be obtained by a time dependent shift of the σ^+-polarised polariton with $\sigma_{st} = 1$ ps and $\hbar\delta\omega^{\sigma^+} = 0.4$ meV, and centred at $t^1_{st} = 6.58$ and $t^2_{st} = 18.15$ ps. The parameters used here and everywhere else, unless otherwise specified, are: $m_{LP} = 2.4 \times 10^{-5} m_e$, where m_e is the mass of the electron, $\omega_h = 4.0\ ps^{-1}$, $\beta = 0.04$ meVμm^2, $\gamma_{LP} = 0.02$ meV.

finite energy splitting between the poles induces the precession of the state vector, which moves it from a σ^+-polarised to a σ^--polarised vortex. Next we make use of another pulse, which arrives at $t = t^2_{st} = 18.15$ ps, to flip the spin-orbit vector from the equator to the $\boldsymbol{\psi_{RA}}$ state. This process can be visualized by considering the population in different states as in Fig. 3.7. The spin-orbit vector then starts to precess, between t^1_{st} and t^2_{st}, oscillating around σ^+-polarised state and σ^--polarised state. This is clear when looking at the upper panel of Fig. 3.7, where the polariton population oscillates between the σ^+ and the σ^- components, and from the lower panels, showing polaritons at different times. Finally a second Stark pulse, again with σ^+-polarisation, which arrives when the state is halfway between the σ^- and the σ^+ vortex (i.e. at $\varphi_2 = 3\pi/2$ as showed in Fig. 3.6), flips the vector at the at the south pole. In fact, at that point, the $\sigma^{\pm}$ components are equal again, and the

polariton distribution and polarisation matches exactly with the one expected for a $\boldsymbol{\psi_{RA}}$ state.

The strategy, proposed above, for the manipulation of a SOV is not unique: for example it is possible to obtain the same result using σ^+ Stark pulses with different intensities, so that the SOV first flips to a non-zero latitude and then to the south or north pole. Furthermore, the same manipulation can be achieved by implementing two Stark pulses having σ^- polarisation or pulses with opposite circular polarisations, and this equivalence can be easily understood if we notice that the σ^- pulse induce a rotation in the opposite direction of the σ^+ polarised pulse. In fact, if the spin-orbit vector considered is at $\varphi_2 = 3\pi/2$, a σ^- polarised Stark pulse would flip it to the north pole, i.e. in the opposite direction of a σ^+ pulse, while if the state is in $\varphi_2 = \pi/2$, the same pulse would flip it to south pole.

The full control of the SOV is achieved by Stark pulses with no particular spatial structure or orbital angular momentum: this is due to the fact that any spin-orbit vector, on a defined sphere, is spanned by a linear superposition of σ^+ and σ^-, having relative magnitudes which vary on the horizontal axis of the sphere, with $\varphi_2 = 0$ corresponding to a pure σ^+ state and $\varphi_2 = \pi$ corresponding to a pure σ^-. Hence a σ^+ or σ^- polarised Stark pulse is sufficient to generate an energy splitting of the points on the sphere having $\varphi_1 = \pi/2$, $\varphi_2 = 0$ and $\varphi_1 = \pi/2$, $\varphi_2 = \pi$, and to the consequent precession of the vector around the axis. By the same argument, linearly polarised Stark pulses cannot be used to move the spin-orbit vector on the sphere, since for any given polarisation angle, all the SOVs states on this sphere will have the same amount of linearly polarised components. The same argument applies on the SOPS with $\boldsymbol{\psi_{RA}}$ and $\boldsymbol{\psi_{HY1}}$ as south and north poles, as depicted Fig. 3.6(c): here the states are made by linear combinations of horizontal-vertical polarisations, hence in order to control the SOV on this particular sphere, it is possible to make use of Stark pulses having H and V polarisation. Using D^+ and D^- polarised pulses it is possible to manipulate every state on the SOPS spanned by $\boldsymbol{\psi_{RA}}$ and $\boldsymbol{\psi_{HY2}}$ at the poles, as depicted in Fig. 3.6(d). Hence a full control of the SOV is made

possible by the use of polarised Stark pulses, each of them acting independently on different SOPS.

We now focus on the radial and the hyperbolic anti-vortex, considering the sphere having these two states as north and south pole. The spin-orbit vectors on this sphere can be written in the following parametric form:

$$|\boldsymbol{\psi_d}\rangle = \left[\cos\left(\frac{\phi_1}{2}\right) e^{-i\frac{\phi_2+\pi}{2}} |\boldsymbol{\psi_{HY2}}\rangle + \sin\left(\frac{\phi_1}{2}\right) e^{i\frac{\phi_2+\pi}{2}} |\boldsymbol{\psi_{RA}}\rangle\right]. \tag{3.58}$$

Using a H polarised Stark pulse, the state can be flipped from the pole to the equator and here it starts to precess, as a consequence of the separation in energy between the $\boldsymbol{\psi_{RA}}$ and the $\boldsymbol{\psi_{HY1}}$ states: however, as can be seen by comparing the upper panel of Fig. 3.7 with the upper panel of Fig. 3.8, as this splitting is smaller with respect to the previous case, the precession at the equator will be slower. Setting the energy splitting between the $\boldsymbol{\psi_{AZ}}$ and the $\boldsymbol{\psi_{RA}}$ states [Fig. 3.6(b) and Fig. 3.7] as ΔE = 0.306 meV, we obtain a corresponding period of precession of 13.4 ps. The splitting between the $\boldsymbol{\psi_{RA}}$ and the $\boldsymbol{\psi_{HY1}}$ states [Fig. 3.6(c) and Fig. 3.8] is ΔE = 0.15 meV, which gives a corresponding period of precession of 26.8 ps. We implement here the same strategy as before, making use of a second pulse: once the SOV, during its rotation on the equator of the SOPS, reaches the middle point ($\varphi_2 = 3\pi/2$) between the H and the V-polarised states, shifting the H-polarised component of exciton line, induces a flip of the SOV toward the north-pole of the sphere, corresponding to the $\boldsymbol{\psi_{HY1}}$ state.

We notice here that all the considered SOPS spheres have the $\boldsymbol{\psi_{RA}}$ state as south pole: this fact allows, in principle, to move the spin-orbit vector on any possible sphere, by applying a sequence of Stark pulses, with diverse polarisations. This demonstrates the possibility of a complete manipulation of the SOV, by means of Stark pulses.

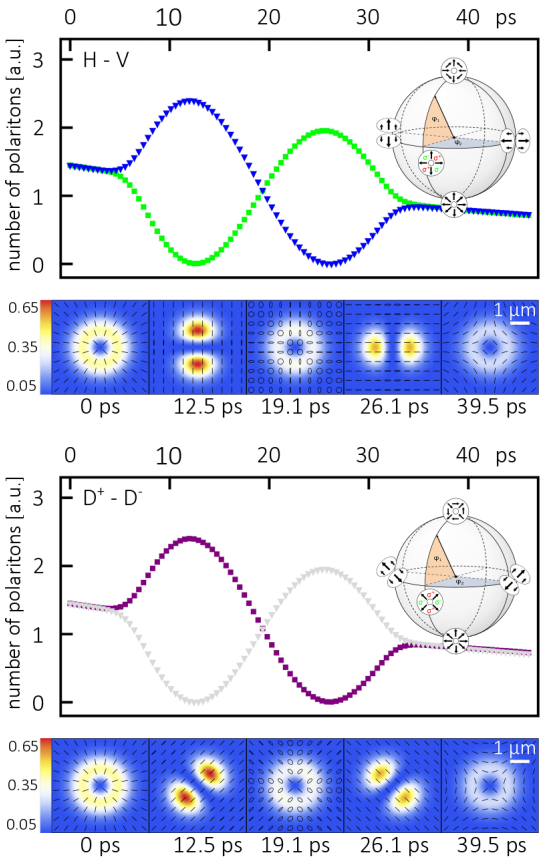

Figure 3.8: From [2]. Control of the SOV using a Stark pulse on the states of the SOPS. Upper panel: the population of polaritons, for H and V polarisation, in the main panel and the corresponding polariton intensity distributions and polarisation. Lower panel: Population in the D_+, D_- basis and the corresponding polariton intensity distribution, during the manipulation of the SOPS. The presence of the decay term in the equations, induces a dissipation of the population, as expected. The manipulation is performed via two H (D^+)-polarised Stark pulses, whose effect can be obtained by a time dependent shift of the polaritons with $H(D^{\pm})$ polarisation, with the following characteristics, σ_{st} = 1 ps and $\hbar\delta\omega^{\sigma^+}$ = 0.4 meV, and centred at t^1_{st} = 6.58 and t^2_{st} = 32.1 ps.

3.3.6 Strong TE-TM splitting

The manipulation proposed in the previous section can be achieved for wide ranges of the parameters: however their mutual dependence may affects the dynamics significantly, in particular concerning the amplitude of the energy shift, its duration and timing. To demonstrate this fact, we show here that by increasing the values of the TE-TM splitting strength β and considering longer polariton lifetimes, it is possible to perform more operations to manipulate the SOV. It is possible to change the value of the splitting by changing the detuning of the cavity mode with respect

to the stop band of the Bragg mirrors, as shown in [61]. Moreover, it is possible to obtain different value for the TE-TM splitting making use of different materials, such as organic structures [62], or considering different geometries like tunable open microcavities [1].

As an example of this, we consider $\beta = 0.006$ meVμm^2. As the energy splitting of

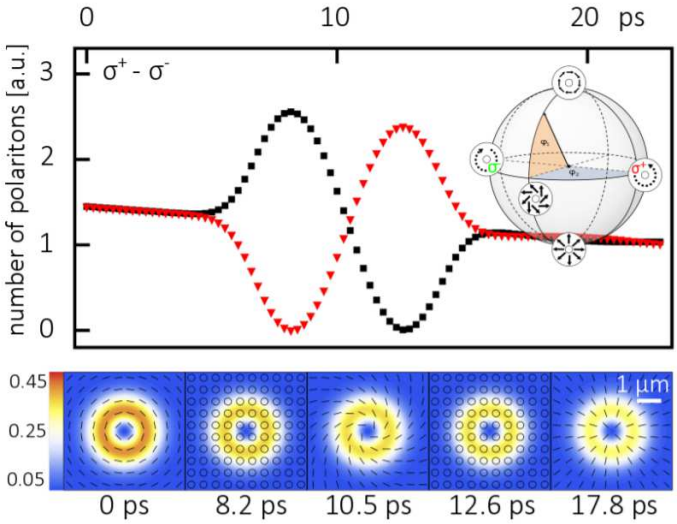

Figure 3.9: From [2]. Control of the SOV using a Stark pulse on the states of the SOPS, initially in $\boldsymbol{\psi_{AZ}}$. Top panel: the population of polaritons, for σ^+, σ^- polarisation. The presence of the decay term in the equations, induces a dissipation of the population, as expected. Lower panel: intensity distribution (colors) and polarisation (lines) taken for various times. The manipulation is performed via two σ^+ polarised Stark pulses, whose effect can be obtained by a time dependent shift of the σ^+-polarised polariton with $\sigma_{st} = 1$ ps and $\hbar\delta\omega^{\sigma^+} = 0.6$ meV, and centred at $t^1_{st} = 6.58$ and $t^2_{st} = 14.15$ ps. Here we consider a TE-TM splitting strength of $\beta = 0.006$ meVμm^2

the levels is bigger, a more intense Stark shift is necessary to manipulate the state. Moreover, the state precesses faster at the equator, compared to the previous case, with smaller β, hence the time window to perform a manipulation is shorter. For $\beta = 0.006$ meVμm^2, as shown in Fig.(3.9) the manipulation is performed in 10 ps, hence faster than the 15 ps needed for the previous case in Fig.(3.7).

Chapter 4

Statistical properties of nonlinear dissipative systems

In this Chapter, we show some of the main results of the research carried out during the Ph.D., concerning quantum effects in nonlinear driven-dissipative systems. Polaritons, which have been introduced in the previous Chapter, provide a useful system to explore such effects, first because of the presence of polariton-polariton interaction, which act as a source of weak nonlinearity in the dynamical evolution equations, and second due to their driven-dissipative nature. However, the results presented here go beyond polaritonics and find application in different branches of physics, ranging from quantum optics to cold atoms. In the first part of this Chapter, we provide an analytical method to find the correlation function of a single Kerr-oscillator, in a driven dissipative regime, using the P-representation. We extend the result numerically, analysing the dynamics under pulsed excitations: here a discussion about the choice of a proper *gauge* representation is necessary. Then we present the same results for a multimode system: in particular we focus on a soliton-state, i.e. a state which is "shape-preserving", arising from the interplay between the repulsive interaction and a negative effective-mass. Such states have been observed experimentally in polariton systems.

4.1 Single-mode case

The single mode Hamiltonian for a bosonic Kerr oscillator is:

$$H = H_0 + H_p + H_{nl}, \tag{4.1}$$

where:

$$\begin{aligned} H_0 &= \omega_0 a^\dagger a \\ H_p &= f a^\dagger e^{-i\omega_p t} + f^* a e^{i\omega_p t} \\ H_{nl} &= \frac{g}{2} a^\dagger a^\dagger a a, \end{aligned} \tag{4.2}$$

which are, respectively, the bosonic field energy, the coherent driving term and the nonlinear Kerr interaction. As we pointed out in Chapter 3, if we consider a single $\boldsymbol{k}$ and we neglect the saturation effect, the above model is suitable for describing a single mode polariton field in a microcavity. The density matrix for the system evolves due to the Hamiltonian, plus the coupling to a reservoir for the mode. We consider here the coupling to an empty reservoir, which leads to the leaking of photons from the cavity, derived in Chapter 2:

$$\partial_t \rho = -i[H, \rho] + \gamma(2a\rho a^\dagger - a^\dagger a \rho - \rho a^\dagger a). \tag{4.3}$$

The next necessary step to address the dynamics of (4.3) in phase-space is to write the density matrix making use of a suitable representation. In the following, we make use of the the P-representation, i.e. we consider the probability distribution for complex conjugate variables α and α^*, and we find analytically the statistical moments of the distribution in the linear regime: this approach gives exactly the same results as in the doubled Hilbert space of the Positive-P, but has the advantage of much simpler mathematics. The application of the conversion rules (2.94), leads

to:

$$\begin{aligned}
&\gamma(2a\rho a^\dagger - a^\dagger a\rho - \rho a^\dagger a) \to \gamma(\partial_\alpha \alpha + \partial_{\alpha^*}\alpha^*)P(\alpha,\alpha^*)\\
&-i\omega_0(a^\dagger a\rho - \rho a^\dagger a) \to -i\omega_0(-\partial_\alpha \alpha + \partial_{\alpha^*}\alpha^*)P(\alpha,\alpha^*)\\
&fe^{-i\omega_p t}(a^\dagger \rho - \rho a^\dagger) \to ife^{-i\omega_p t}\partial_\alpha P(\alpha,\alpha^*) - ife^{i\omega_p t}\partial_{\alpha^*}P(\alpha,\alpha^*),
\end{aligned} \tag{4.4}$$

while for the Kerr nonlinearity, we find terms containing the second derivative in α and α^*, which will enter into the diffusion matrix:

$$-i\frac{g}{2}(a^\dagger a^\dagger aa\rho - \rho a^\dagger a^\dagger aa) \to -ig(-\partial_\alpha|\alpha|^2\alpha + \partial_{\alpha^*}|\alpha^*|^2\alpha^* + \frac{1}{2}\partial^2_{\alpha^2}\alpha^2 + \frac{1}{2}\partial^2_{\alpha^{*2}}\alpha^{*2})P(\alpha,\alpha^*). \tag{4.5}$$

Gathering all the these terms together, we can reconstruct the Fokker-Planck equation for $P(\alpha,\alpha^*)$:

$$\begin{aligned}
\partial_t P(\alpha,\alpha^*) = &-\partial_\alpha(-\gamma\alpha - i\omega_0\alpha - ife^{-\omega_p t} - ig|\alpha|^2\alpha)P(\alpha,\alpha^*) + \frac{1}{2}\partial^2_{\alpha^2}(-ig\alpha^2)P(\alpha,\alpha^*) +\\
&-\partial_{\alpha^*}(-\gamma\alpha^* + i\omega_0\alpha^* + ife^{\omega_p t} + ig|\alpha|^2\alpha^*)P(\alpha,\alpha^*) + \frac{1}{2}\partial^2_{\alpha^{*2}}(ig\alpha^{*2})P(\alpha,\alpha^*).
\end{aligned}$$

4.1.1 Langevin equation

As extensively explained in Chapter 2, equation (4.6) is exactly equivalent to a Fokker-Planck equation: hence we can derive the drift and diffusion matrix, A and D, which can be cast in a system of stochastic Langevin equations:

$$\partial_t \begin{pmatrix} \alpha \\ \alpha^* \end{pmatrix} = A(\alpha,\alpha^*)\begin{pmatrix} \alpha \\ \alpha^* \end{pmatrix} + F(t) + \zeta(t), \tag{4.6}$$

where $\zeta(t) = (\zeta_\alpha\ \zeta_{\alpha^*})^T$, is a vector of delta-correlated random noise terms with correlation matrix:

$$D = \begin{pmatrix} -ig\alpha^2 & 0 \\ 0 & ig\alpha^{*2} \end{pmatrix}, \tag{4.7}$$

i.e., each element of the noise vector $\zeta(t)$ is defined such that: $\langle \zeta_i(t)\zeta_j(t')\rangle = \delta(t - t')D_{ij}$. The drift matrix, $A(\alpha, \alpha^*)$, in equation (4.6), has the following form:

$$A = \begin{pmatrix} -\gamma - i\omega_0 - ig|\alpha|^2 & 0 \\ 0 & -\gamma + i\omega_0 + ig|\alpha|^2 \end{pmatrix}, \tag{4.8}$$

while $F(t)$ is a diagonal matrix containing the driving terms. Writing down explicitly the equation (4.6) we obtain the Langevin equation for α:

$$\partial_t \alpha = (-\gamma - i\omega_0 - ig|\alpha|^2)\alpha - ife^{-\omega_p t} + \zeta_\alpha(t). \tag{4.9}$$

We recall at this point that, using the P-representation, we transformed the master equation for the density operator in an equivalent system of stochastic differential equations for the random variable α. The dynamics of the random variable is described by a classical trajectory α_c, together with the fluctuations $\tilde{\alpha}$, local in time, which describe the quantum corrections:

$$\alpha = \alpha_c + \tilde{\alpha}. \tag{4.10}$$

By taking the ensemble average of each equation, over many realization of the stochastic process, such that the fluctuations are zero, we can derive the mean field equations. Writing $\langle \alpha_c \rangle = \psi$, we obtain:

$$\partial_t \psi = -\gamma\psi - i\omega_0\psi - ife^{-i\omega_p t} - ig|\psi|^2\psi, \tag{4.11}$$

and a similar result is obtained for the equation with α^*. To get rid of the time-dependence in the pump term, we transform the field $\psi \to \psi e^{-i\omega_p t}$, and this replaces the ω_0 term with the bare detuning, $\delta_0 = \omega_0 - \omega_p$. Doing this, we transform equation (4.11) to:

$$\partial_t \psi = -\gamma\psi - i\delta_0\psi - if - ig|\psi|^2\psi, \tag{4.12}$$

and considering the steady state ($\partial_t \psi = 0$), after multiplying the equation by its

complex conjugate, we get:

$$|f|^2 = \left[\gamma^2 + (\delta_0 + g|\psi|^2)^2\right]|\psi|^2, \tag{4.13}$$

which is formally identical to equation (3.34). Hence we recover the bistable behaviour and the S-curve, for $\delta_0 \geq \sqrt{3}\gamma$. Having found the classical solution, we next want to expand the Langevin equation for the quantum system, so that the variables considered are the fluctuations, $\tilde{\alpha}$ around the classical solution. The approach developed here allows the calculation of the statistical moments, as long as the fluctuations are small compared to the field amplitudes: this means that, in the presence of optical bi-stability, as the mean field "jumps" suddenly from low to high density, the method is faulty and it gives a divergent behaviour of the moments. In that case we will need to use numerical methods, which will be discussed in the next section.

We choose to scale the fluctuations by the classical solution, $\alpha \to (\psi + \psi\tilde{\alpha})$, and then we expand to the first order in the fluctuation term, in order to get a tractable linear set of equations. Hence we get the linearised non linear term:

$$|\alpha|^2\alpha = |\psi|^2\psi(1+\tilde{\alpha})(1+\tilde{\alpha}^*)(1+\tilde{\alpha}) \approx |\psi|^2\psi(2\tilde{\alpha}+\tilde{\alpha}^*), \tag{4.14}$$

where we have discarded the terms at the second order in the fluctuations, $\tilde{\alpha}^{*2}$ and $\tilde{\alpha}^2$. Making use of this approximation on the Langevin equation (4.9), it is possible to obtain the equation for the fluctuations:

$$\partial_t\tilde{\alpha} = (-\gamma - i\delta)\tilde{\alpha} - ig|\psi|^2(\tilde{\alpha}+\tilde{\alpha}^*) + \zeta_{\tilde{\alpha}}(t), \tag{4.15}$$

where $\delta = \delta_0 + g|\psi|^2$ is the detuning inclusive of the blue-shift term. We now want to convert these fluctuations to polar coordinates:

$$\tilde{\alpha} = \psi(1+j)e^{-i\theta}, \tag{4.16}$$

with modulus $\psi(1+j)$ and phase θ. For small fluctuations we can perform a Taylor

expansion of the exponential, to get:

$$\tilde{\alpha} \approx \psi(1 + j - i\theta). \tag{4.17}$$

If we compare the expression in (4.17), with the definition of the scaled fluctuations, $\alpha \to (\psi + \psi\tilde{\alpha})$, it is easy to see that the real and imaginary part of $\tilde{\alpha}$ are, respectively, j and $-\theta$. The term ψ, being the classical mean field solution, will follow the equation of motion (4.11). Hence the equations for j and θ can be obtained from (4.15):

$$\partial_t j = -\gamma j - \delta\theta + \eta(t) \tag{4.18}$$

$$\partial_t \theta = -\gamma\theta + (\delta + 2g|\psi|^2)j + \xi(t), \tag{4.19}$$

where we have normalized everything to the classical solution ψ. From the above argument, it follows that the noise terms for j and θ have the expressions:

$$\begin{aligned} \eta &= \mathrm{Re}(\zeta_{\tilde{\alpha}}) = \frac{1}{2}\left(\frac{\zeta_{\tilde{\alpha}}}{\psi} + \frac{\zeta_{\tilde{\alpha}^*}}{\psi^*}\right) \\ \xi &= \mathrm{Im}(\zeta_{\tilde{\alpha}}) = \frac{1}{2}i\left(\frac{\zeta_{\tilde{\alpha}}}{\psi} - \frac{\zeta_{\tilde{\alpha}^*}}{\psi^*}\right), \end{aligned} \tag{4.20}$$

and they have the physical meaning of the normalized intensity and phase fluctuations, respectively. The correlations between the ζ noise terms was given by the original D matrix, hence, we can derive the intensity-phase noise matrix using the following expressions:

$$\langle\eta\eta\rangle = \frac{1}{4}\left(\frac{1}{\psi^2}\langle\zeta_{\tilde{\alpha}}\zeta_{\tilde{\alpha}}\rangle + \frac{1}{\psi^{*2}}\langle\zeta_{\tilde{\alpha}^*}\zeta_{\tilde{\alpha}^*}\rangle\right) = \frac{1}{2}\mathrm{Re}(-ig) = 0 \tag{4.21}$$

$$\langle\xi\eta\rangle = \frac{1}{4}i\left(\frac{1}{\psi^2}\langle\zeta_{\tilde{\alpha}}\rangle\zeta_{\tilde{\alpha}} - \frac{1}{\psi^{*2}}\langle\zeta_{\tilde{\alpha}^*}\zeta_{\tilde{\alpha}^*}\rangle\right) = -\frac{1}{2}\mathrm{Im}(-ig) = \frac{g}{2} \tag{4.22}$$

$$\langle\xi\xi\rangle = -\langle\eta\eta\rangle = 0. \tag{4.23}$$

By doing this, we obtain the diffusion matrix in polar coordinates:

$$D_{j-\theta} = \frac{1}{2}g\begin{pmatrix} 0 & 1 \\ 1 & 0 \end{pmatrix}, \tag{4.24}$$

and the drift matrix:

$$A_{j-\theta} = \begin{pmatrix} -\gamma & -\delta \\ (\delta + 2g|\psi|^2) & -\gamma \end{pmatrix}. \tag{4.25}$$

4.1.2 The second order correlation function

We now wish to evaluate, following the derivation in the previous section, the second order correlation function for the single driven dissipative Kerr oscillator, defined as [8]:

$$g^{(2)}(0) = \frac{\langle \alpha^*(t)\alpha^*(t+\tau)\alpha(t)\alpha(t+\tau)\rangle}{\langle \alpha^*(t)\alpha(t)\rangle^2}. \tag{4.26}$$

In particular, we are interested in obtaining an analytical expression for the second order correlation function at time delay $\tau = 0$:

$$g^{(2)}(0) = \frac{\langle \alpha^*(t)\alpha^*(t)\alpha(t)\alpha(t)\rangle}{\langle \alpha^*(t)\alpha(t)\rangle^2} = \frac{\langle |\alpha(t)|^4\rangle}{\langle |\alpha(t)|^2\rangle^2}. \tag{4.27}$$

In terms of the classical fields and of the fluctuations, the above expression reads:

$$g^{(2)}(0) = \frac{\langle |\alpha(t)|^4\rangle}{\langle |\alpha(t)|^2\rangle^2} = \frac{|\psi|^4 \langle (1+j)^4\rangle}{(|\psi|^2 \langle (1+j)^2\rangle)^2} \approx 1 + 4\langle j^2\rangle . \tag{4.28}$$

What is needed now is the variance $\langle j^2\rangle$ for the intensity fluctuations. To obtain this, we first diagonalize the $A_{j-\theta}$ matrix for the fluctuations (4.25). The eigenvalues of $A_{j-\theta}$ are:

$$\lambda_\pm = -\gamma \pm i\sqrt{\delta(\delta + \tilde{g})}, \tag{4.29}$$

with $\tilde{g} = 2g|\psi|^2$, and the corresponding eigenvectors:

$$E_\pm = \frac{1}{\sqrt{2\delta + g}} \begin{pmatrix} \sqrt{\delta} \\ \mp i\sqrt{\delta + g}. \end{pmatrix} \tag{4.30}$$

The matrix S which diagonalises $A_{j-\theta}$ is then given by:

$$S = \frac{1}{\sqrt{2\delta + g}} \begin{pmatrix} \sqrt{\delta} & \sqrt{\delta} \\ -i\sqrt{\delta + \tilde{g}} & i\sqrt{\delta + \tilde{g}} \end{pmatrix}. \tag{4.31}$$

By defining $\boldsymbol{x} = (j, \theta)^T$ and $\boldsymbol{f}(t) = (\eta(t), \xi(t))$, we can write formally eq. (4.18) as:

$$\partial_t \boldsymbol{x} = A\boldsymbol{x} + \boldsymbol{f}(t), \tag{4.32}$$

which, by defining $u = S^{-1}x$, has the standard solution:

$$u_i(t) = u(0)e^{\lambda_i t} + \int_0^t dt' e^{\lambda_i (t-t')} \sum_{i'} S^{-1}_{ii'} f_i(t'). \tag{4.33}$$

By multiplying equation (4.33) with itself, and taking the average value, we obtain expressions containing $\langle f_i f_{i'} \rangle$, which represent elements of the $D_{j-\theta}$ matrix. Hence, we can express the correlation functions in the following way:

$$\langle u_i(t_1) u_k(t_2) \rangle = (S^{-1} D_{j-\theta} S^{-1T})_{i,k} \int_0^{t_1} dt_1' \int_0^{t_2} dt_2' e^{\lambda_i (t_1 - t_1')} e^{\lambda_k (t_2 - t_2')} \delta(t_1' - t_2'). \tag{4.34}$$

Evaluating the integrals in (4.34), the correlations in the u variables is:

$$\langle u_i(t_1) u_k(t_2) \rangle = -(S^{-1} D_{j-\theta} S^{-1T})_{i,k} \frac{1}{\lambda_i + \lambda_k} \begin{cases} e^{\lambda_i (t_1 - t_2)}, & \text{if } t_1 > t_2 \\ e^{\lambda_j (t_2 - t_1)}, & \text{if } t_2 > t_1. \end{cases} \tag{4.35}$$

The equation above, for $t_1 = t_2$, gives the *covariance matrix* $\tilde{V}$. The covariance matrix contains the information about the variances of the random variables, on the diagonal, and the covariances between them. In fact, in the u_i basis:

$$\tilde{V} = \begin{pmatrix} \langle u_1 u_1 \rangle - \langle u_1 \rangle^2 & \langle u_1 u_2 \rangle - \langle u_1 \rangle \langle u_2 \rangle \\ \langle u_1 u_2 \rangle - \langle u_1 \rangle \langle u_2 \rangle & \langle u_2 u_2 \rangle - \langle u_2 \rangle^2 \end{pmatrix}, \tag{4.36}$$

which, making use of the expressions in (4.35), gives:

$$\tilde{V} = (S^{-1} D_{j-\theta} S^{-1T}) \begin{pmatrix} -\frac{1}{2\lambda_+} & -\frac{1}{\lambda_+ + \lambda_-} \\ -\frac{1}{\lambda_+ + \lambda_-} & -\frac{1}{2\lambda_-} \end{pmatrix} = ig \frac{2\delta + g}{4\sqrt{\delta(\delta + \tilde{g})}} \begin{pmatrix} -\frac{1}{2\lambda_+} & 0 \\ 0 & -\frac{1}{2\lambda_-} \end{pmatrix}. \tag{4.37}$$

From (4.37), going back into the (j, θ) basis through the inverse transformation $\boldsymbol{x} = S\boldsymbol{u}$, we obtain the covariance matrix for the intensity and phase fluctuations, V,

which has the general form:

$$V = \begin{pmatrix} \langle j^2 \rangle & \langle j\theta \rangle \\ \langle j\theta \rangle & \langle \theta^2 \rangle \end{pmatrix}. \tag{4.38}$$

Hence, to evaluate (4.28), we need the first element of V, which, from equation (4.37), is found to be:

$$\langle j^2 \rangle = ig \frac{\delta}{4\sqrt{\delta(\delta+\tilde{g})}} \left(-\frac{1}{2\lambda_+} + \frac{1}{2\lambda_-} \right) = -\frac{g}{4} \frac{\delta}{\gamma^2 + \delta(\delta+\tilde{g})}. \tag{4.39}$$

By substituting the above result in the expression for the $g^{(2)}(0)$ function, we obtain:

$$g^{(2)}(0) = 1 - g\frac{\delta}{\gamma^2 + \delta(\delta+\tilde{g})} = 1 - g\frac{\delta_0 + g|\psi|^2}{\gamma^2 + (\delta_0 + g|\psi|^2)(\delta_0 + 3g|\psi|^2)}, \tag{4.40}$$

which is the expression for the second order correlation function for a single driven-dissipative Kerr-oscillator with small nonlinearities. The sign of $g^{(2)}(0) - 1$ depends on the sign of the blue shifted detuning δ: when $\delta < 0$, increasing the population pulls the system closer to resonance, so bunching is expected. On the contrary, when

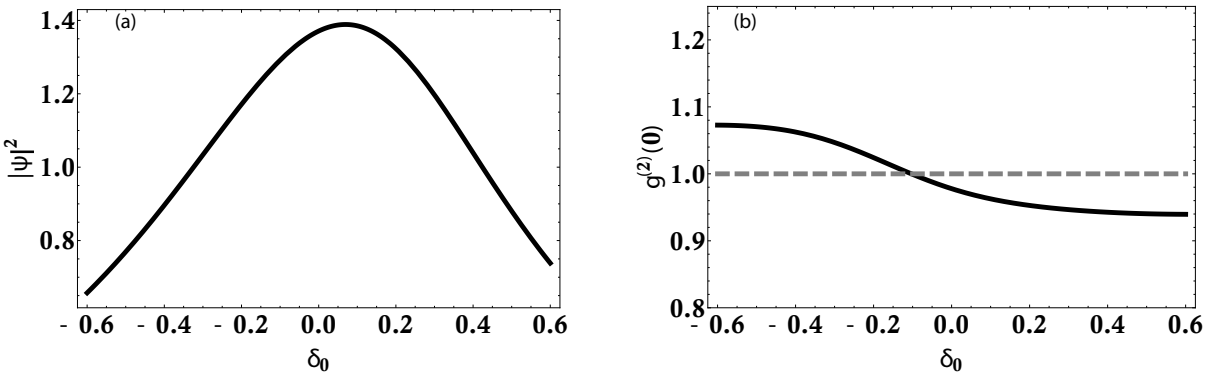

Figure 4.1: (a) Number of particles and (b) $g^{(2)}(0)$ function, for the steady state of equation (4.12), as a function of the cavity-laser detuning δ_0. The pump intensity is fixed, $|f|^2 = 0.9$, and the decay and nonlinearity are respectively $\gamma = 0.6$ and $g = 0.08$. For positive detuning the system is always antibunched. For negative detuning there are regions where bunching is expected.

$\delta > 0$, increasing the population pushes the system away from resonance, leading to antibunching. This result is plotted in Fig. (4.1)(b), where we have fixed the value of the pump intensity and calculated the steady state population(Fig. (4.1)(a)) as

a function of δ_0: $g^{(2)}$ is mostly bunched when $\delta_0 < 0$, while is antibunched for $\delta_0 > 0$.

4.1.3 Stochastic simulation of a single mode

The approach developed in the last section is exact in the limit of a small non-linearity, as we treated the linearised version of the original system of equations. For a single Kerr oscillator, when the detuning $\delta_0 > \sqrt{3}\gamma$, a bistable response is expected: in this regime, as the system jumps discontinuously to the higher occupied state, the linearisation is not applicable, hence the linear equation fails to describe properly the relevant moments of the system. To address the dynamics of the Kerr oscillator in the bistable regime, we need to solve numerically the set of stochastic differential equations (4.6). To guarantee that the diffusion process is always positive semidefinite we move to the positive P-representation, as we showed in Chapter 2: notice that this operation can be easily done by introducing a new phase space variable instead of the complex conjugate of α, i.e., by replacing $\alpha^* \to \beta$. The stochastic differential equations for $\boldsymbol{\alpha} = (\alpha, \beta)$ are then given by:

$$d\boldsymbol{\alpha} = A(\boldsymbol{\alpha}, t)dt + \sum_{ij} B_{ij}(\boldsymbol{\alpha}, t)dW_j(\boldsymbol{\alpha}, t), \tag{4.41}$$

where $dW_j(\boldsymbol{\alpha}, t)$ is the Wiener increment with zero means, satisfying, at each t:

$$\langle dW_i(t)dW_j(t')\rangle = \delta_{ij}\delta(t - t')dt. \tag{4.42}$$

To avoid moving singularities and/or boundary terms arising from the drift and diffusion matrices in the Fokker-Planck equation, we further modify the stochastic evolution, implementing the gauge P-representation. For the particular example of a single driven-dissipative Kerr oscillator, whose dynamical evolution is described by the master equation (4.3), the gauge P-representation in Ito's form is:

$$d\alpha = i\delta\alpha dt - 2ig\alpha^2\beta dt - \frac{\gamma}{2}\alpha dt + f dt + \sum_k B'_{1k}(dW_k - g_k dt) \tag{4.43}$$

$$d\beta = -i\delta\beta dt + 2ig\beta^2\alpha dt - \frac{\gamma}{2}\beta dt + f^* dt + \sum_k B'_{2k}(dW_k - g_k dt) \tag{4.44}$$

$$d\Omega = \Omega \sum_k g_k dW_k, \tag{4.45}$$

with $\delta = \omega_p - \omega$ the laser-mode detuning, where g_k are arbitrary diffusion gauge terms and the noise matrix B is the square root of the diffusion matrix D. In the limit of many trajectories, the statistical moments converge to the quantum mechanical mean values of the relevant quantities. One of the problems concerning the stochastic simulation of nonlinear systems is the rapid growth of statistical errors in the simulation. Even if the simulation can be performed with high accuracy when the number of trajectories is large enough, there might still be issues regarding the number of paths needed to obtain accurate results. For the Kerr oscillator, the uncertainty in phase-dependent observables, like squeezing, grows more than exponentially in time, and any simulation becomes useless, regardless of the number of trajectories. It is possible to demonstrate [32] that a well-behaved simulation, obtained by means of the positive P-representation, lasts for a time:

$$t_{\mathrm{sim}} \approx \frac{1.3 \pm 0.1}{g n^{2/3}}, \tag{4.46}$$

which for large occupation number, n, is not long enough for simulating meaningful time-windows where decoherence effects occur. This computational limitation of the positive P-representation was demonstrated by Drummond et al. in the example of simulation regarding evaporative cooling [63] . In a number of works, Drummond and Deuar [32], performed an extensive investigation on how to improve their effective simulation time, t_{sim}, with an appropriate choice of gauges. What they found is that combining drift and diffusion gauges, i.e., gauge fields acting both on the diffusion (B' in Eq. (4.43)) and on the drift terms (g_k in Eq. (4.43)) of the stochastic equations, gives the longest useful simulation time for highly occupied modes, with good precision beyond the point where the coherence has decayed. The rapid growth of statistical errors, which affect the useful simulation time, is not the only numerical problem concerning many-body stochastic simulations: another important issue is represented by moving singularities, i.e., a solution which diverges at finite times as a result of problems with numerics. Considering eq. (4.43), the equation for the

modulus for α is:

$$d|\alpha| = 2g|\alpha|^2|\beta|\sin(\theta_\alpha + \theta_\beta)dt + ..., \tag{4.47}$$

Deuar [64] demonstrated that, when $|\beta|\sin(\theta_\alpha + \theta_\beta)$ is positive, a moving singularity can occur, as $|\alpha|$ grows more than exponentially, leading to boundary term errors, i.e., errors arising from discarding non-negligible boundary term in any integration which involves the probability distribution.

Hence a suitable gauge needs to be chosen for (4.43), which is able to deal with two different problems: a rapid appearance of massive statistical errors, and systematic biases generated by moving singularities. Concerning the singularities, from equation (4.47), it is clear that the part which leads to a super exponential growth of the fields is the nonlinear term. As α and β are two different complex random variables, the associated number variable will have, in general, a real and an imaginary part, i.e., $n = \mathrm{Re(n)} + i\mathrm{Im(n)}$. It follows from equation (4.47) that the drift terms leading to moving singularities are:

$$\begin{aligned} d\alpha &= 2g\alpha\mathrm{Im}(n)dt..., \\ d\beta &= -2g\beta\mathrm{Im}(n)dt..., \end{aligned} \tag{4.48}$$

as the terms containing the real part of n will only affect the phase of α and β, hence they are harmless. We note here that for coherent states $\beta = \alpha^*$, as the P-distribution is a delta function in phase space, hence the imaginary part of n is always zero. It follows that, the more "quantum" is the state we are sampling, the more likely we are to end up with a moving singularity. The drift gauges g_k are then chosen such that the terms causing the instabilities (the imaginary part of the number variable) are cancelled by the correction. In particular we consider the gauges:

$$g_1 = -\sqrt{2ig}\mathrm{Im}(n)e^{-\Xi} \tag{4.49}$$

$$g_2 = -ig_1, \tag{4.50}$$

where the term $e^{-\Xi}$ is a suitable diffusion gauge, which will be treated in the fol-

lowing. These choices for the drift gauges cause an effective replacement in the stochastic equation,

$$\begin{aligned} -2ig\alpha ndt &\to -2ig\alpha \mathrm{Re}(n)dt \\ 2ig\beta ndt &\to 2ig\beta \mathrm{Re}(n)dt, \end{aligned} \tag{4.51}$$

which prevent the super-exponential growth of the fields, as demonstrated by [64], provided that a well behaved diffusion gauge Ξ is chosen. As mentioned before, the diffusion gauge is needed to improve the useful simulation times, which means that we want to be able to perform the simulation on time-scale of the order of the coherence time. It is important to stress here that this term Ξ is completely arbitrary and then there is not a unique way to optimise the results. In the following, we adopt the approach of Deuar and Drummond, where the local diffusion gauge is dependent on the optimal target time parameter, or precisely on the *remaining target time*, defined as:

$$t_{\mathrm{rem}} = \begin{cases} t_{\mathrm{opt}} - t, & \text{if} \quad t < t_{\mathrm{opt}} \\ 0, & \text{if} \quad t \geq t_{\mathrm{opt}}, \end{cases} \tag{4.52}$$

and is given by:

$$\Xi(t) = \frac{1}{6}\log(8|n(t)|^2 g t_{\mathrm{rem}} + \epsilon^{3/2}(n(t), \gamma t_{\mathrm{rem}})), \tag{4.53}$$

where,

$$\epsilon(n(t), \gamma t_{\mathrm{rem}}) = 1 + 4\mathrm{Im}(n)^2\left(\frac{1 - e^{-2\gamma t_{\mathrm{rem}}}}{2\gamma t_{\mathrm{rem}}}\right) - 2|n|^2\left(\frac{1 - 2\gamma t_{\mathrm{rem}} + 2(\gamma t_{\mathrm{rem}})^2 - e^{-2\gamma t_{\mathrm{rem}}}}{\gamma t_{\mathrm{rem}}}\right)$$

The diffusion gauge (4.53) shows statistical errors that are well controlled by the choise of the target time t_{opt}, hence we expect to the error to be small until the target time is explicitely reached, provided that this lies inside the useful simulation range. Drummond et al. [64] suggested an heuristic approach, which is here implemented, to optimize the simulation time. This goal can be achieved following the steps below:

- Choose an optimal time t_{opt} to be some time that one wants to be able to

simulate.

- Run a simulation and check how long useful observable estimates occur, $t_{\text{sim}}(t_{\text{opt}})$
- If $t_{\text{sim}}(t_{\text{opt}}) < t_{\text{opt}}$ then reduce t_{opt} to some value between $t_{\text{sim}}(t_{\text{opt}})$and t_{opt}. It should give a better simulation time. Hence run the simulation again, as indicated in the previous point. In case $t_{\text{sim}}(t_{\text{opt}}) \approx t_{\text{opt}}$ either keep the simulation or increase t_{opt} and perhaps obtain more simulation time, going back to the previous step.

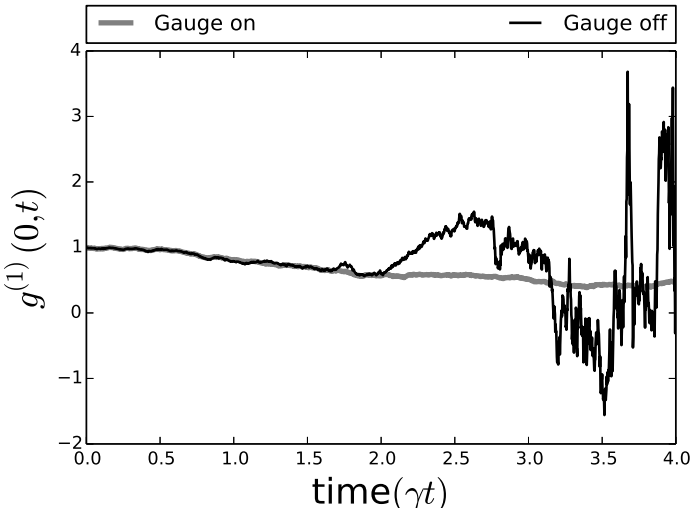

Figure 4.2: $g^{(1)}(0,t)$, first order coherence function, for a single mode Kerr oscillator, with $g = \gamma = 0.1$, driven resonantly by a continuous wave pump with intensity $I = 0.1$. The stochastic simulation without the proposed drift-diffusion gauge (black line) has a lower optimal time t_{opt} for the simulation, as the trajectory quickly diverges, compared to the case with the gauge on (gray line)

In Fig. (4.2), as an example of the computational usefulness of the propose gauge, we follow the example of [32], comparing the evolution of a normalised $g^{(1)}(0,t)$, i.e. the phase coherence function, for a single Kerr oscillator, with and without gauge terms: it is clear that the optimal simulation time t_{opt} increases when the gauge is on, compared to the scenario with no gauge, where a singularity appears.

Having determined an appropriate gauge to treat the system, we now find the value of the $g^{(2)}$ function for the steady states of system (4.43) as a function of the pump power $I = |f|^2$, in a regime where a bistable curve is expected, i.e. $\delta > \sqrt{3}\gamma$. The result is shown in Fig. (4.3) and it reproduces the results of Drummond et al.

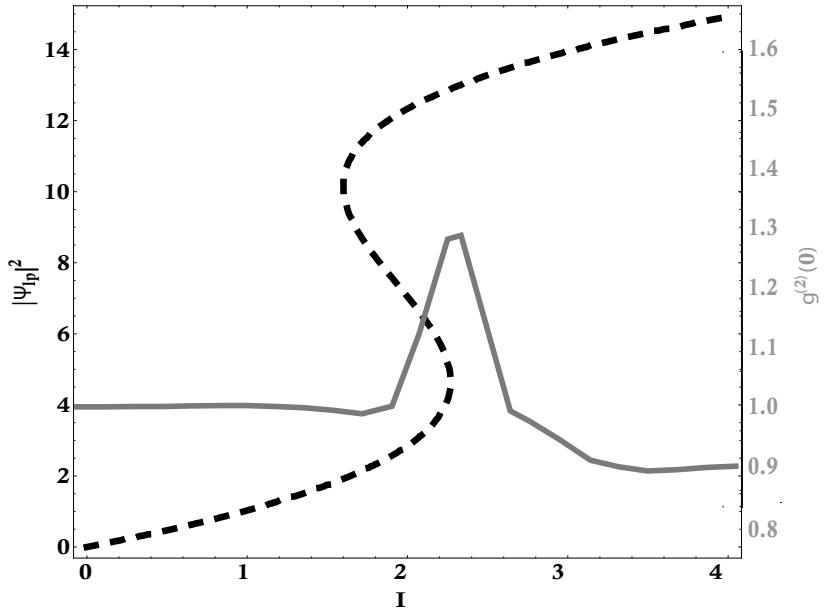

Figure 4.3: (Solid curve) Intensity profile of a single Kerr mode as a function of the CW pump intensity I, in the bistable regime, with g = 0.09, γ = 0.1 and δ = 0.2 > $\sqrt{3}\gamma$. (Dashed curve) $g^{(2)}(0)$ for the single mode: the system is super-Poissonian in the bistable region, as a consequence of the noise enhancement, while is sub-Poissonian in the upper branch of the S-curve.

in [65].

The $g^{(2)}$ value shows an increase near the transition point, as it depends on the variance of the fluctuations, which are enhanced by the random switching between the lower and apper branch of the bistable curve [8]. After the transition point, as the system is basically at resonance with the pump, antibunching is observed, as expected from the linearised analytic results. The magnitude of this antibunching is found to be strongly dependent on the nonlinear term g, in accordance with the analytical result showed in equation (4.40). Hence for polariton systems, where the nonlinearity is usually two order of magnitude smaller than the linewidth γ, we expect a small deviation from coherent statistics.

4.1.4 Pulsed excitation

The stochastic differential equations, (4.41), derived in the previous section, together with a suitable drift-diffusion gauge, enable us to quantify the dynamics of the relevant statistical moments of a bosonic system in presence of a time-dependent

driving field. This fact acquires a high significance for simulation of experiments, especially in quantum-optics, as a lot of experiments make use of lasers which emit pulses with a quasi-Gaussian profile. Practically, we change the constant driving

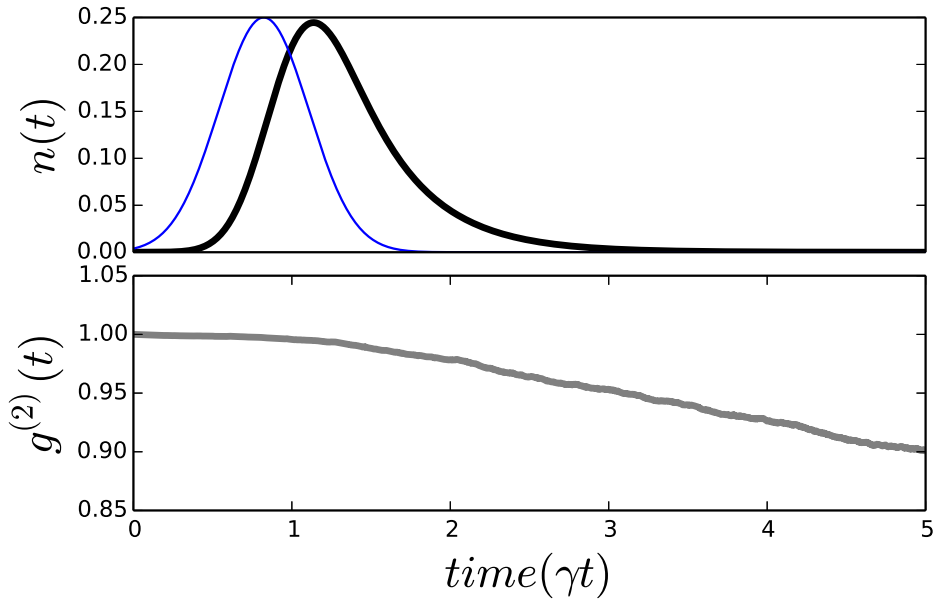

Figure 4.4: (Upper panel) Polariton population in a single mode dissipative system, with $\gamma = 0.05$ and $g = 0.01$, quasi-resonant with a pulsed pump, with maximum intensity $I = 0.25$. The blue line indicates the pulse profile. (Lower panel) $g^{(2)}(t)$ for the single mode: the system shows a sub-Poissonian statistics after reaching the maximum intensity.

field amplitude f in equation (4.41), to a function having a Gaussian profile in time:

$$f(t) = \sqrt{I} e^{-\frac{(t-t_0)^2}{2\sigma^2}},$$

where σ is the width and t_0 is the center of the pulse. As can be seen by looking at figure (4.4), as the number of particles, $n(t) = \langle \alpha\beta \rangle_{\text{stoch}}$ increases, the second order correlation function changes and it moves towards an antibunching regime. When the Gaussian pulse is over, the $g^{(2)}$ is stationary, i.e. it reaches a steady state: the reason behind this will be clarified in the next chapter, where we shall demonstrate that the $g^{(2)}$ function is constant in a system where the number of particles is conserved.

4.2 Quantum soliton in polariton systems

In the previous sections, we have derived and discussed the quantum properties, and specifically the appearance of antibunched light, in a single Kerr-like mode, with the claim that this is suitable for describing a single mode polariton field. However most realistic experimental systems deal with a collection of modes or with continuous systems: for example, photonic waveguides or monolithic microcavities are generally modelled via continuous variables approaches.

In this section we investigate the dynamics of correlation functions in multimode systems: specifically we are interested in the quantum properties of polariton solitons, which were observed experimentally, both in monolithic cavities [66] and in nonlinear waveguide systems [4]. To investigate numerically a multimode systems, we employ the strategy of the previous sections, i.e. we expand the master equation onto a multidimensional coherent basis deriving a set of stochastic differential equation, together with a suitable gauge field which prevents instabilities and sampling errors. We first consider a system made of coupled Kerr oscillators, described by the following Hamiltonian,

$$H = \sum_{i,j} (\omega_i a_i^\dagger a_i + g_i a_i^\dagger a_i^\dagger a_i a_i + \tau_{ij}(a_i^\dagger a_j + a_j^\dagger a_i)), \tag{4.54}$$

where ω_i are the energies of each mode and τ_{ij} is the adjacency matrix, quantifying the hopping probability between the i-th and j-th mode. Following the approach adopted in the previous sections, i.e. making use of the Gauge P representation, we obtain the system of stochastic differential equations:

$$d\alpha_i = i \sum_j (\tau_{ij}\alpha_j) + i\delta\alpha_i dt - 2ig\alpha_i^2\beta_i dt + \sum_k B_{1k}(dW_k - g_k dt) \tag{4.55}$$

$$d\beta_i = -i \sum_j (\tau_{ij}\beta_j) - i\delta\beta_i dt + 2ig\beta_i^2\alpha_i dt + \sum_k B_{2k}(dW_k - g_k dt) \tag{4.56}$$

$$d\Omega_i = \Omega_i \sum_k g_k dW_k. \tag{4.57}$$

The systems above will be used as a basic model to evaluate the statistical moments of multimode systems.

4.2.1 Polariton Solitons

Solitons are particular solutions of nonlinear equations which possess peculiar properties: namely they are non-spreading localized wavepackets and their shape is left unchanged when they interact with each other. Solitons were observed for the first time in a water canal, by John Scott Russell in 1863 [67]. Even though there exists a long list of different kinds of solitons, for our purposes we just mention two of them, namely *dark* and *bright* solitons: dark solitons are defined as a lack of intensity in a continuous beam, i.e., they show a reduction of the intensity compared to the bright background. Bright solitons by contrast, are localized intensity peaks above a less intense background. With technological advancements, it has been possible to observe solitons in a variety of systems, such as optical fibres [68], and Bose-Einstein condensates [69].

Non-spreading wave packets can be found in open quantum systems as well: here, as well as the balancing between the dispersion and the interaction, needed to obtain a stable solution, a balance between the loss and the gain is required. Such states are called *dissipative solitons*. Polariton solitons are generated in microcavity systems: due to the effective repulsive interaction, the formation of polariton dark solitons is allowed when $m_{\text{eff}} > 0$. Conversely, the formation of bright solitons requires a negative effective mass ($m_{\text{eff}} = (\partial_k^2 E(k))^{-1}$), which balances the spreading of the wavepaket due to the nonlinearity. From the polariton dispersion relation it is clear then that, to obtain a bright soliton, it is necessary to excite the system at $k \neq 0$. In [4], in an experimental work led by the University of Sheffield, conservative bright polariton solitons were observed in a AlGaAs/GaAs waveguide, with an embedded InGaAs quantum well. Such systems are assumed to be conservative, as the excitations, injected in the waveguide, propagate in the material through total internal reflection, hence minimizing the losses. The lower polariton branch has a negative effective mass for every k, allowing the formation of bright solitons. The initial quasi-Gaussian pulse, at low excitation power, starts to broaden, as an effect of the large polariton dispersion. However, when the pulse power is increased, the

output pulse narrows in time, which is a signature of the bright soliton formation.

In 2012, Sich et al. [66] demonstrated the formation of a bright dissipative polari-

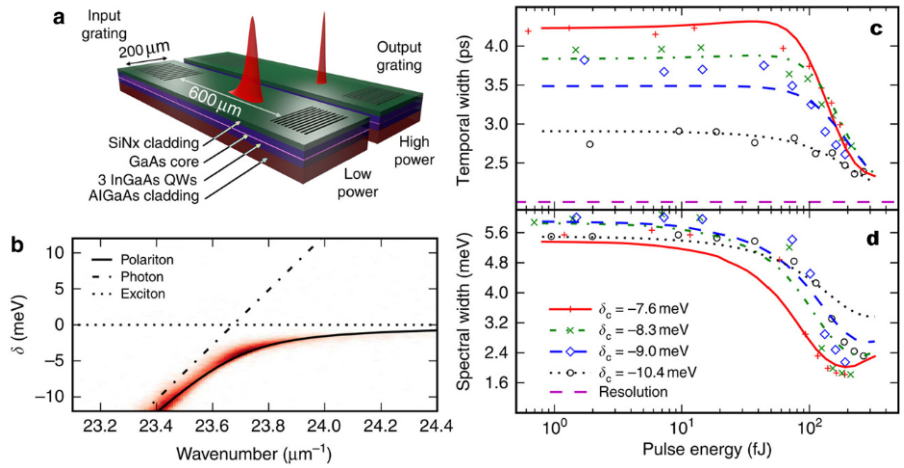

Figure 4.5: From [3]. (a) Schematic diagram of the waveguide system implemented in the experiment. (b)In red: the measured emitted light coming from the lower polariton mode. (c) Experimental and numerically temporal duration (pulsed regime) as function of the energy, for different detunings δ_C of the pulse frequency from the exciton.(d) Spectral width of the polariton as function of the pulse energy for equal detuning. The plot shows both the experimental measurements (in symbols) and the numerical simulations (lines) performed by [4].

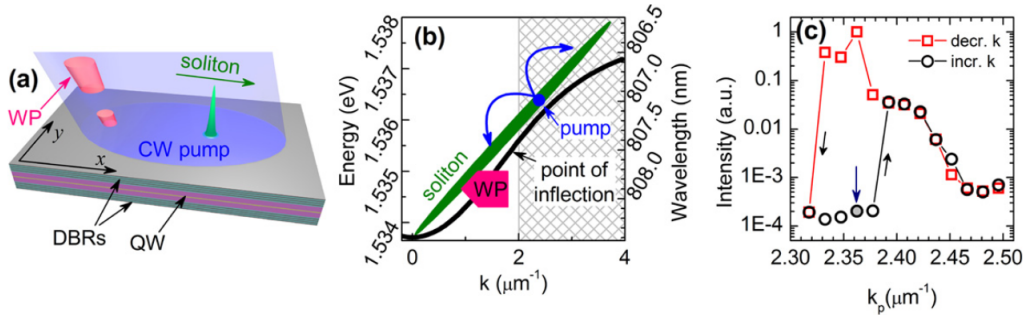

Figure 4.6: (a) Scheme of the experiment by Sich et al. [3]. A picosecond writing pulse (WP) (red) triggers the soliton pattern formation, on an area driven quasiresontantly by a weak CW pump. (b) The pumping scheme adopted, where the solid black line is the lower polariton dispersion. (c) Bistable behaviour of polariton intensity as a function of pump momentum.

ton soliton in a semiconductor microcavity with InGaAs quantum wells: Fig (4.6) shows the experimental setup designed by the authors and the results of part of the measurement performed. A CW quasi-resonant laser is applied at a k such that the effective mass is negative, i.e., close to the inflection point of the LP branch: this

writing Gaussian beam with a duration of 5 ps triggers the soliton formation. An additional weak CW pump, broad in space, sustains the soliton propagation: this step is necessary to allow an efficient experimental detection of the soliton state, before the losses destroys it. In this setup the localisation is taking place both in the x and in the y direction, as a consequence of the isotropy of the local polariton field, therefore a spatial 2D soliton is formed.

To investigate the quantum properties of polariton solitons, in the following we will refer to the last situation, without taking into account a sustaining driving field. As the localisation is happening simultaneously in both dimensions on the plane, we consider a cut along the y direction and then we analyse the whole temporal dynamics, giving a Gaussian wave-packet as initial condition.

4.2.2 Quantum model for 1D solitons

As anticipated in the previous section, in the following we consider a quantum model for bright soliton, following the experimental results obtained by Sich et al. As mentioned in the previous section, the geometry and the phenomenological features of the 2D-polariton solitons, allows us to treat the system in one spatial dimension, as the dynamics is mimicked in the other one. Given the repulsive nature of polariton-polariton interaction, in order to generate a bright soliton we need to take into account the balancing effect of a negative effective mass, $m_{\text{eff}} = (\partial_k^2 E(k))^{-1}$, which gives an effective confinement of the wave-packet. In microcavity polaritons the effective mass is negative close to the inflection point of the dispersion: from this consideration it follows that any bright soliton generated in such systems will move on the plane with a wavevector k. The formalism used to characterized the quantum properties of polariton solitons follows the approach of Drummond and Carter [70], which basically consists of discretising the 1D Hamiltonian of a Kerr optical fibre, neglecting the high order nonlinear terms. It can be demonstrated that this results in:

$$H_0 = \sum_j^M (\omega_j a_j^\dagger a_j + g a_j^\dagger a_j^\dagger a_j a_j + \tau(a_j^\dagger a_{j+1} + a_{j+1}^\dagger a_j)), \tag{4.58}$$

which is the 1D analogue of eq. (4.54), with M sites. In the limit of large M, the model converges to the continuum. To take into account the effect of dissipation it is necessary to consider the master equation formalism:

$$\partial_t \rho = -i[H_0, \rho] + \gamma \sum_j (2a_j \rho a_j^\dagger - a_j^\dagger a_j \rho - \rho a_j^\dagger a_j), \tag{4.59}$$

where each site emits with the same rate γ in a vacuum environment. As we want to model interacting polaritons in 1D, we need to consider a repulsive interaction, i.e. $g > 0$, which in general enhances the spreading of the wave-packet, together with the kinetic term, proportional to τ. In principle the Hamiltonian (4.58) does not display any negative effective mass region in the dispersion, hence bright solitons should not be allowed to form. However, Smerzi et al. in [5] demonstrated that, even in this simple model, it is possible to obtain a discrete bright soliton solution by accurately choosing the system's parameters. They used a variational ansatz on a chain of repulsive bosons in an optical lattice to determine the conditions to obtain a non dispersive wave packet. Let us consider the mean field Hamiltonian corresponding to (4.58), given by:

$$H_{\mathrm{mf}} = \sum_j^M ((\omega_j - g)|\psi_j|^2 + g|\psi_j|^4 + \tau(\psi_j \psi_{j+1}^* + \psi_{j+1}\psi_j^*)), \tag{4.60}$$

where ψ_j and $i\psi_j^*$ are canonically conjugate variables. In order to find the bright soliton condition, we need to study the dynamics of the ansatz wave-function:

$$\psi_j^{var} = \sqrt{I} \exp\left[-\frac{(j - j_0)^2}{\sigma^2} + ik(j - j_0) \right], \tag{4.61}$$

where k is the wave-vector of the Gaussian wave-packet and σ is the width. The dynamics of the wave-function can be obtained by calculating the Lagrangian $\mathcal{L}(\psi_j = \psi_j^{var}) = \sum_j i\psi_j^* \psi_j - H_{\mathrm{mf}}$, and the associated *Euler-Lagrange equations* for the variational parameters, σ and k. Following this approach, it is possible to derive the variational Hamiltonian:

$$H_{var} = \frac{g}{2\sqrt{\pi}\sigma} - \cos(k) e^{-1/2\sigma^2}, \tag{4.62}$$

and the corresponding equations of motion:

$$\begin{aligned} \dot{k} &= 0 \\ \dot{\sigma} &= \sigma \cos(k) e^{\frac{1}{2\sigma^2}}. \end{aligned} \tag{4.63}$$

Imposing in (4.63) the condition for a non-dispersive propagating wave-packet, i.e., $\dot{\sigma} = 0$, it is possible to find the set of parameters which give a discrete bright soliton. Notice here that, following the approach proposed by Smerzi, the variational Hamiltonian does not depend on the amplitude of the ansatz wavefunction, $\sqrt{I}$: in the limit of $\sigma \gg 1$, in fact it is possible to demonstrate that:

$$I = \sqrt{\frac{2}{\pi\sigma^2}}. \tag{4.64}$$

In [5] the authors found that in order to obtain a soliton, the following relation

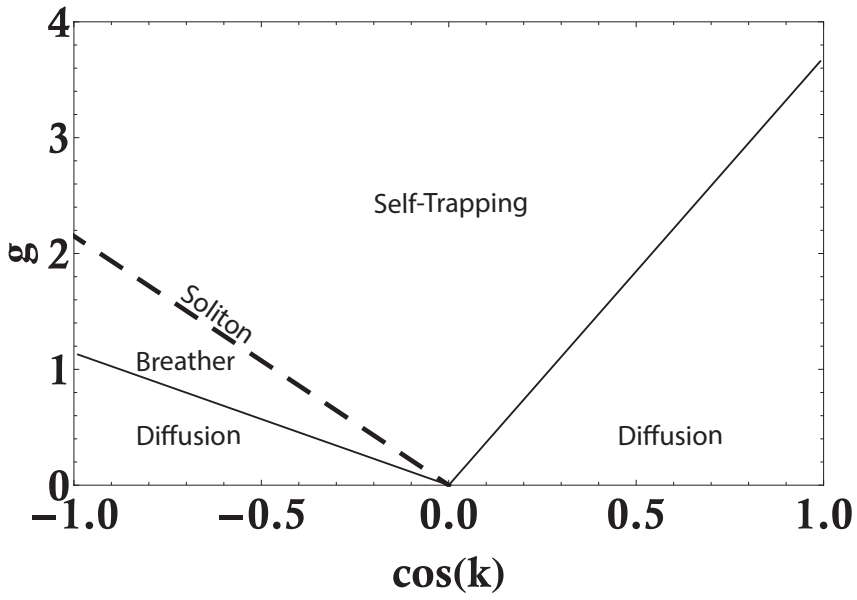

Figure 4.7: Adapted from [5]. The phase diagram for the Gaussian variational ansatz of (4.58), with $j_0 = 0$ and $\tau = 0.5$. The solution shows a rich variety of behaviour, ranging from a diffusive phase, to the breather solution, i.e. a wave-packet with oscillating localization. In particular a soliton solution is obtained imposing the condition $\partial_t \sigma = 0$, for negative values of $\cos(k)$.

between the non-linearity and the momentum (for $\tau = 0.5$), needs to hold:

$$g = 2\sqrt{\pi}\frac{|\cos(k)|}{\sigma} e^{-1/2\sigma^2}, \tag{4.65}$$

which is a line in the $k-g$ phase plane as in Fig. (4.7). We require $\cos(k) < 0$ to satisfy the requirement of negative effective mass: in fact, in term of the variational Hamiltonian,

$$(m_{\text{eff}})^{-1} = \partial^2_{p^2} H_{var} = \cos(k) e^{-1/2\sigma^2}, \tag{4.66}$$

hence giving negative values for $\cos(k)$. The dependence on the momentum k in equation (4.66), allows us to explore a wide range of possible solution. For example, the limit case of $m_{\text{eff}} \to \infty$, gives a self-trapping (hence non-propagating) wavepacket. The results obtained with the variational approach are exact for the closed system described by (4.58): however in the dissipative case a real soliton cannot exist, unless the dissipation is balanced by a constant driving field. Still, for a limited time window, a focusing of the Gaussian wave can occur. We call this state formed with the above mechanism a *quasi-soliton* or a *full-dissipative-soliton*.

From the Hamiltonian (4.58) and the master equation (4.59), using the gauge P-representation, we derive a set of stochastic differential equations for the 1D chain of interacting bosons, which, for the j-th mode, have the form:

$$d\alpha_j = -\gamma\alpha_j + i\tau(\alpha_j + \alpha_{j-1}) + i\delta\alpha_j dt - 2ig\alpha_j^2\beta_j dt + \sum_k B_{1k}(dW_k - g_k dt) \tag{4.67}$$

$$d\beta_j = -\gamma\beta_j - i\tau(\beta_j + \beta_{j-1}) - i\delta\beta_j dt + 2ig\beta_j^2\alpha_j dt + \sum_k B_{2k}(dW_k - g_k dt) \tag{4.68}$$

$$d\Omega_j = \Omega_j \sum_k g_k dW_k. \tag{4.69}$$

The noise has the same structure as the single mode case, i.e., is localized on each site and is proportional to the nonlinear interaction strength. It follows that we can make use of the same drift-diffusion gauge terms as in the single mode scenario:

$$\begin{aligned} -2ig\alpha_j n_j dt &\to -2ig\alpha \text{Re}(n_j) dt \\ 2ig\beta_j n_j dt &\to 2ig\beta_j \text{Re}(n_j) dt, \end{aligned} \tag{4.70}$$

together with the diffusion gauge (4.53), on each site. We perform our numerical analysis on (4.67) considering a set of $M = 21$ sites, which we group, for notation purposes, in a single vector $\hat{x} = (\alpha_{-10}, ..., \alpha_0, ..., \alpha_{10})$. At time $t = 0$, the system is

initialized as a Gaussian-like wave packet, which mimics the effect of the writing pulse on the sample, and serves to trigger the propagation of the state in the k direction:

$$x_j(t=0) = X_0 \exp(-\frac{j^2}{2\sigma} + ikj), \tag{4.71}$$

with X_0 being the intensity on the central site at $t = 0$.

To make a proper comparison with the soliton regime, we first investigate the dynamics in the diffusive regime, with a repulsive interaction $g > 0$ and $k = 0$. In this case we expect that the combined effects of the repulsion between particles and the positiveness of the effective mass, will give rise to a spreading of the wave packet during the time evolution. To show this, we solve the stochastic equation on a set of trajectories, S, and we evaluate the intensity on each site:

$$\frac{\langle \alpha_i(t)\beta_i(t)\Omega(t)\rangle_{\text{stoch}}}{\langle \Omega(t)\rangle_{\text{stoch}}} \approx \langle n_i(t)\rangle\,, \tag{4.72}$$

where Ω is the gauge field, as described in (4.67). The result is plotted in Fig. (4.8)(a): it can be clearly seen that the initial wave-packet dissipates over time, as a result of the decay term in the master equation, and loses the initial localisation, spreading all over the lattice sites. We can quantify the spreading by calculating the time evolution full-width-half-maximum (FWHM) of the intensity distribution. We expect that the FWHM for a spreading Gaussian beam will increase because of the diffusion process, as confirmed numerically in the case considered in Fig.(4.9).

Following the same approach, we evaluate the second order correlation function from each site, which numerically is equivalent to averaging over an appropriate sample set, S, the quantity:

$$\frac{\langle \alpha_i(t)\beta_i(t)\Omega(t)\alpha_i(t)\beta_i(t)\Omega(t)\rangle_{\text{stoch}}}{\langle \alpha_i(t)\beta_i(t)\Omega(t)\rangle^2_{\text{stoch}}} \approx g_i^{(2)}(t). \tag{4.73}$$

The coupling between each site induces a deviation in the value of the second order correlation function, compared to the single mode case. In Fig. (4.8)(b) it can be seen that the correlation functions show almost everywhere antibunching, especially

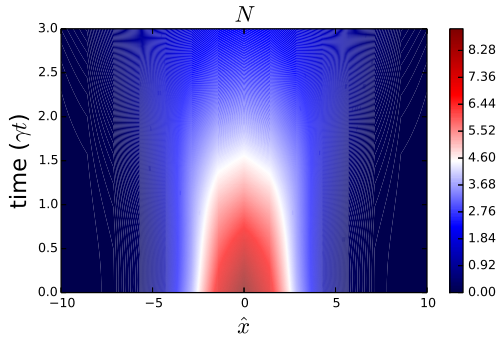

(a)

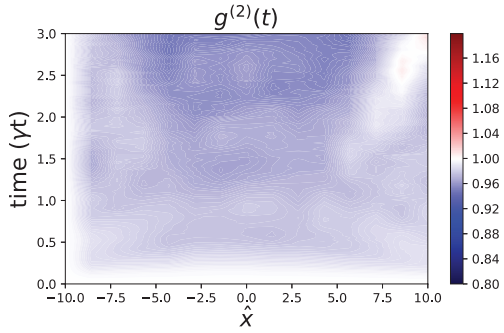

(b)

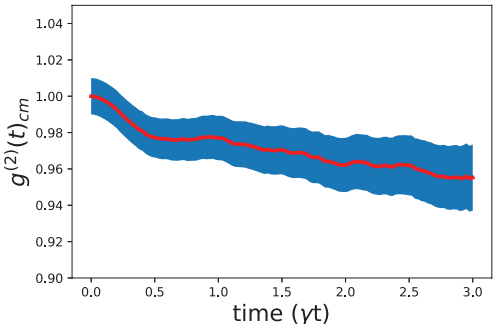

(c)

Figure 4.8: (a) Evolution of the Gaussian wave-packet in the diffusive regime, with $\tau = 0.5$, $g = 0.03$, $\gamma = 0.1$ and $X_0 = 3$, $\sigma_0 = 5$, for a system made of $|\hat{x}| = 21$ sites. (b) Evolution of the second order equal times autocorrelation function, $g_i^{(2)}$, for each site of the system in the diffusive regime. The system experiences a deviation from the coherent statistics. In particular the central site (c), which corresponds to the center of mass of the beam, has sub-Poissonian behaviour, with $\min(g_{cm}^{(2)}(0)) = 0.96$. The blue region in the plot describes the standard error associated to the stochastic evolution.

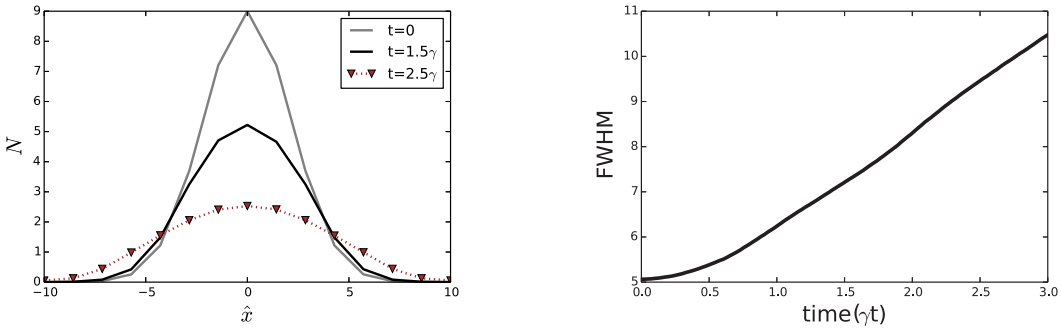

(a) (b)

Figure 4.9: (a) Profile of the Gaussian beam at different times, with $\tau = 0.5$, $g = 0.03$, $\gamma = 0.1$ and $X_0 = 3$, $\sigma_0 = 5$, at $k = 0$. As the Gaussian beam spreads over the lattice, the FWHM increases as shown in (b).

at late times : the centre of mass, which corresponds in this case to the central site (Fig. (4.8)(c)), is maximally antibunched, with a minimum value of the correlation function, $\min(g_0^{(2)}) \approx 0.96$. However, light emitted is most antibunched when the intensity of the beam is close to zero: hence, as it can be seen from Fig. (4.8)(a), in this region the system is basically empty, which means that the probability of detecting photons with the expected statistics is low.

We now analyse what happens when the system has a negative effective mass ($\cos(k) < 0$) and repulsive on-site interactions ($g > 0$), with parameters chosen to satisfy the soliton condition as in eq. (4.65). Starting again with a initial Gaussian-like state, we notice that, as with the experimental results, at low power the wave-packet still experiences a spreading effect due to the unbalancing effect between the nonlinearity (which is, by definition, intensity-dependent) and the dispersion. However, at higher power, self focusing takes place and, for a certain time window, a *bright soliton* is formed. This can be seen in Fig. (4.10): the wave-packet, with an initial width σ_0, is gradually focusing to a state with a $\sigma < \sigma_0$. We can quantify the focusing of the state, again by calculating the time dependent full-width-half-maximum (FWHM) of the intensity distribution. As shown in Fig.(4.11)(a), the FWHM decreases from its initial value, demonstrating the focusing of the initial distribution. After it reaches a minimum, the FWHM is approximatively constant in the time window considered, hence the state there can be properly described as a discrete

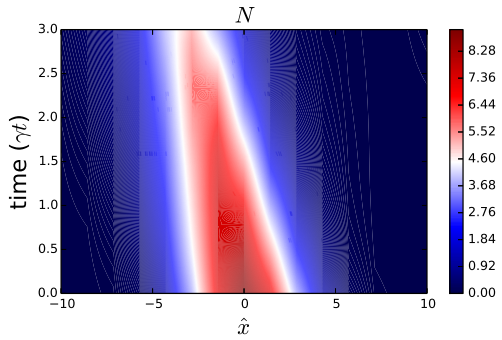

(a)

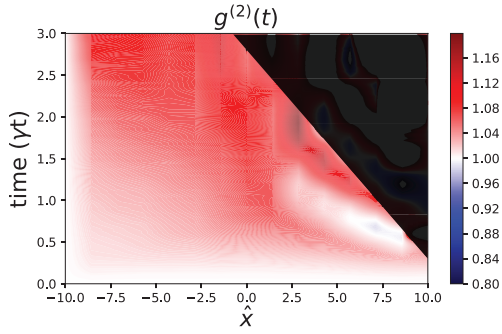

(b)

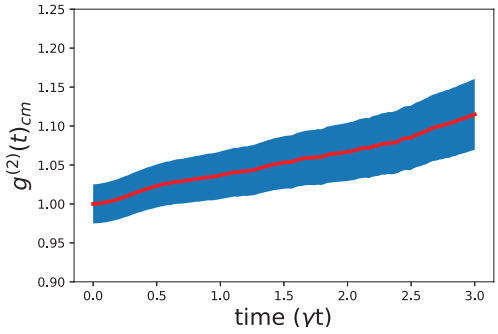

(c)

Figure 4.10: Evolution of the Gaussian wave-packet in the case of negative effective mass, with $\tau = 0.5$, $g = 0.03$, $\gamma = 0.1$, $X_0 = 3$, and $\sigma_0 = 5$, $k = 1.6$ for a system made of $|\hat{x}| = 21$ sites. (b) Evolution of the second order equal times autocorrelation function, $g_i^{(2)}$, for each site of the system close to the soliton regime. The system experiences a deviation from the coherent statics, along the soliton propagation direction. In particular $g_i^{(2)} \geq 1$, hence is always super-Poissonian. (c) The second order correlation function for the soliton center of mass, showing bunching statistics for all times. The blue region describes the standard error associated to the stochastic evolution.

bright soliton, as it is evident from the intensity profile in Fig. (4.11)(b).

An analysis of the behaviour of the $g_i^{(2)}(t)$ reveals a different scenario from the diffusive case: as it can be seen in Fig. (4.10)(b), in the region where the soliton is propagating, the correlation function is mostly coherent or super-Poissonian. The

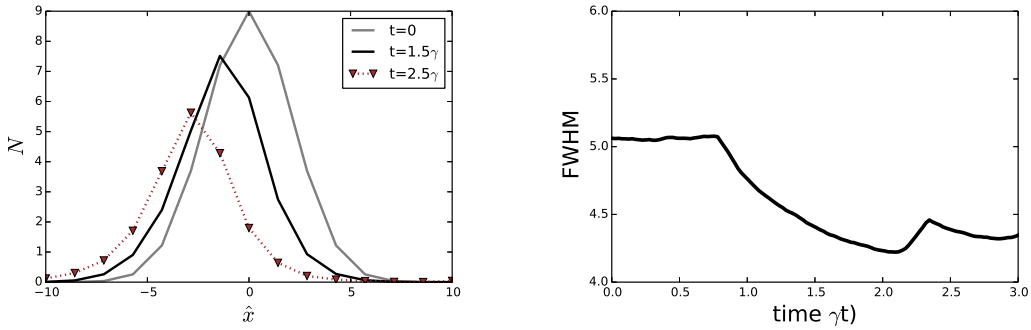

(a) (b)

Figure 4.11: (a) Profile of the Gaussian beam at different times, in the quasi-soliton regime, with $\tau = 0.5$, $g = 0.03$, $\gamma = 0.1$ and $X_0 = 3$, $\sigma_0 = 5$, at $k = 1.6$. As the Gaussian beam is focusing, the FWHM decreases as shown in (b).

empty region is physically meaningless, as the stochastic analysis is susceptible to high fluctuations and divergences. In particular, the dynamics of the correlation function for the center of mass of the soliton reveals a super-Poissonian statistics as shown in Fig. (4.10) (c). When considering multi-mode systems, to quantify the statistical properties of the total emission, it is necessary to take into account the inter-mode correlation function, also called cross-correlation function, which statistically corresponds to the covariance between, say, mode i and mode j. Computationally this corresponds to evaluate the quantities:

$$\frac{\langle \alpha_i(t)\beta_i(t)\Omega(t)\alpha_j(t)\beta_j(t)\Omega(t)\rangle_{\text{stoch}}}{\langle \alpha_i(t)\beta_i(t)\Omega(t)\rangle_{\text{stoch}}\langle \alpha_j(t)\beta_j(t)\Omega(t)\rangle_{\text{stoch}}} \approx g^{(2)}_{ij}(t). \tag{4.74}$$

If we add up the second order correlation functions for each mode, together with any possible cross-correlations, normalizing respect to the total intensity, we obtain a definition for the total second order correlation function. Both in the diffusive and in the soliton case total second order correlation function is stationary, i.e., its initial value is unchanged during the whole dynamics. This fact is a consequence of a general result that will be presented and investigated in the next Chapter.

4.2.3 Squeezing in polariton solitons

We want now to measure the quadrature variances of the *quasi-soliton* state, to see whether or not squeezing occurs. Squeezing in solitons has been extensively studied

in the context of optical fibres [71], and they were proposed as possible candidates to perform quantum non-demolition measurements, i.e., a set of measurement which avoids any increase of the uncertainty of the measured observable. As mentioned in Chapter 2, a squeezed state shows a noise reduction, with respect to a coherent state, in one of the quadratures and, correspondingly, a noise enhancement in the orthogonal quadrature, such that the Heisenberg relation is always satisfied. We need to consider the generalized quadrature operator:

$$\begin{aligned} X(\phi) &= e^{i\phi}a + e^{-i\phi}a^\dagger, \\ X\left(\phi + \frac{\pi}{2}\right) &= e^{i(\phi+\frac{\pi}{2})}a + e^{-i(\phi+\frac{\pi}{2})}a^\dagger, \end{aligned} \tag{4.75}$$

with $\phi \in [0, \frac{\pi}{2}]$. A state is squeezed if for one of the quadrature:

$$\Delta X(\phi)^2 < 1. \tag{4.76}$$

We solve the dynamics of the system (4.67) for the set of parameters giving a dissipative soliton, thus in the negative mass condition. We then evaluate the stochastic variances (4.75) for each pair of orthogonal quadratures, $X(\phi)$ and $X\left(\phi + \frac{\pi}{2}\right)$, on a finite set of values of ϕ: as it is sufficient to demonstrate the violation (6.48) for at least one of the quadratures, we consider the value of the rotation angle in phase space for which a minimum of the variance is obtained, $\min(S(\phi))$. As shown in Fig.(4.12)(a), the system shows squeezing mostly in the region where the wave packet is propagating. In Fig.(4.12) (b), we track the variances for the centre of mass of the wave packet: it is clear that as soon as the soliton is formed, thus from the very beginning of the time evolution, the variances start to deviate from the the coherent state value. In particular one of the quadratures shows a variance that goes below the lower limit expected for coherent states, which means the state is squeezed in that quadrature. However when the intensity decreases, due to the dissipation, both the variances return to values greater than or equal to the coherent state prescription, $\Delta X(\phi)^2 \geq 1$. In conclusion, we demonstrated that in the simple model implemented to study polariton bright solitons, quantum squeezing can be

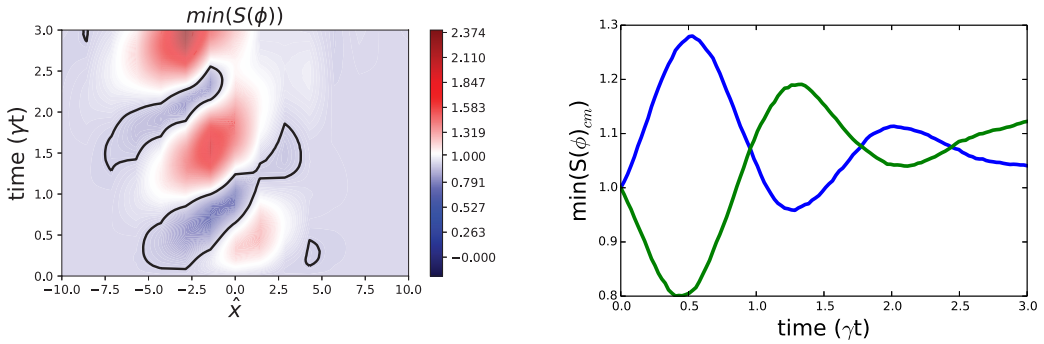

(a) (b)

Figure 4.12: (a) Evolution of the minimum quadrature variance, $\min(S(\phi))$, for each site of the system in the soliton regime, with $\tau = 0.5$, $g = 0.03$, $\gamma = 0.1$ and $X_0 = 3$, $\sigma_0 = 5$, at $k = 1.6$. The dark lines define the region where squeezing occurs, hence where $\min(S(\phi)) < 1$. (b) Evolution of the minimum variance for the two orthogonal quadratures of the peak of the moving soliton: as soon as the initial wave packet focuses the system shows a pronounced quadrature squeezing.

observed: this result might have a potential impact on the research field of quantum polaritonics, as the squeezing of polariton soliton might be detectable via homodyne detection.

Chapter 5

Conservation of correlation functions in U(1)-symmetric systems

In this Chapter, we analyse and describe a theoretical study of the conservation of correlation functions in U(1)-symmetric systems. The following results have been condensed in the form of a scientific publication, published in *Physical Review Letter* [72]. As suggested in the previous chapters, the intensity correlation function, especially at equal times, is widely used to characterize the statistical properties of optical and condensed matter systems. In particular, it may be used as a first measure of the "quantumness" of the systems under investigation. Here we derive the conditions under which the intensity correlation function is a conserved quantity: with this statement, we mean that the aforementioned quantity is stationary over a time interval. The conservation theorem concerns both closed and open quantum system, where in the latter case additional restrictions on the dissipation are needed to guarantee the validity of the result. In particular, we found that a general feature of a system possessing a stationary intensity correlation function is to be $U(1)$-symmetric, i.e., to be invariant under a global gauge transformation. Hence, in systems where the $U(1)$ symmetry is broken, the second order correlation function will be a non stationary function of time. As we shall demonstrate in the following, such a theoretical link provides a new tool to investigate the symmetry properties of

a variety of systems, and the corresponding phase transitions, using photon counting measurements.

Let us consider a multimode system: as we mentioned in the previous Chapter, it is possible to define the second-order quantum correlation function for each measured mode, whose expression at equal times are:

$$g_{ij}^{(2)}(t,t) = \frac{\langle c_i^\dagger c_j^\dagger c_i c_j \rangle}{\langle c_i^\dagger c_i \rangle \langle c_j^\dagger c_j \rangle}, \tag{5.1}$$

where $c_i^\dagger$, c_i and $c_j^\dagger$, c_j are ladder operators for generic i and j quantum fields (bosonic or fermionic). If $i \neq j$, the above expression describes the correlations between each mode, otherwise it quantifies the fluctuations within a mode. This definition is not limited to second order correlations, as it can be extended to higher orders correlation functions, containing m creation and annihilation operators.

The normalised equal times total m^{th} order correlation function for a multimode system is given by:

$$g_{tot}^{(m)}(t,t) = \frac{\langle J \rangle}{\langle N \rangle^m}, \tag{5.2}$$

where

$$\langle J \rangle = \langle : (\sum_i c_i^\dagger c_i)^m : \rangle \tag{5.3}$$

and the normalisation factor is given by the total number of excitation

$$\langle N \rangle = \langle \sum_i c_i^\dagger c_i \rangle \tag{5.4}$$

where the summation is extended over all the modes. The symbol $\langle : \cdots : \rangle$ in Eq.(5.3) indicates that the operators inside are normally ordered. We regard our definition in (5.2) as a natural way to extend the concept of single mode normalised correlation function to a multimode system, as the contribution of each mode is weighted according to its occupation. If we consider a system made of purely photonic modes, having identical coupling with the environment, Eq.(5.2) quantifies the correlation function obtained by measuring the total emission without resolving each mode individually. Notice that if $m = 2$ and the systems is made of a single mode, Eq.(5.2)

reduces to Eq.(5.1), with $i = j$.

5.1 U(1) symmetry

Let us consider a quantum field defined on a continuous configuration space. The creation and annihilation operator, $a(x)$, $a^\dagger(x)$, in general satisfy the following commutation relation rule:

$$[a(x), a^\dagger(y)] = \delta(x - y). \tag{5.5}$$

The number operator N is denoted as:

$$N = \int a^\dagger(x)a(x)dx. \tag{5.6}$$

A system preserves the number of particles if its Hamiltonian commutes with N. The commutation rules between N and $a(x)$ (and $a^\dagger(x)$) can be easily obtained from the definitions above, giving:

$$Na(x) = a(x)(N - 1), \quad Na^\dagger(x) = a^\dagger(x)(N + 1). \tag{5.7}$$

From (5.7) follows that any polynomial combination with equal number of $a(x)$, $a^\dagger(x)$ will commute with N:

$$[a^\dagger(x_1)....a^\dagger(x_n)..a(x_1)...a(x_n)..]N = N[a^\dagger(x_1)....a^\dagger(x_n)..a(x_1)...a(x_n)..]. \tag{5.8}$$

A global unitary gauge transformation, with one parameter θ, is given by the rules:

$$a(x) \to a(x)e^{i\theta} \quad a^\dagger(x) \to a^\dagger(x)e^{-i\theta}, \tag{5.9}$$

and belongs to the one parameter unitary group, $U(1)$. If the Hamiltonian of the system is invariant upon the application of the transformation (5.9), it is said to possess a global $U(1)$ symmetry. The gauge transformation in (5.9) represents a rotation of the global phase angle of the fields $a(x)$ and $a(x)^\dagger$, with the rotation determined by the complex variable θ. From the above argument, it follows that

any polynomial with the same number of creation and annihilation operators will be $U(1)$ invariant. At this point, it is clear that a system where the number operator commutes with the Hamiltonian is globally $U(1)$-symmetric, and vice-versa, the $U(1)$ symmetry guarantees the commutation of the Hamiltonian with N.

In condensed matter systems and in optics, the breaking of such a symmetry is associated with a variety of phenomena, depending on how the breaking occurs. For example, in the closed Bose-Hubbard model, a spontaneous $U(1)$ symmetry breaking happens in the ground state, leading to a Mott-superfluid phase transition [73]. The $U(1)$ symmetry breaking in the ^{4}He (an isotope of helium), below a certain critical temperature, leads to superfluidity [74]. In the Rabi model, i.e., light-matter coupling beyond the rotating wave approximation, the spontaneous breaking of the $U(1)$ symmetry generates a diffusion of Goldstone modes. This is a general result of quantum field theory [75]: according to the *Goldstone theorem*, associated to a global spontaneous symmetry breaking, there is always a gapless excitation for each generator of the symmetry that does not leave the ground state invariant. In the case of the Rabi model such gapless excitations are represented by polaritons, i.e., the eigenstates of the system in the dressed state basis.

5.2 Closed quantum system

In order to determine the condition that the total correlation function (5.2) is conserved, we equate its time derivative to zero, giving

$$\left(\frac{d}{dt}\langle J\rangle\right)\langle N\rangle^m - \left(m\langle N\rangle^{m-1}\frac{d}{dt}\langle N\rangle\right)\langle J\rangle = 0. \tag{5.10}$$

For closed system that is guaranteed by:

$$\frac{d}{dt}\langle N\rangle = 0, \quad \frac{d}{dt}\langle J\rangle = 0, \tag{5.11}$$

which means that the Hamiltonian must commute with both N and J. Now, the normally ordered operator J can be written as a power expansion in the total number operator, $J = \sum_k^m d_k N^k$, where d_k are numerical coefficient related to the order of

the expansion [76]. The condition $[H, J] = 0$ is thus satisfied provided $[H, N] = 0$, so this is our only requirement. The condition $[H, N] = 0$ is equivalent to invariance under the gauge transformation, as shown in the previous section:

$$\begin{cases} \tilde{c_i}^\dagger = c_i^\dagger e^{i\phi} \\ \tilde{c_i} = c_i e^{-i\phi}, \quad \forall i \end{cases}$$

which corresponds to a global $U(1)$ symmetry of the Hamiltonian H. This result can be summarized in a general theorem:

Theorem: *For any closed system with an arbitrary number of modes, described by Hamiltonian H, then the total m^{th} order equal time correlation function $g_{tot}^{(m)}(t,t)$ is a conserved quantity, if H globally possess a $U(1)$ symmetry, i.e. , $[H, N] = 0$, where N is the total number operator.*

To underline the link between the global $U(1)$ symmetry of the Hamiltonian and the conservation of the second order correlation functions, we first consider the case of two closed, undriven linear bosonic modes, coherently coupled. This system can be described by a Hamiltonian of the form

$$H_{tm} = \omega_1 a_1^\dagger a_1 + \omega_2 a_2^\dagger a_2 + \tau(a_1^\dagger a_2 + a_2^\dagger a_1), \tag{5.12}$$

where ω_i are the energies of each mode and τ is the coupling strength between modes. Note that we can add non-linear terms with no effect provided that they commute with the number operators for each mode, so this discussion could equally apply to a two-mode Bose-Hubbard model. We need to evaluate the time derivative for three correlators: the two auto-correlation functions $(g_1^{(2)}, g_2^{(2)})$ and the cross correlation function $(g_{1,2}^{(2)} = g_{2,1}^{(2)})$. It is easy to obtain the dependence of the auto-correlation, $\langle a_1^\dagger a_1^\dagger a_1 a_1 \rangle$, from the hopping terms:

$$\begin{aligned} \frac{d}{dt}\langle a_1^\dagger a_1^\dagger a_1 a_1 \rangle = &- i\tau(2\langle a_1^\dagger a_1 a_1 a_2^\dagger \rangle - 2\langle a_1^\dagger a_1^\dagger a_1 a_2 \rangle + \langle a_1^\dagger a_2 \rangle \\ &- \langle a_2^\dagger a_1 \rangle), \end{aligned}$$

while the derivative of the number of particles for mode 1, $\langle n_1 \rangle$, is:

$$\frac{d}{dt}\langle n_1 \rangle = -i\tau \langle a_1^\dagger a_2 - a_2^\dagger a_1 \rangle , \tag{5.13}$$

with an equivalent form for mode 2. The autocorrelation function for mode 1 (and analogously for mode 2) is not conserved. However, considering now our **Theorem**, we note that though the Hamiltonian does not commute with the number operator for each mode ($[H_{tm}, n_{1,2}] \neq 0$), i.e. the $U(1)$ symmetry is locally broken, it does commute with the total number operator $N = n_1 + n_2$. This is a consequence of the global $U(1)$ symmetry of the Hamiltonian. Therefore, it can be expected that total $m-th$ order correlation function, $g_{tot}^{(m)}$ is conserved. This can be confirmed by evaluating the time derivative of the cross correlation between the two modes. the expression contains terms which precisely cancel the derivative of the auto-correlation function:

$$\begin{aligned}\frac{d}{dt}\langle a_2^\dagger a_2 a_1^\dagger a_1 \rangle =& i\tau(\langle a_2^\dagger a_2 a_1^\dagger a_2 \rangle + \langle a_2^\dagger a_1 a_1^\dagger a_1 \rangle - \\ & \langle a_1^\dagger a_2 a_1^\dagger a_1 \rangle - \langle a_2^\dagger a_2 a_2^\dagger a_1 \rangle).\end{aligned}$$

Increasing the number of modes, the above argument encompasses the 1D Bose-Hubbard Hamiltonian. It can also be extended to bosonic quantum networks [77], which can describe a huge variety of physical systems, like photonic or polaritonic lattices (Lieb [78], Kagome [79] and Graphene [80]), quantum networks and collective phenomena involving stimulated parametric processes (like parametric up/down conversion). The correlation function for each mode of the network changes dynamically, as a consequence of the interaction with other modes and this change is dependent on the structure of the network itself, and on the strength of the coupling terms (τ in the two mode case). This leads to the possibility of controlling the statistics of the emitted photons by engineering the geometry of the networks, as it has been shown for photonic molecules in [81].

5.2.1 Jaynes-Cummings Hamiltonian

It is also interesting to consider the case of mixed bosonic and fermionic systems, for example, the Jaynes-Cummings-Hubbard model [82], the spin-boson network model [83], and light-matter coupled systems [84]. The simplest case is the Jaynes Cummings model, for a single-mode cavity, containing one two-level atom:

$$H_{JC} = \omega_0 a^\dagger a + \omega_a \sigma^+\sigma^- + \eta(a^\dagger\sigma^- + a\sigma^+), \tag{5.14}$$

where ω_0 and ω_a are the energies of the mode and atom, η is the vacuum Rabi frequency that characterizes the photon-atom interaction strength and $\sigma^\pm$ are the atomic raising and lowering operators. We have written this Hamiltonian using the rotating wave approximation (RWA), since it then commutes with the total number of excitations, $[H_{JC}, N] = 0$, where $N = n_a + n_\sigma$, $n_\sigma = \sigma^+\sigma^-$ is the number operator for fermions, and $n_a = a^\dagger a$ is the number operator for bosons. The total $G^{(2)}_{tot}$ for this system is made up of three elements: the atomic autocorrelation, $\langle\sigma^+\sigma^+\sigma^-\sigma^-\rangle$, the cavity mode autocorrelation $\langle a^\dagger a^\dagger aa\rangle$, and the cross correlation term $\langle a^\dagger a\sigma^+\sigma^-\rangle$. It is possible to calculate the derivative of each component, using the same approach as in the previous sections:

$$\begin{aligned}
\frac{d}{dt}G^{(2)}_\sigma &= \frac{d}{dt}\langle\sigma^+\sigma^+\sigma^-\sigma^-\rangle = -i\eta[\sigma^+\sigma^+\sigma^-\sigma^-, (a^\dagger\sigma^- + a\sigma^+)] = i\eta\langle 2\sigma^+\sigma^-\sigma^-a^\dagger - 2\sigma^+\sigma^+\sigma^-a\rangle \\
\frac{d}{dt}G^{(2)}_a &= \frac{d}{dt}\langle a^\dagger a^\dagger aa\rangle = -i\eta[a^\dagger a^\dagger aa, (a^\dagger\sigma^- + a\sigma^+)] = i\eta\langle 2a^\dagger aa\sigma^+ - 2a^\dagger a^\dagger a\sigma^-\rangle \\
\frac{d}{dt}G^{(2)}_{\sigma,a} &= \frac{d}{dt}\langle a^\dagger a\sigma^+\sigma^-\rangle = -i\eta[a^\dagger a\sigma^+\sigma^-, (a^\dagger\sigma^- + a\sigma^+)] = \\
&= -i\eta\langle a^\dagger aa\sigma^+ - a^\dagger a^\dagger a\sigma^- + \sigma^+\sigma^-\sigma^-a^\dagger - \sigma^+\sigma^+\sigma^-a\rangle\,.
\end{aligned}$$

In a similar way, the derivative of the total number of particles is zero,

$$\frac{d}{dt}\mathcal{N}_{tot} = \frac{d}{dt}(n_\sigma + n_a) = 0, \tag{5.15}$$

where $n_a = a^\dagger a$ and $n_\sigma = \sigma^+\sigma^-$. We compute the total $g^{(2)}$ adding up all the terms, and we find that is conserved:

$$\frac{d}{dt}g^{(2)}_{tot}(t,t) = \frac{d}{dt}\left(\frac{G^{(2)}_\sigma + G^{(2)}_a + 2G^{(2)}_{\sigma,a}}{\langle n_a + n_\sigma\rangle^2}\right) = 0, \tag{5.16}$$

hence confirming the validity of the **Theorem**. In Fig.(5.1) we show numerical

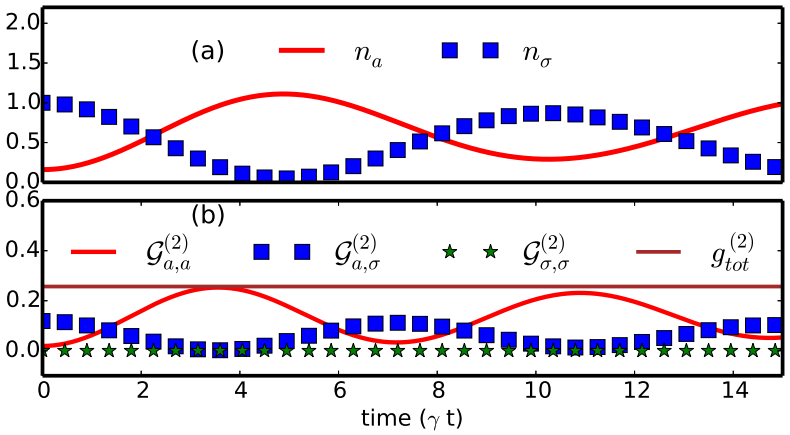

Figure 5.1: Numerical solution for H_{JC}, with a Rabi term $\eta = 0.25$ and $\omega_a = \omega_\sigma = 0$, prepared in an initial state with $|\alpha_0|^2 = 0.18$ particles in the cavity mode and the atom in the excited state. (a) The number of photons, n_a, and excitation level of the atom, n_σ. $n_\sigma = 0$ corresponds to the atom in its ground state, $n_\sigma = 1$ to the excited state. (b) The correlation functions $\mathcal{G}^{(2)}_{i,j} = \langle a^\dagger_i a^\dagger_j a_i a_j\rangle / N^2$ for the atomic, bosonic and for the cross terms. The total correlations for the emitted light is a constant of motion; here it is always sub-Poissonian ($g^{(2)}_{tot} < 1$).

calculations, performed using the positive P-representation and the corresponding stochastic equations, of the dynamics of the Jaynes-Cummings model described by H_{JC}, preparing the system in an initial state $|\psi(0)\rangle = |\alpha_0, e\rangle$, with $|\alpha_0|^2 = 0.18$ particles in the field mode, and the two level system in the excited state $|e\rangle$. As expected, we find that the atomic and the field correlations change in time, while $g^{(2)}_{tot}(t,t)$ remains constant, since the $U(1)$ symmetry is locally broken, $[H_{JC}, n_\sigma] \neq 0$ and $[H_{JC}, n_a] \neq 0$, but globally is maintained. In order to lose the stationarity, it is sufficient to break the symmetry with respect to the total number operator, for example having a coherent driving term like $\Omega_\sigma(t) = h(t)(\sigma^+ + \sigma^-)$ $\Omega_a(t) = h(t)(a^\dagger + a)$ [85]. The Jaynes Cummings model beyond the rotating wave approximation (so called Rabi model [86]), also contains terms which break the $U(1)$ symmetry,

allowing creation and destruction of excitations. Then, when the coupling strength Ω is increased, a phase transition occurs occurs where particles are spontaneously created. This generates a dynamics of the total second order correlation functions, as we will briefly show in the following.

The Hamiltonian for the Rabi model reads:

$$H_{Rb} = \omega_0 a^\dagger a + \omega_a \sigma^+ \sigma^- + \eta(a^\dagger + a)(\sigma^- + \sigma^+), \tag{5.17}$$

where the interaction term contain now both the rotating and the counter-rotating terms:

$$a^\dagger \sigma^- + \sigma^+ a \quad \rightarrow \textit{rotating terms} \tag{5.18}$$

$$a^\dagger \sigma^+ + \sigma^- a \quad \rightarrow \textit{counter-rotating terms.} \tag{5.19}$$

As we showed above, the rotating terms commute with the total number operator: however the counter-rotating terms break the commutation relation. In order to evaluate the commutator:

$$[a^\dagger \sigma^+ + \sigma^- a, a^\dagger a + \sigma^+ \sigma^-], \tag{5.20}$$

we use the fact that the Pauli matrices, $(\sigma^x, \sigma^y, \sigma^z)$, form a closed algebra [87],

$$[\sigma^i, \sigma^j] = 2i\epsilon_{ijk}\sigma^k, \tag{5.21}$$

with ϵ_{ijk} the *Levi-Cita tensor*. From the definition of the spin ladder operators, $\sigma^+ = \sigma^x + i\sigma^y$ and $\sigma^- = \sigma^x - i\sigma^y$, we obtain:

$$[a^\dagger \sigma^+ + \sigma^- a, a^\dagger a + \sigma^+ \sigma^-] = -a^\dagger \sigma^+ + \sigma^- a + 4(a^\dagger \sigma^+ \sigma^z + a\sigma^z \sigma^-)], \tag{5.22}$$

which clearly implies that $[H, N] \neq 0$, leading to a breaking of the $U(1)$ symmetry. The consequence is again a non-stationary total correlation function: we analyse this scenario numerically, considering the same set of parameters as in Fig. (5.1), but this time for the Rabi model (5.17). As can clearly be seen in Fig. (5.2)(a)

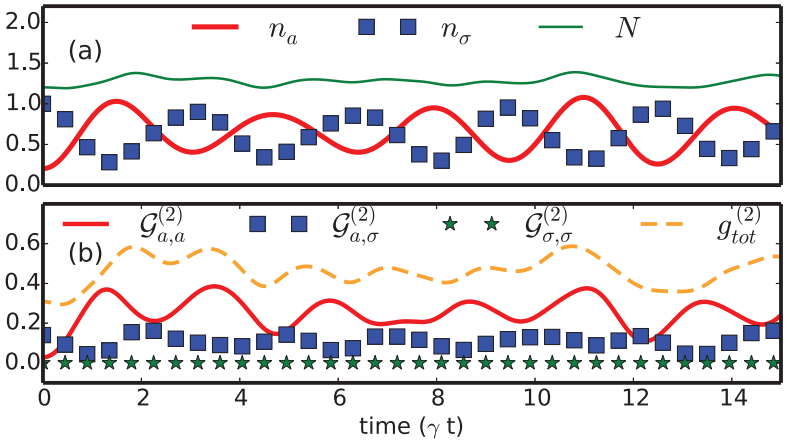

Figure 5.2: Numerical solution for H_{Rb}, with a Rabi term $\eta = 0.25$ and $\omega_a = \omega_\sigma = 0$, prepared in an initial state with $|\alpha_0|^2 = 0.18$ particles in the cavity mode and the atom in the excited state. (a) The number of photons, n_a, and excitation level of the atom, n_σ. $n_\sigma = 0$ corresponds to the atom in its ground state, $n_\sigma = 1$ to the excited state. (b) The correlation functions $\mathcal{G}^{(2)}_{i,j} = \langle a_i^\dagger a_j^\dagger a_i a_j \rangle / N^2$ for the atomic, bosonic and for the cross terms. The total number of excitation is not stationary, as a consequence of the broken $U(1)$ symmetry for the Rabi model, and correspondingly the total correlation function is for the emitted light is not a constant of motion ; here it is always sub-Poissonian ($g^{(2)}_{tot} < 1$).

the presence of the counter-rotating terms in the Hamiltonian (5.17) breaks the conservation of the total number of excitations: consequently $g^{(2)}_{tot}$ is not stationary (5.2)(b).

Similar behaviour should be seen in any system which breaks a $U(1)$ symmetry while undergoing a phase transition, for example, in the case of Hubbard Hamiltonians inside a cavity [88].

5.3 Dissipative systems

We now consider dissipative systems, whose dynamics is described by a master equation in the Lindblad form[89]:

$$\frac{d}{dt}\rho = -i[H, \rho] + \mathcal{D}(\rho) \tag{5.23}$$

where

$$D(\rho) = \sum_i \frac{\gamma_i}{2}(2c_i^\dagger \rho c_i - c_i^\dagger c_i \rho - \rho c_i^\dagger c_i) \tag{5.24}$$

In this case, the time derivatives of $\langle N \rangle$ and $\langle J \rangle$ are not zero, but, from (5.10), the conservation of the correlation functions is guaranteed by the conditions:

$$\frac{d}{dt}\langle N \rangle = \kappa \langle N \rangle \tag{5.25}$$

$$\frac{d}{dt}\langle J \rangle = m\kappa \langle J \rangle , \tag{5.26}$$

where κ is an arbitrary constant and m is the order of correlation function. The physical meaning of the conditions (5.25) can be easily understood by evaluating the formal solutions of the differential equations: these give an exponential behaviour in time for $\langle N \rangle$ and $\langle J \rangle$, depending on the sign and magnitude of κ.

The time derivative of the mean value of an operator, using the Schrödinger picture, can be expressed as:

$$\frac{d}{dt}\langle A \rangle = \mathrm{Tr}\left\{ \frac{d}{dt}(A\rho) \right\} = \mathrm{Tr}\left\{ A \frac{d}{dt}\rho \right\}. \tag{5.27}$$

Using this, with Eq.(5.23) for $\frac{d}{dt}\rho$, the conditions for the conservation of the total correlation function in Eq.(5.25) become

$$-i\langle [H, N] \rangle + \sum_i \frac{\gamma_i}{2} \langle (2c_i^\dagger N c_i - c_i^\dagger c_i N - N c_i^\dagger c_i) \rangle = \kappa \langle N \rangle \tag{5.28}$$

$$-i\langle [H, J] \rangle + \sum_i \frac{\gamma_i}{2} \langle (2c_i^\dagger J c_i - c_i^\dagger c_i J - J c_i^\dagger c_i) \rangle = \kappa m \langle J \rangle \tag{5.29}$$

In general these conditions cannot be satisfied, but if we consider the case where all the loss rates are equal, $\gamma_i = \gamma$, the second terms on the left hand side of each equation can be evaluated to $-\gamma \langle N \rangle$ and $-\gamma m \langle J \rangle$. Thus, with $[H, N] = 0 = [H, J]$ as before, and $\kappa = \gamma$, the total correlation function is conserved.

This result can be summarized in a Corollary:

Corollary: *For any dissipative system with an arbitrary number of modes, described by an Hamiltonian H, and with a linear dissipator $\mathcal{D}(\rho)$, where each mode decays with the same rate γ, iff H globally possess a $U(1)$ symmetry, i.e. iff $[H, N] = 0$, where N is the total number operator, then the total m^{th} order equal time correlation*

function $g^{(m)}_{tot}(t,t)$ *is a conserved quantity.*

The corollary also applies to the case of linear gain instead of loss (swapping the c and $c^\dagger$ operators in Eq.(5.24)), but not nonlinear dissipative processes (c replaced by c^2 etc).

Although the requirement for all the modes to have equal loss rates is a significant restriction, there are many physical systems made of identical elements, for which the losses are expected to be equal, so the theorem applies. For examples we can look to photonic lattice structures [90, 91], arrays of semiconductor micro-cavities with the same detuning [92] and continuous systems, like waveguide or waveguide networks with isotropic geometry [93]. Furthermore, let us we consider the system analysed in [94]: here optical patterns have been observed, above a certain threshold of the pump power, as a consequence of the parametric scattering between polaritons on the same ring in k space. In such a system the $U(1)$ symmetry is spontaneously broken by the parametric process and each mode possesses the same decay rate: it follows from the Corollary that the total second order correlation function for the optical patterns is not a conserved quantity.

The results and the consequences of the **Theorem** and of the **Corollary** can be summarised as follows: the m^{th} order quantum correlation function is a constant of motion, for systems where the Hamiltonian possess global $U(1)$ symmetry and any dissipation is identical for each mode of the system and linear in the system operators. For a multimode system, the m^{th} order quantum correlation function may change dynamically in each mode, due to the their mutual interactions. However, the total correlation function will still be a constant of motion.

In general terms, when a global symmetry possessed by a system is spontaneously broken, a phase transition takes place, i.e., the geometrical and/or the statistical properties of the system can change drastically. When the system considered has a spatial structure, it is possible to characterize each phase transitions by studying the behaviour of the equal times two-points correlation functions: this is the standard approach used to investigate the order-disorder transitions. To give a

conceptual example, let us consider a ferromagnetic spin system, as showed in [95]. The equal times correlation function, $C(r, \tau = 0)$, as a function of the relative distance r between each spin, shows different scaling properties, which depend on the temperature of the system. Above a certain critical temperature, T_c, when the system is highly disordered for the thermal effects, the correlation function $C(r, \tau = 0)$ exhibits a mixed exponential and power-law behaviour. At the critical temperature $C(r, \tau = 0)$ follows a power-low behaviour, while below T_c, thus in the most ordered phase, it shows again a mixed feature. Hence an order-disorder phase transition can be investigated by measuring the scaling properties of the correlation function and, in particular, how these properties change as a function of some meaningful parameters (the temperature in the example).

Following the above argument, the results presented in the **Theorem** and in the **Corollary** suggest that the total correlation function may be an interesting parameter to measure in systems which undergo phase transitions characterized by the breaking of a global $U(1)$ symmetry. To clarify this point, let us consider an Hamiltonian depending on a parameter ζ and suppose that above a critical value of the parameter, ζ_c, the $U(1)$ symmetry is spontaneously broken. It follows that, when tracking the dynamics of the system, below ζ_c the total m^{th} order correlation function is stationary. Conversely, when $\zeta \geq \zeta_c$ the total m^{th} order correlation function will have a non-stationary dynamical evolution. Hence it is possible to make use of the total m^{th} order correlation function, which can be measured via photon counting, to detect phase transitions involving the breaking of the $U(1)$ symmetry. Together with the possibility of detecting phase transitions, the **Theorem** suggests a methodological approach to measure the second order correlation functions in a multimode system. The Theorem states, in fact, that care is necessary when using the second order correlation function as a probe for non-classical physics: in systems with $U(1)$ symmetry, it may be necessary to isolate light from individual modes, rather than looking at the statistics of the total emitted light. For example, in the $U(1)$-symmetric case, the total second order correlation function can show a

stationary bunched statistics, while the $g^{(2)}(0)$ for an individual mode can reveal purely non-classical features, i.e., antibunching.

5.3.1 Single mode with a dissipative term and with a driving pump

To show explicitly the results stated in the previous section, and their consequences, we consider here a single bosonic mode, with a Kerr nonlinearity, in a linear dissipative regime and driven by a coherent pump:

$$H_{sm} = \omega_0 a^\dagger a + g a^\dagger a^\dagger a a + f(t)(e^{-i\omega_p t} a^\dagger + e^{i\omega_p t} a), \tag{5.30}$$

where g describes the strength of the nonlinear interaction and ω_0 is the energy of the mode, $f(t)$ is the amplitude of the driving force, and ω_p is the frequency of the pump. We want to calculate the dynamics of the normalized second order quantum correlation function,

$$\frac{d}{dt} g^{(2)}(t,t) = \frac{\frac{d}{dt}\langle a^\dagger a^\dagger a a\rangle \langle a^\dagger a\rangle^2 - \langle a^\dagger a^\dagger a a\rangle \frac{d}{dt}\langle a^\dagger a\rangle^2}{\langle a^\dagger a\rangle^4}, \tag{5.31}$$

for the above Hamiltonian, in a linear dissipative regime. To address the dissipative dynamics, we consider the master equation, in the general form:

$$\frac{d}{dt}\rho = -i[H,\rho] + \mathcal{D}(\rho) = \mathcal{L}\rho \tag{5.32}$$

where $\mathcal{D}(\rho) = -\frac{\gamma}{2}(2a\rho a^\dagger - a a^\dagger \rho - \rho a a^\dagger)$ describes the linear dissipation, and $\mathcal{L}$ is the Lindblad superoperator.

We first focus on H_{sm} without the driving term. Using (5.32), it is possible to evaluate the derivative of the correlation function (in the following we omit the

explicit time dependence of the mean values):

$$\begin{aligned}\frac{d}{dt}G^{(2)} &= \frac{d}{dt}\langle a^\dagger a^\dagger aa\rangle = \\ &= \mathrm{Tr}\{a^\dagger a^\dagger aa(\frac{d}{dt}\rho)\} = \mathrm{Tr}\{i\omega[a^\dagger a^\dagger aa, a^\dagger a]\rho\} + \mathrm{Tr}\{ig[a^\dagger a^\dagger aa, a^\dagger a^\dagger aa]\rho\} \\ &- \mathrm{Tr}\{\frac{\gamma}{2}[\mathcal{D}(a^\dagger a^\dagger aa)]\rho\} \\ &= i\omega\mathrm{Tr}\{a^\dagger a^\dagger aaa^\dagger a\rho\} - i\omega\mathrm{Tr}\{a^\dagger a^\dagger aaa^\dagger a\rho\} + ig\mathrm{Tr}\{a^\dagger a^\dagger aaa^\dagger aa^\dagger a\rho\} \\ &- ig\mathrm{Tr}\{a^\dagger a^\dagger aaa^\dagger aa^\dagger a\rho\} - \frac{\gamma}{2}\mathrm{Tr}\{2a^\dagger a^\dagger a^\dagger aa\rho - a^\dagger a^\dagger aaa^\dagger a\rho - a^\dagger aa^\dagger a^\dagger aa\rho\}.\end{aligned}$$

Using the cyclic property of the trace, one can see that the terms in ω cancel out, and the same happens to the terms in g. For the last term, using the commutation relation for creation and annihilation operators, together with the cyclic property of the trace, we get:

$$\frac{d}{dt}G^{(2)} = -\gamma\mathrm{Tr}\{a^\dagger a^\dagger aa\rho\} = -2\gamma\langle a^\dagger a^\dagger aa\rangle, \tag{5.33}$$

which can be integrated to:

$$\langle a^\dagger a^\dagger aa\rangle = e^{-2\gamma t}\langle a^\dagger a^\dagger aa\rangle_{t=0}, \tag{5.34}$$

where $\langle a^\dagger a^\dagger aa\rangle_{t=0}$ is the initial amount of auto-correlation. Using the same method, it is possible to evaluate the derivative of the total number of particles in the system,

$$\frac{d}{dt}\langle n\rangle = \frac{d}{dt}\langle a^\dagger a\rangle = -\gamma\mathrm{Tr}\{a^\dagger a\rho\} = -\gamma\langle a^\dagger a\rangle, \tag{5.35}$$

as the number operator commutes with the Hamiltonian. Integrating (5.35), we find again:

$$\langle n\rangle = e^{-\gamma t}\langle n\rangle_{t=0}, \tag{5.36}$$

where $\langle n\rangle_{t=0}$ is the number of particles at $t = 0$. The dynamical evolution, both for the correlator and for the number of particles, is following an exponential law: this is a crucial element for the conservation of the second order correlation function, and it is related to the structure of the Lindblad term. Using now equations (5.33)

and (5.35) in (5.31), the time derivative of the $g^{(2)}(t,t)$ is:

$$\frac{d}{dt}g^{(2)}(t,t) = \frac{-2\gamma\langle a^\dagger a^\dagger aa\rangle\langle a^\dagger a\rangle^2 + 2\gamma\langle a^\dagger a^\dagger aa\rangle\langle a^\dagger a\rangle^2}{\langle a^\dagger a\rangle^4} = 0,$$

hence it is stationary, as expected from the **Corollary**.

Let us now consider the complete scenario in which a coherent pump is driving the system. Making use of (5.32), and of the following commutation relations, $[a, a^\dagger a] = a, [a^\dagger, a^\dagger a] = -a^\dagger$, it is possible to calculate the time derivative of $G^{(2)}$ and $\langle n\rangle$:

$$\frac{d}{dt}G^{(2)} = \mathrm{Tr}\{a^\dagger a^\dagger aa\mathcal{L}\rho\} = -2\gamma G^{(2)} + \mathrm{Tr}\{if(t)[a^\dagger a^\dagger aa, (e^{-i\omega_p t}a^\dagger + e^{i\omega_p t}a)]\rho\}$$
$$\frac{d}{dt}\langle n\rangle = \mathrm{Tr}\{a^\dagger a\mathcal{L}\rho\} = -\gamma\langle n\rangle\,\mathrm{Tr}\{if(t)[(e^{-i\omega_p t}a^\dagger + e^{i\omega_p t}a), a^\dagger a]\rho\},$$

which give,

$$\frac{d}{dt}G^{(2)} = -if(t)(e^{-i\omega_p t}2\langle a^\dagger aa\rangle - e^{i\omega_p t}2\langle a^\dagger a^\dagger a\rangle + \langle a^\dagger\rangle - \langle a\rangle) - 2\gamma G^{(2)},$$
$$\frac{d}{dt}\langle n\rangle = \mathrm{Tr}\{a^\dagger a\mathcal{L}\rho\} = -if(t)(e^{-i\omega_p t}\langle a^\dagger\rangle - +e^{i\omega_p t}\langle a\rangle) - \gamma\langle n\rangle$$
$$= -2f(t)\langle P_{\omega_p}\rangle - \gamma\langle n\rangle,$$

where $\langle P_{\omega_p}\rangle = \frac{i}{2}(\langle a^\dagger\rangle e^{-i\omega_p t} - \langle a\rangle e^{i\omega_p t})$ is the optical phase space coordinate. Making use of the previous expressions, the derivative of the SOQC function is then:

$$\frac{d}{dt}g^{(2)} = -i\frac{f(t)}{\langle n\rangle^2}[e^{-i\omega_p t}\langle 2a^\dagger aa\rangle - e^{i\omega_p t}\langle 2a^\dagger a^\dagger a\rangle + (e^{-i\omega_p t}\langle a\rangle - e^{i\omega_p t}\langle a^\dagger\rangle)(1 - 2\langle n\rangle g^{(2)})],$$

which in general is not zero.

5.3.2 1-D Bose-Hubbard chain

We now show explicitly the validity of the results for a system composed of M-modes. For simplicity we focus on a 1D Bose Hubbard Hamiltonian, with nearest neighbour interaction, described by the following Hamiltonian:

$$H_{BH} = \sum_{i=1}^{M}\tau(a_i^\dagger a_{i+1} + a_{i-1}^\dagger a_i) + g(a_i^\dagger a_i^\dagger a_i a_i). \tag{5.37}$$

We start by considering a closed system and, as before, we evaluate the total second order correlation function:

$$\frac{d}{dt}g^{(2)}_{tot} = \frac{d}{dt}\left(\frac{\sum_{j,k=1}^{M}\langle a_j^\dagger a_j a_k^\dagger a_k\rangle}{\langle N\rangle^2}\right) = \\ = \left(\frac{\frac{d}{dt}\sum_{j,k=1}^{M}\langle a_j^\dagger a_j a_k^\dagger a_k\rangle\langle N\rangle^2 - \frac{d}{dt}\langle N\rangle^2\sum_{j,k=1}^{M}\langle a_j^\dagger a_j a_k^\dagger a_k\rangle}{\langle N\rangle^4}\right).$$

We can split the expression for the derivative of the total $G^{(2)}$, in terms of the derivative of the cross terms and of the autocorrelations:

$$\frac{d}{dt}\sum_{j,k=1}^{M}\langle a_j^\dagger a_j a_k^\dagger a_k\rangle = \sum_{j,k=1}^{M}\frac{d}{dt}\langle a_j^\dagger a_j a_k^\dagger a_k\rangle = \sum_{j=1}^{M}\frac{d}{dt}\langle a_j^\dagger a_j a_j^\dagger a_j\rangle + \sum_{j,k=1,k\neq j}^{M}(\frac{d}{dt}\langle a_j^\dagger a_j a_k^\dagger a_k\rangle \\ + \frac{d}{dt}\langle a_k^\dagger a_k a_j^\dagger a_j\rangle).$$

Let us first consider the time derivatives of all the autocorrelations ($j = k$):

$$\sum_{j=1}^{M}\frac{d}{dt}\langle a_j^\dagger a_j^\dagger a_j a_j\rangle = i\tau\sum_{j=1}^{M}(\langle a_j^\dagger a_j a_j^\dagger a_{j+1}\rangle + \langle a_j^\dagger a_j a_j^\dagger a_{j-1}\rangle + \langle a_j^\dagger a_{j+1} a_j^\dagger a_j\rangle + \langle a_j^\dagger a_{j-1} a_j^\dagger a_j\rangle \\ - \langle a_{j+1}^\dagger a_j a_j^\dagger a_j\rangle - \langle a_{j-1}^\dagger a_j a_j^\dagger a_j\rangle - \langle a_j^\dagger a_j a_{j+1}^\dagger a_j\rangle - \langle a_j^\dagger a_j a_{j-1}^\dagger a_j\rangle).$$

Then, consider the case of the cross-correlations ($j \neq k$):

$$\sum_{j,k=1,k\neq j}^{M}\frac{d}{dt}\langle a_j^\dagger a_j a_k^\dagger a_k\rangle = \sum_{j,k=1,k\neq j}^{M}(i\tau(\langle a_j^\dagger a_j a_k^\dagger a_{k+1}\rangle + \\ \langle a_j^\dagger a_j a_k^\dagger a_{k-1}\rangle + \langle a_j^\dagger a_{j+1} a_k^\dagger a_k\rangle + \langle a_j^\dagger a_{j-1} a_k^\dagger a_k\rangle - \\ \langle a_{j+1}^\dagger a_j a_k^\dagger a_k\rangle - \langle a_{j-1}^\dagger a_j a_k^\dagger a_k\rangle - \langle a_j^\dagger a_j a_{k+1}^\dagger a_k\rangle \\ - \langle a_j^\dagger a_j a_{k-1}^\dagger a_k\rangle)).$$

Substituting the relations (5.38)-(5.38) in (5.38), we can evaluate the total derivative of the $G^{(2)}$. To demonstrate that the total summation gives zero, let us consider the terms with $k = j + 1$ in (5.38):

$$\frac{d}{dt}\langle a_j^\dagger a_j a_{j+1}^\dagger a_{j+1}\rangle = i\tau(\langle a_j^\dagger a_j a_{j+1}^\dagger a_{j+2}\rangle + \langle a_j^\dagger a_j a_{j+1}^\dagger a_j\rangle + \langle a_j^\dagger a_{j+1} a_{j+1}^\dagger a_{j+1}\rangle \\ + \langle a_j^\dagger a_{j-1} a_{j+1}^\dagger a_{j+1}\rangle - \langle a_{j+1}^\dagger a_j a_{j+1}^\dagger a_{j+1}\rangle - \langle a_{j-1}^\dagger a_j a_{j+1}^\dagger a_{j+1}\rangle \\ - \langle a_j^\dagger a_j a_{j+2}^\dagger a_{j+1}\rangle - \langle a_j^\dagger a_j a_j^\dagger a_{j+1}\rangle).$$

we can see that all the terms containing a combination of the $(j, j+1)$ indices in (5.38) cancel out with the equivalent terms in (5.38), while the terms containing combinations of $(j, j+1, j+2)$,$(j-1, j, j+1)$ remain. They get cancelled by considering the terms with $k = j-1$ and $k = j+2$ in (5.38): these terms will give again correlators containing combinations of $(j+1, j+2, j+3)$, which are cancelled by the next term in the k series, and so on until we reach the boundaries of the system. Hence, iterating the process described above, we find that the sum of the series is exactly zero. In conclusion we have demonstrated that, in a 1D chain of interacting boson, the correlation will be re-distributed among the modes during the dynamical evolution, while the total $G^{(2)}$ remains stationary:

$$\frac{d}{dt}G^{(2)}_{tot} = \sum_{j,k=1}^{M} \frac{d}{dt}\left\langle a_j^\dagger a_j a_k^\dagger a_k \right\rangle = 0, \tag{5.38}$$

and the same demonstration holds for the total number of particles:

$$\frac{d}{dt}\left\langle N \right\rangle = 0. \tag{5.39}$$

Adding a Lindblad term in the master equation, $\mathcal{L}(\rho) = \sum_{i=1}^{M} \frac{\gamma}{2}(2a_i\rho a_i^\dagger - a_i a_i^\dagger \rho - \rho a_i a_i^\dagger)$, leads to an exponential decay of our statistical quantities,

$$\frac{d}{dt}\left\langle N \right\rangle = -\gamma \sum_{j=1}^{M} \left\langle a_j^\dagger a_j \right\rangle, \tag{5.40}$$

$$\frac{d}{dt}G^{(2)}_{tot} = \sum_{j,k=1}^{M} \frac{d}{dt}\left\langle a_j^\dagger a_j a_k^\dagger a_k \right\rangle = -2\gamma \sum_{j,k=1}^{M} \left\langle a_j^\dagger a_j a_k^\dagger a_k \right\rangle. \tag{5.41}$$

Using expressions (5.40) and (5.41) inside (5.38), it is possible to calcutate the total derivative of the second order correlation function for the multimode system:

$$\begin{aligned}
&\frac{d}{dt}g^{(2)}(t,t)_{tot} = \\
&= \left(- \frac{2\gamma \sum_{j=1}^{M}\sum_{k=1}^{M} \left\langle a_j^\dagger a_j a_k^\dagger a_k \right\rangle \sum_i^M \left\langle a_i^\dagger a_i \right\rangle^2 + 2\gamma \sum_{j=1}^{M}\sum_{k=1}^{M}\sum_i^M \left\langle a_i^\dagger a_i \right\rangle^2 \left\langle a_j^\dagger a_j a_k^\dagger a_k \right\rangle}{\sum_{j=1}^{M} \left\langle a_j^\dagger a_j \right\rangle^4} \right) \\
&= 0.
\end{aligned} \tag{5.42}$$

So $g^{(2)}(t,t)_{tot}$, again, is a conserved quantity. The $U(1)$ symmetry is locally broken, i.e. $[H, n_i] \neq 0$, where $n_i = a_i^\dagger a_i$, hence the corresponding second order correlation function is not stationary. However, the global $U(1)$ is preserved, giving as a result the conservation of the total correlation function.

To show the validity of the result numerically, we consider the case of two undriven bosonic modes, coherently coupled with the same linear dissipation for each mode. Using the master equation approach it is easy to show that the dissipation terms appearing in eqs.(5.13) and (5.13) are exactly cancelled by those in the autocorrelation functions, (5.14), so, as expected, the total second order correlation function is conserved. However, it is instructive to look in more detail at the development of non-classical correlations in a two mode system with Kerr non-linearities.

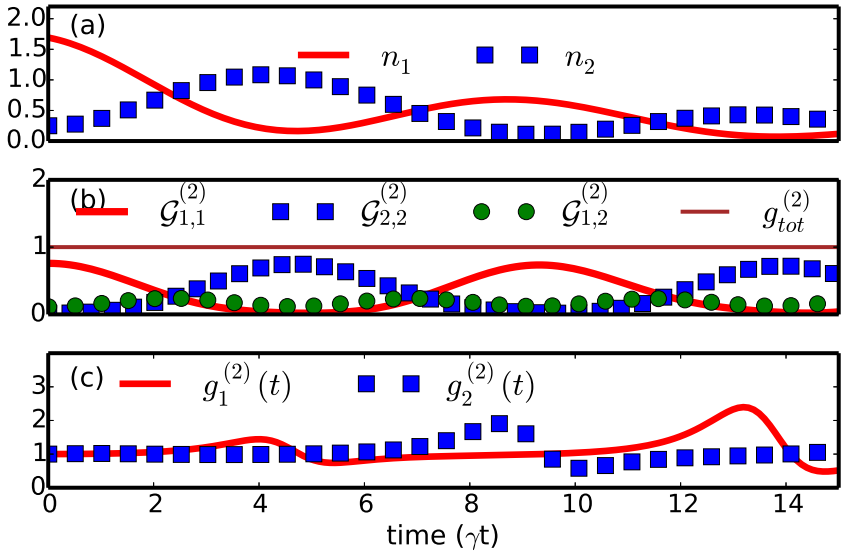

Figure 5.3: Numerical solutions for the number of excitation for two coupled bosonic modes, with coupling $\tau = 1.5\gamma$ and nonlinearity $g = 0.25\gamma$, prepared into an initial state with $|\alpha_1|^2 = 1.7$ particles in mode 1 and $|\alpha_2|^2 = 0.22$ particles in mode 2 (α_1 and α_2 both real and positive), and $\omega_1 = \omega_2 = 0$. (a) Populations of the two modes, n_1 and n_2. (b) The correlation functions $\mathcal{G}^{(2)}_{i,j} = \langle a_i^\dagger a_j^\dagger a_i a_j \rangle / N^2$ for each mode and for the cross terms. The total correlation function for the emitted light is a constant of motion; in this case $g^{(2)}_{tot} = 1$, as the initial state is coherent.(c) The time evolution of the normalized second order correlation functions for the individual modes; each shows a non-trivial behavior, even though the total correlation function is stationary.

We use the positive-P representation developed by Drummond et al. [96], to

transform the master equation, Eq(5.23), into a set of stochastic differential equations which are solved using Monte-Carlo methods. We consider a system of two non-linear bosonic modes described by the Hamiltonian H_{tm}, with the addition of on-site non-linearities $g(a_1^{\dagger 2}a_1^2+a_2^{\dagger 2}a_2^2)$, prepared in an initial coherent state, $|\psi(0)\rangle = |\alpha_1, \alpha_2\rangle$, with $|\alpha_1|^2$ particles in one mode and $|\alpha_2|^2$ particles in the other mode. We evaluate the normalized second order correlation function for each mode and for the cross-correlations. While the particles move between cavities and disappear due to dissipation, the quantities $\mathcal{G}_{i,j}^{(2)} = \langle a_i^\dagger a_j^\dagger a_i a_j \rangle / N^2$, describing the correlation functions normalized to the total number of particles, undergo a dynamical evolution. However, it can be clearly seen that the total correlation function is constant in the whole time interval, as our theorem requires. The conserved $g_{tot}^{(2)} = 1$, as the initial state is coherent. By contrast,if we look at the the individual cavity second order correlations, $g_1^{(2)}(t,t)$ and $g_2^{(2)}(t,t)$, non-classical behaviour is apparent, with their values falling below one at some stages of the evolution. This demonstrates a situation where the total emission has classical statistics, but quantum effects can be observed if the individual modes are resolved.

5.3.3 The continuum limit

Until now we have considered a discrete collection of quantum systems. However, our **Theorem** can be extended to the case of a system with a continuum of modes, for example, the optical field in a waveguide. If the Hamiltonian commutes with the total number operator[97],

$$N = \int_{-\infty}^{+\infty} dx\, a^\dagger(x) a(x), \tag{5.43}$$

then the total second order correlation function,

$$g_{tot}^{(2)} = \frac{1}{\langle N \rangle^2} \langle \int_{-\infty}^{+\infty} dx\, dx'\, a^\dagger(x) a^\dagger(x') a(x) a(x') \rangle \tag{5.44}$$

is stationary, provided any losses are linear and independent of x. This is true even when individual point-like components, $g^{(2)}(x,x')$, experience temporal dynamics.

To show this explicitly, we consider the Hamiltonian for a single mode bosonic waveguide:

$$H_c = \int_{-\infty}^{+\infty} dx(\omega_0 a^\dagger(x)a(x) - iva^\dagger(x)\partial_x a(x)) \tag{5.45}$$

where v is the group velocity of the wavepacket. We first want to show that, if $[H, n] = 0$, then $g^{(2)}(t,t) = 0$. To show that H_c commutes with the number operator, we need to evaluate $[a^\dagger(x)a(x), a^\dagger(x')\partial_{x'}a(x')]$,

$$\begin{aligned}&\int_{-\infty}^{+\infty}\int_{-\infty}^{+\infty} dxdx'[a^\dagger(x)a(x), a^\dagger(x')\partial_{x'}a(x')] = \\ &= \int dxa^\dagger(x)\partial_x a(x) + \int dxa^\dagger(x)\int dx'\partial_{x'}\delta(x-x')a(x'),\end{aligned} \tag{5.46}$$

we have used here the properties of the Dirac delta function and

$$[A(x), B(x')] = C(x,x') \rightarrow [A(x), \partial_{x'}B(x')] = \partial_{x'}C(x,x'), \tag{5.47}$$

and this property comes from the fact that the derivative acts only on the x' variable. Using now the property of the derivative of the Dirac delta in equation (5.46),

$$\int dx\partial_x\delta_x f(x) = -\partial_x f(0), \tag{5.48}$$

we find,

$$\begin{aligned}&\int_{-\infty}^{+\infty}\int_{-\infty}^{+\infty} dxdx'[a^\dagger(x)a(x), a^\dagger(x')\partial_{x'}a(x')] = \\ &= \int_{-\infty}^{+\infty} dxa^\dagger(x)\partial_x a(x) - \int_{-\infty}^{+\infty} dxa^\dagger(x)\partial_x a(x) = 0.\end{aligned} \tag{5.49}$$

So H_c commutes with the total number of excitation. Similarly it is possible to demonstrate that, in this case, the derivative of the total SOQC function is

$$\begin{aligned}\frac{d}{dt}g^{(2)}_{tot}(t,t) &= \frac{d}{dt}\int\int dxdx'\frac{\langle a^\dagger(x)a^\dagger(x')a(x)a(x')\rangle}{\langle a^\dagger(x)a(x)\rangle\langle a^\dagger(x')a(x)'\rangle} \\ &= \int\int dxdx'\partial_t\frac{\langle a^\dagger(x)a^\dagger(x')a(x)a(x')\rangle}{\langle a^\dagger(x)a(x)\rangle\langle a^\dagger(x')a(x')\rangle} \\ &= 0.\end{aligned}$$

Each x-dependent component, by contrast, changes dynamically. Explicitly:

$$\begin{aligned}\frac{d}{dt}G^{(2)}_{x,x'} &= \frac{d}{dt}\int_{-\infty}^{+\infty} dx\,\langle a^\dagger(x')a^\dagger(x')a(x')a(x')\rangle \\ &= 2v\int_{-\infty}^{+\infty} dx\,\langle a^\dagger(x')a(x')a^\dagger(x')\partial_{x'}a(x')\rangle \\ &+ \langle a^\dagger(x')\partial_{x'}a(x')a^\dagger(x')a(x')\rangle\,, \end{aligned} \tag{5.50}$$

which is not zero, in general.

Chapter 6

Quantum effects in cascades of nonlinear optical systems

In this Chapter we illustrate a result of the theoretical investigation of the quantum properties of nonlinear optical systems, arranged in a *cascade configuration*: the output of one system (source) is used as the input of another system (target). This configuration allows, in principle, to drive the target system with a light source having arbitrary statistical properties.

We first introduce, briefly, the formalism used to describe such configuration, derived by Carmichael [98] and Gardiner: the approach consists of an extension of the *input-output* formalism, leading to a master equation formulation. We then make use of the positive P-representation to evaluate the dynamics of the cascade master equation, in the particular scenario of sub-systems made up of Kerr nonlinear medium: hence the results are suitable for describing cascades made of microcavity polaritons, Rydberg atoms and, to some extend, superconducting qubits. We quantify the effect of the cascade coupling on the second-order correlation function and then we demonstrate that the two systems coupled through this dissipative coupling, can be driven into an entangled state.

6.1 Theoretical methods: input-output and cascade master equation

In this section we introduce the basic idea behind the input-output model and the quantum stochastic differential equation.

We consider a bosonic reservoir, interacting with a localised quantum system:

$$H = H_{\text{sys}} + H_B + H_{\text{int}}, \tag{6.1}$$

where H_{sys} is left unspecified and we define the reservoir Hamiltonian with a continuous spectrum:

$$H_B = \int \omega b^\dagger(\omega) b(\omega) d\omega, \tag{6.2}$$

with $b(\omega)$ having the units of the square root of time, and satisfying $[b(\omega), b^\dagger(\omega')] = \delta(\omega - \omega')$. Assuming a linear interaction between the system and the reservoir, in the interaction picture and within the usual RWA and Born-Markov approximations, H_{int} reads:

$$H_{\text{int}} = i\sqrt{\frac{\gamma}{2\pi}} \int (c b^\dagger(\omega) - c^\dagger b(\omega)) d\omega, \tag{6.3}$$

with γ the coupling factor between the system and the reservoir, assumed to be constant within a certain interval of frequencies as required by the Markovian approximation, and c are the system operators. We first define the input field b_{in} in terms of the bosonic field operators $b(\omega)$:

$$b_{\text{in}}(t) = \frac{1}{\sqrt{2\pi}} \int b_0(\omega) e^{-i\omega t} d\omega, \tag{6.4}$$

where b_0 corresponds to the value of $b(\omega)$ at $t = 0$, obeying to the same commutation rules as for $b(\omega)$. Eq. (6.4) basically represents the amplitude of the field incident on the system at time t. The terms $b_{\text{in}}(t)$ are also called *noise terms*: however, interpreting the b_{in} operators as noise is exact only if the state of the system is initially factorized and the field b_{in} is incoherent. Normally this means that we are

dealing with thermal states, i.e.:

$$\langle b^\dagger(t)b(t')\rangle = \bar{N}(\omega,T)\delta(t-t'), \tag{6.5}$$

where $\bar{N}(\omega,T)$ is the thermal distribution function of the bosonic field. From the canonical commutation relation for $b(\omega)$, it can be seen that $[b_{\text{in}}(t), b^\dagger_{\text{in}}(t')] = \delta(t-t')$. Hence, following the approach of Gardiner and Collet in [99], it is possible to derive the Heisenberg equation of motion for the arbitrary system operator a:

$$\partial_t a(t) = -i[a(t), H_{\text{sys}}] - [a(t), c^\dagger(t)]\left[\frac{\gamma}{2}c(t) + \sqrt{\gamma}b_{\text{in}}(t)\right] - \left[\frac{\gamma}{2}c^\dagger(t) + \sqrt{\gamma}b^\dagger_{\text{in}}(t)\right][a^\dagger(t), c(t)]. \tag{6.6}$$

The output field operator is defined as:

$$b_{\text{out}}(t) = \int e^{-i\omega(t-t_1)}b_1(\omega)d\omega, \tag{6.7}$$

where $b_1(\omega)$ is the value of the field $b(\omega)$ at time $t_1 > t$, hence b_{out} is the value of the field at some time t_1, after the interaction with the system. Following the approach of Gardiner, it can be demonstrated, using the relations above, that the input and output fields are related by the relation:

$$b_{\text{out}}(t) = b_{\text{in}}(t) + \sqrt{\gamma}c(t), \tag{6.8}$$

which models the scattering of the input mode in the output mode after the interaction with the system.

Now, let us consider the time-integrated quantities:

$$B_{\text{in}}(t) = \int_0^t ds b_{\text{in}}(s), \qquad B^\dagger_{\text{in}}(t) = \int_0^t ds b^\dagger_{\text{in}}(s), \tag{6.9}$$

and the increments:

$$dB_{\text{in}}(t) = \int_t^{t+dt} ds b_{\text{in}}(s), \qquad dB^\dagger_{\text{in}}(t) = \int_t^{t+dt} ds b^\dagger_{\text{in}}(s), \tag{6.10}$$

which are called *quantum stochastic increments*: the name comes from the fact that, from the commutation relation $[b_{\text{in}}(t), b^\dagger_{\text{in}}(t')] = \delta(t-t')$, it follows that $[dB^\dagger_{\text{in}}(t), dB_{\text{in}}(t')] =$

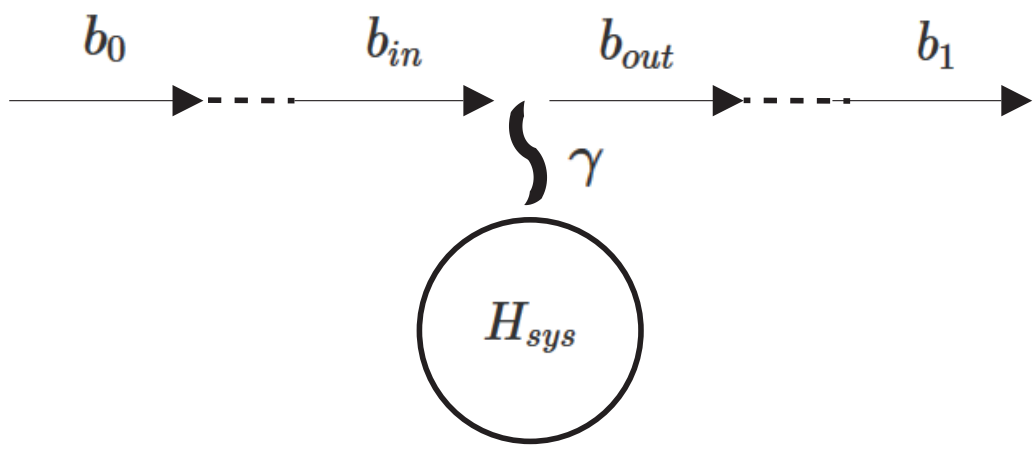

Figure 6.1: Schematic representation of the input-output model.

dt if $t - t' = 0$ and zero otherwise. Hence they can be treated as the quantum equivalent of classical Wiener increments. From the commutation relations for $b_{\rm in}$, it follows that the vacuum expectation values for the stochastic increments are:

$$\langle dB^\dagger(t)dB(t')\rangle = \langle dB^\dagger(t)dB^\dagger(t')\rangle = \langle dB^\dagger(t)dB(t')\rangle = 0 \tag{6.11}$$

$$\langle dB(t)dB^\dagger(t')\rangle = dt. \tag{6.12}$$

Making use on (6.10) and (6.11) of the rules of *Ito Calculus*, Gardiner et al. [99], derived the Ito form of the *quantum stochastic differential equation* for the input-output system:

$$da = -i[a, H_{\rm sys}]dt + \frac{\gamma}{2}(\bar{N}+1)(2c^\dagger ac - ac^\dagger c - c^\dagger ca)dt + \frac{\gamma}{2}\bar{N}(2cac^\dagger - acc^\dagger - cc^\dagger a)dt - \sqrt{\gamma}[a, c^\dagger]dB_{\rm in}(t) + \sqrt{\gamma}[a, c]dB^\dagger_{\rm in}(t). \tag{6.13}$$

For $\bar{N} = 0$, which is the case we will consider in the following, equation (6.13) is equivalent to (6.6): to see this is sufficient to change $dB_{\rm in}(t) \to b_{\rm in}dt$. The Ito form of the quantum evolution equation is computationally convenient, as the stochastic increments commute with the system operator, but it presents some inconveniences. First, as we mentioned already, the rules of the Ito calculus are slightly different from the standard one. Moreover the bath distribution $\bar{N}$ explicitly appears in (6.13),

hence a complete knowledge of the bath statistics is, in general, necessary.

For practical purposes, it is convenient to work with the quantum master equation, corresponding to (6.13). To derive the master equation for the system, we first assume again that, initially, the system is factorized, i.e. $\rho(0) = \rho_{\text{sys}}(0) \otimes \rho_B$. Considering equation (6.13), with $\bar{N} = 0$, the mean value of the operator is given by:

$$\langle da \rangle = \langle -i[a, H_{sys}] + \frac{\gamma}{2}(2c^\dagger ac - ac^\dagger ca - c^\dagger ca) \rangle \, dt, \tag{6.14}$$

as the terms proportional to the stochastic increments $dB_{\text{in}}(t)$ have zero mean. For any operator O, $\langle O \rangle = \text{Tr}(O\rho)$, hence:

$$\langle da \rangle = \text{Tr}((-i[a, H_{sys}] + \frac{\gamma}{2}(2c^\dagger ac - ac^\dagger ca - c^\dagger ca))\rho) dt. \tag{6.15}$$

Using the cyclic property of the trace, we derive:

$$\frac{d}{dt}\langle a \rangle = \text{Tr}(a(i[\rho, H_{sys}] + \frac{\gamma}{2}(2c^\dagger \rho c - \rho c^\dagger c - c^\dagger c\rho))), \tag{6.16}$$

and, as we know that $\frac{d}{dt}\langle O \rangle = \text{Tr}(O\frac{d}{dt}\rho)$, we finally obtain:

$$\frac{d}{dt}\rho = i[\rho, H_{\text{sys}}] + \frac{\gamma}{2}(2c^\dagger \rho c - \rho c^\dagger c - c^\dagger c\rho) = \mathcal{L}(\rho), \tag{6.17}$$

which is the master equation, in the Lindblad form, for the system considered.

6.1.1 Cascaded quantum systems

The problem of cascaded quantum systems, i.e., where the output of a system is used as an input field for another system, was first examined by Gardiner in [100] and Carmichael in [98], using different approaches. Consider the case where the output reflected from a single sided cavity, feeds another cavity: this configuration is different from the the usual coherent coupling, as the field moves, unidirectionally, from one system to another, with ideally no scattering from the mirror of the second cavity. Following the approach of Carmichael, the Hamiltonian of the cavity mode

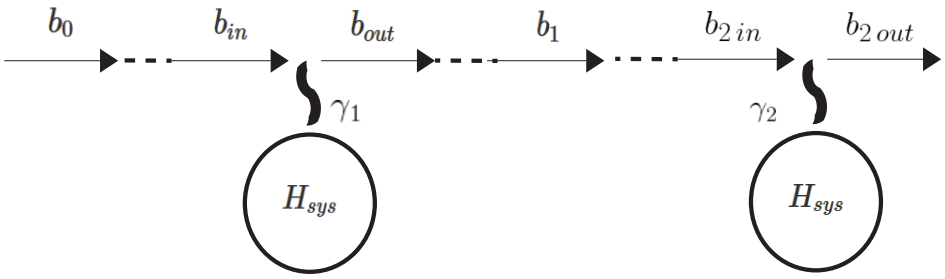

Figure 6.2: Schematic representation of cascade quantum system.

and of the propagating field, reads:

$$H = H_{\text{sys1}} + H_{\text{sys2}} + \int b^\dagger(\omega)b(\omega)d\omega + i\sqrt{\frac{\gamma_1}{2\pi}}\int (c_1 b^\dagger(\omega) - c_1^\dagger b(\omega))d\omega + i\sqrt{\frac{\gamma_2}{2\pi}}\int (c_2 b^\dagger(\omega)e^{-i\omega\tau} - c_2^\dagger b(\omega)e^{i\omega\tau})d\omega,$$

where c_i is the field operator describing the cavity mode and τ is the time needed to the light to propagate between the two systems. Making use of the same procedure as in the previous section, it is possible to derive the Langevin equation for any degree of freedom of the intra-cavity field, a:

$$\begin{aligned}\partial_t a = &-i[a(t), H_{\text{sys1}} + H_{\text{sys2}}] - [a(t), c_1^\dagger(t)](\frac{\gamma_1}{2}c_1(t) + \sqrt{\gamma_1}b_{in}(t)) - (\frac{\gamma_1}{2}c_1^\dagger(t) \\ &+ \sqrt{\gamma_1}b_{in}^\dagger(t))[a^\dagger(t), c_1^\dagger(t)] - [a(t), c_2^\dagger(t)](\frac{\gamma_2}{2}c_2(t) + \sqrt{\gamma_1\gamma_2}c_1(t-\tau) + \sqrt{\gamma_2}b_{\text{in}}(t-\tau)) \\ &- (\frac{\gamma_2}{2}c_2^\dagger(t) + \sqrt{\gamma_1\gamma_2}c_1^\dagger(t-\tau) + \sqrt{\gamma_2}b_{\text{in}}^\dagger(t-\tau))[a^\dagger(t), c_2^\dagger(t)].\end{aligned}$$

We consider the limit of vanishing time of propagation, i.e. $\tau \to 0$, hence giving for (6.18):

$$\begin{aligned}\partial_t a = &-i[a(t), H_{\text{sys1}} + H_{\text{sys2}}] - [a(t), c_1^\dagger(t)](\frac{\gamma_1}{2}c_1(t) + \sqrt{\gamma_1}b_{in}(t)) - (\frac{\gamma_1}{2}c_1^\dagger(t) \\ &+ \sqrt{\gamma_1}b_{in}^\dagger(t))[a^\dagger(t), c_1^\dagger(t)] - [a(t), c_2^\dagger(t)](\frac{\gamma_2}{2}c_2(t) + \sqrt{\gamma_1\gamma_2}c_1(t) + \sqrt{\gamma_2}b_{\text{in}}(t)) \\ &- (\frac{\gamma_2}{2}c_2^\dagger(t) + \sqrt{\gamma_1\gamma_2}c_1^\dagger(t) + \sqrt{\gamma_2}b_{\text{in}}^\dagger(t))[a^\dagger(t), c_2^\dagger(t)],\end{aligned}$$

this approximation is valid as long as $\tau < \frac{1}{\gamma_i}$, with $\frac{1}{\gamma_i}$ being the typical time scale of the emission process. Equation (6.18) demonstrates the main idea behind the cascaded systems, which is the fact that information flows unidirectionally from

one system to another: if a is an operator for the first system, all the commutator containing the operators c_2 are zero, i.e. the dynamics of the first system is not affected, while if a represents an operator for the second system, the commutators containing c_2 are potentially non-zero, so that the dynamics is influenced by c_1, b_{in} and c_2. The output of the whole system can be found by cascading the relation (6.8):

$$b_{\text{out}}(t) = b_{\text{out},2}(t) = b_{\text{in},2}(t) + \sqrt{\gamma_2}c_2(t) = b_{\text{in}}(t) + \sqrt{\gamma_1}c_1(t) + \sqrt{\gamma_2}c_2(t), \qquad (6.18)$$

which implies that the effective coupling between the input and the output field of the whole system is given by $\sqrt{\gamma_1}c_1(t) + \sqrt{\gamma_2}c_2(t)$. With the same procedure as in the previous sections, it is possible to derive the master equation for the cascade quantum systems:

$$\frac{d}{dt}\rho = i[\rho, H_{\text{sys1}} + H_{\text{sys2}}] + \frac{\gamma_1}{2}(2c_1^\dagger \rho c_1 - \rho c_1^\dagger c_1 - c_1^\dagger c_1 \rho) + \frac{\gamma_2}{2}(2c_2^\dagger \rho c_2 - \rho c_2^\dagger c_2 - c_2^\dagger c_2 \rho) - \sqrt{\gamma_1\gamma_2}([c_2^\dagger, c_1\rho] + [\rho c_1^\dagger, c_2]),$$

where the last term models the coupling between the two systems, which, as required, is incoherent and unidirectional.

6.2 Cascade of nonlinear optical systems

We first consider two Kerr cavities in cascade: our aim is to calculate the second-order correlation function. In order to do that we make use of the Positive-P representation, which allows us to derive the Fokker-Planck equation for the P-distribution, and to rewrite the master equation as a set of stochastic differential equation, as described in the previous chapters. Then, taking the mean value of each random variable, we derive and solve the mean field equations for the steady state. To evaluate the correlation functions it is then necessary to find the equations for the fluctuations: the information about the field variances and covariances are contained in the covariance matrix σ, which is the key quantity for the evaluation of the $g^{(2)}$ function.

The two bosonic modes, with an onsite Kerr nonlinearity, in a linear dissipative regime, one of them driven by a coherent, continuous wave pump, are modelled by the following Hamiltonian:

$$H_{\text{sys}} = \omega_1 a_1^\dagger a_1 + \omega_2 a_2^\dagger a_2 + k_1 a_1^\dagger a_1^\dagger a_1 a_1 + k_2 a_2^\dagger a_2^\dagger a_2 a_2 + f(t)(e^{-i\omega_P t} a_1^\dagger + e^{i\omega_P t} a_1). \quad (6.19)$$

The two modes are interacting through an incoherent and unidirectional channel. To model such configuration we need to make use of the master equation for cascade systems, (6.19):

$$\begin{aligned}\partial_t \rho = &- i[H_{\text{sys}}, \rho] + \frac{\gamma_1}{2}(2a_1^\dagger \rho a_1 - a_1^\dagger a_1 \rho + \rho a_1^\dagger a_1) + \frac{\gamma_2}{2}(2a_2^\dagger \rho a_2 - a_2^\dagger a_2 \rho - \rho a_2^\dagger a_2) - \\ &- \sqrt{\eta\gamma_1\gamma_2}([a_2^\dagger, \rho a_1] + [\rho a_1^\dagger, a_2]), \end{aligned} \quad (6.20)$$

where the first two Lindblad terms describe the dissipation for each mode, while the third one is the cascade coupling of the first mode into the second. The effective coupling parameter, $0 \leq \eta \leq 1$, describes what fraction of particles emitted by the first system is entering the second one: it takes into account a variety of phenomena like scattering, absorption and so on. In the following we are considering identical systems, unless differently specified, with $\gamma_1 = \gamma_2 = \gamma$ and $k_1 = k_2 = k$, and a perfect coupling between the modes in cascade ($\eta = 1$).

To quantify the relevant statistical quantities associate to the cascade system, we make use again of the positive P-representation:

$$\rho = \int d\alpha d\beta \frac{|\alpha\rangle \langle\beta|}{\langle\alpha\beta\rangle} P(\alpha, \beta) \quad (6.21)$$

where $|\alpha\rangle, |\beta\rangle$ are coherent states vectors, that form a basis for a doubled Hilbert space. We make use of the usual correspondence rules:

$$\begin{aligned} a\rho &\to \alpha P(\alpha,\beta), \;\; a^\dagger \rho \to (\beta - \partial_\alpha) P(\alpha,\beta) \\ \rho a &\to (\alpha - \partial_\beta) P(\alpha,\beta), \;\; \rho a^\dagger \to \beta P(\alpha,\beta) \end{aligned}$$

In the following, for the analytical evaluation of the statistical moments, we consider

the P-representation variables (α, α^*), as this simplifies the mathematics without changing the final result. We follow the same procedure described in the previous Chapters: we convert the operator-valued master equation, in a system of stochastic differential equations for c-numbers, $(a_1, a_2) \Rightarrow (\alpha_1, \alpha_1^*, \alpha_2, \alpha_2^*)$. In particular for (6.20), the equation of motion have the form:

$$\partial_t \begin{pmatrix} \alpha_1 \\ \alpha_1^* \\ \alpha_2 \\ \alpha_2^* \end{pmatrix} = \begin{pmatrix} A'(\alpha_1, \alpha_1^*, \alpha_2, \alpha_2^*) \\ A'^*(\alpha_1, \alpha_1^*, \alpha_2, \alpha_2^*) \\ A''(\alpha_1, \alpha_1^*, \alpha_2, \alpha_2^*) \\ A''^*(\alpha_1, \alpha_1^*, \alpha_2, \alpha_2^*) \end{pmatrix} + \zeta(t), \tag{6.22}$$

where $\zeta(t)$ is a vector of delta correlated random noise terms with correlation matrix:

$$D = \begin{pmatrix} -ik\alpha_1^2 & 0 & 0 & 0 \\ 0 & ik\alpha_1^{*2} & 0 & 0 \\ 0 & 0 & -ik\alpha_2^2 & 0 \\ 0 & 0 & 0 & ik\alpha_2^{*2} \end{pmatrix}, \tag{6.23}$$

whose entries come from the second derivatives in the Fokker-Planck equation. The drift matrix elements are:

$$A'(\alpha_1, \alpha_1^*, \alpha_2, \alpha_2^*) = -\gamma\alpha_1 - i\omega\alpha_1 - ife^{-i\omega_P t} - ik|\alpha_1|^2\alpha_1,$$
$$A''(\alpha_1, \alpha_1^*, \alpha_2, \alpha_2^*) = -\gamma\alpha_2 - i\omega\alpha_2 - ik|\alpha_2|^2\alpha_2 + \gamma\alpha_1,$$

which come from the terms proportional to the first derivatives in the Fokker-Planck equation.

The next step is to obtain the classical solution, taking the ensemble average of each equation, such that the fluctuations average to zero. Defining $\langle\alpha_1\rangle = S_1$ and $\langle\alpha_2\rangle = S_2$, then the classical equations are:

$$\begin{cases} \partial_t S_1 = -\gamma S_1 - i\omega S_1 - ife^{-i\omega_P t} - ik|S_1|^2 S_1 \\ \partial_t S_2 = -\gamma S_2 - i\omega S_2 - ik|S_2|^2 S_2 + \gamma S_1 \end{cases} \tag{6.24}$$

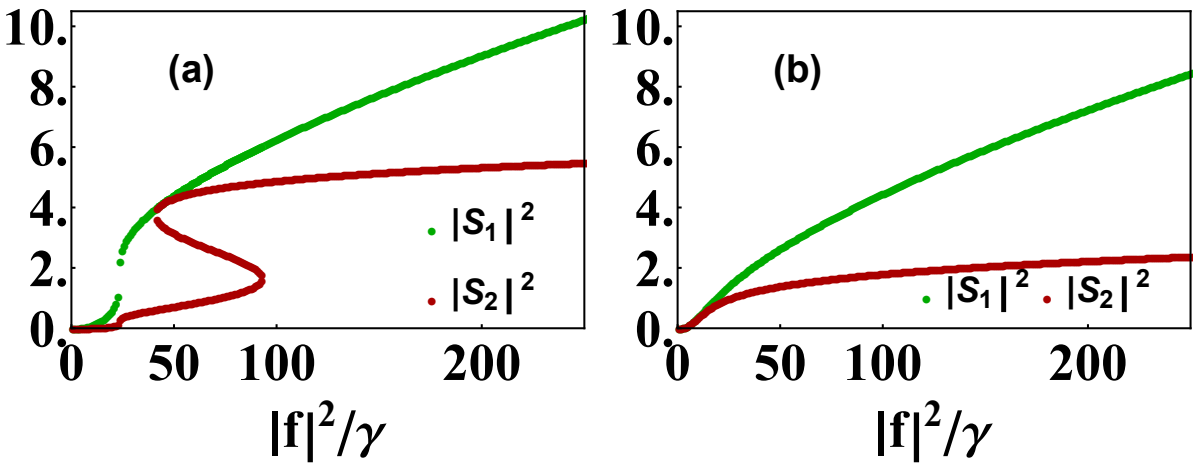

Figure 6.3: (a) Bistable and multi-stable behavior for the number of particles, as function of the relative pump intensity, $|f|^2/\gamma$, with $\gamma = 0.2$, $k = \gamma$, $\delta = 2 * \sqrt{3}\gamma$. (b) The resonant case, $\delta = 0$, where the system (6.25) has only one stable solution.

To get rid of the time dependence in the pump term, we need to transform the fields, $S_1 \to S_1 e^{-i\omega_P t}$ and $S_2 \to S_2 e^{-i\omega_P t}$. This transformation replaces ω with $\delta = \omega - \omega_P$. Looking for the steady state, the time derivative is set to zero and the classical equations simplify to:

$$\begin{aligned} -i\gamma S_1 + (\delta + k|S_1|^2)S_1 &= -f \\ -i\gamma S_2 + (\delta + k|S_2|^2)S_2 &= -i\gamma S_1. \end{aligned} \tag{6.25}$$

Taking the modulus squared of the equations above gives,

$$\begin{aligned} (\gamma^2 + (\delta + k|S_1|^2)^2)|S_1|^2 &= |f|^2 \\ (\gamma^2 + (\delta + k|S_2|^2)^2)|S_2|^2 &= \gamma^2|S_1|^2. \end{aligned} \tag{6.26}$$

The first equation is completely independent from the second one, and it gives a bistable behavior, as a function of the pump intensity, when $\delta > \sqrt{3}\gamma$. The second equation is effectively driven by the first field, with an intensity $\gamma^2|S_1|^2$, so it can experience a doubly bistable behavior: one inherited from the multiple solutions for S_1 and the other coming from the intrinsic nonlinearity for S_2, again if $\delta > \sqrt{3}\gamma$. We now need to expand the Langevin equation for the quantum system, so that the variables are fluctuations about the classical solutions. It is convenient to scale again

the fluctuations by the classical solutions, that is $\alpha_1 \to S_1(1+\tilde{\alpha_1})$ and $\alpha_2 \to S_2(1+\tilde{\alpha_2})$. Hence we need to expand the nonlinear terms and linearise the results:

$$\begin{aligned} |\alpha_1|^2\alpha_1 &= |S_1|^2 S_1(1+\tilde{\alpha_1}) \to |S_1|^2 S_1(2\tilde{\alpha_1} + \tilde{\alpha_1^*}), \\ |\alpha_2|^2\alpha_2 &= |S_2|^2 S_2(1+\tilde{\alpha_2}) \to |S_2|^2 S_2(2\tilde{\alpha_2} + \tilde{\alpha_2^*}), \end{aligned} \tag{6.27}$$

then we get:

$$\begin{aligned} \partial_t\tilde{\alpha_1} &= (-\gamma - i\delta)\tilde{\alpha} - ik|\tilde{\alpha_1}|^2(2\tilde{\alpha_1} + \tilde{\alpha_1^*}), \\ \partial_t\tilde{\alpha_2} &= (-\gamma - i\delta)\tilde{\alpha_2} - ik|\tilde{\alpha_2}|^2(2\tilde{\alpha_2} + \tilde{\alpha_2^*}) + \gamma\tilde{\alpha_1}\frac{S_1}{S_2}. \end{aligned}$$

From equation (6.25), it is possible to express S_1/S_2 as:

$$\frac{S_1}{S_2} = 1 + \frac{i}{\gamma}(\delta + k|S_2|^2) \tag{6.28}$$

Now we convert the fluctuations into polar coordinates:

$$\alpha_1 = S_1(1+i_1)e^{-i\theta_1}, \tag{6.29}$$

where i_1 is the modulus of the fluctuation and θ_1 the phase. For small fluctuations it is convenient to approximate the exponential and write:

$$\alpha \approx S_1(1 + i_1 - i\theta_1). \tag{6.30}$$

Comparing the expression above with the definition of $\tilde{\alpha}$, it is possible to recognize i_1 and θ_1 as the real and imaginary part of $\tilde{\alpha}$ respectively. Making this association, we obtain:

$$\begin{aligned} \partial_t i_1 &= -\gamma i_1 - \delta\theta_1 - k|S_1|^2\theta_1 + \eta_1(t), \\ \partial_t i_2 &= -\gamma i_2 - \delta\theta_2 - k|S_2|^2\theta_2 + \gamma i_1 + (\delta + k|S_2|^2)\theta_1 + \eta_2(t), \\ \partial_t \theta_1 &= -\gamma\theta_1 + \delta i_1 + 2k|S_1|^2 i_1 + \xi_1(t), \\ \partial_t \theta_2 &= -\gamma\theta_2 + \delta i_2 + 2k|S_2|^2 i_2 + \gamma\theta_1 - (\delta + k|S_2|^2)i_1 + \xi_2(t) \end{aligned}$$

where the noise terms are

$$\begin{aligned}\eta_i &= \frac{1}{2}\left(\frac{\zeta_i}{S_i} + \frac{\zeta_{i^*}}{S_i^*}\right),\\ \xi_i &= \frac{i}{2}\left(\frac{\zeta_i}{S_i} - \frac{\zeta_{i^*}}{S_i^*}\right).\end{aligned} \tag{6.31}$$

We can now write the matrix $\tilde{A}$ for the fluctuations,derived from (6.31), as:

$$\tilde{A} = \begin{pmatrix} -\gamma & -(\delta + k|S_1|^2) & 0 & 0 \\ (\delta + 3k|S_1|^2) & -\gamma & 0 & 0 \\ \gamma & (\delta + k|S_2|^2) & -\gamma & (\delta + k|S_2|^2) \\ (\delta + k|S_2|^2) & \gamma & (\delta + 3k|S_2|^2) & -\gamma \end{pmatrix}$$

and $\tilde{D}$, the noise matrix for the intensity phase equations, using the expressions:

$$\begin{aligned}\langle \eta_i \eta_i \rangle &= \frac{1}{4}\left(\frac{1}{S_i^2}\langle \zeta_i \zeta_i \rangle + \frac{1}{S_i^{*2}}\langle \zeta_{i^*} \zeta_{i^*} \rangle\right) = \frac{1}{2} Re\left(\frac{1}{S_i^2}\langle \zeta_i \zeta_i \rangle\right) = 0,\\ \langle \eta_i \xi_i \rangle &= \frac{i}{4}\left(\frac{1}{S_i^2}\langle \zeta_i \zeta_i \rangle - \frac{1}{S_i^{*2}}\langle \zeta_{i^*} \zeta_{i^*} \rangle\right) = -\frac{1}{2} Im\left(\frac{1}{S_i^2}\langle \zeta_i \zeta_i \rangle\right) = \frac{k}{2}.\end{aligned}$$

Hence the $\tilde{D}$ matrix is

$$\tilde{D} = \frac{k}{2}\begin{pmatrix} 0 & 1 & 0 & 0 \\ 1 & 0 & 0 & 0 \\ 0 & 0 & 0 & 1 \\ 0 & 0 & 1 & 0 \end{pmatrix}. \tag{6.32}$$

We now focus our attention on the calculation for the second order correlation functions for the two modes. The procedure showed above is the identical to the one showed in Chapter 4, but extended to the case of a two mode system. The $g_1^{(2)}(0)$ for the first mode is:

$$g_1^{(2)}(0) = \frac{\langle \alpha_1^*(t)\alpha_1^*(t)\alpha_1(t)\alpha_1(t)\rangle}{\langle \alpha_1^*(t)\alpha_1(t)\rangle^2} \approx 1 + 4\langle i_1^2 \rangle, \tag{6.33}$$

and the same for the second mode in cascade:

$$g_2^{(2)}(0) = \frac{\langle \alpha_2^*(t)\alpha_2^*(t)\alpha_2(t)\alpha_2(t)\rangle}{\langle \alpha_2^*(t)\alpha_2(t)\rangle^2} \approx 1 + 4\langle i_2^2 \rangle. \tag{6.34}$$

The information about the square of the mean values of the fluctuations (variances) are contained in the covariance matrix, σ, of the system. The covariance matrix is

defined such that its entry in the i, j position is the covariance between the i-th and j-th elements of a vector of random variables. For the fluctuations, as the mean values disappear, σ has the simple formal expression:

$$\sigma = \begin{pmatrix} \langle i_1^2 \rangle & \langle i_1\theta_1 \rangle & \langle i_1 i_2 \rangle & \langle i_1\theta_2 \rangle \\ \langle i_1\theta_1 \rangle & \langle \theta_1^2 \rangle & \langle i_2\theta_1 \rangle & \langle \theta_1\theta_2 \rangle \\ \langle i_2 i_1 \rangle & \langle i_2\theta_1 \rangle & \langle i_2^2 \rangle & \langle i_2\theta_2 \rangle \\ \langle \theta_2 i_1 \rangle & \langle \theta_2\theta_1 \rangle & \langle \theta_2 i_2 \rangle & \langle \theta_2^2 \rangle \end{pmatrix} \tag{6.35}$$

As the first system is completely decoupled from the second one, it is possible to limit our attention to the covariance matrix σ_1 for the reduced system, considering the diffusion and noise submatrices :

$$\tilde{A}_1 = \begin{pmatrix} -\gamma & -(\delta + k|S_1|^2) \\ (\delta + 3k|S_1|^2) & -\gamma \end{pmatrix}, \tag{6.36}$$

$$\tilde{D}_1 = \frac{k}{2}\begin{pmatrix} 0 & 1 \\ 1 & 0 \end{pmatrix}. \tag{6.37}$$

The eigenvalues for $\tilde{A}_1$ are,

$$\lambda_\pm = -\gamma \pm i\sqrt{(\delta + k|S_1|^2)(\delta + 3k|S_1|^2)}, \tag{6.38}$$

and the matrix E_1, made by the eigenvectors of $\tilde{A}_1$, which diagonalize $\tilde{A}_1$ is:

$$E_1 = \psi_1 \begin{pmatrix} \sqrt{(\delta + k|S_1|^2)} & \sqrt{(\delta + k|S_1|^2)} \\ -i\sqrt{(\delta + 3k|S_1|^2)} & i\sqrt{(\delta + 3k|S_1|^2)} \end{pmatrix},$$

$$E_1^{-1} = \psi_2 \begin{pmatrix} i\sqrt{(\delta + k|S_1|^2)} & -\sqrt{(\delta + k|S_1|^2)} \\ -i\sqrt{(\delta + k|S_1|^2)} & \sqrt{(\delta + k|S_1|^2)} \end{pmatrix},$$

where $\psi_1 = \frac{1}{\sqrt{(2\delta+4k|S_1|^2)}}$ and $\psi_2 = \frac{\sqrt{(2\delta+4k|S_1|^2)}}{2i\sqrt{(\delta+k|S_1|^2)(\delta+3k|S_1|^2)}}$.

In this new basis, the D_1 matrix gets the following expression:

$$E_1^{-1} D_1 E_1^{-1T} = ik \frac{(2\delta + 4k|S_1|^2)}{4\sqrt{(\delta + k|S_1|^2)(\delta + 3k|S_1|^2)}} \begin{pmatrix} 1 & 0 \\ 0 & -1 \end{pmatrix}.$$

In this way it is possible to express the covariance matrix $\tilde{\sigma_1}$ in the eigenbasis of $\tilde{A}$, as:

$$(\tilde{\sigma_1})_{i,j} = \frac{1}{-(\lambda_i + \lambda_j)} (E_1^{-1} D_1 E_1^{-1T})_{i,j}. \tag{6.39}$$

Equation (6.39) is the steady state solution, in the chosen basis, for the equation of motion for the covariance matrix:

$$\frac{d}{dt}\sigma(t) = A\sigma(t) + \sigma(t)A + D, \tag{6.40}$$

which can be derived by making used of the *quantum regression theorem* [101]. To transform it back into the i_1, θ_1 basis we make the following transformation:

$$\sigma_1 = E_1 \tilde{\sigma_1} E_1^T. \tag{6.41}$$

The first element of σ_1 is the variance of the real part of the fluctuation, which is what we need for calculating the second order correlation function:

$$\langle i_1^2 \rangle = -\frac{k}{4} \frac{\delta + k|S_1|^2}{\gamma^2 + (\delta + k|S_1|^2)(\delta + 3k|S_1|^2)}, \tag{6.42}$$

giving for the first mode:

$$g_1^{(2)}(0) = 1 - k \frac{\delta + k|S_1|^2}{\gamma^2 + (\delta + k|S_1|^2)(\delta + 3k|S_1|^2)}, \tag{6.43}$$

which is exactly the same relation obtained in Chapter 4, as expected, for a single mode Kerr oscillator. In order to calculate the variance $\langle i_2^2 \rangle$, we need to follow the same procedure as above, this time considering the whole matrix $\tilde{A}$. From the calculation for the steady state classical solution, we can get rid of the dependence on $|S_1|^2$ in the expressions above. Indeed, we find that:

$$|S_1|^2 = \left(1 + \frac{1}{\gamma^2}(\delta + k|S_2|^2)^2\right)|S_2|^2. \tag{6.44}$$

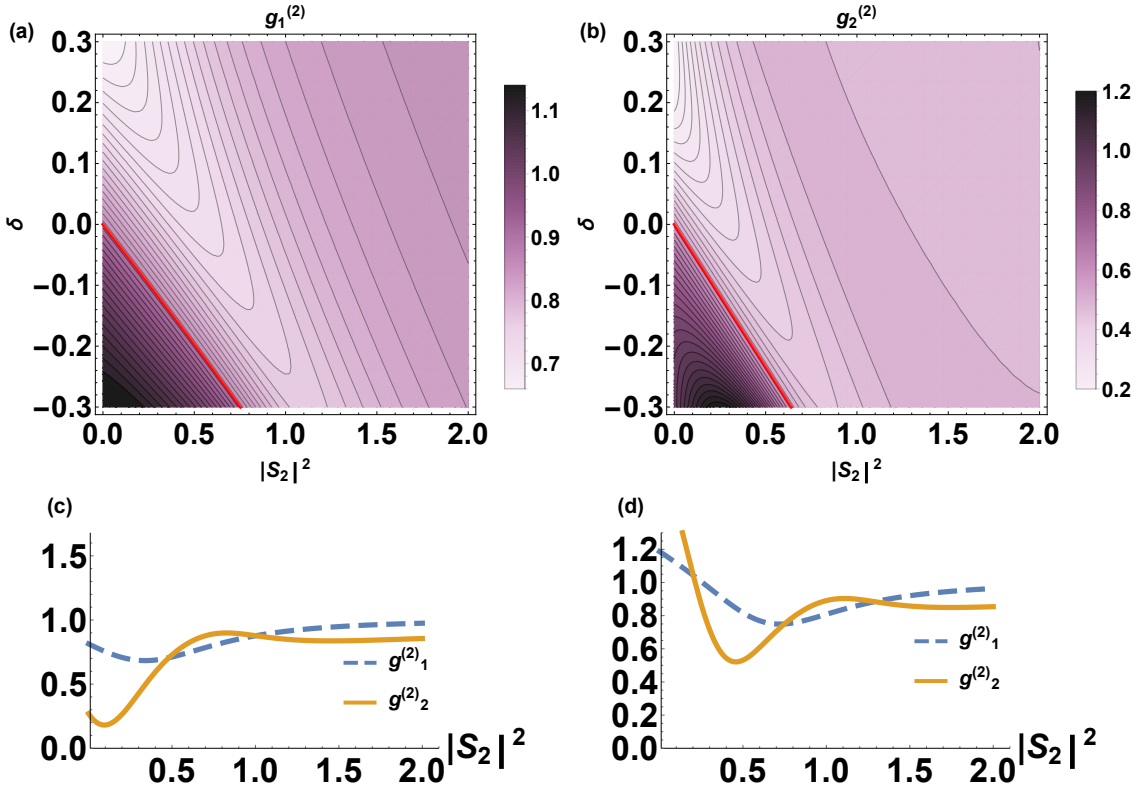

Figure 6.4: **(a)** $g_1^{(2)}$ and **(b)** $g_2^{(2)}$ for the cascade system as a function of the population in cavity two and of the detuning, with $\gamma = 0.4$, $k = \gamma$. The oblique red curve corresponds to $g_m^{(2)} = 1$, while the light colour regions are the ones where the systems are antibunched. The correlation function for the first cavity has a minimum value of 0.65, while for the second cavity it goes down to 0.2. **(c)** Section of the parameters space for the correlation functions for the two modes, with $\delta = 0.1$ and **(d)** with $\delta = -0.1$.

In this way, $g_2^{(2)}$ is a function of the detuning, the decay rate, the nonlinear interaction strength and of $|S_2|^2$, and the same for $g_1^{(2)}$. The expression for $\langle i_2^2 \rangle$, needed to calculate $g_2^{(2)}(0)$, is long and not-straightforward: it is then more useful, in order to visualize the effect of the cascade coupling on the correlation function, to analyse the results for a range of parameters. In Fig. (6.4) we show the correlation functions for each of the two cavities as functions of the populations in the second cavity and of the detuning from the pump, with a fixed set of parameters.

For $\delta > 0$, both modes show sub-Poissonian statistics and for small values of $|S_2|^2$ one can identify a region of the phase-space where the second mode shows a strongly improved antibunching, with respect to the first one. In particular, considering the situation shown in Fig. (6.4), the minimum value of the second order cor-

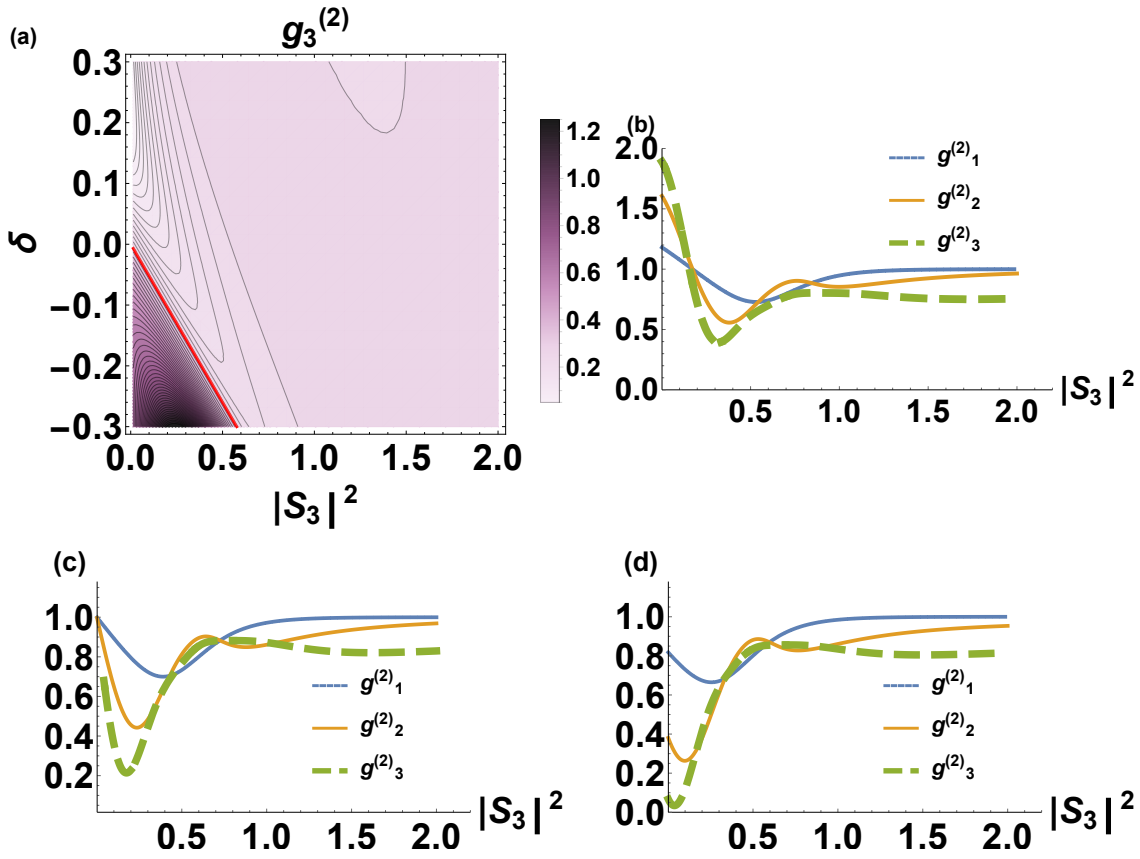

Figure 6.5: **(a)** $g_3^{(2)}$ for the cascade system as a function of the population in mode 3 and of the detuning, with $k = \gamma = 0.4$. The red line corresponds to the values for which $g_3^{(2)} = 1$, while the light color region is the one where the system is antibunched. The third mode in the cascade shows a further improvement of the antibunching, in particular, for this set of parameters, $\min(g_3^{(2)}) = 0.05$. **(b)** Section of the parameters space for the correlation functions for the three modes, with $\delta = -0.1$, **(c)** $\delta = 0$, **(d)** $\delta = 0.1$.

relation function for the first mode is $\min(g_1^{(2)}) = 0.65$, while for the second one $\min(g_2^{(2)}) = 0.2$.

It is interesting to study the possibility whether the gain of the antibunching follows an additivity principle: i.e., if having more systems in the cascade results in an improved value of the quantum correlations. However, given the nonlinear nature of the equation we are considering it is not an easy task to demonstrate this analytically, therefore we limit the our study to the case of three nonlinear systems in cascade using the same semi-analytical procedure adopted in the previous section. The second order correlation function for the third mode is shown in Fig. (6.5). As before, it is possible to perform this analysis as a function of the population in the

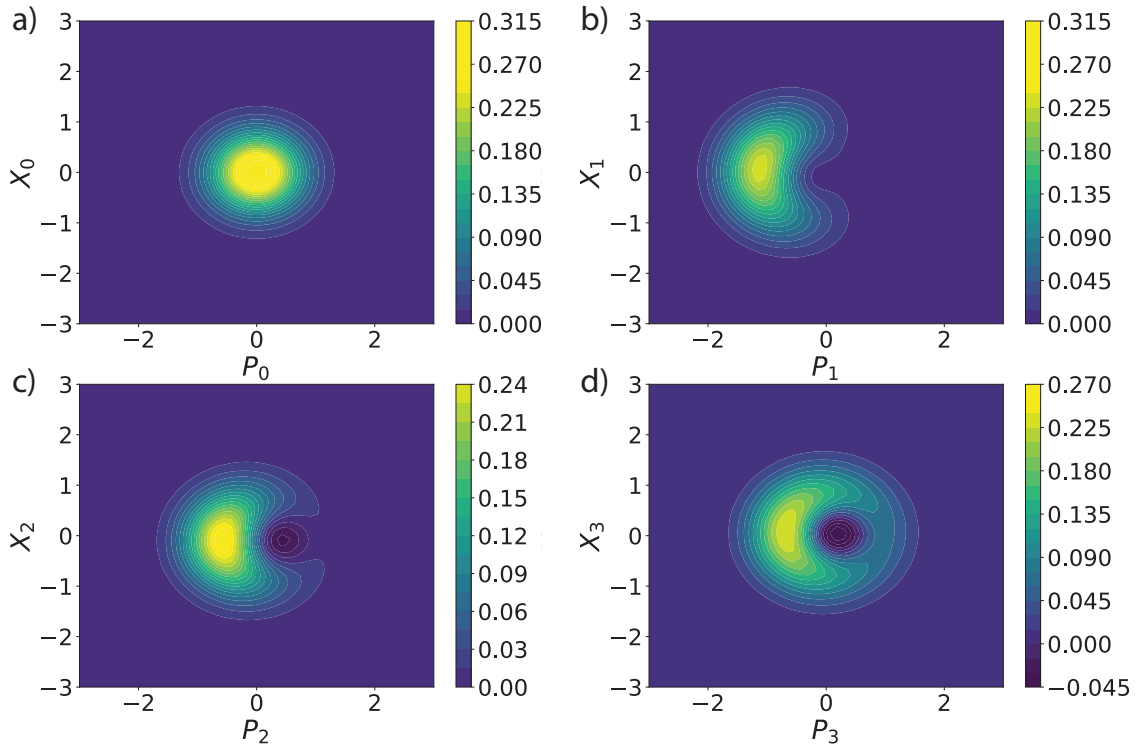

Figure 6.6: Wigner functions of the steady state for the coherent state **(a)**, representing the driving laser field, for the first **(b)**, the second **(c)** and the third **(d)** system in cascade, respectively, with $\delta = 0$, $\gamma = 0.3$, $k = \gamma$ and pump intensity, $f = 0.05\gamma$. The Wigner function becomes negative as we add more systems in cascade: the third mode **(c)** already shows a fidelity of 0.7 with a single photon state.

last mode in cascade, since $|S_2|^2 = (1 + \frac{1}{\gamma^2}(\delta + k|S_3|^2)^2)|S_3|^2$. As shown in Fig. (6.5), the minimum value of the correlation function for the third mode, $\min(g_3^{(2)}) = 0.05$, is a further improvement, compared to the two mode configuration.

6.2.1 Wigner function of the cascade system

To analyse the effect of the cascade coupling on the quantum state of each subsystem, we evaluate numerically the time evolution of the Wigner function [102] for three systems in a cascade, with a Quantum Monte Carlo approach [35]: expanding the total system on a properly truncated Fock basis, the expression for the Wigner function is

$$W(\alpha_2) = \frac{1}{\pi} \sum_{n,m} \rho_{n,m} \langle n| T(\alpha_2) |m\rangle , \tag{6.45}$$

with $\rho_{n,m}$ the density matrix on the Fock basis and $T(\alpha_2) = \int \exp(\alpha_2 \zeta^* - \alpha_2^* \zeta) D(\zeta) d^2\zeta$, $D(\zeta)$ being the displacement operator. Fig. (6.6) shows the result of the numerical

analysis, after a steady-state is reached. Starting from the coherent state injection of the laser source, the first driven mode shows, as expected [103], a crescent like shape, which is a signature of intensity squeezing, due to the Kerr nonlinearity. The Wigner function for the second mode in cascade is intensity squeezed, but also slightly negative: for a pure state, which is valid for our system at low excitation powers, the negativity of the Wigner distribution indicates that the state of the system is non-Gaussian [104]. Additionally, the negativity of the Wigner function is considered a key resource for quantum computing. In fact, a certain class of algorithms can be implemented by using only classical resources, even if they are expressed in the language of quantum mechanics. This result is described by the Gottesman–Knill theorem [105] which, for finite-dimensional Hilbert spaces, demonstrates that there exists a set of quantum processes that can be emulated efficiently on a classical computer. Generalizing this theorem to the continuous-variable case [106], it can be shown that, likewise, a class of continuous-variable quantum computations can be simulated using only classical analogue computations. In particular, for the continuous variable case, the theorem is always valid for Gaussian channels, i.e., quantum channels made of Hamiltonians which are quadratic in the field operators. In particular, Eisert et al. in [107] demonstrated that, when the Wigner quasiprobability representations of all the quantities involved in a computation process are non-negative, then they can be interpreted as ordinary probability distributions, indicating that the computation can be modelled as an essentially classical one. On the contrary, negative Wigner distributions of the quantities involved in the process can be used as resources in quantum computing, as the outcome of the computation cannot be efficiently sampled using classical algorithms. In this sense, the cascade system configuration can be implemented to generate interesting quantum states, with potential applications in continuous variable quantum computing.

As an additional system is added to the cascade, the output state moves from intensity squeezing to a quasi-number state, as indicated by the ring-shape feature of the probability distribution. To confirm this observation, we evaluate the fidelity

between the cascade state and a single photon state [108]:

$$\mathcal{F} = Tr(\sqrt{\sqrt{\rho}\sigma\sqrt{\rho}})^2 \tag{6.46}$$

where ρ is the system density matrix and σ is the target density matric, which is a single photon in this case. In particular, the fidelity is one if the two systems are described by the same density matrix, and zero if they are completely orthogonal. While the first mode in cascade has a fidelity of $\mathcal{F} \approx 0.5$, for the second one we get $\mathcal{F} \approx 0.7$. This trend of increasing non-Gaussianity is confirmed by the Wigner function for the third mode in the cascade: the distribution is more negative, compared to the previous case, and the fidelity between the mode and the single photon state is $\mathcal{F} \approx 0.8$.

6.2.2 Weak nonlinear systems

So far we have considered systems with a strong on-site Kerr nonlinearity, $k = \gamma$. However, this is not the case in many realistic experimental setups, like III-V semiconductor microcavity-polariton systems. In such systems the strength of the nonlinearity is two orders of magnitude smaller than the linewidth, $k \approx 10^{-2}\gamma$. Nevertheless, it is still interesting to investigate quantum effects in these systems [109]. Since the nonlinearity is weak, the deviation from a coherent statistics is small and therefore, is interesting to study the cascade configuration, to enhance the quantum effects. For example, as shown in Fig. 6 (a), a single Kerr quantum system with $k = 0.005$ and $\gamma = 0.4$, reveals an optimal value for the $g_1^{(2)}(0) \approx 0.98$, as expected from Drummond et al. [110]. Using a further system in cascade, it is possible to achieve a lower value for the antibunching, down to $g_2^{(2)}(0) \approx 0.92$, as shown in Fig.(6.7)(b).

Notice here that, in the case of weak nonlinearity, the Wigner function for the cascade system is always positive, at least when the size of the system itself (the number of modes considered) is limited. Further investigation are necessary, at the time of writing, to find out the optimal values of the system parameters, when

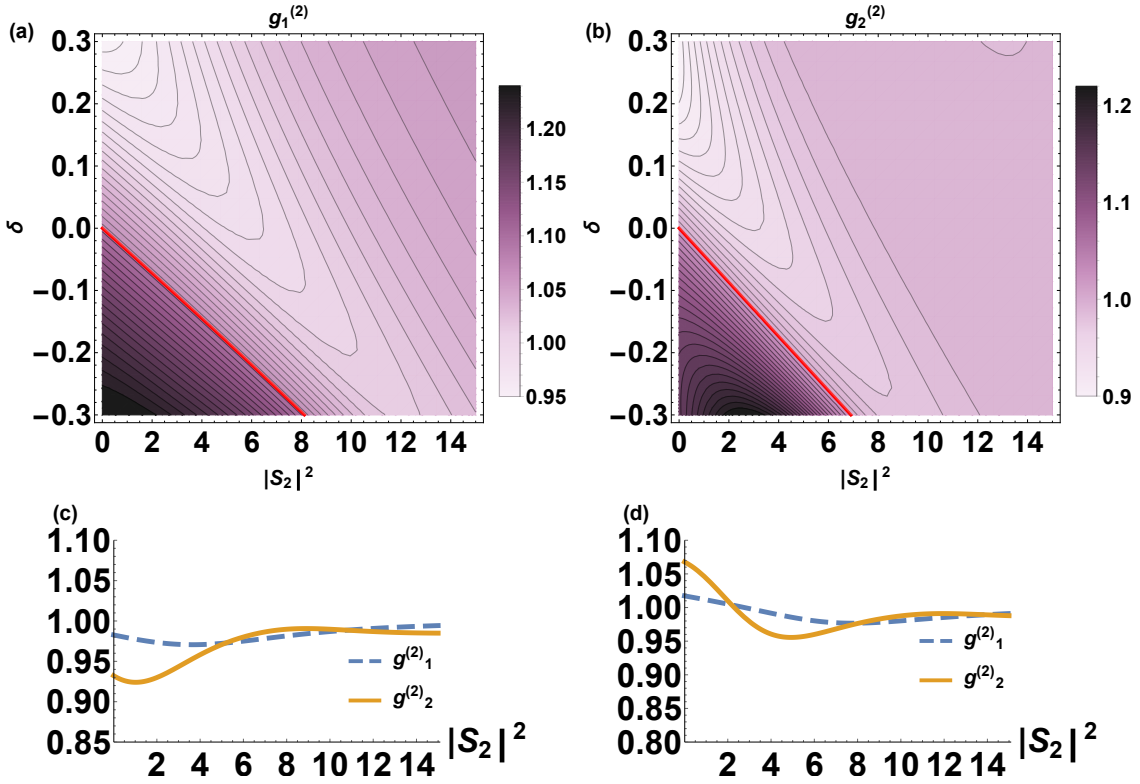

Figure 6.7: **(a)** $g_1^{(2)}$ and **(b)** $g_2^{(2)}$ for the cascade system as a function of the population in cavity two and of the detuning,with $\gamma = 0.4$, in the weak nonlinearity regime, $k = 0.005$. The oblique red curve corresponds to $g_m^{(2)} = 1$, while the light colour regions are the ones where the systems shows antinbunching. The correlation function for the first cavity has a minimum value of 0.98, while for the second cavity it goes down to 0.92. **(c)** Section of the parameters space for the correlation functions for the two modes, with $\delta = 0.1$ and **(d)** with $\delta = -0.1$.

considering weak nonlinearity, which give negative Wigner functions.

6.2.3 Bipartite Entanglement through dissipation

Entanglement is a key resource for quantum information processing and quantum communication [111]: the presence of such non-intuitive correlations between two or more systems has been investigated experimentally in a variety of physical situations, from parametric down converted photons, to nuclear magnetic resonance. In particular, entanglement can be found both in discrete variable systems, i.e., systems with a discrete number of degrees of freedom like spin qubits, and in continuous variable systems, where the system dynamics is described by continuous functions. The main motivation for using continuous variables in quantum information, is based

on a practical observation: efficient preparation, manipulation and measurements of entangled quantum states can be achieved, in optics, by making use of quadrature amplitudes of the electromagnetic field, and for example, using homodyne detection and feedforward techniques, it is possible to measure quadratures with nearly unitary efficiency [112].

Let us consider now a system made of two bosonic modes in a cascade, with an on-site Kerr nonlineraity: our aim is to check if such a conifuration allows the system to be driven into a bipartite entangled state. Bipartite continuous variable entanglement can be tested according to a criterion established by Duan et al. [113], which gives a sufficient condition for any CV state and a necessary condition for Gaussian states: the criterion is based on the variances of the combination of the quadrature operators, namely $x_1 + x_2$ and $p_1 - p_2$:

$$E_N = V(p_1 - p_2) + V(x_1 + x_2), \tag{6.47}$$

where $x_1 = (a_1 + a_1^\dagger)/2$ and $p_1 = (a_1 - a_1^\dagger)/2i$, and V is the variance. A bipartite system is said to be in an entangled state if:

$$E_N < 1. \tag{6.48}$$

To be sure that the inequality (6.48) properly determines the presence of entanglement, it is necessary to minimize its value over the possible phase references used for the detection scheme, and that can be done considering local transformation of the form $a_1 \to ae^{i\phi_1}$. If $\min_\phi(E_N) = \tilde{E}_N < 1$, with $\phi = \phi_1 + \phi_2$ the system is in an entangled state, while for $\tilde{E}_N \geq 1$, they are separable. In this case, the minimum value of E_N is found for $\phi = \pi/2$.
Following the argument above, $\tilde{E}_N$ can be written as ([114]):

$$\tilde{E}_N = 1 + \langle a_1^\dagger a_1\rangle + \langle a_2^\dagger a_2\rangle - \langle a_1^\dagger\rangle\langle a_1\rangle - \langle a_2^\dagger\rangle\langle a_2\rangle - 2\sqrt{\langle a_1^\dagger a_2^\dagger\rangle - \langle a_1^\dagger\rangle\langle a_2^\dagger\rangle}\sqrt{\langle a_1 a_2\rangle - \langle a_1\rangle\langle a_2\rangle}. \tag{6.49}$$

The expectation values entering this equation can be calculated following the same

approach of the previous sections, i.e. using the mean field equation and the covariance matrix to evaluate the correlations. Explicitly, in terms of the polar expansion, the bipartite CV entanglement witness reads:

$$E_N^{i,\theta} = 1 + |S_1|^2 \langle i_1^2 \rangle + |S_2|^2 \langle i_2^2 \rangle - 2|S_1||S_2|\sqrt{(\langle i_1 i_2 \rangle - \langle \theta_1 \theta_2 \rangle)^2 + (\langle i_1 \theta_2 \rangle + \langle i_2 \theta_1 \rangle)^2}.$$

As shown in Fig. (6.8)(a), for low values of the population (i.e. dark region on the

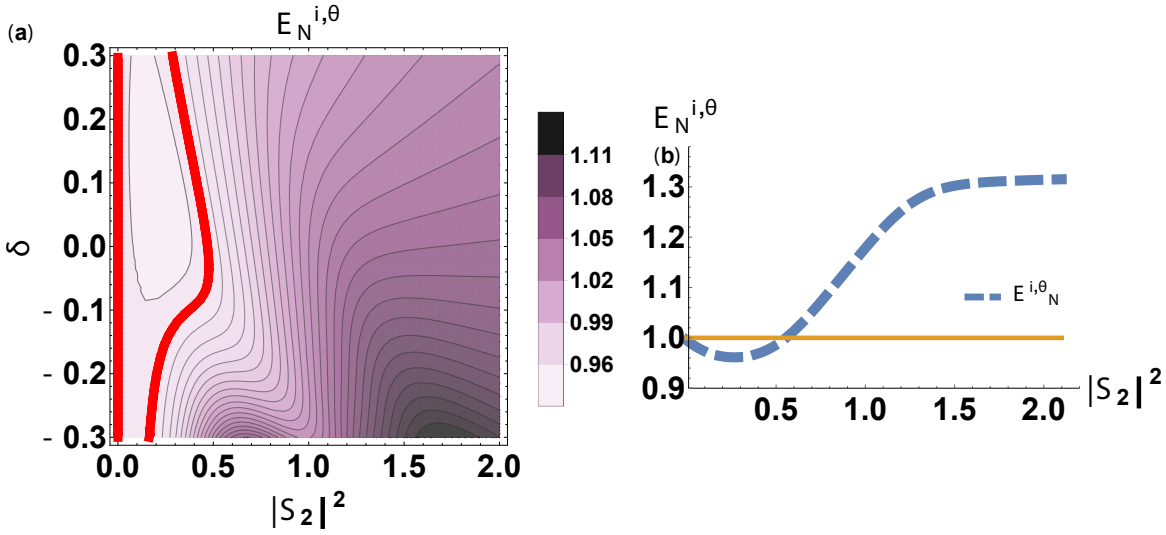

Figure 6.8: **(a)** Bipartite Entanglement between the modes, as a function of the population $|S_2|^2$ and of the detuning δ, with $\gamma = 0.2$, $k = \gamma$. The red curve specifies the point where the inequality saturates to 1 while the highlighted region corresponds to values where the systems are effectively entangled.**(b)** A 1D section of the 2D plot which underlines the range of the violation of the inequality, with $\delta = 0$.

left side) the two modes are in an entangled state. This is particularly interesting, because it shows that entanglement can be generated through dissipative coupling. In order to give an intuitive motivation for the formation of bipartite entanglement in this particular system, we move onto a reduced Fock states basis: $\{|0,0\rangle, |1,0\rangle, |0,1\rangle\}$ and we consider the effective Hamiltonian:

$$H_{\text{eff}} = H_{\text{sys1}} + H_{\text{sys2}} + i\sqrt{\gamma_1\gamma_2}(a_1^\dagger a_2 - a_2^\dagger a_1) - i\frac{\gamma_2}{2}a_1^\dagger a_1 - i\frac{\gamma_2}{2}a_2^\dagger a_2. \tag{6.50}$$

It can be noticed immediately, from equation (6.50), that the cascade term has the form of an effective imaginary coupling between the two modes, hence allowing quantum interference effects to take place. In particular, evaluating the eigenstates

of the Hamiltonian (6.50) expanded in the Fock basis, we found :

$$|\psi_{\text{ent}}\rangle = \left(\chi_1 |0,1\rangle - e^{i\phi}\chi_2 |1,0\rangle\right), \tag{6.51}$$

which is an entangled state, where the normalization factors, χ_1 and χ_2, and the relative phase, ϕ, depend upon the choice of the parameters of the system.
The generation of entangled state through dissipation is potentially relevant for quantum communication protocols, in particular for generating entanglement between systems which are spatially separated [115], and for quantum foundation experiments, like measuring Bell's inequalities [116] with CV systems.

From Fig. (6.8)(a), it can be seen that the violation of the inequality quickly disappears, as the number of excitation in mode 2 increases. At that point, the occupation number for the two modes starts to be significantly different, which means that in the number operator basis, the two systems become increasingly distinguishable (separable). Notice here that the minimum of the entanglement

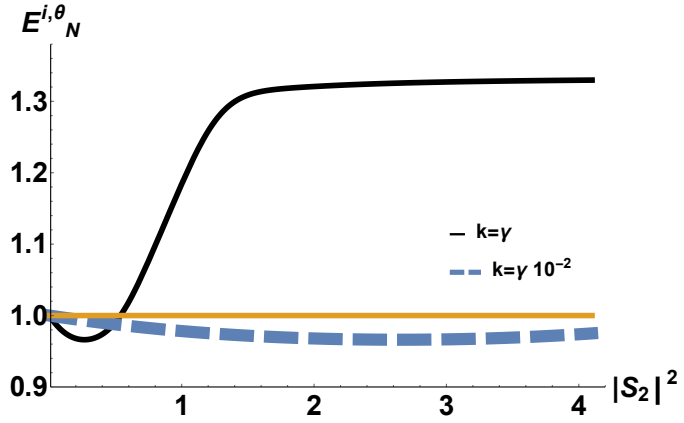

Figure 6.9: Bipartite Entanglement between the modes, as a function of the population in the second cavity, with $\gamma = 0.4$ and $k = \gamma$ and $k = \gamma 10^{-2}$, hence both in the strong and in the weak nonlinear regime. The maximum violation of the entanglement witness is unaffected by the nonlinearity.

witness (6.48) does not change as a function of the onsite Kerr nonlinearity, but is rather a function of the effective coupling strength between the cascade modes, as shown in Fig. (6.9): changing the nonlinearity simply shifts the driving field value for which the minimum of the entanglement witness occurs.

Chapter 7

Quantum optics of nonlinear $\mathcal{PT}$-symmetric systems

In this Chapter, we investigate the quantum optical properties of non-Hermitian systems: these have recently attracted great attention both for fundamental investigations [117], as their quantum-mechanical properties are mostly unknown, and for potential applications. In particular, we focus our attention on the interplay between non-Hermitian phenomena and non-linear effects, which lead, as shown in the previous chapters, to non-classical effects in the field correlation functions. We first give a brief introduction about $\mathcal{PT}$-symmetric systems, considering the example of linear gain-loss dimers: this constitutes a basic model for non-Hermitian dynamics, that shows all the peculiar features of the $\mathcal{PT}$-symmetry on the mean field solutions. We then move to a model for nonlinear non-Hermitian system, inspired by laser theory, for which we evaluate the second-order correlation function and the Wigner distribution, showing the quantum effects in correspondence to the different phases arising from the $\mathcal{PT}$-symmetry property of the system.

7.1 $\mathcal{PT}$-symmetry

In Quantum mechanics, physically observable quantities correspond to the eigenvalues of measurement operators, and the reality requirements, i.e., the fact that these quantities are measurable, demand that the eigenvalues must all be real numbers. Hermitian operators ensure that the eigenvalues are always real, and that is the rea-

son why quantum mechanics postulates that all the observables must be described by this class of operators, together with the fact that they generate a unitary time evolution. In a seminal work, Bender et al. [118] investigated the spectrum of a class of non-Hermitian Hamiltonians, discovering that in fact their spectrum is still real if they are $\mathcal{PT}$-symmetric, i.e., the operator is invariant under parity and time transformation. These systems possess, in many cases, a parameter-dependent threshold, above which the spectrum is not completely real: the threshold marks the border between the so-called $\mathcal{PT}$-symmetric phase, when the eigenvalues are real, and the broken phase, where the $\mathcal{PT}$ symmetry is spontaneously broken.

The $\mathcal{PT}$-symmetry condition replaces the Hermiticity, in non-Hermitian Hamiltonian theory: the actions of the parity P and time T operators are defined as,

$$P : p \to -p, \quad x \to -x \quad T : p \to -p, \quad x \to x, \quad i \to -i, \tag{7.1}$$

where x and p are, respectively, the position and momentum operator, and $[P, T] = 0$. The application of time reversal operator T generates a change of the sign of the imaginary unit, as it is required to preserve the quantum-mechanical commutation relation, $[x, p] = i$.

In general we can define a Hamiltonian as:

$$H = \frac{p^2}{2m} + V(x), \tag{7.2}$$

where m is the mass and $V(x)$ is an arbitrary potential term. The Hamiltonian is $\mathcal{PT}$-symmetric if it shares the same eigenfunctions with the $\mathcal{PT}$ operators and the following relation holds:

$$\mathcal{PT}H = H\mathcal{PT}. \tag{7.3}$$

The fact that $[H, \mathcal{PT}] = 0$ does not automatically imply that the two operators share common eigenfunctions, since $\mathcal{T}$ is an anti-linear operator, meaning that its action on any linear combination of state vectors gives:

$$\mathcal{T}(c_1\psi_1 + c_2\psi_2) = (c_1^*\mathcal{T}\psi_1 + c_2^*\mathcal{T}\psi_2). \tag{7.4}$$

If (7.3) is respected, but the eigenfunction of the Hamiltonian are different from the eigenfunction of $\mathcal{PT}$, the system is said to be in the broken $\mathcal{PT}$-symmetry phase.

7.2 Linear $\mathcal{PT}$-symmetric systems

To illustrate the consequences of these assumptions, we briefly consider a simple but intensively used model, which capture the basics of non-Hermitian physics. Consider a two-level non-Hermitian Hamiltonian:

$$H = \begin{pmatrix} i\gamma & \tau \\ \tau & -i\gamma \end{pmatrix}. \tag{7.5}$$

Hamiltonian (7.5) is used to model, under certain approximation, a two level system, with Rabi term τ and with one energy level having a *gain* term $+i\gamma$ and the other a *loss* term $-i\gamma$, or equivalently two bosonic modes, coherently coupled through τ, in the single particle regime, again respectively with a linear gain/loss term. The Hamiltonian is clearly non-Hermitian, as $H^\dagger \neq H$. The eigenvalues of (7.5) are given by:

$$E_\pm = \pm\sqrt{\tau^2 - \gamma^2}. \tag{7.6}$$

As it can be seen from Fig. (7.1), if $\gamma < \tau$ the eigenvalues are real, and the $\mathcal{PT}$-symmetry is unbroken. As γ increases the two eigenvalues start to converge until they become degenerate at the breaking threshold, $\gamma = \tau$. After this point the $\mathcal{PT}$-symmetry is completely broken and the eigenvalues are imaginary. To evaluate the normalised eigenvectors we need to consider separately the two regions corresponding to $\gamma < \tau$ and $\gamma > \tau$. In the former case the eigenstates are:

$$\psi_+ = \frac{1}{\sqrt{2}} \begin{pmatrix} \dfrac{\tau}{i\gamma - \sqrt{\tau^2 - \gamma^2}} \\ 1 \end{pmatrix}, \tag{7.7}$$

$$\psi_- = \frac{1}{\sqrt{2}} \begin{pmatrix} \dfrac{\tau}{i\gamma + \sqrt{\tau^2 - \gamma^2}} \\ 1 \end{pmatrix}, \tag{7.8}$$

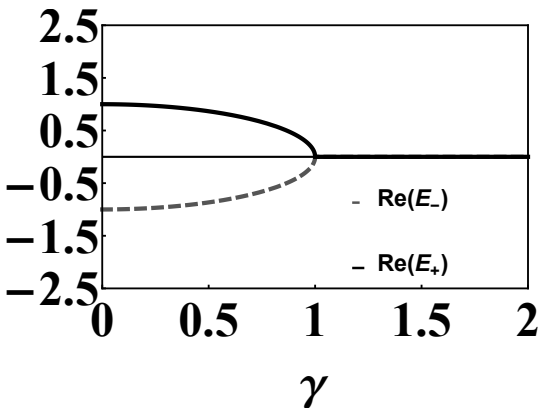

(a)

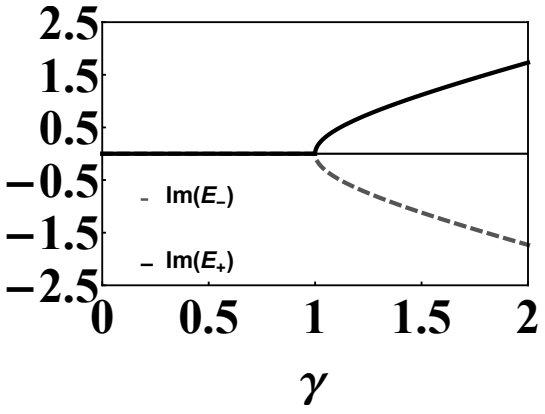

(b)

Figure 7.1: (a) Real part of the spectrum of Hamiltonian (7.5), as a function of γ with $\tau = 1$. Before the branching point, $\gamma = \tau$ the spectrum is completely real. After the branching point (b), the real part goes to zero and the spectrum is completely imaginary.

so that when $\gamma = 0$, H is Hermitian and the two eigenvectors are orthonormal. As γ increases, still remaining below the breaking point, $\psi_\pm$ are no longer orthonormal, but they remain linearly independent, hence they span the entire subspace. At the breaking point the two eigenvectors are parallel, which reflects the degeneracy of the system. For $\gamma > \tau$ the eigenvectors need new normalization, as this time the term $\sqrt{\tau^2 - \gamma^2}$ is purely imaginary. In this case the normalised eigenvectors are:

$$\psi_+ = \left(\frac{2\gamma^2 - \tau^2 - 2\gamma\sqrt{\gamma^2 - \tau^2}}{2\gamma^2 - 2\gamma\sqrt{\gamma^2 - \tau^2}} \right)^{1/2} \begin{pmatrix} \dfrac{\tau}{i\gamma - i\sqrt{-\tau^2 + \gamma^2}} \\ 1 \end{pmatrix}, \tag{7.9}$$

$$\psi_- = \left(\frac{2\gamma^2 - \tau^2 + 2\gamma\sqrt{-\gamma^2 + \tau^2}}{2\gamma^2 + 2\gamma\sqrt{-\gamma^2 + \tau^2}} \right)^{1/2} \begin{pmatrix} \dfrac{\tau}{i\gamma + i\sqrt{-\tau^2 + \gamma^2}} \\ 1 \end{pmatrix}, \tag{7.10}$$

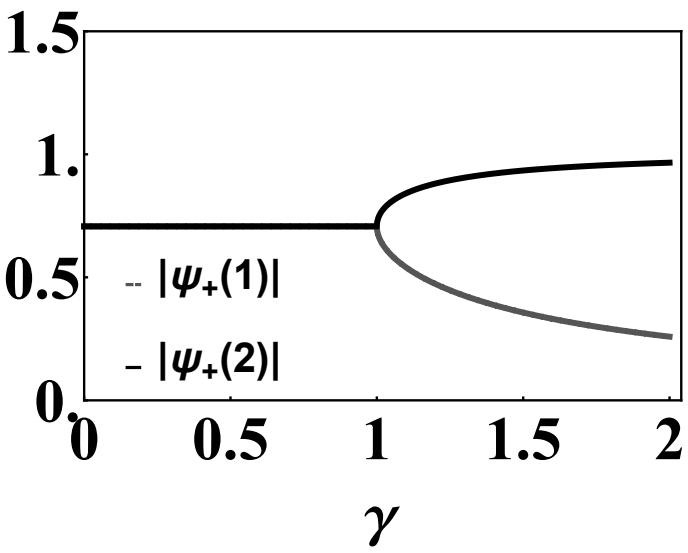

Figure 7.2: Eigenvectors for the excited state of the two modes, as a function of γ

which again are not orthonormal but linearly independent. Fig (7.2) shows the effect of the symmetry breaking on the amplitude of the excited state eigenvectors for the two sites. Before $\gamma = \tau$, the two amplitudes are identical, i.e. the states have the same probability distribution. In the broken phase, the resulting eigenvector amplitudes are now asymmetric. Broken $\mathcal{PT}$ symmetry has consequences for the time evolution of a system: the presence of complex eigenvalues gives an exponential increase or decay (depending upon the sign) of the amplitude.

7.3 A model for $\mathcal{PT}$-symmetric nonlinear system

In this section, we address the properties of a system with nonlinear gain and loss when it undergoes $\mathcal{PT}$-symmetry breaking, considering a basic model described by [7]. As shown in the previous section, the phase dynamics of the system is obtained by changing the magnitude of the non-Hermitian terms, γ, which, in a two-mode system, has alternating signs on each mode. Nonlinear gain-loss terms, i.e. terms proportional to a nonlinear function of the wavefunction, can be physically obtained in different ways. To name a few examples, consider multi-photon absorption/emission processes [119], which are very common in semiconductor based photonic systems, or optical and electrical cooling and pumping [120], which can be used to induce balanced gain and loss in mechanical resonators. The system that we investigate in

the following is based on a coupled resonator model, but is in principle suitable to describe the essential features different of different physical situations.

The semi-classical description of such a system is based on a set of coupled equations with nonlinear gain/loss containing saturation, derived from the standard theory of laser gain:

$$\begin{cases} \partial_t S_1 = \left(-\gamma + \dfrac{\Gamma}{1 + \dfrac{|S_1|^2}{n_0}} \right) S_1 + i\tau S_2 \\ \partial_t S_2 = \left(-\gamma - \dfrac{\Gamma}{1 + \dfrac{|S_2|^2}{n_0}} \right) S_2 - i\tau S_1 \end{cases} \tag{7.11}$$

where γ is the damping rate, assumed equal on each mode, Γ is the strength of the nonlinear gain/loss, n_0 the saturation intensity and τ the coupling term. Conveniently, in polar coordinates, defining $S_1 = \psi_1 e^{-i\theta_1}$ and $S_2 = \psi_2 e^{-i\theta_2}$, we can rewrite (7.11) as:

$$\begin{cases} \partial_t \psi_1 = \left(-\gamma + \dfrac{\Gamma}{1 + \dfrac{\psi_1^2}{n_0}} \right) \psi_1 - \tau \sin(\phi) \psi_2 \\ \partial_t \psi_2 = \left(-\gamma - \dfrac{\Gamma}{1 + \dfrac{\psi_2^2}{n_0}} \right) \psi_2 + \tau \sin(\phi) \psi_1 \\ \partial_t \phi = \tau \left(\dfrac{\psi_1}{\psi_2} - \dfrac{\psi_2}{\psi_1} \right) \cos(\phi) \end{cases} \tag{7.12}$$

where $\phi = \theta_1 - \theta_2$. Note that if we perform a simultaneous rotation of both S_1 and S_2 the system is invariant: Therefore the evolution of the total phase $\theta_1 + \theta_2$ can be neglected. For the last equation we see that there are two fixed points for the phase, $\phi_{ss} = \pm\pi/2$. Due to finite γ, the stationary occupation number of the gain mode is always slightly larger than that of the loss mode, which makes $\phi_{ss} = \pi/2$ is the stable solution. We therefore set $\phi = \pi/2$ and henceforth study the two-dimensional dynamical system with variables ψ_1 and ψ_2.

We analyse numerically (7.12), using the MatLab package *MatCont* [121], looking for steady state solutions as a function of Γ. The software gives directly the stable solutions, found by evaluating the *Jacobian* of the system, i.e., the dynamical

matrix of the system linearised around each stationary state [122]. The analysis

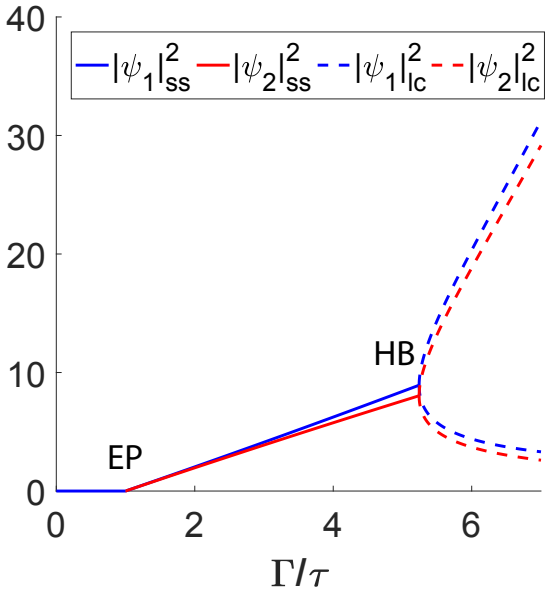

Figure 7.3: Bifurcation diagram for the populations $|\psi_1|^2_{SS}, |\psi_2|^2_{SS}$, of the two modes, with $n_0 = 2$ and $\gamma = 0.01$: after the exceptional point (EP) in **I**, the steady states are deviating from the trivial solutions $|\psi_1|^2_{SS} = 0, |\psi_2|^2_{SS} = 0$, but the $\mathcal{PT}$-symmetry is still preserved, as no population imbalance is observed. After **II** the system moves towards another regime, characterized by an Hopf bifurcation (HB), where the temporal dynamics is oscillatory, $|\psi_1|^2_{lc}, |\psi_2|^2_{lc}$: the dotted lines corresponds to the minimum and maximum oscillation amplitudes, thus enclosing the region within which the limit cycle happens. In this regime $\mathcal{PT}$-symmetry is spontaneously broken locally, as the different periods of the oscillations might give a population imbalance, but not globally.

reveals the presence of an exceptional point (EP): this special point in phase-space is defined as the coalescence point between two (or more) eigenstates of the system. Below the exceptional point, the population in the two modes is zero. After the exceptional point, the populations start to increase linearly as a function of Γ/τ, but the states are still $\mathcal{PT}$-symmetric: as long as the amplitudes ψ_1, ψ_2 are identical, the gain and the loss terms are still exactly the same. For $\Gamma/\tau \approx 5$, we observe a *Hopf bifurcation*, beyond which the system enters a limit cycle, i.e., a closed orbit attractor in the phase plane: without going into details, the Hopf bifurcation is critical point where periodic solutions appear. The limit cycle here is always formed symmetrically around a central point, $|\psi_{1c}| = |\psi_{2c}|$, hence the $\mathcal{PT}$-symmetry here is spontaneously broken locally, but is preserved when averaging over the cycle. No-

tice, from Fig.(7.3), that there is always a small difference between the population of each mode: this asymmetry is induced by the presence of the linear loss term γ. In fact it would disappear in an ideal model, with $\gamma = 0$, as confirmed by numerical simulations. The dynamical analysis of this transition was first investigated in [7], where it was found that the value at which the Hopf bifurcation occurs is:

$$\left(\frac{\Gamma}{\tau}\right)_{\text{Hopf}} \approx 1 + 2 + \sqrt{5}, \tag{7.13}$$

independent of all the other parameters of the system.

7.3.1 Quantum model

In order to address the quantum equivalent of (7.11), it is necessary to find a suitable description in term of Lindblad operators of the nonlinear gain/loss term. As there is no known functional form of annihilation and creation operators which describes it, we focus on a Taylor series expansion, truncating at second order:

$$\pm\frac{\Gamma}{1+\frac{\psi^2}{n_0}} = \pm\sum_{j=0}^{\infty}(-1)^j\frac{\psi^{2*j}\Gamma}{n_0^j} \approx \pm\left(\Gamma - \frac{\psi^2\Gamma}{n_0}\right). \tag{7.14}$$

The first order terms are, respectively, a linear gain and a linear loss: quantum-mechanically, they are both described by:

$$\Gamma\mathcal{L}(\rho)_{lgain} = \Gamma(2a_1^\dagger\rho a_1 - a_1^\dagger a_1\rho + \rho a_1^\dagger a_1) \tag{7.15}$$

$$\Gamma\mathcal{L}(\rho)_{lloss} = \Gamma(2a_2\rho a_2^\dagger - a_2 a_2^\dagger\rho + \rho a_2 a_2^\dagger), \tag{7.16}$$

which exactly correspond to the standard Lindblad dissipation and driving terms, as showed in the previous Chapters. The second order terms can be obtained from the quadratic nonlinear gain/loss Lindblad:

$$\frac{\Gamma}{n_0}\mathcal{L}(\rho)_{nlgain} = \frac{\Gamma}{n_0}(2a_2^{\dagger 2}\rho a_2^2 - a_2^{\dagger 2}a_2^2\rho + \rho a_2^{\dagger 2}a_2^2) \tag{7.17}$$

$$\frac{\Gamma}{n_0}\mathcal{L}(\rho)_{nlloss} = \frac{\Gamma}{n_0}(2a_1^2\rho a_1^{\dagger 2} - a_1^2 a_1^{\dagger 2}\rho + \rho a_1^2 a_1^{\dagger 2}). \tag{7.18}$$

The linear coupling between each mode is modeled by the Hamiltonian:

$$H = \tau(a_1^\dagger a_2 - a_2^\dagger a_1), \tag{7.19}$$

so that the complete master equation describing the truncated nonlinear gain/loss system reads:

$$\partial_t \rho = -i[H,\rho] + \gamma\mathcal{L}(\rho)_{loss} + \Gamma\mathcal{L}(\rho)_{lgain} + \frac{\Gamma}{n_0}\mathcal{L}(\rho)_{nlloss} + \Gamma\mathcal{L}(\rho)_{lloss} + \frac{\Gamma}{n_0}\mathcal{L}(\rho)_{nlgain},$$

where $\mathcal{L}(\rho)_{loss}$ is a standard Lindblad dissipative term, with decay rate γ.
When solving the master equation (7.20), we will consider cases where the expansion (7.14) formally is not valid, i.e., values of $|\phi|^2$ significantly greater than zero, where (7.14) is not valid. However we can still capture the main physics behind the model, as we show in what follows.

We now want to prove that the choice made for the Lindblad operators produce proper mean field equations containing the terms of the expansion (7.14). Making use of the P representation, we transform (7.20), according to the correspondence rules, defined in Chapter 2:

$$a\rho \to \alpha P(\alpha,\alpha^*),\ \ a^\dagger\rho \to (\alpha^* - \partial_\alpha)P(\alpha,\alpha^*)$$
$$\rho a \to (\alpha - \partial_{\alpha^*})P(\alpha,\alpha^*),\ \ \rho a^\dagger \to \alpha^* P(\alpha,\alpha^*).$$

We then convert the operator-valued master equation into a system of stochastic differential equations for c-numbers, $(a_1, a_2) \Rightarrow (\alpha_1, \alpha_1^*, \alpha_2, \alpha_2^*)$. In particular for (7.20), the equations of motion have the form:

$$\partial_t \begin{pmatrix} \alpha_1 \\ \alpha_1^* \\ \alpha_2 \\ \alpha_2^* \end{pmatrix} = \begin{pmatrix} A'(\alpha_1,\alpha_1^*,\alpha_2,\alpha_2^*) \\ A'^*(\alpha_1,\alpha_1^*,\alpha_2,\alpha_2^*) \\ A''(\alpha_1,\alpha_1^*,\alpha_2,\alpha_2^*) \\ A''^*(\alpha_1,\alpha_1^*,\alpha_2,\alpha_2^*) \end{pmatrix} + \zeta(t), \tag{7.20}$$

where $\zeta(t)$ is a vector of delta correlated random noise terms with correlation matrix:

$$D = \begin{pmatrix} -\frac{\Gamma}{n_0}\alpha_1^2 & \Gamma & 0 & 0 \\ \Gamma & -\frac{\Gamma}{n_0}\alpha_1^{*2} & 0 & 0 \\ 0 & 0 & \frac{\Gamma}{n_0}\alpha_2^2 & 0 \\ 0 & 0 & 0 & \frac{\Gamma}{n_0}\alpha_2^{*2} \end{pmatrix}, \tag{7.21}$$

while the drift matrix elements are:

$$A'(\alpha_1, \alpha_1^*, \alpha_2, \alpha_2^*) = (-\gamma + \Gamma)\alpha_1 - \frac{\Gamma}{n_0}|\alpha_1|^2\alpha_1 - i\tau\alpha_2,$$
$$A''(\alpha_1, \alpha_1^*, \alpha_2, \alpha_2^*) = (-\gamma - \Gamma)\alpha_2 + \frac{\Gamma}{n_0}|\alpha_2|^2\alpha_2 + i\tau\alpha_1.$$

7.3.2 Mean field equations and stability analysis

Considering now the mean-field equation for (7.20), which corresponds to taking the mean values of the quantities, $S_1 = \langle\alpha_1\rangle$ and $S_2 = \langle\alpha_2\rangle$, we obtain the equivalent of system (7.11) for the Taylor expanded terms:

$$\begin{cases} \partial_t S_1 = (-\gamma + \Gamma - \frac{\Gamma}{n_0}S_1^2)S_1 + i\tau S_2 \\ \partial_t S_2 = (-\gamma - \Gamma + \frac{\Gamma}{n_0}S_2^2)S_2 - i\tau S_1 \end{cases}. \tag{7.22}$$

We move into a polar representation of the mean-fields, as in (7.12), and assuming $\phi = \pi/2$, we find:

$$\begin{cases} \partial_t \psi_1 = (-\gamma + \Gamma - \frac{\Gamma}{n_0}\psi_1^2)\psi_1 - \tau\psi_2, \\ \partial_t \psi_2 = (-\gamma - \Gamma + \frac{\Gamma}{n_0}\psi_2^2)\psi_2 + \tau\psi_1. \end{cases} \tag{7.23}$$

As shown in Fig. (7.4), the dynamics of the fields around zero is identical to the original case, where the gain/loss terms are not expanded in Taylor series. After the exceptional point the $\mathcal{PT}$-symmetry is still preserved, as the populations of the two modes are identical. As Γ increases, the system reaches a point where a population imbalance is observed. Hence the $\mathcal{PT}$-symmetry is broken.

The results shown in Fig. (7.4) are obtained numerically with *MatCon*. However it

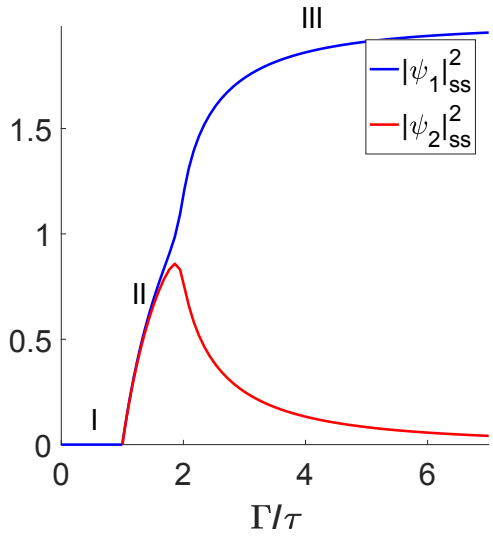

Figure 7.4: Bifurcation diagram for the populations $|\psi_1|^2_{SS}, |\psi_2|^2_{SS}$, of the two modes, with $n_0 = 2$ and $\gamma = 0.01$: after the exceptional point (EP) in **I**, the steady states are deviating from the trivial solutions $|\psi_1|^2_{SS} = |\psi_2|^2_{SS} = 0$, but the $\mathcal{PT}$-symmetry is still preserved, as no population imbalance is observed. After **II** the $\mathcal{PT}$-symmetry is spontaneously broken, generating an imbalance of the population in the two modes. Unlike the previous case, a Hopf bifurcation does not occur.

is possible to calculate analytically the position of the exceptional point performing a stability analysis. In order to do this, we rewrite the equations (7.23) for the first order Taylor approximation of the original model, setting $x = \psi_1$ and $y = \psi_2$,

$$\dot{x} = -\left[\gamma - \Gamma + \frac{\Gamma}{n_0}x^2\right]x - \tau y,$$
$$\dot{y} = -\left[\gamma + \Gamma - \frac{\Gamma}{n_0}y^2\right]y + \tau x.$$

It is easy to see that $(0,0)$ is an equilibrium point. The system can show up to 8 steady states in $\mathbb{R}^2$, not all with physical significance, that are solutions of

$$0 = \left[\gamma + \Gamma - \frac{\Gamma x^2}{n_0\tau^2}\left(\gamma - \Gamma + \frac{\Gamma}{n_0}x^2\right)^2\right]\left(\gamma - \Gamma + \frac{\Gamma}{n_0}x^2\right) - \tau^2$$
$$y = -\frac{x}{\tau}\left(\gamma - \Gamma + \frac{\Gamma}{n_0}x^2\right)$$

Among all the possible roots, we are interested in the positive ones since x and y are moduli. We can avoid the analytic calculation for the explicit expression of the equilibria by using a phase plane analysis. Specifically, we can plot in the x-y plane

the isoclines where $\dot{x} = 0$ and $\dot{y} = 0$. The equilibria of the system are the points of intersection between two *isocline*.

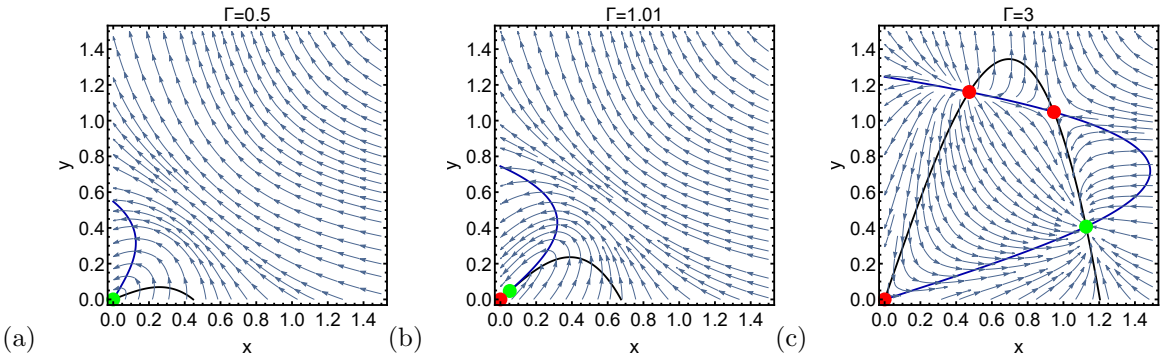

Figure 7.5: x-y phase plane for different values of Γ and $\tau = 1$. x-isocline is marked in black and y-isocline in blue. Green dots represent stable steady state and red is for unstable ones. The arrows show the dynamic of the trajectories.

As can be seen in Fig.7.5a for low values of Γ the origin is the only stable equilibrium. When Γ increases, a positive stable equilibrium appears through a pitchfork bifurcation (Fig.7.5b). At higher values of Γ, two unstable equilibria are generated by a fold bifurcation (Fig.7.5c).

It is possible to compute the critical value of Γ at which the first pitchfork bifurcation occurs, i.e. when the origin loses its stability. The Jacobian matrix evaluated at the origin is

$$J(0,0) = \begin{pmatrix} -\gamma + \Gamma & -\tau \\ \tau & -\gamma - \Gamma \end{pmatrix}$$

and its determinant is equal to zero if

$$\Gamma = \Gamma_{crit} = \sqrt{\gamma^2 + \tau^2},$$

which corresponds exactly to the point computed numerically in Fig. (7.4).
It is important to notice here that the population of the first mode is bounded from above by the saturation parameter n_0: in fact, considering $\psi_{1ss}^2 = n_1 > n_0$ in the steady-state equations, we have:

$$0 = \left(-\gamma + \Gamma - \frac{\Gamma}{n_0} n_1\right) - \tau\psi_2. \tag{7.24}$$

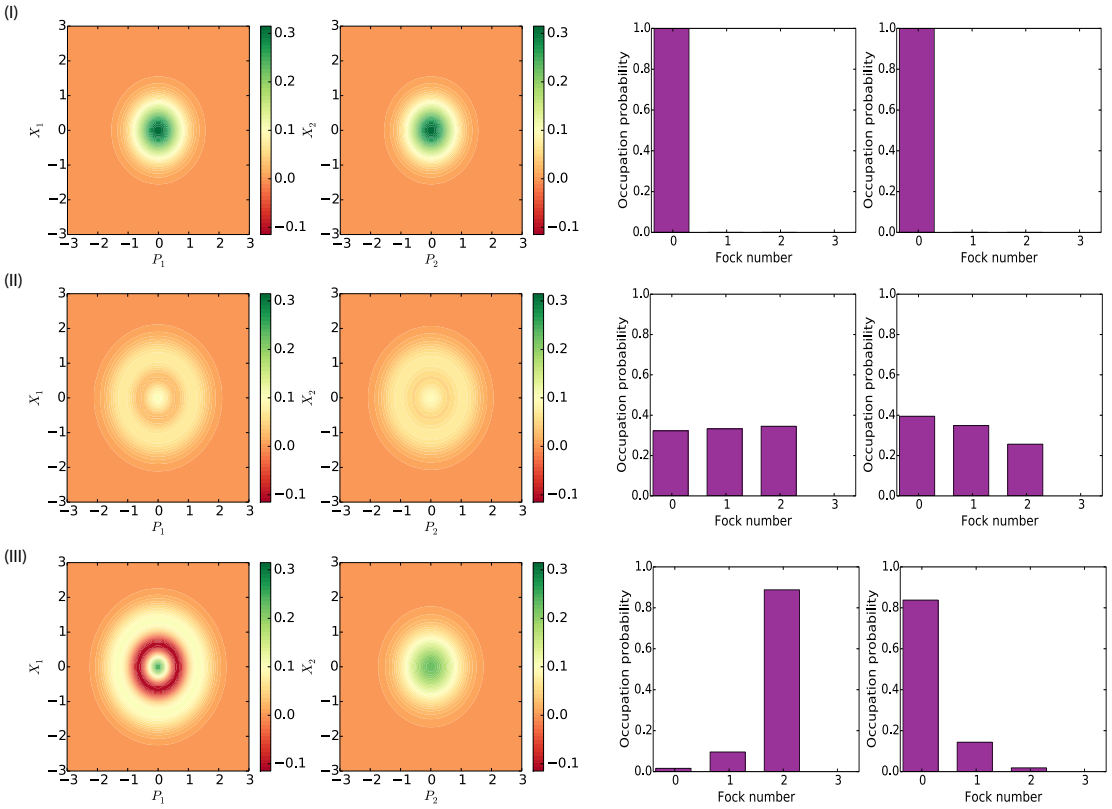

Figure 7.6: Wigner function and Fock-distribution of the two modes, with $\gamma = 0.1$ and $n_0 = 2$ and $\tau = 1$, for the three cases indicated in Fig. (7.4). For the unbroken phase **I**, and at the exceptional point **II**, the two modes posses a comparable probability distribution, being first a coherent vacuum state and then a mixed ensemble of Fock states. In the broken phase, the two probability distributions differ significantly: the one for the nonlinear loss mode (mode 1) is strongly non-classical while the other shows a thermal probability distribution.

Since $\frac{n_1}{n_0} > 1$ by construction, it is easy to demonstrate that $\psi_2 < 0$, which is clearly impossible as we are considering absolute values.

7.3.3 Quantum effects

In order to investigate the quantum properties of the the nonlinear gain/loss system (7.22), we make use of the Quantum Monte Carlo approach which enables us to study the dynamics of the full master equation (7.20). In particular we are interested in what happens to the quantum states of the modes at three particular point, shown in Fig.2: **I**, in the unbroken phase, before the EP, **II** in the region between the EP and the $\mathcal{PT}$-broken phase, **III** in the broken symmetry regime. In the following, we evaluate the Wigner function and the Fock distribution for these three regimes, as

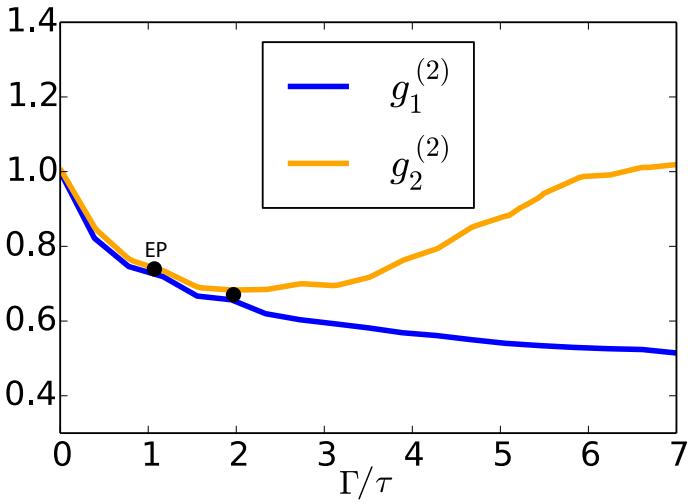

Figure 7.7: $g^{(2)}$ function for the two modes, with $\gamma = 0.1$, $n_0 = 2$ and $\tau = 1$. The two functions are nearly identical, until the $\mathcal{PT}$-symmetry is broken, and then they deviate significantly. The gain mode moves towards a coherent (vacuum) state ($g_2^{(2)} \approx 1$), while the loss mode is antibunched with $g_1^{(2)} \approx 0.5$.

shown in Fig.(7.6). In **I,** both modes stay in the initial configuration, the vacuum. In **II**, the nonlinear effects of the gain/loss terms are important, moving the modes towards a statistical mixture of Fock states. When the symmetry breaking occurs, in **III**, the statistics and the quantum properties of the two modes start to diverge drastically: while the first mode, with nonlinear loss, is moving towards a 2 photon Fock state $\psi_1 \approx |n_2\rangle$, with sub-Poissonian statistics, $g_1^{(2)}(0) \approx 0.5$, the nonlinear gain mode possess Poissonian statistics, as shown by the number distribution, with $g_2^{(2)}(0) \approx 1$, for high values of Γ (as shown in Fig.(7.7)). Numerical checks made with different values of n_0 have shown that, for large *Gamma* the loss mode can always be approximate to a Fock state with n_0 excitations.

It is clear that, at the exceptional point and in the broken-phase, quantum effects start to modify significantly the probability distributions, and hence the statistics, of the coupled mode system. As the maximum of the population is bounded by the saturation intensity n_0, it is possible to visualize the structure of the density matrix, with a good approximation, performing an expansion onto the Fock basis, $\rho = \sum_{i,j=0}^{n_0} |i\rangle \langle j|$. As shown in Fig. (7.8) the density matrix is approximatively diagonal, and pure, both in **I** and in **III**. Just after the EP, as the population starts

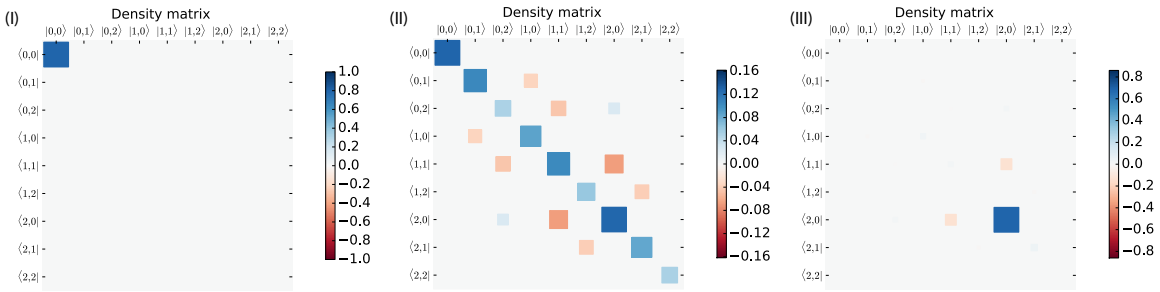

Figure 7.8: Density matrix for the system with $n_0 = 2$, $\gamma = 0.1$ and $\tau = 1$, expanded on a two-photon Fock state basis, for each of the three phase regime. In (I) for $\Gamma = 0$, we see that the density matrix is prepared in a pure state. In (II), just above the EP, for $\Gamma = 1.2$, the density matrix is non-diagonal and mixed. In (III) for large values of Γ, the density matrix is again almost diagonal and the system is in a pure state.

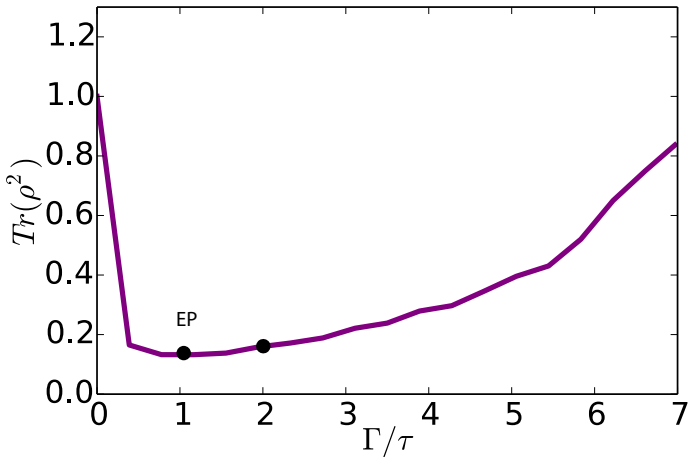

Figure 7.9: Purity of the total density matrix, with $n_0 = 2$, $\gamma = 0.1$ and $\tau = 1$. The system gradually lose the original purity until it reaches a minimum before the EP. It then starts to lose the mixedness, undergoing a process which can be called *$\mathcal{PT}$-breaking purification*.

to deviate significantly from zero, the off-diagonal elements of the density matrix are non-zero, and the state is fully mixed. It is worth at this point to quantify the purity of the whole system. The purity is defined as:

$$\mathrm{Tr}(\rho^2) \leq 1, \tag{7.25}$$

being equal to one for a pure state. In a mixed state, where $\mathrm{Tr}(\rho^2) < 1$, it can be used as a measure of the amount of mixing. As shown in Fig.(7.8), starting from a pure

vacuum state, $\rho_{in} = |0\rangle\langle 0|$, the system loses its initial purity, as Γ/τ increases, until reaching a minimum at the exceptional point, then, when the transition happens, the purity gradually increases: hence, as $\Gamma/\tau \to \infty$, we expect, from what we showed above, the system to be in the product state $|\Psi\rangle \approx |n_0\rangle \otimes |0\rangle$, confirming the results showed in Fig (7.6). This fact reveals that, in principle, it is possible to make use of nonlinear $\mathcal{PT}$-symmetric systems to perform Fock state production.

Chapter 8

Conclusion

8.1 Summary of Thesis Achievements

In conclusion, we give a brief summary of the main achievements presented in this thesis.

First we built a basic model for studying the quantum optical properties of polariton solitons. In particular, we focused on dissipative bright solitons, of the kind observed in monolithic microcavities and polaritonic waveguides. We demonstrated that the intensity-correlation function for such a state is always super-Poissonian and that quadrature squeezing is present.

We then derived and demonstrated a Theorem stating that the total intensity correlation function, of any order, are stationary when the multimode system considered possess a global $U(1)$ symmetry. Moreover, we extended the validity of the result for open quantum system, provided that the incoherent processes are linear in the basis of the operator for the system and that the decay rates for each mode are identical. This result provides a useful tool to link photon counting measurement to the probing of phase transitions related to the $U(1)$ symmetry breaking. Furthermore, as the individual correlation functions for each mode composing a multimode system can be non-stationary, the Theorem suggests that, when using a second order correlation function to quantify the nonclassicality of a given system, care is necessary: in fact, when the systems exhibits $U(1)$ symmetry, it may be necessary to isolate light from individual modes, rather than looking at the statistics of the

total emitted light.

We then proposed a set-up based on cascading nonlinear optical systems, to enhance the quantum mechanical properties of the output light. In particular we showed that a cascade of systems with high Kerr nonlinearity generates states of light with negative Wigner function: this result is particularly relevant, as a negative Wigner function is regarded as a fundamental resource for quantum computing. Additionally, we demonstrated that the cascade configuration is able to enhance the amount of antibunching for the emitted light. This is true both for strong nonlinearities and for the weak nonlinear case, which is particularly relevant for polaritonic systems. Finally, regarding the cascade system, we showed that, for bipartite system, the dissipative coupling between the two modes is able to put the sub-systems into an entangled state.

In the last Chapter, we studied the interplay between non-Hermitian physics, in particular considering system with $\mathcal{PT}$-symmetry, and quantum optics. We derived a classical model for a nonlinear $\mathcal{PT}$-symmetric system, which has a specific quantum mechanical counterpart. Hence, we demonstrated that, for this particular system, the Wigner functions for the gain and the loss mode show completely different features after the exceptional point, which delimits the unbroken symmetry phase from the broken phase. While the nonlinear loss mode moves toward a pure Fock state, the nonlinear gain approaches a thermal state. Hence, we demonstrated that this peculiar PT-symmetric system can be used, in principle, to generate pure Fock states, which are required for different technological applications, such as quantum cryptography and quantum communication protocols.

8.2 Future Work

We finish by offering different directions for near future extensions of the work presented.

First, it is interesting to consider whether realistic polariton solitons can be used as squeezed state source and if the amount of squeezing is sufficient to make use of

them for metrology applications, such as quantum interferometry [123].

As explicitly demonstrated in Chapter 4, the Theorem that enstablish the conservation of the total correlation function in multimode systems, establish a link between photon counting measurements and the symmetry properties of the system considered. In a recent work [124], Imamoglu et al. demonstrated that it is possible to make use of photon correlation measurements to determine the behaviour of the Liouvillian gap, which is ultimately related to quantum phase transitions [125]. Hence, it is legitimate to investigate the possibility of using photon correlations, of any order, to detect what kind of phase transition or symmetry breaking the system in experiencing. The possible finding would, in principle, provide an operational tool to explore the physics of complex systems, such as strongly correlated states of matter.

Concerning the cascade configuration, a possible way to extend the investigation is to consider quantum optical networks. Quantum networks have recently attracted a lot of attention from the scientific community. In fact they are essential elements of a quantum computer, especially because they allow the transmission of quantum information between spatially separated systems [6]. Generally the systems considered in literature are made of quantum dots in photonic crystal or superconductors [126]: it is then interesting to extend the analysis to networks made by microcavities, in the strong coupling regime, hence using the polariton-polariton interaction as a source of nonlinearity. The goal of this investigation would be to demonstrate

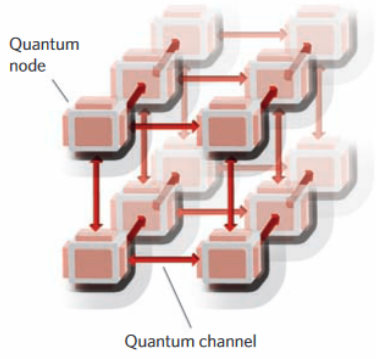

Figure 8.1: From [6], schematic of a quantum network. Each node corresponds to a particular physical system, connected by transmission lines or quantum channels.

the possibility of performing a class of quantum operations via a *cascade optical continuous variable quantum computer*, where the attribute "continuous variable" is used because microcavities are not, in general, a source of discrete-variable quantum states.

Finally, concerning the $\mathcal{PT}$-symmetric system analysed in the last Chapter, it is

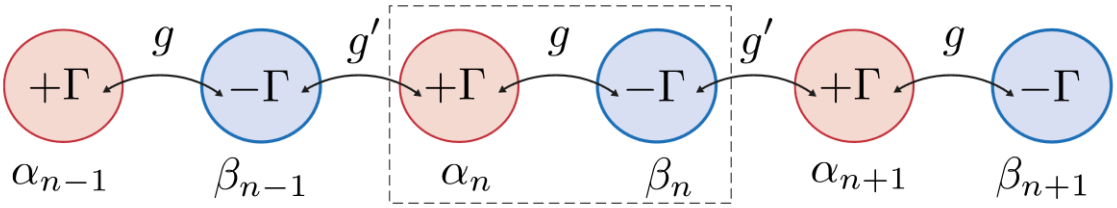

Figure 8.2: From [7], schematic representation of an array of coupled nonlinear gain/loss system, where each unit cell contains a $\mathcal{PT}$-symmetric system.

interesting to go beyond the two-mode case, for example considering an extended chain of gain and loss systems, as shown in Fig. (8.2), where each unit cell of the chain is made of a PT-symmetric system. The interest here includes both the classical features of the system, whether or not it shows Hopf bifurcations or other peculiar dynamical properties, and the quantum optical properties.

Bibliography

[1] S. Dufferwiel, F. Li, E. Cancellieri, L. Giriunas, A. A. P. Trichet, D. M. Whittaker, P. M. Walker, F. Fras, E. Clarke, J. M. Smith, M. S. Skolnick, and D. N. Krizhanovskii, "Spin textures of exciton-polaritons in a tunable microcavity with large te-tm splitting," *Phys. Rev. Lett.*, vol. 115, p. 246401, Dec 2015.

[2] F. Li, E. Cancellieri, G. Buonaiuto, M. S. Skolnick, D. N. Krizhanovskii, and D. M. Whittaker, "Full stark control of polariton states on a spin-orbit hypersphere," *Phys. Rev. B*, vol. 94, p. 201301, Nov 2016.

[3] M. Sich, D. V. Skryabin, and D. N. Krizhanovskii, "Soliton physics with semiconductor excitonpolaritons in confined systems," *Comptes Rendus Physique*, vol. 17, no. 8, pp. 908 – 919, 2016. Polariton physics / Physique des polaritons.

[4] P. M. Walker, L. Tinkler, D. V. Skryabin, A. Yulin, B. Royall, I. Farrer, D. A. Ritchie, M. S. Skolnick, and D. N. Krizhanovskii, "Ultra-low-power hybrid light-matter solitons," *Nature Communications*, vol. 6, pp. 8317 EP –, Sep 2015. Article.

[5] A. Trombettoni and A. Smerzi, "Discrete Solitons and Breathers with Dilute Bose-Einstein Condensates," *Phys. Rev. Lett.*, vol. 86, pp. 2353–2356, Mar 2001.

[6] H. J. Kimble, "The quantum internet," *Nature*, vol. 453, pp. 1023 EP –, Jun 2008.

[7] K. V. Kepesidis, T. J. Milburn, J. Huber, K. G. Makris, S. Rotter, and P. Rabl, "PT -symmetry breaking in the steady state of microscopic gainloss systems," *New Journal of Physics*, vol. 18, no. 9, p. 095003, 2016.

[8] D. Walls and G. Milburn, *Quantum Optics*. SpringerLink: Springer e-Books, Springer Berlin Heidelberg, 2008.

[9] H. Carmichael, *Statistical Methods in Quantum Optics 1: Master Equations and Fokker-Planck Equations*. Physics and Astronomy Online Library, Springer, 1999.

[10] F. P. Heinz-Peter Breuer, "The Theory of Open Quantum Systems," *OUP Oxford, 2007*, 2007.

[11] K. Sanaka, K. J. Resch, and A. Zeilinger, "Filtering Out Photonic Fock States," *Phys. Rev. Lett.*, vol. 96, p. 083601, Feb 2006.

[12] B. T. H. Varcoe, S. Brattke, and H. Walther, "Generation of Fock states in the micromaser," *Journal of Optics B: Quantum and Semiclassical Optics*, vol. 2, no. 2, p. 154, 2000.

[13] M. Hofheinz, E. M. Weig, M. Ansmann, R. C. Bialczak, E. Lucero, M. Neeley, A. D. O'Connell, H. Wang, J. M. Martinis, and A. N. Cleland, "Generation of Fock states in a superconducting quantum circuit," *Nature*, vol. 454, pp. 310 EP –, Jul 2008.

[14] B. Lounis and M. Orrit, "Single-photon sources," *Reports on Progress in Physics*, vol. 68, no. 5, p. 1129, 2005.

[15] H. Flayac and V. Savona, "Unconventional photon blockade," *Phys. Rev. A*, vol. 96, p. 053810, Nov 2017.

[16] D. P. R. Munro, "Introduction to the Theory of Coherence and Polarization of Light, by E. Wolf," *Contemporary Physics*, vol. 50, no. 6, pp. 661–662, 2009.

[17] *Optical Coherence and Photon Statistics*. Wiley-Blackwell, 2007.

[18] R. Feynman, R. Leighton, and M. Sands, *The Feynman Lectures on Physics*. No. v. 1 in The Feynman Lectures on Physics, Addison-Wesley, 1963.

[19] L. Mandel and E. Wolf, *Optical Coherence and Quantum Optics*. Cambridge University Press, 1995.

[20] R. J. Glauber, M. Kleber, A. K. Patnaik, M. O. Scully, and H. Walther, "A simple study of photon correlations from Hanbury-Brown and Twiss to Einstein, Podolsky, Rosen and beyond," *Journal of Physics B: Atomic, Molecular and Optical Physics*, vol. 38, no. 9, p. S521, 2005.

[21] L. Davidovich, "Sub-Poissonian processes in quantum optics," *Rev. Mod. Phys.*, vol. 68, pp. 127–173, Jan 1996.

[22] L. Davidovich, "Sub-poissonian processes in quantum optics," *Rev. Mod. Phys.*, vol. 68, pp. 127–173, Jan 1996.

[23] R. Hudson, "When is the wigner quasi-probability density non-negative?," *Reports on Mathematical Physics*, vol. 6, no. 2, pp. 249 – 252, 1974.

[24] A. Gilchrist, C. W. Gardiner, and P. D. Drummond, "Positive P representation: Application and validity," *Phys. Rev. A*, vol. 55, pp. 3014–3032, Apr 1997.

[25] L. Kadanoff, *Statistical Physics: Statics, Dynamics and Renormalization*. Statistical Physics: Statics, Dynamics and Renormalization, World Scientific, 2000.

[26] P. D. Drummond and M. Hillery, *The Quantum Theory of Nonlinear Optics*. Cambridge University Press, 2014.

[27] D. Sels and F. Brosens, "Variational truncated Wigner approximation," *Phys. Rev. E*, vol. 89, p. 042107, Apr 2014.

[28] C. Gardiner, P. Zoller, and P. Zoller, *Quantum Noise: A Handbook of Markovian and Non-Markovian Quantum Stochastic Methods with Applications to Quantum Optics*. Springer Series in Synergetics, Springer, 2004.

[29] C. W. Gardiner and P. Zoller. second ed.

[30] J. L. Garcia-Palacios, "Introduction to the theory of stochastic processes and Brownian motion problems," *arXiv e-prints*, pp. cond–mat/0701242, Jan. 2007.

[31] C. Gardiner, *Handbook of Stochastic Methods for Physics, Chemistry, and the Natural Sciences*. Springer complexity, Springer, 2004.

[32] P. Deuar, *First-principles quantum simulations of many-mode open interacting Bose gases using stochastic gauge methods*. PhD thesis, PhD Thesis, 2005, Oct. 2005.

[33] P. Kloeden and E. Platen, *Numerical Solution of Stochastic Differential Equations*. Stochastic Modelling and Applied Probability, Springer Berlin Heidelberg, 2013.

[34] H. Carmichael, *An Open Systems Approach to Quantum Optics: Lectures Presented at the Université Libre de Bruxelles, October 28 to November 4, 1991*. Lecture Notes in Physics Monographs, Springer Berlin Heidelberg, 2009.

[35] J. Johansson, P. Nation, and F. Nori, "Qutip: An open-source python framework for the dynamics of open quantum systems," *Computer Physics Communications*, vol. 183, no. 8, pp. 1760 – 1772, 2012.

[36] J. Kasprzak, M. Richard, S. Kundermann, A. Baas, P. Jeambrun, J. M. J. Keeling, F. M. Marchetti, M. H. Szymanska, R. André, J. L. Staehli, V. Savona, P. B. Littlewood, B. Deveaud, and L. S. Dang, "Bose-Einstein condensation of exciton polaritons," *Nature*, vol. 443, pp. 409 EP –, Sep 2006. Article.

[37] A. Amo and J. Bloch, "Exciton-polaritons in lattices: A non-linear photonic simulator," *Comptes Rendus Physique*, vol. 17, no. 8, pp. 934 – 945, 2016. Polariton physics / Physique des polaritons.

[38] Y. Yamamoto, F. Tassone, and H. Cao, *Semiconductor Cavity Quantum Electrodynamics*. Springer Tracts in Modern Physics, Springer Berlin Heidelberg, 2003.

[39] A. Kavokin, J. J. Baumberg, G. Malpuech, and F. P. Laussy, *Microcavities*. New York, NY, USA: Oxford University Press, Inc., 2008.

[40] J. J. Hopfield, "Theory of the contribution of excitons to the complex dielectric constant of crystals," *Phys. Rev.*, vol. 112, pp. 1555–1567, Dec 1958.

[41] C. Ciuti, V. Savona, C. Piermarocchi, A. Quattropani, and P. Schwendimann, "Threshold behavior in the collision broadening of microcavity polaritons," *Phys. Rev. B*, vol. 58, pp. R10123–R10126, Oct 1998.

[42] A. Baas, J. P. Karr, H. Eleuch, and E. Giacobino, "Optical bistability in semiconductor microcavities," *Phys. Rev. A*, vol. 69, p. 023809, Feb 2004.

[43] D. M. Whittaker and P. R. Eastham, "Coherence properties of the microcavity polariton condensate," *EPL (Europhysics Letters)*, vol. 87, no. 2, p. 27002, 2009.

[44] A. Kavokin, J. Baumberg, G. Malpuech, and F. Laussy, *Microcavities*. Series on Semiconductor Science and Technology, OUP Oxford, 2017.

[45] T. Byrnes, N. Y. Kim, and Y. Yamamoto, "Exciton-polariton condensates," *Nature Physics*, vol. 10, pp. 803 EP –, Oct 2014. Review Article.

[46] M. Kira and S. Koch, *Semiconductor Quantum Optics*. Cambridge University Press, 2011.

[47] N. Takemura, M. D. Anderson, S. Trebaol, S. Biswas, D. Y. Oberli, M. T. Portella-Oberli, and B. Deveaud, "Dephasing effects on coherent exciton-polaritons and the breakdown of the strong coupling regime," *Phys. Rev. B*, vol. 92, p. 235305, Dec 2015.

[48] J. Rogel-Salazar, "The GrossPitaevskii equation and BoseEinstein condensates," *European Journal of Physics*, vol. 34, no. 2, p. 247, 2013.

[49] D. Ballarini, M. De Giorgi, E. Cancellieri, R. Houdré, E. Giacobino, R. Cingolani, A. Bramati, G. Gigli, and D. Sanvitto, "All-optical polariton transistor," *Nature Communications*, Apr 2013.

[50] D. Ballarini, M. De Giorgi, E. Cancellieri, R. Houdré, E. Giacobino, R. Cingolani, A. Bramati, G. Gigli, and D. Sanvitto, "All-optical polariton transistor," *Nature Communications*, vol. 4, pp. 1778 EP –, Apr 2013. Article.

[51] D. D. Solnyshkov, I. A. Shelykh, M. M. Glazov, G. Malpuech, T. Amand, P. Renucci, X. Marie, and A. V. Kavokin, "Nonlinear effects in spin relaxation of cavity polaritons," *Semiconductors*, vol. 41, pp. 1080–1091, Sep 2007.

[52] A. Bramati and M. Modugno, *Physics of Quantum Fluids: New Trends and Hot Topics in Atomic and Polariton Condensates*. Springer Series in Solid-State Sciences, Springer Berlin Heidelberg, 2013.

[53] M. Z. Maialle, E. A. de Andrada e Silva, and L. J. Sham, "Exciton spin dynamics in quantum wells," *Phys. Rev. B*, vol. 47, pp. 15776–15788, Jun 1993.

[54] I. A. Shelykh, G. Pavlovic, D. D. Solnyshkov, and G. Malpuech, "Proposal for a mesoscopic optical berry-phase interferometer," *Phys. Rev. Lett.*, vol. 102, p. 046407, Jan 2009.

[55] A. Kavokin, G. Malpuech, and M. Glazov, "Optical spin hall effect," *Phys. Rev. Lett.*, vol. 95, p. 136601, Sep 2005.

[56] A. Gerrard and J. Burch, *Introduction to Matrix Methods in Optics*. Dover Books on Physics, Dover, 1994.

[57] M. J. Padgett and J. Courtial, "Poincaré-sphere equivalent for light beams containing orbital angular momentum," *Opt. Lett.*, vol. 24, pp. 430–432, Apr 1999.

[58] H. Flayac, D. D. Solnyshkov, I. A. Shelykh, and G. Malpuech, "Transmutation of skyrmions to half-solitons driven by the nonlinear optical spin hall effect," *Phys. Rev. Lett.*, vol. 110, p. 016404, Jan 2013.

[59] L. Allen, M. W. Beijersbergen, R. J. C. Spreeuw, and J. P. Woerdman, "Orbital angular momentum of light and the transformation of Laguerre-Gaussian laser modes," *Phys. Rev. A*, vol. 45, pp. 8185–8189, Jun 1992.

[60] Hayat, Alex and Lange, Christoph and Rozema, Lee A. and Darabi, Ardavan and van Driel, Henry M. and Steinberg, Aephraim M. and Nelsen, Bryan and Snoke, David W. and Pfeiffer, Loren N. and West, Kenneth W., "Dynamic stark effect in strongly coupled microcavity exciton polaritons," *Phys. Rev. Lett.*, vol. 109, p. 033605, Jul 2012.

[61] G. Panzarini, L. C. Andreani, A. Armitage, D. Baxter, M. S. Skolnick, V. N. Astratov, J. S. Roberts, A. V. Kavokin, M. R. Vladimirova, and M. A. Kaliteevski, "Exciton-light coupling in single and coupled semiconductor microcavities: Polariton dispersion and polarization splitting," *Phys. Rev. B*, vol. 59, pp. 5082–5089, Feb 1999.

[62] S. Kéna-Cohen, M. Davanço, and S. R. Forrest, "Strong exciton-photon coupling in an organic single crystal microcavity," *Phys. Rev. Lett.*, vol. 101, p. 116401, Sep 2008.

[63] P. D. Drummond and J. F. Corney, "Quantum dynamics and coherence properties of evaporatively cooled Bose-Einstein condensates," in *Technical Digest.*

Summaries of Papers Presented at the Quantum Electronics and Laser Science Conference, pp. 38–39, May 1999.

[64] P. Deuar and P. D. Drummond, "Gauge P representations for quantum-dynamical problems: Removal of boundary terms," *Phys. Rev. A*, vol. 66, p. 033812, Sep 2002.

[65] P. D. Drummond and D. F. Walls, "Quantum theory of optical bistability. I. Nonlinear polarisability model," *J. Phys. A: Math. Gen.*, vol. 13, no. 2, pp. 725–741, 1999.

[66] M. Sich, D. N. Krizhanovskii, M. S. Skolnick, A. V. Gorbach, R. Hartley, D. V. Skryabin, E. A. Cerda-Méndez, K. Biermann, R. Hey, and P. V. Santos, "Observation of bright polariton solitons in a semiconductor microcavity," *Nature Photonics*, vol. 6, pp. 50 EP –, Nov 2011. Article.

[67] L. Debnath, "A brief historical introduction to solitons and the inverse scattering transforma vision of scott russell," *International Journal of Mathematical Education in Science and Technology*, vol. 38, no. 8, pp. 1003–1028, 2007.

[68] L. Mollenauer and J. Gordon, *Solitons in Optical Fibers: Fundamentals and Applications*. Elsevier Science, 2006.

[69] C. Becker, S. Stellmer, P. Soltan-Panahi, S. Dörscher, M. Baumert, E.-M. Richter, J. Kronjäger, K. Bongs, and K. Sengstock, "Oscillations and interactions of dark and dark-bright solitons in bose-einstein condensates," *Nature Physics*, vol. 4, pp. 496 EP –, May 2008. Article.

[70] P. D. Drummond and S. J. Carter, "Quantum-field theory of squeezing in solitons," *J. Opt. Soc. Am. B*, vol. 4, pp. 1565–1573, Oct 1987.

[71] P. D. Drummond, R. M. Shelby, S. R. Friberg, and Y. Yamamoto, "Quantum solitons in optical fibres," *Nature*, vol. 365, pp. 307 EP –, Sep 1993.

[72] G. Buonaiuto, D. M. Whittaker, and E. Cancellieri, "Conservation of Quantum Correlations in Multimode Systems with $U(1)$ Symmetry," *Phys. Rev. Lett.*, vol. 121, p. 020404, Jul 2018.

[73] Q. Feng, H. Hong-Bin, Q. Guan-Xiao, and S. Cai-Kang, "Spontaneous U(1) symmetry breaking and BoseEinstein condensation," *Chinese Physics*, vol. 15, no. 7, p. 1577, 2006.

[74] G. Volovik and O. U. Press, *The Universe in a Helium Droplet*. International Series of Monographs on Physics, Clarendon Press, 2003.

[75] A. Zee, *Quantum Field Theory in a Nutshell: Second Edition*. In a Nutshell, Princeton University Press, 2010.

[76] J. Vargas-Martanez, H. Moya-Cessa, and M. Fernandez Guasti, "Normal and anti-normal ordered expressions for annihilation and creation operators," *Revista mexicana de Fisica E*, vol. 52, pp. 13 – 16, 06 2006.

[77] S. Baier, M. J. Mark, D. Petter, K. Aikawa, L. Chomaz, Z. Cai, M. Baranov, P. Zoller, and F. Ferlaino, "Extended Bose-Hubbard models with ultracold magnetic atoms," *Science*, vol. 352, no. 6282, pp. 201–205, 2016.

[78] C. E. Whittaker, E. Cancellieri, P. M. Walker, D. R. Gulevich, H. Schomerus, D. Vaitiekus, B. Royall, D. M. Whittaker, E. Clarke, I. V. Iorsh, I. A. Shelykh, M. S. Skolnick, and D. N. Krizhanovskii, "Exciton-polaritons in a two-dimensional Lieb lattice with spin-orbit coupling," *ArXiv e-prints*, May 2017.

[79] S. Endo, T. Oka, and H. Aoki, "Tight-binding photonic bands in metallophotonic waveguide networks and flat bands in kagome lattices," *Phys. Rev. B*, vol. 81, p. 113104, Mar 2010.

[80] T. Jacqmin, I. Carusotto, I. Sagnes, M. Abbarchi, D. D. Solnyshkov, G. Malpuech, E. Galopin, A. Lemaître, J. Bloch, and A. Amo, "Direct ob-

servation of dirac cones and a flatband in a honeycomb lattice for polaritons," *Phys. Rev. Lett.*, vol. 112, p. 116402, Mar 2014.

[81] T. C. H. Liew and V. Savona, "Single photons from coupled quantum modes," *Phys. Rev. Lett.*, vol. 104, p. 183601, May 2010.

[82] S. Schmidt and G. Blatter, "Strong coupling theory for the jaynes-cummings-hubbard model," *Phys. Rev. Lett.*, vol. 103, p. 086403, Aug 2009.

[83] S. Mandt, D. Sadri, A. A. Houck, and H. E. Treci, "Stochastic differential equations for quantum dynamics of spin-boson networks," *New Journal of Physics*, vol. 17, no. 5, p. 053018, 2015.

[84] H. Deng, G. S. Solomon, R. Hey, K. H. Ploog, and Y. Yamamoto, "Spatial coherence of a polariton condensate," *Phys. Rev. Lett.*, vol. 99, p. 126403, Sep 2007.

[85] T. H. Stievater, X. Li, D. G. Steel, D. Gammon, D. S. Katzer, D. Park, C. Piermarocchi, and L. J. Sham, "Rabi oscillations of excitons in single quantum dots," *Phys. Rev. Lett.*, vol. 87, p. 133603, Sep 2001.

[86] Q. Xie, H. Zhong, M. T. Batchelor, and C. Lee, "The quantum rabi model: solution and dynamics," *Journal of Physics A: Mathematical and Theoretical*, vol. 50, no. 11, p. 113001, 2017.

[87] C. J. Isham, "Lectures on Groups and vector spaces for physicists," *World Sci. Lect. Notes Phys.*, vol. 31, pp. 1–219, 1989.

[88] Y. Chen, Z. Yu, and H. Zhai, "Quantum phase transitions of the Bose-Hubbard model inside a cavity," *Phys. Rev. A*, vol. 93, p. 041601, Apr 2016.

[89] B.-G. Englert and G. Morigi, "Five lectures on dissipative master equations," pp. 55–106, 2002.

[90] T. Ozawa, A. Amo, J. Bloch, and I. Carusotto, "Klein tunneling in driven-dissipative photonic graphene," *Phys. Rev. A*, vol. 96, p. 013813, Jul 2017.

[91] W. Casteels, R. Rota, F. Storme, and C. Ciuti, "Probing photon correlations in the dark sites of geometrically frustrated cavity lattices," *Phys. Rev. A*, vol. 93, p. 043833, Apr 2016.

[92] S. R. K. Rodriguez, A. Amo, I. Sagnes, L. Le Gratiet, E. Galopin, A. Lemaître, and J. Bloch, "Interaction-induced hopping phase in driven-dissipative coupled photonic microcavities," *Nature Communications*, vol. 7, pp. 11887 EP –, Jun 2016. Article.

[93] S. Mukherjee, D. Mogilevtsev, G. Y. Slepyan, T. H. Doherty, R. R. Thomson, and N. Korolkova, "Dissipatively coupled waveguide networks for coherent diffusive photonics," *Nature Communications*, vol. 8, no. 1, p. 1909, 2017.

[94] C. E. Whittaker, B. Dzurnak, O. A. Egorov, G. Buonaiuto, P. M. Walker, E. Cancellieri, D. M. Whittaker, E. Clarke, S. S. Gavrilov, M. S. Skolnick, and D. N. Krizhanovskii, "Polariton Pattern Formation and Photon Statistics of the Associated Emission," *Phys. Rev. X*, vol. 7, p. 031033, Aug 2017.

[95] J. Yeomans, *Statistical Mechanics of Phase Transitions*. Clarendon Press, 1992.

[96] A. Gilchrist, C. W. Gardiner, and P. D. Drummond, "Positive p representation: Application and validity," *Phys. Rev. A*, vol. 55, pp. 3014–3032, Apr 1997.

[97] R. S. J. Mikusiski, *The elementary theory of distributions (II)*. Instytut Matematyczny Polskiej Akademi Nauk, 1961.

[98] H. J. Carmichael, "Quantum trajectory theory for cascaded open systems," *Phys. Rev. Lett.*, vol. 70, pp. 2273–2276, Apr 1993.

[99] C. W. Gardiner and M. J. Collett, "Input and output in damped quantum systems: Quantum stochastic differential equations and the master equation," *Phys. Rev. A*, vol. 31, pp. 3761–3774, Jun 1985.

[100] C. W. Gardiner, "Driving a quantum system with the output field from another driven quantum system," *Phys. Rev. Lett.*, vol. 70, pp. 2269–2272, Apr 1993.

[101] P. Meystre and M. Sargent, *Elements of Quantum Optics*. Springer Berlin Heidelberg, 2013.

[102] J. E. Moyal, "Quantum mechanics as a statistical theory," *Mathematical Proceedings of the Cambridge Philosophical Society*, vol. 45, no. 1, p. 99124, 1949.

[103] A. D. Wilson-Gordon, V. Buek, and P. L. Knight, "Statistical and phase properties of displaced kerr states," *Phys. Rev. A*, vol. 44, pp. 7647–7656, Dec 1991.

[104] R. L. Hudson, "When is the wigner quasi-probability density non-negative?," *Reports on Mathematical Physics*, vol. 6, pp. 249–252, Oct. 1974.

[105] S. Aaronson and D. Gottesman, "Improved simulation of stabilizer circuits," *Phys. Rev. A*, vol. 70, p. 052328, Nov 2004.

[106] S. D. Bartlett, B. C. Sanders, S. L. Braunstein, and K. Nemoto, "Efficient classical simulation of continuous variable quantum information processes," *Phys. Rev. Lett.*, vol. 88, p. 097904, Feb 2002.

[107] A. Mari and J. Eisert, "Positive Wigner Functions Render Classical Simulation of Quantum Computation Efficient," *Phys. Rev. Lett.*, vol. 109, p. 230503, Dec 2012.

[108] M. A. Nielsen and I. L. Chuang, *Quantum Computation and Quantum Information: 10th Anniversary Edition*. New York, NY, USA: Cambridge University Press, 10th ed., 2011.

[109] J. C. López Carreño, C. Sánchez Muñoz, D. Sanvitto, E. del Valle, and F. P. Laussy, "Exciting polaritons with quantum light," *Phys. Rev. Lett.*, vol. 115, p. 196402, Nov 2015.

[110] P. D. Drummond and D. F. Walls, "Quantum theory of optical bistability. i. nonlinear polarisability model," *Journal of Physics A: Mathematical and General*, vol. 13, no. 2, p. 725, 1980.

[111] M. A. Nielsen and I. L. Chuang, *Quantum Computation and Quantum Information: 10th Anniversary Edition*. New York, NY, USA: Cambridge University Press, 10th ed., 2011.

[112] S. L. Braunstein and P. van Loock, "Quantum information with continuous variables," *Rev. Mod. Phys.*, vol. 77, pp. 513–577, Jun 2005.

[113] L.-M. Duan, G. Giedke, J. I. Cirac, and P. Zoller, "Inseparability criterion for continuous variable systems," *Phys. Rev. Lett.*, vol. 84, pp. 2722–2725, Mar 2000.

[114] T. C. H. Liew and V. Savona, "Multimode entanglement in coupled cavity arrays," *New Journal of Physics*, vol. 15, no. 2, p. 025015, 2013.

[115] H. Krauter, C. A. Muschik, K. Jensen, W. Wasilewski, J. M. Petersen, J. I. Cirac, and E. S. Polzik, "Entanglement generated by dissipation and steady state entanglement of two macroscopic objects," *Phys. Rev. Lett.*, vol. 107, p. 080503, Aug 2011.

[116] O. Thearle, J. Janousek, S. Armstrong, S. Hosseini, M. Schünemann (Mraz), S. Assad, T. Symul, M. R. James, E. Huntington, T. C. Ralph, and P. K. Lam, "Violation of bell's inequality using continuous variable measurements," *Phys. Rev. Lett.*, vol. 120, p. 040406, Jan 2018.

[117] R. El-Ganainy, K. G. Makris, M. Khajavikhan, Z. H. Musslimani, S. Rotter, and D. N. Christodoulides, "Non-Hermitian physics and PT symmetry," *Nature Physics*, vol. 14, pp. 11 EP –, Jan 2018. Review Article.

[118] C. M. Bender, "Introduction to -symmetric quantum theory," *Contemporary Physics*, vol. 46, no. 4, pp. 277–292, 2005.

[119] E. Caparelli, V. Dodonov, and S. Mizrahi, "Photon distribution drift in multiphoton absorption-emission processes due to one-photon perturbations," *Physics Letters A*, vol. 232, no. 3, pp. 175 – 182, 1997.

[120] K. V. Kepesidis, S. D. Bennett, S. Portolan, M. D. Lukin, and P. Rabl, "Phonon cooling and lasing with nitrogen-vacancy centers in diamond," *Phys. Rev. B*, vol. 88, p. 064105, Aug 2013.

[121] A. Gurumoorthy and J. Picardo, "Evaluation of matcont of matlab for constructing bifurcation diagrams of chemical process systems," 09 2011.

[122] S. Strogatz, *Nonlinear Dynamics and Chaos: With Applications to Physics, Biology, Chemistry, and Engineering.* Studies in Nonlinearity, Avalon Publishing, 2014.

[123] R. Schnabel, "Squeezed states of light and their applications in laser interferometers," *Physics Reports*, vol. 684, pp. 1 – 51, 2017. Squeezed states of light and their applications in laser interferometers.

[124] T. Fink, A. Schade, S. Höfling, C. Schneider, and A. Imamoglu, "Signatures of a dissipative phase transition in photon correlation measurements," *Nature Physics*, vol. 14, no. 4, pp. 365–369, 2018.

[125] E. M. Kessler, G. Giedke, A. Imamoglu, S. F. Yelin, M. D. Lukin, and J. I. Cirac, "Dissipative phase transition in a central spin system," *Phys. Rev. A*, vol. 86, p. 012116, Jul 2012.

[126] A. Faraon, A. Majumdar, D. Englund, E. Kim, M. Bajcsy, and J. Vukovi, "Integrated quantum optical networks based on quantum dots and photonic crystals," *New Journal of Physics*, vol. 13, no. 5, p. 055025, 2011.